The characterization of the components of the energy and water balance within hedgerow orchards for the verification of a two-dimensional water balance and energy interception model for fruit trees

by

N. du Sautoy

Submitted in partial fulfilment of the requirements for the degree
PHILOSOPHIAE DOCTOR AGRICULTURAE: PLANT PRODUCTION
in the Faculty of Natural and Agricultural Science
University of Pretoria

Supervisor: Prof J. G. Annandale
Co-Supervisor: Dr N. Z. Jovanovic

February 2005

CONTENTS

Acknowledgement v
List of tables vi
List of figures vii
List of acronyms and symbols xii
Abstract xv

INTRODUCTION 1
1 MODEL DESCRIPTION 5
1.1. Two-dimensional water balance and energy interception model for hedgerow fruit trees (SWB -2D) 6
1.1.1. Two dimensional energy interception model 6
1.1.2. Spatial distribution of soil evaporation 9
1.1.3. Two-dimensional finite difference soil water balance model 13
1.1.3.1. The soil profile 13
1.1.3.2. Two-dimensional water flow 15
1.1.3.3. Upper boundary condition 22
1.1.3.4. Lower boundary condition 23
1.1.3.5. Model stability 23
1.1.4. Link between the two-dimensional radiation and soil water balance model 24
1.1.5. Required inputs ... 25
1.2. FAO-based crop factor model 26
1.2.1. FAO-type crop factor modification 27
1.2.2. Soil water balance with localised irrigation 30
1.2.2.1. Water redistribution 30
1.2.2.2. Evaporation 30
1.2.2.3. Transpiration 31
1.2.3. Yield predictions with the FAO model 33
2 MATERIALS AND METHODS 35
2.1. Experimental set-up at the University of Pretoria 35
2.1.1. Location and environmental characteristics 35
2.1.2. Orchard lay-out, irrigation and cultivation practices 36
2.1.3. Lysimeter characteristics 37

2.1.4. Calculation of evapotranspiration and crop coefficient from lysimeter data 38
2.1.5. Weather monitoring 40
2.1.6. Soil measurements 40
2.1.6.1. Soil physical properties 40
2.1.6.2. Soil matric potential 41
2.1.6.3. Soil water content 48
2.1.7. Plant measurements 56
2.1.7.1. Root distribution 56
2.1.7.2. Canopy radiation interception 56
2.1.7.3. Leaf area index and density 57
2.1.7.4. Canopy size and row orientation 57
2.1.8. Leucaena trial 58
2.2. Experimental set-up at the University of the North 58
2.2.1. Location and environmental characteristics 58
2.2.2. Orchard lay-out, irrigation and cultivation practices 58
2.2.3. Weather monitoring 62
2.2.4. Soil measurements 62
2.2.5. Plant measurements 62
2.3. Field trial at Brits 63
3 MODELLING 65
3.1. Evaluation of the SWB model 65
3.2. Calibration of the FAO-type model and field observations 66
3.3. Evaluation of the two-dimensional energy interception model 81
3.3.1. Overview of the field trials 81
3.3.2. Peach trial (Hatfield) 82
3.3.3. Leucaena trial (Hatfield) 94
3.3.4. Citrus trial (Syferkuil) 104
3.3.5. Citrus trial (Brits) 108
3.4. Evaluation of the two-dimensional water balance model 112
3.5. Scenario modelling and sensitivity analysis 127
3.5.1 Row orientation 127
3.5.2 Wetted diameter and canopy width 128
3,5,3 Root density 129
3,5,4 Interpretation of results 130
4 CONCLUSIONS AND RECOMMENDATIONS 136
5 REFERENCES 140

Appendix A 143
Program code used with Campbell Scientific data-loggers 143
A.1 Hatfield Automatic Weather Station 143
A.2 Mobile Automatic Weather Station at Syferkuil clementine orchard..... 146
A.3 Lysimeter and tube solarimeter control program peach orchard..... 151
A.4 Program to control tube solarimeters & line quantum sensors 154
A.5 Heat dissipation sensors (HDS) program; 16 sensors 158
A.6 Heat dissipation sensors (HDS) program; 24 sensors 167
A.7 Heat dissipation sensors (HDS) program; 28 sensors 181
A.8 TDR cable length measurement for 28 TDR probes in clementine orchard..... 186
A.9 TDR cable length measurement for 40 TDR probes in peach orchard 189
A.10 TDR Water Content measurement for 28 TDR probes in clementine orchard.. 197
A.11 TDR Water Content measurement for 40 TDR probes in peach orchard 200
A.12 Mobile Weather station & light penetration of hedge-rows..... 208
A.13 Programme to calibrate seven tube solarimeters..... 211

ACKNOWLEDGEMENTS

While one is in the midst of tackling a challenging project it is easy to overlook or take for granted the assistance of colleagues who have made a useful contribution to the fulfilment of the enterprise and thus failed to express the rightful gratitude that was deserved. I, no doubt, have been guilty of committing this offence during the course of this research. To those who I have so offended, I extend a sincere word of apology and take this opportunity to make amends by extending a word of thanks now.

During this research, besides learning a tremendous amount, I have made many friends and have many fond memories. Coming from a BC (Before Computers) era, and getting involved with crop modelling presented some interesting challenges and changes in one's mindset. Associated with this were some unforgettable comments, for example, Dr Nico Benade's words of wisdom when he quietly stated: " .. *if I can produce a program that Neil cannot foul-up it will be completely foolproof* " ! On one particularly trying task, while Nebo and I were trying to get some new technology working via an old laptop, somehow the electrical connections were incorrectly connected and the unit burn out. The conclusion was then reached that "*it was bad for computers to smoke*". On another occasion, whilst taking measurements an irrigation unit sprayed a computer and the valuable lesson gained was "*it's bad to irrigate computers*". So to these two fellows, for passing on this valuable information, I honestly don't know how to adequately express my thanks!

The Personnel of the Department of Plant Production and Soil Science were particularly helpful and friendly and certainly made the time spent at TUKS enjoyable, for this I thank you all. A particular word of thanks goes to Ms Joey Herman who on many occasions has phoned me and politely related the riot act to encourage me to "put digits to keyboard" and get the Thesis written.

This study would not have begun if it were not for Prof Paul Fouché who motivated that I join the Research Project funded by the Water Research Commission. For this instigation, I extend grateful thanks to Prof Fouché. I am also indebted to the WRC for the funding and to Dr G Backeberg for his assistance and encouragement.

Dr Nebo Jovanovic played a pivotal role in assisting me with this research. Without his quite encouragement, unstinting help and reliability I doubt whether I could have completed the task. Dr Jovanovic and Dr Lobit's input into the final draft of the WRC report "Two-dimensional energy interception and water balance model for hedgerow tree crops", which is the precursor for this thesis, was massive. Their assistance in this final draft cannot be over emphasised and for this I thank you both.

During this study many individuals and institutions gave very valuable advice and information. In particular, Ms T Volschenk from the Agricultural Research Council – Infruitec, Stellenbosch, Dr George Green of the WRC and Dr Tom Fyfield, ARC – Institute for Soil, Climate and Water, Pretoria, come quickly to mind. Your contributions are appreciated.

On the personal side, the support received from my wife and children has been tremendous. They have patiently accepted the inconvenience in our daily lives that were associated with conducting this project; for this I'm indebted and very grateful. In addition, the MD of, and colleagues in Techniland, your encouragement and support in the final stages of this thesis are appreciated, many thanks.

Finally, sincere thanks are extended to my promoter, Prof John Annandale. He has managed to take a virtually computer illiterate "old school soil scientist" who was very sceptical about the value of modelling and convert him to a "computer illiterate believer". The most important point I have gained from this project is the realization of the importance of realistic numerical quantification of "soil-plant-atmosphere" inter-relationships and what a powerful tool this can be in modern agriculture. For this I am really grateful and wish you every success in passing this extremely valuable concept onto your future students. If you can teach me this, you will get it right with anybody.

LIST OF TABLES

Table 2.1 Field capacity water content per depth interval for soil at Hatfield peach trial site

Table 2.2 Weighting factors used in calculate respective NWM access tube contribution to the water status of the whole row at Hatfield peach trial site

Table 3.1. List of tree crops monitored and their locality specifications.

Table 3.2. Distances (m) from centre line of the canopies for tube solarimeters (No. 1 to 7) installed in different hedge-rows.

Table 3.3. Radiation data collection programme and canopy parameters for crops monitored.

LIST OF FIGURES

Figure 1.1. Three-dimensional scheme of a tree; c is half the height, a half the width and b half the depth of the canopy. z_o is the height from the ground to the centre of the canopy, and z_b the height of the base of the canopy.

Figure 1.2. Schematic representation of a ray of sunlight passing through the tree canopy. S is the path length; θ is the elevation angle, Q is the position where the ray enters the canopy, N where it exits and P where it is intercepted on the soil surface. Three cases are shown: (1) both Q and N are on the ellipsoidal part of the canopy, (2) N is at the base of the canopy, (3) the ray of sunlight is not intercepted by the canopy.

Figure 1.3. Schematic illustration of the system simulated; n is the tree row number, h is the row spacing, x, y and z the cartesian axes, and the soil surface over which radiant transmittance is estimated is between 3/2h and 5/2h.

Figure 1.4. Flow diagram of the two-dimensional energy interception model for hedgerow fruit trees.

Figure 1.5. The two-dimensional nodal system. Element [i, j] has been divided into quarters: ul (upper left); ur (upper right); ll (lower left) and lr (lower right). Element [i-1, j] shows the soil properties which are fixed for a particular element: b is the slope of a log-log water retention function; Ψ_e the air entry potential; K_s the saturated hydraulic conductivity; ρ_b is bulk density and θ_s the saturated volumetric water content.

Figure 1.6. Nodal grid system showing symmetry planes and hedgerow. The soil layers for the cascading model are also represented.

Figure 1.7. Detail of element [i, j] (see Figure 2.5), with K, θ and Φ calculated for each quarter (ul, ur, ll and ul). For demonstration purposes, nodes [i, j] and [i, j+1] are below Ψ_e whilst nodes [i+1, j] and [i+1, j+1] are above Ψ_e.

Figure 1.8. Control volume [i, j] illustrating the eight water fluxes.

Figure 1.9. Flow diagram of the two-dimensional soil water balance model for hedgerow fruit trees.

Figure 1.10. Flow diagram of the FAO-type crop factor model.

Figure 1.11. Flow diagram of the cascading soil water balance for tree crops under localized irrigation.

Figure 2.1. Calibration curves of the lysimeters (east and west)

Figure 2.2. Diagrammatic grid indicating monitoring and soil sampling locations in the soil profile for the Hatfield and Syferkuil hedgerow system.

Figure 2.3. Variation of soil texture of B horizon (~0.4 m depth) across tree row.

Figure 2.4. Variation of soil texture (mean for row width) with depth.

Figure 2.5. Variation of soil penetration resistance with depth.

Figure 2.6. Effect of soil water content on soil penetration resistance.

Figure 2.7. View of tube solarimeters and LQS installed under the peach hedgerow to record solar irradiance under a developing canopy.

Figure 2.8. Diagrammatic representation of the Heat Dissipation Sensor (HDS) system used in the Hatfield field trial.

Figure 2.9. Dimensions used to determine profile volumetric water (θ) content from NWM measurements

Figure 2.10. Dimensions used to establish weighting factors (wt_j) for each NWM access tube (t_j) to correctly establish water status for the whole row having a width of 4.5 m.

Figure 2.11. Installing HDS and TDR sensors in clementine hedgerow at Syferkuil.

Figure 2.12. Completed installation of HDS and TDR sensors and control units in the clementine hedgerow at Syferkuil.

Figure 2.13. Diagrammatic representation of the Time Domain Reflectometry (TDR) system used in the field trial.

Figure 2.14. View of the clementine hedgerow and tube solarimeter in the inter-row. Note jagged shade line.

Figure 2.15. View of leucaena N-S axis hedgerow and tube solarimeters. This is with full canopy (LAD = 1.55 m^{-2} m^3) with afternoon sunshine.

Figure 2.16. View of the leucaena E-W axis hedgerow and tube solarimeters. This is with totally stripped canopy (LAD = 0.39 m^{-2} m^3) with late afternoon sunshine.

Figure 2.17. View of the valencia tramline hedgerow with tube solarimeter and AWS in middle of tramline.

Figure 2.18. View of the valencia tramline hedgerow and tube solarimeters installed under canopy to record solar irradiance under tramline canopy.

Figure 2.19. View of LAI-2000 Plant Canopy Analyser (PCA) optical sensor with 45º view cap to block out 315º field-of-view.

Figure 2.20. Diagrammatic representation of the dimensions of the valencia tramline hedgerow at Brits showing the positioning of the solarimeters.

Figure 3.1. Daily Kc (dots) and Kcb (+ and line0), as well as growth periods for first leaf season of peaches.

Figure 3.2. Daily Kc (dots) and Kcb (+ and line), as well as growth periods for second leaf season of peaches.

Figure 3.3a. Predicted (solid line) and measured (squares) soil water deficit for first leaf season of peaches (stress treatment).

Figure 3.3b. Predicted (solid line) and measured (squares) soil water deficit for first leaf season of peaches (non-stressed treatment).

Figure 3.4. Predicted (solid line) and measured (squares) soil water deficit for second leaf season of peaches.

Figure 3.5. Soil water deficit predicted with the SWB model (SWB Soil water deficit) vs. deficit measured with the neutron water meter (NWM Soil water deficit). The comparison was carried out by using NWM measurements for the whole area, 2 m from tree and at centre of row.

Figure 3.6. Distribution of irrigation application measured with a grid of rain gauges vs. distance from tree row.

Figure 3.7. Distribution of % penetrating the peach canopy for five rainfall events; measured with a grid of rain gauges and expressed as % of recorded rainfall vs. distance from tree row.

Figure 3.8. Variation of irradiance reaching the soil surface with distance from tree row for three full sunshine days (second leaf peach tree) (DOY = Day of year).

Figure 3.9. Variation of irradiance reaching the soil surface with distance from tree row for three full sunshine days (second leaf peach tree) (DOY = Day of year).

Figure 3.10a. Root length density with soil depth for peaches (Grass sod inter-row is solid lines while Bare soil inter-row is broken lines).

Figure 3.10b. Root length density with distance from the trunk for peaches (Grass sod inter-row is solid lines while Bare soil inter-row is broken lines).

Figure 3.11a. Root length density with soil depth for clementines.

Figure 3.11b. Root length density with distance from the trunk for clementines.

Figure 3.12. Volumetric soil water content across the row at 6, 26, 56 and 86 cm soil depth, and 2 and 36 h after irrigation of peaches (grass sod or bare soil in the inter-row area).

Figure 3.13. Soil matric potential across the row at 6 and 26 cm soil depth, and 2 and 10 days after irrigation of peaches (grass sod or bare soil in the inter-row area).

Figure 3.14. Volumetric soil water content across the row at 6, 26 and 56 cm soil depth, and 1, 6, 11 and 16 days after irrigation of clementines.

Figure 3.15. Variations in soil temperature measured at 6 cm during a summer day in the peach orchard at Hatfield (Squares indicate Bare soil, Dots indicate Grass sod and Diamonds indicate under tree).

Figure 3.16. Measured (symbols) and simulated (lines) daily solar radiation at different sides and distances from the tree row in a hedgerow peach orchard for period 9 to 19 September (initial stage of the crop).

Figure 3.17. Measured (symbols) and simulated (lines) hourly solar radiation at different sides and distances from the tree row in a hedgerow peach orchard for period 9 to 19 September 1999 (initial stage of the crop).

Figure 3.18. Measured (symbols) and simulated (lines) daily solar radiation across the peach hedgerow on 12 September 1999 (initial stage of the crop).

Figure 3.19. Measured (symbols) and simulated (lines) hourly solar radiation across the peach hedgerow on 12 September 1999 at 13h00 (initial stage of the crop).

Figure 3.20. Measured (symbols) and simulated (lines) daily solar radiation at different sides and distances from the tree row in a hedgerow peach orchard for period 13 to 19 October 1999 (development stage of the crop).

Figure 3.21. Measured (symbols) and simulated (lines) hourly solar radiation at different sides and distances from the tree row in a hedgerow peach orchard for period 13 to 19 October 1999 (development stage of the crop).

Figure 3.22. Measured (symbols) and simulated (lines) daily solar radiation at different sides and distances from the tree row in a hedgerow peach orchard for period 15 to 21 November 1999 (at harvest).

Figure 3.23. Measured (symbols) and simulated (lines) hourly solar radiation at different sides and distances from the tree row in a hedgerow peach orchard for period 15 to 21 November 1999 (at harvest).

Figure 3.24. Canopy dimensions (m) and shape for the E-W row axis Leuceana hedge-row and the positions of the solarimeters. Note: 1) On the northern side, the coppice stems are virtually parallel to the solar irradiance (dashed arrows) and thus little solar irradiance is intercepted. 2) Due to the “Feather-duster” shape, the solarimeters on the northern side have little foliage interception of solar irradiance. 3) In addition, the canopy is not symmetrical and does not conform to an elliptical shape (dashed outline).

Figure 3.25. Measured (symbols) and simulated (lines) hourly solar radiation at different sides and distances from the tree row in a hedgerow leucaena orchard for period 29 to 30 May 1999 (row axis N-S; LAD = 1.55 m^2 leaf m^{-3} canopy).

Figure 3.26. Measured (symbols) and simulated (lines) hourly solar radiation at different sides and distances from the tree row in a hedgerow leucaena orchard on 31 May 1999 (row axis N-S; LAD = 1.22 m^2 leaf m^{-3} canopy).

Figure 3.27. Measured (symbols) and simulated (lines) hourly solar radiation at different sides and distances from the tree row in a hedgerow leucaena orchard on 1 June 1999 (row axis N-S; LAD = 0.46 m^2 leaf m^{-3} canopy).

Figure 3.28. Measured (symbols) and simulated (lines) hourly solar radiation at different sides and distances from the tree row in a hedgerow leucaena orchard for period 2 to 3 June 1999 (row axis N-S; LAD = 0.23 m^2 leaf m^{-3} canopy).

Figure 3.29. Measured (symbols) and simulated (lines) hourly solar radiation at different sides and distances from the tree row in a hedgerow leucaena orchard for period 5 to 9 June 1999 (row axis E-W; LAD = 1.40 m^2 leaf m^{-3} canopy).

Figure 3.30. Measured (symbols) and simulated (lines) hourly solar radiation at different sides and distances from the tree row in a hedgerow leucaena orchard on 10 June 1999 (row axis E-W; LAD = 1.00 m^2 leaf m^{-3} canopy).

Figure 3.31. Measured (symbols) and simulated (lines) hourly solar radiation at different sides and distances from the tree row in a hedgerow leucaena orchard on 11 June 1999 (row axis E-W; LAD = 0.39 m^2 leaf m^{-3} canopy).

Figure 3.32. Measured (symbols) and simulated (lines) daily solar radiation at different sides and distances from the tree row in a hedgerow clementine orchard for period 3 to 11 December 1999.

Figure 3.33. Measured (symbols) and simulated (lines) hourly solar radiation at different sides and distances from the tree row in a hedgerow clementine orchard for period 3 to 9 December 1999.

Figure 3.34. Measured (symbols) and simulated (lines) photosynthetically active radiation (PAR) at different sides and distances from the tree row in a hedgerow clementine orchard for period 3 to 9 December 1999.

Figure 3.35. Measured (symbols) and simulated (lines) hourly solar radiation at different sides and distances from the tree row in a hedgerow valencia orchard for period 7 to 13 July 1999.

Figure 3.36. Measured (symbols) and simulated (lines) hourly solar radiation at different sides and distances from the tree row in a hedgerow mandarin orchard for period 30 July to 5 August 1999.

Figure 3.37. Simulated (line) and measured (squares) volumetric soil water content at 6 cm depth, 3.75; 2.5 and 1.25 m on the NE side of the trunk, as well as directly under the tree, for the Clementine hedgerow for the period 13 to 23 February 2000.

Figure 3.38. Simulated (line) and measured (squares) volumetric soil water content at 26 cm depth, 3.75; 2.5 and 1.25 m on the NE side of the trunk, as well as directly under the tree, for the Clementine hedgerow for the period 13 to 23 February 2000.

Figure 3.39. Simulated (line) and measured (squares) volumetric soil water content at 90 cm depth, 3.75; 2.5 and 1.25 m on the NE side of the trunk, as well as directly under the tree, for the Clementine hedgerow fot the period 13 to 23 February 2000.

Figure 3.40a. Simulated (line) and measured (squares) volumetric soil water content on the SW side of the Clementine hedgerow at 6, 26, 56, and 86 cm depths for the period 9 to 17 February, i.e. during a heavy irrigation.

Figure 3.40b. Simulated (line) and measured (squares) volumetric soil water content on the NE side of the Clementine hedgerow at 6, 26, 56, and 86 cm depths for the period 9 to 17 February, i.e. during a heavy irrigation.

Figure 3.41a. Simulated (line) and measured (squares) volumetric soil water content on the SW side of the Clementine hedgerow at 6, 26, 56, and 86 cm depths for the period 18 to 26 February, i.e. during a 22.6 mm rainfall event.

Figure 3.41b. Simulated (line) and measured (squares) volumetric soil water content on the NE side of the Clementine hedgerow at 6, 26, 56, and 86 cm depths for the period 18 to 26 February, i.e. during a 22.6 mm rainfall event.

Figure 3.42a. Simulated (line) and measured (squares) volumetric soil water content on the SW side of the Clementine hedgerow at 6, 26, 56, and 86 cm depths for the period 26 February to 11 March, i.e. during a heavy rainfall (34.9 mm) event.

Figure 3.42b. Simulated (line) and measured (squares) volumetric soil water content on the NE side of the Clementine hedgerow at 6, 26, 56, and 86 cm depths for the period 26 February to 11 March, i.e. during a heavy rainfall (34.9 mm) event.

Figure 3.43a. Simulated (line) and measured (squares) volumetric soil water content on the SW side of the Clementine hedgerow at 6, 26, 56, and 86 cm depths for the period 18 to 29 March, i.e. during a light rainfall (8.3 mm) event.

Figure 3.43b. Simulated (line) and measured (squares) volumetric soil water content on the NE side of the Clementine hedgerow at 6, 26, 56, and 86 cm depths for the period 18 to 29 March, i.e. during a light rainfall (8.3 mm) event.

Figure 3.44. Variation in measured volumetric soil water content (WC %) with depth across the Clementine hedgerow one day after a 48 mm rainfall (14 February 2000) and 10 days later (24 February 2000). Negative distances on the x-axis are for the SW side of the row, and positive values are for the NE side.

Figure 3.45. Simulated evaporation (E), transpiration (T) and evapotranspiration (ET) as a function of row orientation for two orchards at Kakamas and Stellenbosch (from 01/01/1998 to 28/02/1998).

Figure 3.46. Simulated transpiration (T) as a function of canopy width and wetted diameter for two orchards at Kakamas and Stellenbosch for period 1 January to 28 February 1998.

Figure 3.47. Simulated transpiration (T) in % of evapotranspiration (ET) as a function of canopy width and wetted diameter for two orchards at Kakamas and Stellenbosch for period 1 January to 28 February 1998.

Figure 3.48. Simulated transpiration (T) and evaporation (E) as a function of the fraction of roots in the wetted volume of soil for two orchards at Kakamas and Stellenbosch for period 1 January to 28 February 1998.

LIST OF SYMBOLS AND ACRONYMS

List of acronyms

CROPWAT	CROP WATer requirements model (FAO, Rome Italy)
FAO	Food and Agriculture Organization of the United Nations (Rome Italy)
HDS	Heat dissipation sensor
SWB	Soil Water Balance model (University of Pretoria, South Africa)
PEST	ASP Model-Independent Parameter ESTimation (Watermark Numerical Computing, Australia)

List of symbols

a	Half the width of the tree canopy
Acb	Canopy base unit area (m^2 ground)
b	Half the depth of the tree canopy
Cr_{di}	NWM Count ratio for depth interval i
Ct_{Std}	Mean of NWM standard counts
c	Half the height of the tree canopy
D	Drainage
D	Index of agreement of Willmott (1982)
DOY	Day of year
E	Evaporation
ETo	Penman-Monteith grass reference evapotranspiration (mm)
ET_{Gross}	Gross daily evapotranspiration from lysimeters
ET_{lys}	Evapotranspiration determined from lysimeters
FI_{evap}	Canopy cover fraction
FI_{irrig}	Irrigated surface fraction
g	Gravitational constant (9.8 m s^{-1})
h_c	Canopy humidity
hs	Soil surface humidity
Hc	Crop height (m)
Hc_{max}	Maximum crop height (m)
HDS	Heat dissipation sensors
i	Vertical position of a node
I	Infiltration
Ir	Irrigation
j	Horizontal position of a node
k	Extinction coefficient Kcb
K	Hydraulic conductivity (kg s m^{-3})
Kc	Daily crop coefficient
Kcb	FAO basal crop coefficients
Kc_{max}	Maximum value for Kc following rain or irrigation
K_{PAR}	Canopy extinction coefficient for PAR
K_s	Saturated hydraulic conductivity
K_y	Yield Stress factor
l_j	Distance from tree trunk to NWM access tube j (m)
l_r	Row width (m)
LAb	Leaf area per canopy base unit area (m^2 leaf m^{-2} soil surface)
LAD	Leaf area density (m^2 leaves m^{-3} canopy volume)
LAI	Leaf area index (m^2 leaf area m^{-2} soil surface)
$Ly_{(i)}$	Lysimeter water status for day i (mm)
LyEast	Eastern lysimeter

LyWest	Western lysimetr
M	Molar mass of water (0.018 kg mol^{-1})
MAE	Mean absolute error
MBE	Mass balance error
N	Number of observations
N	Days in growth stage for estimated yield calculation
NIR	Near-infrared radiation (range 0.7 – 3 µm)
NWM	Neutron water meter
PAR	Photosynthetically active radiation (range 0.4 – 0.7 µm)
PE	Potential evaporation (mm)
PET	Potential evapotranspiration (mm)
PT	Potential crop transpiration (mm)
R	Rain (mm)
R	Gas constant (8.314 J K^{-1} mol^{-1})
RD	Root depth (m)
RD_{max}	Maximum root depth (m)
RH	Relative humidity (%)
RH_{min}	Daily minimum relative humidity (%)
RMSE	Root mean square error
Rn	Net radiation (W m^2)
r^2	Coefficient of determination
S	Path length of radiation through the canopy (m)
SI	Stress index
SVP	Saturation vapour pressure (kPa)
SWC	Soil water content (m water m^{-1} soil)
SWD	Soil water deficit (mm)
t	Time (s)
t_j	NWM access tube j
T	Kelvin temperature (^{0}K)
T	Actual crop transpiration (mm)
TDR	Time domain reflectometry
T_{max}	Maximum transpiration rate (mm d^{-1})
U	Wind speed (m s-1)
U_2	Mean daily wind speed at 2 m height (m s^{-1})
Vc	Canopy unit volume (m^{-3})
VP	Vapour pressure (kPa)
VPD	Vapour pressure deficit (kPa)
wt_j	Weighting fractor for NWM access tube j
Y	Estimated yield (Mg ha^{-1})
Y_{pot}	Potential yield (Mg ha^{-1})
Y_{red}	Percentage yield reduction (%)
$Y_{rel(Init)}$	Relative yield for initial stage
$Y_{rel(Dev)}$	Relative yield for development stage
$Y_{rel(Mid)}$	Relative yield for mid-season stage
$Y_{rel(Late)}$	Relative yield for late-season stage
z_o	Distance between the soil surface and the centre of the canopy (m)
z_b	Height at which the base of the canopy is cut off (skirting height) (m)

α	Leaf absorptivity for solar radiation
α_{nir}	Leaf absorptivity for near infrared radiation (0.2)
α_p	Leaf absorptivity for photosynthetically active radiation (0.8)
α_s	Leaf absorptivity for total solar radiation (0.5)
Δd_i	Depth interval for NWM measurements (m)

$\Delta Ly_{(i)}$	Average change in water status for both lysimeters on day i (mm)
$\Delta LyEast_{(i)}$	Change in water status of eastern lysimeter on day i (mm)
$\Delta LyWest_{(i)}$	Change in water status of western lysimeter on day i (mm)
θ	Volumetric water content (m water m^{-1} soil)
θ_{di}	Volumetric water content for depth layer i (m water m^{-1} soil)
θ_{Di}	Water deficit for depth interval i (m water m^{-1} soil)
θ_p	Profile volumetric water content (m water m^{-1} soil)
θ_{ea}	Elevation angle (º).
θ_{fc}	Volumetric soil water content at field capacity (m water m^{-1} soil)
θ_{fcdi}	FC for each depth interval
θ_{pwp}	Volumetric soil water content at permanent wilting point (m water m^{-1} soil)
θ_s	Saturated volumetric water content (m water m^{-1} soil)
ρ_b	Bulk density (Mg m^{-3})
ρ_f	Foliage density (m^2 leaf m^{-3} canopy)
ρ_s	Particle density (Mg m^{-3})
ρ_w	Density of water (1000 kg m^{-3})
τ	Fractional transmission of radiation
τ_d	Daily diffuse transmission coefficient
ϕ	Azimuth angle
Φ	Matric flux potential (kg m^{-1} s^{-1})
ψ	Solar zenith angle (º)
Ψ	Soil water potential (J kg^{-1})
Ψ_e	Air entry potential (J kg^{-1})
Ψ_{fc}	Soil matric potential at field capacity (J kg^{-1})
Ψ_{lm}	Leaf water potential at maximum transpiration, generally occurring in the early afternoon hours (J kg^{-1})
Ψ_m	Soil matric potential (J kg^{-1})
Ψ_{pwp}	Soil matric potential at permanent wilting point (J kg^{-1})

ABSTRACT

Objective of Research

The interest in crop modelling started since the introduction and popularisation of computer technology, which facilitated the dynamic simulation of complex natural systems. In particular, crop growth and soil water balance models for irrigation scheduling are popular at locations where water is a limiting factor for crop production.

In a Water Research Commission project, the soil water balance model (SWB) for irrigation scheduling under full and deficit irrigation was made available. The SWB model is a relatively simple generic crop growth model based on sound physical and physiological principles, (i.e. mechanistic) using daily climatic inputs for daily time-step calculations of the soil-plant-atmosphere water balance to estimate plant growth water use. The SWB model was primarily developed for predicting real-time soil water deficit of field crops with a one-dimensional canopy light interception and water redistribution procedure.

Hedgerow tree crops are planted in widely spaced rows to allow access between trees to carry out necessary management practices (e.g. pest control and harvesting). Distribution of energy is not uniform in widely spaced crops. In addition, localised under tree irrigation is often used for tree crops to reduce system installation costs. This irrigation (micro- or drip) only wets a limited area under the canopy of the trees so that evaporation from the soil surface is also not uniform. One can expect root density to vary with depth as well as with distance between the rows so water uptake for transpiration will also vary in two dimensions. It is also essential to take into account the limited volume of soil wetted under micro-irrigation. If this is not done, the soil capacity will be incorrectly estimated with a standard one-dimensional approach, leading to undesirable over-irrigation in the wetted zone, as well as possible crop stress resulting from a too long an irrigation interval. In order to accurately estimate canopy growth, water balance and yield, it is therefore essential to model canopy radiant interception and soil water balance of hedgerow tree crops in two dimensions and on an hourly time step, based on sound physical principles.

Lack of suitable user-friendly tools to mechanistically describe the two-dimensional energy and soil water balance of tree crops was identified. Due to the importance of fruit crops, on the export as well as local markets, as well as the encouraging results from the initial SWB model, it was decided to improve the SWB model by incorporating a two-dimensional system for use in hedgerow plantings. This thesis reports on the methodology developed to monitor the energy and soil moisture differences within various hedgerows through 24 hour cycles

and the results obtained, as well as the subsequent use of the results to evaluate the 2-dimensional water balance model.

This research was an integral, but independent, part of a larger research thrust, i.e. the development of a two-dimensional fruit tree water balance model that can account for the unique fractional interception of solar radiation associated with hedgerow orchards as opposed to the horizontal planar interception encountered in agronomic crops. The primary objective of this thesis is not the actual programming and mathematical manipulations of the relevant algorithms but to create a reliable data base and then evaluate the model. The primary objective of this thesis was to evaluate the model for deciduous fruit trees using peaches as an example and evaluate the model for evergreen fruit trees using citrus as an example.

Model description

In the overall research thrust two types of model, both predicting crop water requirements on a daily time step, were developed for hedgerow tree crops and included in SWB:

i) A mechanistic two-dimensional energy interception and finite difference, Richards' equation based soil water balance model; and

ii) An FAO-based crop factor model, with a quasi-2D cascading soil water balance model.

For the sake of clarity and completeness, the principles of the models are presented in the thesis and are briefly described in this subsection.

The first model calculates the two-dimensional energy interception for hedgerow fruit trees, based on solar and row orientation, tree size and shape, as well as leaf area density. The two-dimensional soil water redistribution is calculated with a finite difference solution. The two-dimensional energy interception model assumes leaves to be uniformly distributed within an ellipsoid truncated at its base, and radiation penetrating the canopy is attenuated according to Beer's law. This geometry is very versatile as many different shapes can be generated. In order to determine the spatial distribution of soil irradiance across the tree row, the canopy path length through which the radiation must travel to reach a certain point on the soil surface is calculated. Radiation can penetrate neighbouring rows, so two rows on either side of the simulated row are considered.

Beam or direct radiation and diffuse radiation for the PAR (photosynthetically active radiation) and NIR (near-infrared radiation) wavebands are calculated separately, as they interact differently with the canopy. The ratio of actual measured to potential radiation is used to estimate the proportion of direct and diffuse radiation in these two spectral bands.

The attenuation of beam radiation by the canopy is strongly dependent on zenith angle, and, for crops planted in rows, azimuth angle and row orientation will also be crucial. Elevation and azimuth angles are calculated from latitude, solar declination that depends on day of year, and time of day. Before the length of canopy through which radiation penetrates can be calculated, azimuth angle needs to be adjusted to take row orientation into account.

Input data required to run the two-dimensional canopy interception model are: day of year (DOY), latitude, standard meridian, longitude, daily solar radiation, row width and orientation, canopy height and width, bare stem height and distance from the ground to the bottom of the canopy, extinction coefficient, absorptivity and leaf area density.

In order to simulate two-dimensional water movement in the soil, a grid of nodes were established. This divides the soil up into a number of elements. The distances between nodes are selected so that model output can easily be compared to field measured values. Each element has its own physical properties, so this scheme allows variation in soil properties in two dimensions. Symmetry planes are assumed to occur mid-way between two rows on either side of the hedgerow and no water flux is allowed across these planes. The model redistributes water in the soil in two-dimensions using a finite difference solution to Richards' continuity equation for water flow. The aim is to find the matric potentials, which will cause the mass balance error to be negligible. This is done using the Newton-Raphson procedure. Two lower boundary conditions can be chosen in the model: i) gravity drainage for well-drained soils, and ii) zero-flux lower boundary to simulate an impermeable layer.

A precipitation or irrigation in mm is converted to a flux in kg m^{-1} s^{-1} by dividing the time step and multiplying by the horizontal distance over which the water is distributed. The infiltration does not have to be uniform over the surface. Non-uniform infiltration is especially important in very coarse soils where lateral redistribution is likely to be limited, or in the case of micro-irrigation. As with the infiltration flux, evaporation is multiplied by the horizontal distance over which it occurs in order to get an evaporative flux in kg m^{-1} s^{-1}. Potential evapotranspiration (PET) is calculated from weather data using the Penman-Monteith equation and the maximum crop factor after rainfall occurs. PET is then partitioned at the soil surface into potential evaporation and potential transpiration depending on solar orientation, row direction and canopy size, shape and leaf area density. Crop water uptake (transpiration) can either be limited by atmospheric demand or soil-root water supply. Root densities at different soil depths are accounted for in the calculation of root water uptake. The user can specify root depth and the fraction of roots in the wetted volume of soil.

Required inputs for the two-dimensional soil water balance model are: starting and planting dates, altitude, rainfall and irrigation water amounts, as well as maximum and minimum daily

temperature. Two points on the water retention function (usually field capacity and permanent wilting point), initial volumetric soil water content and bulk density are required for each soil layer. Soil saturated hydraulic conductivity can also be entered as input for each soil layer, or calculated by the model using the water retention curve. Row distance, wetted diameter of micro-jets or drippers, fraction of roots in the wetted volume of soil as well as distance of the nodes from the tree row are also required as input.

The second, simpler model, based on the FAO crop factor approach, was developed to enable users to predict crop water requirements with limited input data. This model includes a semi-empirical approach for partitioning of aboveground energy, a cascading soil water redistribution that separates the wetted and non-wetted portion of the ground, as well as prediction of crop yields. The FAO-based crop factor procedure was combined with the mechanistic SWB model, thereby still allowing evaporation and transpiration to be modelled separately as supply and demand limited processes. The crop factor model does not grow the canopy mechanistically and therefore the effect of water stress on canopy size is not simulated. The simpler crop factor model should, however, still perform satisfactorily if the estimated canopy cover closely resembles that found in the field.

The following input parameters are required to run the FAO-type crop factor model: planting date, latitude, altitude, maximum and minimum daily air temperatures, FAO crop factors and duration of crop stages. The input data required to run the two-dimensional cascading model are rainfall and irrigation amounts, volumetric soil water content at field capacity and permanent wilting point, as well as initial volumetric soil water content for each soil layer. Row spacing, wetted diameter, distance between micro-irrigators or drippers and the fraction of roots in the wetted volume of soil are also required. Required input data for yield prediction with the FAO model are FAO stress factors for growing stages and potential yield.

Field Trial

Evaluation of the model was carried out for a wide range of conditions (row orientation, period of the year and canopy density). For this purpose, two field trials were set up. The first trial was established in a peach (*Prunus persica* cv Transvaalia) orchard on the lysimeter facilities at Hatfield (Pretoria University experimental farm). This provided a site where detailed observations could be easily recorded to evaluate the SWB model for deciduous trees. The second trial was established in a citrus clementine (*Citrus reticulata* cv. *Nules Clementine*) orchard at the Syferkuil experimental farm of the University of the North. This was the site where measured data were collected to evaluate the SWB model for evergreen trees.

In both field trials, the following field measurements were carried out and used to evaluate the two-dimensional energy interception and soil water balance model:

i) Weather measurements (temperature and relative humidity, wind speed, solar radiation and rainfall).
ii) Soil texture, bulk density, penetrometer resistance.
iii) Volumetric soil water content with neutron water meter and time domain reflectometry (TDR).
iv) Soil matrix potential with heat dissipation sensors.
v) Root distribution by taking soil core samples and washing out roots to determine root length.
vi) Soil irradiance at different distances from the tree row with tube solarimeters.
v) Leaf area index and density with a LAI-2000 plant canopy analyser.
vi) Canopy size and row orientation.

In addition, load cell lysimeters were used in the peach orchard at Hatfield in order to measure crop water use.

An additional field trial was carried out at the Hatfield experimental station on Leuceaena (*Leucaena leucocephela*) trees in order to test the two-dimensional radiant interception model for different environmental conditions (tree size and shape as well as row orientation). For the same purpose, two other trials were carried out on two commercial orchards at Brits in Empress Mandarin (*Citrus reticulata* cv. *Empress*) and Delta Valencia (*Citrus sinensis* [L.] cv. Osbeck) orchards. In these field trials, weather data were recorded, soil irradiance across the row was measured with tube solarimeters, as well as leaf area index and density, canopy size and row orientation.

Results

The simple, quasi two-dimensional, cascading soil water balance model was calibrated using data from the peach trial at the Hatfield experimental station. In the process, FAO basal crop coefficients (*Kcb*) were determined for first and second leaf peach trees. The daily crop factor (*Kc*) was calculated using evapotranspiration measurements from the lysimeters and the grass reference evapotranspiration calculated from weather data. The *Kcb* values for the various growth stages were determined by fitting an appropriate line through the lower values of *Kc*, which were taken to reflect the condition where the soil surface was dry (negligible evaporation), subsoil drainage was negligible and there was sufficient water not to restrict transpiration. There was good agreement between predicted and measured daily soil water deficit for water stressed and non-stressed treatments. This was expected since the calibration data came from the trial.

Field measurements in Hatfield also indicated that in hedgerow plantings the whole area across the row must be borne in mind when assessing soil water content. The practice of using single or restricted locality measurements, as utilised in agronomic crops, can be misleading in orchards. The reason for this is the effect of the irrigation distribution and rain interception by the canopy, the variation in radiation interception by the canopy across the row, the irradiance reaching the soil surface as the season progresses, the presence of a grass sod or bare soil in the inter-row region and the root density across the row. In both field trials at Hatfield and Syferkuil, it was found that there are significant amounts of roots in the inter-row region and thus this portion of the rooting volume must not be disregarded when assessing the water balance.

The two-dimensional energy interception and soil evaporation components were evaluated separately. The crucial interactions between the model components were integrated in the validation of the two-dimensional soil water balance model, which uses the energy interception and soil evaporation sub-models to split evaporation and transpiration.

The radiant interception model predictions and the tube solarimeter measured soil irradiance generally gave very good agreement at different distances from the tree row and in different orchards. However, some discrepancies between measurements and model predictions occurred. This was attributed to the presence of trunks and branches shading the tube solarimeters at low leaf area densities, irregularities in the shape of the hedgerow, and non-uniform distribution of leaves within the canopy. In one case the canopy shape differed drastically from that used in the model.

The output obtained with the two-dimensional soil water balance model was compared to independent field measurements in order to evaluate the full SWB two-dimensional model. Volumetric soil water content data collected with the TDR system in the peach and citrus orchards were compared to SWB simulations. Results of model simulations done during drying cycles showed that the surface layer predictions were generally very good. However, in certain situations discrepancies between measurements and simulations were observed, in particular, for deeper soil layers. This could have been due to spatial variability of soil properties, as well as soil disturbance during the installation of TDR probes. It is clear that TDR probes can be used in irrigation scheduling to determine crop water use over certain periods. Caution should, however, be exercised in the interpretation of absolute values of volumetric soil water content obtained from the probes.

Scenario modelling and sensitivity analyses were carried out by varying some input parameters and observing variations in certain output variables. The aim was to show an application of this tool to identify the most suitable management practice in order to

maximise water use efficiency. Two case studies were considered for two “virtual” orchards located at different latitudes and in different climates (Kakamas in the Northern Cape and Stellenbosch in the Western Cape). The results of the scenario simulations indicated that, based on the inputs used, the orchards should be planted in a N-S row orientation, a wetted diameter of 0.5 m should be applied when the canopy width is 2 m, in order to minimise water losses through evaporation. As the canopy width increased to 3 m, so the wetted diameter should be increased to 1.5 m. If the wetted diameter is too small, transpiration and thus yield will be reduced.

A sensitivity analysis was also carried out for both case studies varying the fraction of roots in the wetted volume of soil, and observing variations in the output results of evaporation and transpiration. The contribution to crop water uptake from the inter-row volume of soil can be high, in particular under high atmospheric evaporative demand, and this needs to be accounted for in irrigation management in order to maximise rainfall use efficiency in areas of higher summer rainfall.

Conclusions and recommendations

The methodologies developed to measure the temporal and spatial variation in solar radiation and thus the energy distribution within Hedgerow orchards worked well. The methods used to measure the temporal and spatiial variation of the soil water balance also worked well. Thus a very good data set was generated that enabled the sound evaluation of the 2-D SWB model. Thus one can conclude that the two-dimensional energy interception and soil water balance model that was developed in the overall research thrust and included in the Soil Water Balance irrigation scheduling model worked well. The simpler model, based on the FAO crop factor approach and a cascading soil water balance, that was also developed to enable users to predict crop water requirements with a limited set of input data, also gave very satisfactory results.

The FAO-based model and the cascading soil water balance were calibrated for first leaf and second leaf peaches at Hatfield.

The two-dimensional model was fully evaluated for deciduous orchards using data obtained in field trials on peaches and Leucaena (Hatfield). For model validation in evergreen citrus orchards, data obtained in field trials set up at the Syferkuil experimental station (University of the North) and on two commercial farms in Brits were used.

Irregular trunks and branches could cause inaccuracies in predictions of the energy balance. At low leaf area densities, the shade from trunks and branches is not accounted for in the

SWB model. The relative importance of non-symmetric canopy shape as opposed to non-uniform leaf distribution did have an effect but indications where that this was not critical.

The major difficulties encountered in the evaluation of the soil water balance were due to spatial variability of soil properties and disturbance of the soil when the water status monitoring sensors were installed. Careful installation is therefore recommended when using sensors that give localised measurements like those used in this study (heat dissipation sensors and TDR probes).

The successful evaluation of the two-dimensional energy interception and soil water balance model opens the opportunity to develop a useful yield predictor and productivity efficiency measure if one knows the canopy to fruit ratio. This information could also be useful for fruit colour and internal quality research.

As demonstrated with data from the peach trial at Hatfield, soil or cover crops between rows can also have a large effect on the efficient use of rainfall, and this could be further investigated.

The biggest contribution of this model is likely to be the quantification of the contribution that rainfall can make to crop water use by taking the non-irrigated inter-row soil reservoir into account. It is recommended to accurately estimate the root fraction in the wetted and non-wetted volume of soil by digging a trench across the row, taking core soil samples and determining root densities.

The two-dimensional energy interception and finite difference soil water balance model is expected to be more accurate than the cascading soil water balance, due to the sound physical principles on which it is based. The mechanistic detailed approach could give guidance with respect to the magnitude of errors made by using simpler, more empirical approaches. However, the two-dimensional model will also require more input parameters compared to the simpler cascading model. In particular, the most difficult parameters to determine will be the leaf area density for the radiation energy interception part due to the cost of the instrumentation, and the hydraulic conductivity for the soil part due to the specialised knowledge and scientific equipment required. On the other hand, the cascading model requires calibrated FAO crop factors in order to reasonably partition evaporation and transpiration. It would be interesting to compare the cascading and the two-dimensional soil water balance models against field measurements in order to determine the level of accuracy in predictions.

The two-dimensional energy and soil water balance model is primarily meant to be a real-time, irrigation scheduling tool for commercial orchards. Results from this study should guide

irrigation scheduling consultants, extension officers and farmers to more efficiently use scarce water resources on high value tree crops. The two-dimensional model, however, can also be used for planning purposes as demonstrated in the scenario simulations. The mechanistic canopy radiation interception routine which has been shown to be very accurate will make it possible to evaluate the effect of row orientation and spacing as well as the effect of wetted diameter and pruning practices on water use

This model also holds tremendous potential as a teaching aid to allow students to do "*what-if ?*" scenario analyses and thus study cause and effect interactions of various orchard designs and practices.

INTRODUCTION

Problem

The interest in crop modelling started after the introduction and popularisation of computer technology, which facilitated the dynamic simulation of complex natural systems (Sinclair and Seligman, 1996). Several crop models are described in the Agronomy Monograph No. 31 (Hanks and Ritchie, 1991). Advantages and disadvantages, as well as research needs, were discussed in this publication. Crop models have been developed with different levels of complexity depending on the specific requirements (Whisler *et al*., 1986). The most common applications are in irrigation management and planning, fertilisation and herbicide recommendations, pollution prevention, soil erosion impact and control, pests and disease forecasting, as well as yield prediction and risk management. In particular, crop growth and soil water balance models for irrigation scheduling are popular at locations where water is a limiting factor for crop production (Bennie *et al*., 1988; Smith, 1992a; Crosby, 1996; Annandale *et al*., 2000). For irrigation scheduling purposes, models should simulate growth and development of the crop well. Several mechanistic irrigation scheduling models are available (Campbell and Stockle, 1993; Singels and de Jager, 1991a, b and c; Hodges and Ritchie, 1991). Mechanistic crop growth models require, however, specific crop growth input parameters (Jovanovic and Annandale, 1999), which are not readily available, in particular this is true for trees.

In simulating crop growth and the field soil water balance, many models use canopy radiant interception for two purposes: a) to determine the photosynthetic rate and dry matter production from the amount of energy intercepted by the crop canopy (Monteith, 1977), and b) to estimate soil water evaporation and crop transpiration from the amount of energy available for these two processes (Ritchie, 1972). Canopy radiant interception represents the fraction of solar radiation available to the crops. In the horizontal planar interception encountered in agronomic, vegetable and pasture crops, which cover the whole surface area uniformly, this can be quantified in one dimension as the fraction of ground covered by the canopy, often referred to as “canopy cover”.

Tree hedgerow crops are planted in widely spaced rows to allow access between trees to carry out necessary management practices (e.g. pest control and harvesting). Distribution of energy is not uniform in widely spaced crops. The one-dimensional assumption could therefore lead to serious inaccuracies caused by adjacent row shading, which depends on solar and row orientation, tree size and shape, as well as slope and land aspect. The

amount and spatial distribution of intercepted solar radiation will influence evaporation and transpiration, which must be quantified.

In addition, localised irrigation is often used for tree crops to reduce system installation costs. Localised irrigation (micro- or drip) used in orchards only wets a limited area under the canopy of the trees so evaporation from the surface is not spatially uniform. This must be taken into account in modelling the water balance by simulating shading of the wetted portion of the ground. The lack of radiant energy in the shaded portion of the row may limit evaporation, whilst dry soil may limit the process between the rows. Interception of rain by trees is also channelled down the stem and drips from the edge of the canopy, so rain is also not evenly distributed at the surface. Root density varies with depth and with distance between the rows so water uptake for transpiration will also vary in two dimensions. It is important to quantify water uptake between rows in order to estimate the effectiveness of rain and the competition for water from cover crops or weeds growing between rows. It is also essential to take into account the limited volume of soil wetted under micro-irrigation or its capacity will easily be exceeded with a standard one-dimensional approach, leading to undesirable over irrigation in the wetted zone, and possibly crop stress due to too long an irrigation interval.

In order to accurately estimate canopy growth, water balance and yield, it is therefore essential to model canopy radiant interception and soil water balance of hedgerow tree crops in two dimensions, based on sound physical principles and taking cognisance of the changes that occur during the day as a result of the movement of the sun.

Background

Campbell and Diaz (1988) published a simple soil water balance model to predict crop water use. Two outstanding features of this model were:

i) Keeping the model simple with minimal soil, plant, and atmospheric data requirements; and
ii) Developing the model on sound physical and physiological principles (referred to as mechanistic) as opposed to an empirical approach.

Annandale *et al.* (2000) tested the model on green peas. Based on the results, it was decided to:

i) Further develop the program's user friendliness and practicality; and
ii) Determine the necessary crop parameters for other irrigated crops in South Africa.

This materialised in the development of a simple, but mechanistic, generic crop growth and soil water balance model (SWB) for irrigation scheduling under full and deficit irrigation (Annandale *et al*., 1999). The SWB model was mainly developed for predicting real-time soil water deficit of field crops with a one-dimensional canopy radiation interception and water redistribution procedure.

There is a lack of suitable tools to mechanistically describe the energy and soil water balance of tree crops. Due to the importance of fruit crops, on the export as well as local markets, it was decided to improve the SWB model by incorporating a two-dimensional system for use in hedgerow plantings. This was done by Annandale et.al (2002). To evaluate this model, it was necessary to develop the appropriate measurement techniques that could be used in hedgerow orchards, and to generate a database of reliable data for the evaluation of the model.

Objectives

The objectives of this study were:

i) To develop techniques to measure and record the components of the energy and soil water balances within the unique situation associated with hedgerow orchards.
ii) To verify the model for deciduous fruit trees using peaches as an example.
iii) To verify the model for evergreen fruit trees using citrus as an example.

Approach

An extensive literature search was carried out on two-dimensional energy and water balance models. In this thesis, no separate chapter on literature review is included. References are, however, presented in the various Sections as applicable.

The two-dimensional energy and soil water balance model was developed by Prof Annlandale in consultation with Prof Gaylon Campbell during a visit by Prof Annandale to Washington State University (Annandale *et al*., 2002). Verification of the model comprised the inspection of the internal consistency of the model and its software implementation (CAMASE, 1995).

According to the guidelines of CAMASE (1995), the usefulness and relevance of a model needs to be established for the specific purpose for which it was developed. Also, evaluation should be representative of the situations in which the model is to be used. Evaluation of the model presented in this study was therefore carried out for a wide range of conditions (row

orientation, period of the year and canopy density), and for both deciduous and evergreen tree crops.

For this purpose, two field trials were set up. The first trial was established in a peach orchard on the lysimeter facilities at Pretoria University's experimental farm in Hatfield. This provided a site where detailed observations could easily be recorded to evaluate the SWB model for deciduous trees. The second trial was established in a citrus orchard at the Syferkuil experimental farm of the University of the North. This was the site where measured data were collected to evaluate the SWB model for evergreen trees. During the course of the study and for the purpose of evaluating the energy interception model for different conditions (tree size and shape, row orientation etc.), contact was made with private farming enterprises and two field trials were carried out in Brits. Light Leucaena fodder trees on the Hatfield experimental farm.

CAMASE (1995) also suggested that, if the subject of the model is too large for regular evaluation, the model is to be divided into sub-models that are separately evaluated. For this reason, the two-dimensional energy interception and soil evaporation components were evaluated separately. The crucial interactions between the model components were integrated in the evaluation of the two-dimensional soil water balance model, which uses the energy interception and soil evaporation sub-models to split evaporation and transpiration.

This thesis firstly presents the theoretical description of the two-dimensional energy interception and soil water balance model for hedgerow fruit trees, as developed by Annandale *et al*. (2002) (Chapter 2). A simple, quasi two-dimensional cascading soil water balance model based on the FAO crop factor approach is also presented.

Chapter 2 describes material and methods of the field trials used to evaluate the model. Chapter 3 presents the evaluation of the two-dimensional energy interception and soil water balance model for deciduous and evergreen fruit trees (objectives ii) and iii)), as well as the calibration of the simple FAO-based cascading model for peaches, including the most relevant field observations.

Scenario simulations were then carried out to perform logical sensitivity analyses. According to the definition of CAMASE (1995), logical sensitivity analysis is the effort to establish by inspection of results whether the model is sensitive to changes in input.

CHAPTER 1

MODEL DESCRIPTION

Two types of model were developed for hedgerow tree crops during the course of the Water Research Commission's project on the Soil Water Balance and included in SWB model:

i) A two-dimensional energy interception and finite difference soil water balance model; and

ii) An FAO-based crop factor model, with a quasi 2-D soil water balance.

The first model calculates the two-dimensional energy interception for hedgerow fruit trees, based on solar and row orientation, tree size and shape, as well as leaf area density. A two-dimensional soil water redistribution is also calculated with a finite difference solution. This model is based on sound physical principles, but it requires certain input parameters that are not always easy to obtain (e.g. leaf area density and soil saturated hydraulic conductivities).

A second simpler model, based on the FAO crop factor approach, was therefore developed to enable users to predict crop water requirements with limited input data. This model includes a semi-empirical approach for partitioning above-ground energy, a cascading soil water redistribution that separates the wetted and non-wetted portion of the ground, as well as prediction of crop yields according to the CROPWAT model developed by the FAO (Smith, 1992a).

Due to the large size of the SWB two-dimensional model, the code for each subroutine was written in separate files or procedures. The model interface was also developed so as to subdivide the model into components. This facilitated the evaluation of the various components of the model separately and also improved the user-friendliness during the technology transfer phase of the research program.

The SWB model is written in Delphi v. 5.0 (Inprise Corp.), and is available for use with Windows 95 on an IBM-PC or compatible computer. The minimum requirement is 16 Mb RAM and a CD-ROM drive.

In this chapter of the thesis, the theoretical description is presented for both models.

1.1 Two-dimensional water balance and energy interception model for hedgerow fruit trees (SWB-2D)

1.1.1 Two dimensional energy interception model

The radiation interception model described here is based on the work of Charles-Edwards and Thornley (1973) and Charles-Edwards and Thorpe (1976). The model assumes leaves to be uniformly distributed within an ellipsoid, and radiation penetrating the canopy is attenuated according to Beer's law. Fractional transmission of radiation (τ) through a canopy can be described as follows:

$$\tau = e^{-kl} \qquad (1.1.1)$$

where *k* is the extinction coefficient which represents the horizontal projection of leaves relative to one sided leaf area as defined by Campbell and Norman (1998), and *l* is the leaf area index. The transmission of radiation to a certain point on the ground will clearly depend on the distance (*s*) within the canopy through which the beam travels. Norman and Welles (1983) showed that:

$$\rho_f s = \frac{l}{\cos\Psi} \qquad (1.1.2)$$

where ρ_f is foliage density (m^2 leaf m^{-3} canopy), *s* in metres is the path length of radiation through the canopy, and ψ is the solar zenith angle. Campbell and Norman (1998) derived the extinction coefficient for leaves with a spherical leaf angle distribution, which is a good approximation for most canopies:

$$k = \frac{1}{2\cos\Psi} \qquad (1.1.3)$$

The transmissivity calculated in Eq. (1.1.1) now becomes:

$$\tau = e^{(-0.5\rho_f s\sqrt{\alpha})} \qquad (1.1.4)$$

where the absorptivity of leaves for solar radiation (α) equals 0.5, and this term takes radiation scattering (transmission and reflection) within the canopy into account. The same Eq. (1.1.4) can be used for photosynthetically active radiation (PAR, 0.4-0.7 μm) by setting α to 0.8 and to 0.2 for the near infrared range (NIR, 0.7-3 μm).

In order, therefore, to determine the spatial distribution of soil irradiance, the canopy path length through which the radiation must travel to reach a certain point on the soil surface

must be calculated. A method to calculate this path length, based on Charles-Edwards and Thornley (1973), describes an ellipsoidal tree canopy surface as follows:

$$\frac{x^2}{a^2}+\frac{y^2}{b^2}+\frac{z^2}{c^2}=1 \qquad (1.1.5)$$

where x, y and z are the Cartesian co-ordinate axes, and a is half the width, b half the depth and c half the height of the tree canopy. An ellipsoid is very versatile as many different shapes can be generated by adjusting a, b and c. For a hedgerow canopy however, the dimension b can be made very large so the y^2/b^2 term tends to zero and can therefore be neglected. Also, in order to lift the ellipsoid above the ground surface the vertical axis needs to be offset and Eq. (1.1.5) becomes:

$$\frac{x^2}{a^2}+\frac{(z-z_o)^2}{c^2}=1 \qquad (1.1.6)$$

with z_o the distance between the soil surface and the centre of the canopy. This is illustrated in Figure 1.1.

In order to determine the diffuse transmission coefficient, s needs to be evaluated for all azimuth (ϕ) and elevation angles (θ) . If Q (x_q, y_q, z_q) denotes the position where the ray penetrates the canopy, and P (x_p, y_p, z_p) the point where the ray is intercepted on the soil surface, then:

$$\frac{x_q-x_p}{\sin\theta\cos\phi}=\frac{z_q}{\cos\theta} \qquad (1.1.7)$$

If N (x_n, y_n, z_n) denotes the lower surface of the canopy where the ray exits, then the path length s through which the beam travels and along which it can be attenuated is given by:

$$s=\frac{z_q-z_n}{\cos\theta} \qquad (1.1.8)$$

This is schematically presented in Figure 1.2. z_q and z_n can be determined by rearranging Eq. (1.1.7) to give an expression for x_q which can be used to eliminate this term by substitution in Eq. (1.1.6). This results in a quadratic equation in z_q of the form:

$$uz_q^2+vz_q+w=0 \qquad (1.1.9)$$

where the coefficients are:

$$u = c^2 \sin^2\theta\cos^2\phi + a^2\cos^2\theta \qquad (1.1.10)$$

$$v = 2\left[c^2 \sin\theta\cos\theta\cos\phi x_p - a^2\cos^2\theta z_o\right] \qquad (1.1.11)$$

$$w = c^2\cos^2\theta\left[xp^2 + a^2(z_o^2/c^2 - 1)\right] \qquad (1.1.12)$$

If a ray from a particular direction penetrates a row, the height of entry into the canopy z_q and that at which it exits the canopy z_n are given by the roots r_1 and r_2 ($r_1 \geq r_2$) of Eq. (1.1.9). If the ray misses the canopy the roots will be imaginary.

The model also makes provision for elliptical shapes with the base cut off. If the base of the canopy is cut off at a height z_b, an additional condition is added to describe the canopy shape:

$$z \geq z_b \qquad (1.1.13)$$

Three cases can then be distinguished:

- Case 1: $r_1 \geq z_b$ and $r_2 \geq z_b$. Both roots belong to the canopy: $z_q = r_1$ and $z_n = r_2$
- Case 2: $r_1 \geq z_b$ and $r_2 < z_b$. Root r_1 belongs to the surface of the canopy but r_2 is below the cut base: $z_q = r_1$, $z_n = z_b$
- Case 3: $r_1 < z_b$ (and therefore $r_2 < z_b$). The ray misses the canopy.

Radiation can penetrate neighbouring rows, so more than one row needs to be considered. In this model, two rows on either side of the simulated row were considered (Charles-Edwards and Thorpe, 1976). Eq. (1.1.6) then becomes:

$$\frac{(x - nh)^2}{a^2} + \frac{(z - z_o)^2}{c^2} = 1 \qquad (1.1.14)$$

with n the row number from 0 to 4, and h the row spacing. This is illustrated in Figure 1.3, and the soil surface over which radiant transmittance is calculated is also shown. If a ray penetrates more than one row then *s* will be the sum of the individual path lengths through each canopy.

It is essential that beam or direct radiation and diffuse radiation be treated separately, as they will interact differently with the canopy. Weiss and Norman (1985) gave an example for a canopy with a leaf area index (LAI) of 2 that would typically have a diffuse transmittance of 0.25 but direct beam transmittance could vary from near zero to 0.4 depending on solar zenith angle. A daily diffuse transmission coefficient (τ_d) is calculated by determining the path lengths of radiation penetration through the canopy for all azimuth and zenith angles. τ_d

is therefore dependent only on tree size and canopy density. Diffuse and beam radiation is not usually measured separately so it is necessary to estimate the relative contributions of these two components from measured global radiation. The method of Weiss and Norman (1985) has been followed, where diffuse and direct beam radiation for the PAR and NIR wavebands are estimated from total incoming solar radiation. They developed relationships for potential values of direct and diffuse PAR and NIR from clear day experiments. The ratio of actual measured to potential measured radiation is then used to estimate the proportion of direct and diffuse radiation in these two spectral bands.

As illustrated earlier, the attenuation of beam radiation by the canopy is strongly dependent on zenith angle, and for crops planted in rows, azimuth angle and row orientation will also be crucial. Elevation and azimuth angles can be calculated from latitude, solar declination that depends on day of year, and time of day (Campbell and Norman, 1998). Before the length of canopy through which radiation penetrates can be calculated, azimuth angle needs to be adjusted to take row orientation into account. Azimuth angle is calculated in degrees clockwise from N, so E is 90^{o}, S is 180^{o} and W is 270^{o}. The X-axis must always be oriented perpendicular to the row direction for these simulations.

Input data required to run the two-dimensional canopy interception model are: latitude, standard meridian, longitude, daily solar radiation, row width and orientation, canopy height and width, stem height and distance to the bottom of the canopy, extinction coefficient, absorptivity and leaf area density. Extinction coefficient can be assumed to be 0.5 for leaves with a spherical leaf angle distribution. Absorptivity of leaves for total solar radiation can also be assumed to be 0.5. The most difficult input parameter to estimate is the leaf area density. During the course of this study, a method for the estimation of leaf area density was developed using the LAI-2000 plant canopy analyzer (Li-Cor, Lincoln, Nebraska).

A flow diagram of the two-dimensional energy interception model for hedgerow fruit trees is shown in Figure 1.4. The source code of the energy interception model written in Delphi can be obtained in Appendix A of Annandale *et al*. (2002).

1.1.2 Spatial distribution of soil evaporation

The model calculates the special distribution of evaporation at the soil surface in two steps:

i) Potential evaporation at each node (PE_j) is estimated by applying the Penman-Monteith equation (Allen *et al*., 1998), using radiation estimated locally as input.

ii) Evaporation from the soil surface at each node (E_j) is calculated as a function of potential evaporation , air humidity h_c, and humidity of the soil surface h_j (given by the two-dimensional model of soil water redistribution, explained in Sectiion 1.1.3), according to Campbell (1985):

$$E_j = PE_j \frac{(h_j - h_c)}{(1 - h_c)} \qquad (1.1.15)$$

where h_c and h_j are the canopy humidity and the humidity of the soil surface at node j respectively.

The surface humidity depends on the soil water potential Ψ_j (J kg^{-1}) at the surface and is calculated after Campbell (1977) as:

$$h_j = \exp\left(\frac{M\Psi}{RT}\right) \qquad (1.1.16)$$

with M the molar mass of water (0.018 kg mol^{-1}), R the gas constant (8.314 J K^{-1} mol^{-1}) and T the Kelvin temperature.

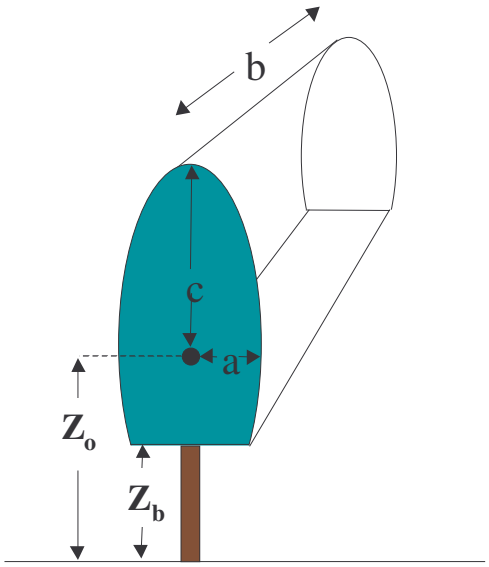

Figure 1.1. Three-dimensional scheme of a tree. c is half the height, a half the width and b half the depth of the canopy. z_o is the height from the ground to the centre of the canopy, and z_b the height of the base of the canopy.

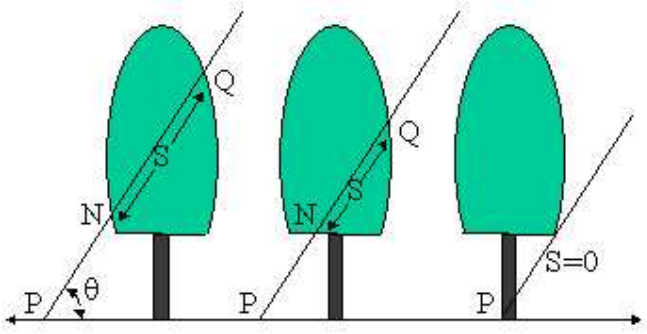

Figure 1.2. Schematic representation of a ray of sunlight passing through the tree canopy. S is the path length, θ is the elevation angle, Q is the position where the ray enters the canopy, N where it exits and P where it is intercepted on the soil surface. Three cases are shown: (1) both Q and N are on the ellipsoidal part of the canopy, (2) N is at the base of the canopy, (3) the ray of sunlight is not intercepted by the canopy.

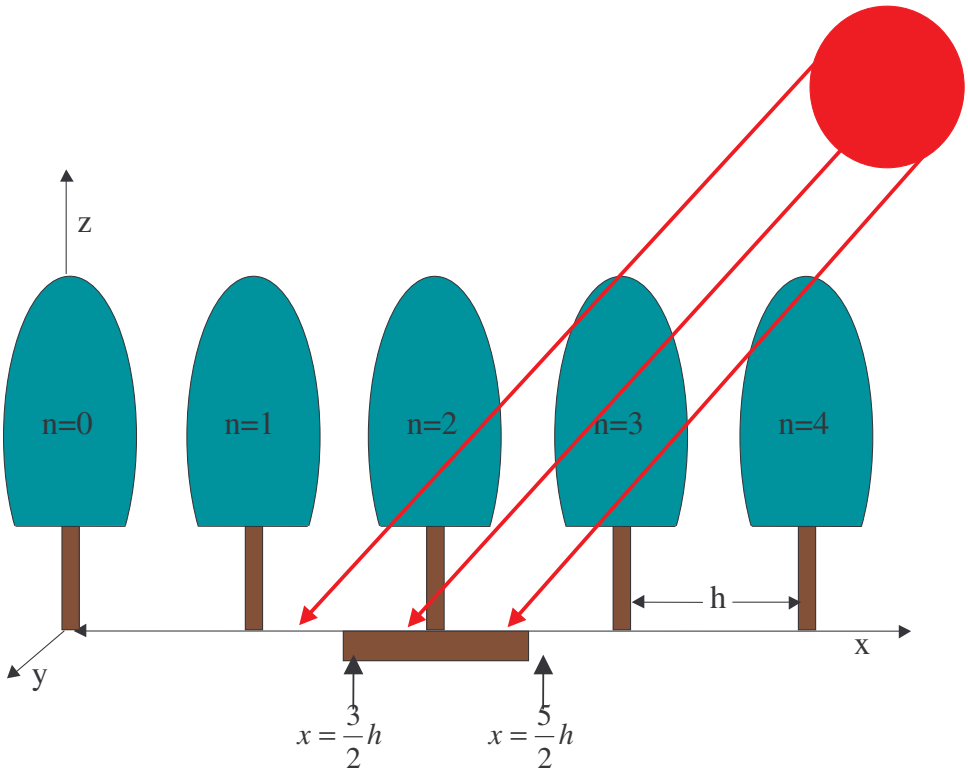

Figure 1.3. Schematic illustration of the system simulated; n is the tree row number, h is the row spacing, *x*, *y* and *z* the cartesian axes, and the soil surface over which radiant transmittance is estimated is between 3/2h and 5/2h.

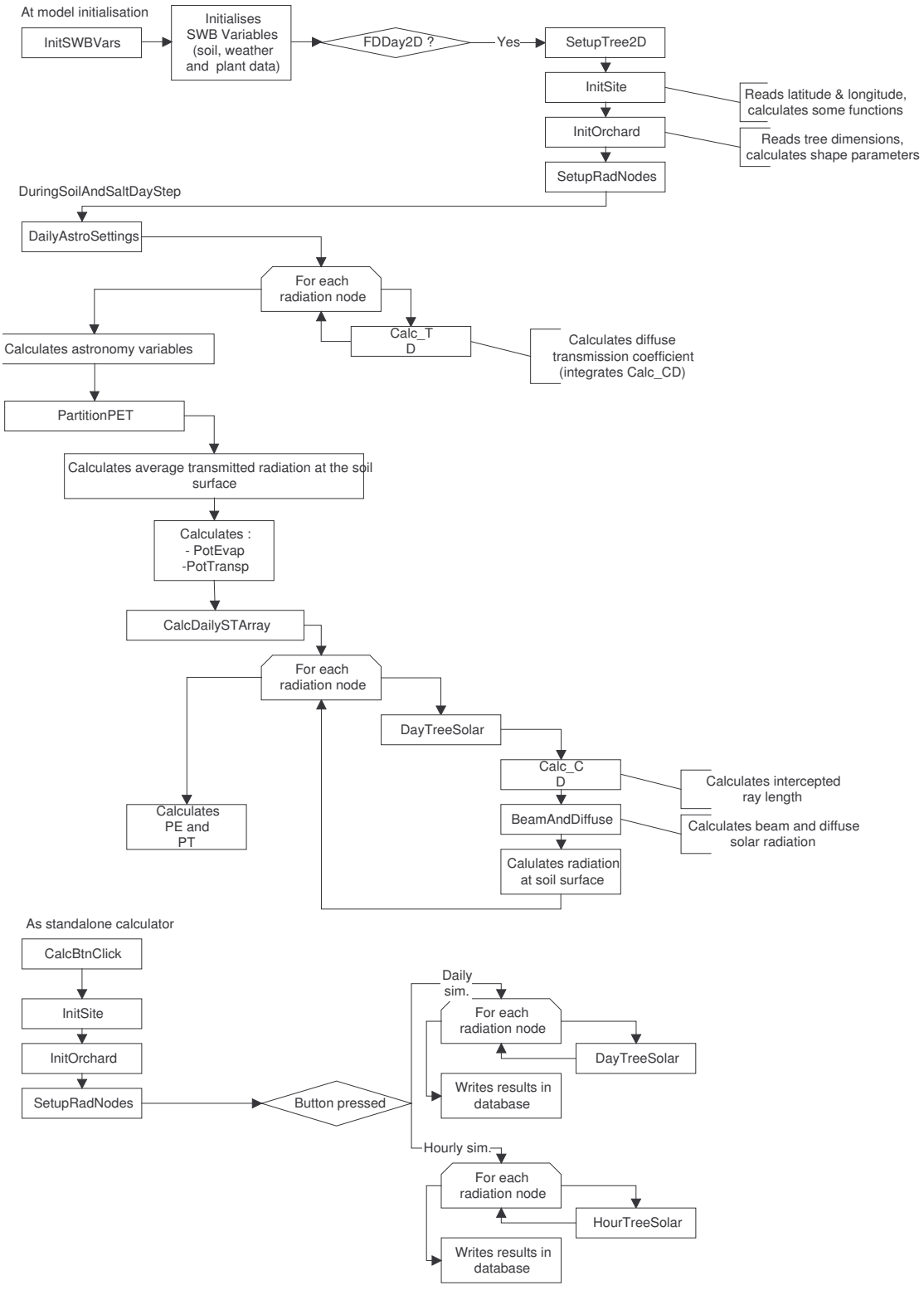

Figure 1.4. Flow diagram of the two-dimensional energy interception model for hedgerow fruit trees.

1.1.3 Two-dimensional finite difference soil water balance model

1.1.3.1. The soil profile

In order to simulate two-dimensional water movement in the soil, a grid of nodes had to be established. This nodal system is set up like the one in Campbell (1985) with i representing the vertical position of a node and j the horizontal position. This divides the soil into a number of elements. Each element is referenced by the node reference of the upper left corner of the element. This is illustrated in Figure 1.5.

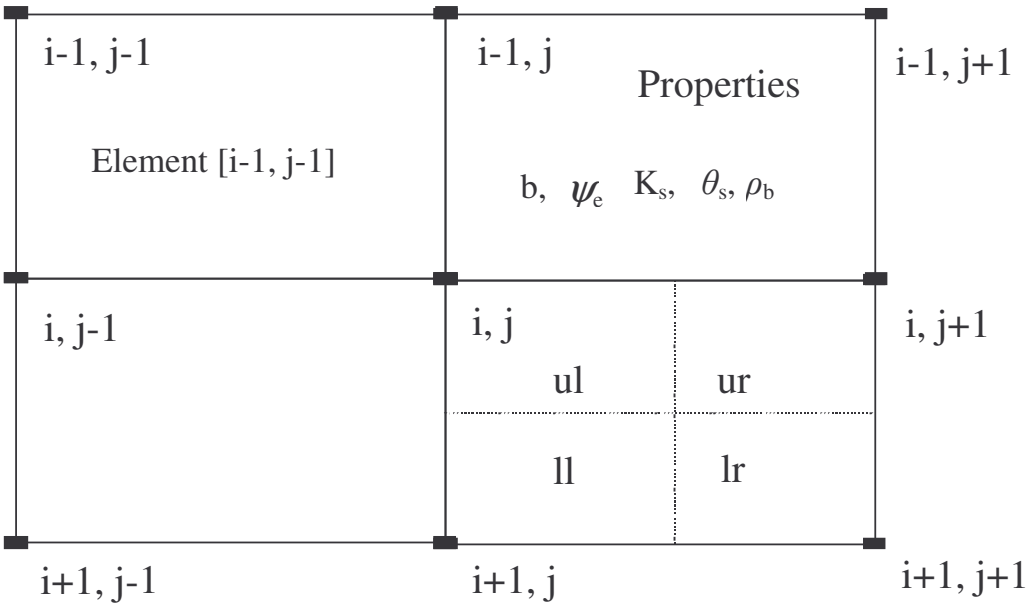

Figure 1.5. The two-dimensional nodal system. Element [i, j] has been divided into quarters: ul (upper left); ur (upper right); ll (lower left) and lr (lower right). Element [i-1, j] shows the soil properties which are fixed for a particular element: b is the slope of a log-log water retention function; Ψ_e the air entry potential; K_s the saturated hydraulic conductivity; ρ_b is bulk density and θ_s the saturated volumetric water content.

The distances between nodes are selected so that model output can easily be compared to field measured values. Each element has its own physical properties, so this scheme allows variation in soil properties in two dimensions. The properties referred to are bulk density (ρ_b), the Campbell 'b' value or slope of a log-log water retention function, the air entry potential (Ψ_e), saturated hydraulic conductivity (K_s) and the saturated water content (θ_s). A fixed set of properties for element [i –1, j] can be seen in Figure 2.5, as can the division of element [i, j]

into quarters labelled ul (upper left), ur (upper right), ll (lower left) and lr (lower right). The reason for this division will be explained in the next section.

The soil bulk density values to be used in this model will be based on field measurements. These values are used to estimate saturated volumetric water contents using Eq. (1.1.17):

$$\theta_s = 1 - \frac{\rho_b}{\rho_s} \qquad (1.1.17)$$

where ρ_s is particle density , assumed to be 2.65 Mg m^{-3}.

The Campbell '*b*' values and air entry potential, Ψ_e, can be determined from water release curves (Campbell, 1985).

$$b = \frac{\ln(\Psi_{pwp}/\Psi_{fc})}{\ln(\theta_{fc}/\theta_{pwp})} \qquad (1.1.18)$$

$$\Psi_e = \Psi_{fc}\left(\frac{\theta_{fc}}{\theta_s}\right)^b \qquad (1.1.19)$$

$$K_s = \frac{0.001}{\Psi_e^2} \qquad (1.1.20)$$

The soil matric potential at field capacity (Ψ_{fc}) and permanent wilting point (Ψ_{pwp}), as well as the volumetric soil water content at field capacity (θ_{fc}) and permanent wilting point (θ_{pwp}) are model inputs.

The complete grid system used in this model can be seen in Figure 1.6. The soil profile is enclosed by the heavy solid line and all nodes falling outside the profile are there merely to generalise the flux equations. Symmetry planes are assumed to occur mid way between two rows on either side of the hedgerow and no water flux is allowed across these planes. The distances between nodes should be selected so that model output can easily be compared to measured data.

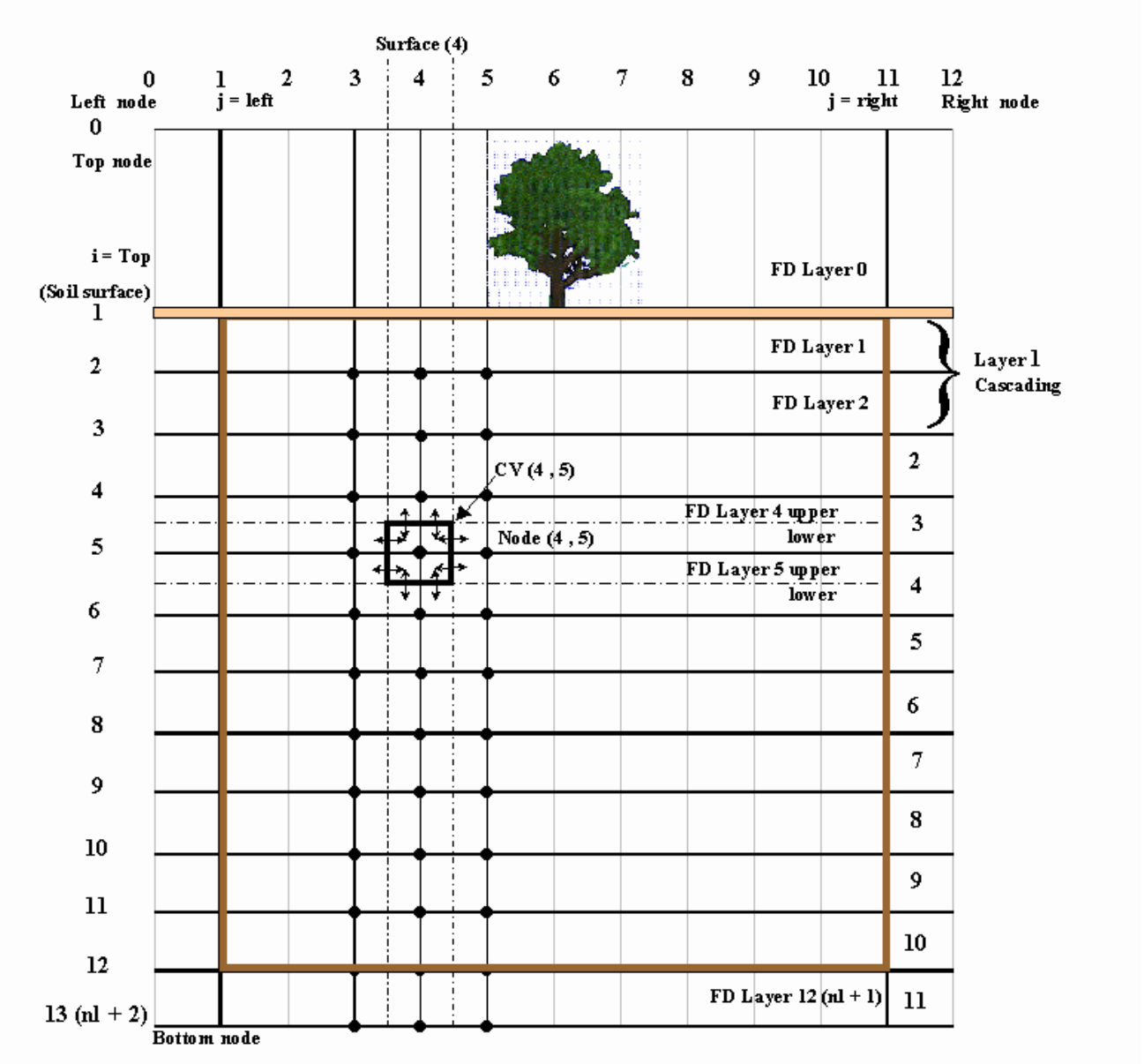

Figure 1.6. Nodal grid system showing symmetry planes and hedgerow. The soil layers for the cascading model are also represented.

1.1.3.2. Two-dimensional water flow

The model redistributes water in the soil in two-dimensions using a finite difference solution to Richards' continuity equation for water flow. The two-dimensional differential equation for water flow is:

$$\rho_w \frac{\partial \theta}{\partial t} = \frac{\partial}{\partial x}\left(k \frac{\partial \Psi}{\partial x}\right) + \frac{\partial}{\partial z}\left(k \frac{\partial \Psi}{\partial z}\right) - g \frac{\partial k}{\partial z} + S \qquad (1.1.21)$$

The left hand side of the equation represents the change in water storage with time, and for mass conservation this must equal the difference between the influx and outflux of water, plus any changes in storage due to a sink term. The density of water ρ_w is 1000 kg m^{-3}, θ is volumetric water content, and t is time in seconds. The horizontal coordinate x is parallel to the soil surface and perpendicular to the row direction (y), and z is the vertical coordinate. The hydraulic conductivity *K* (kg s m^{-3}), is a function of matric potential Ψ (J kg^{-1}) and is expressed by Campbell (1985) as

$$K = Ks\left(\frac{\Psi}{\Psi_e}\right)^{-n} \qquad \Psi < \Psi_e \qquad (1.1.22)$$

$$K = Ks \qquad \Psi \geq \Psi_e \qquad (1.1.23)$$

with *n* an empirical constant related to the slope of the water retention curve

$$n = 2 + \frac{3}{b} \qquad (1.1.24)$$

The flux of water due to gravity g (9.8 m s^{-2}) is taken into account in the term $-g(\delta K/\delta z)$. The sink-source term S includes evaporation, infiltration and crop water uptake. Some of the non-linearity of Eq (1.1.21) can be reduced by using the Kirchhoff transform which defines a new variable Φ, the matrix flux potential. Campbell (1985) defined this variable as

$$\Phi = \int_{-\infty}^{\Psi} K(\Psi) d\Psi \qquad (1.1.25)$$

Substituting Eqs. (1.1.22) or (1.1.23) and integrating gives

$$\Phi = \frac{K\Psi}{1-n} \qquad \Psi < \Psi_e \qquad (1.1.26)$$

$$\Phi = Ks\left(\frac{\Psi_e}{1-n} + \Psi - \Psi_e\right) \qquad \Psi \geq \Psi_e \qquad (1.1.27)$$

with Φ in kg m^{-1} s^{-1}.

The two-dimensional continuity equation expressed in terms of matric flux potential is

$$\rho_w \frac{\partial \theta}{\partial t} = \frac{\partial^2 \Phi}{\partial x^2} + \frac{\partial^2 \Phi}{\partial z^2} - g\frac{\partial k}{\partial z} + S \qquad (1.1.28)$$

In difference form

$$\frac{\rho_w\left(\theta_{i,j}^{t+\Delta t}-\theta_{i,j}^{t}\right)}{\Delta t}=\frac{\left(\frac{\Phi_{i,j+1}-\Phi_{i,j}}{x_{j+1}-x_j}-\frac{\Phi_{i,j}-\Phi_{i,j-1}}{x_j-x_{j-1}}\right)}{\left(\frac{x_{j+1}-x_{j-1}}{2}\right)}+\frac{\left(\frac{\Phi_{i+1,j}-\Phi_{i,j}}{z_{j+1}-z_i}-\frac{\Phi_{i,j}-\Phi_{i-1,j}}{z_i-z_{i-1}}-g\left(K_{i,j}-K_{i-1,j}\right)\right)}{\left(\frac{z_{i+1}-z_{i-1}}{2}\right)}+S \qquad (1.1.29)$$

The volumetric water contents at the beginning and end of the time step are θ^{t} and $\theta^{t+\Delta t}$ respectively. Campbell (1985): related volumetric water content to water potential as follows:

$$\theta=\theta_s\left(\frac{\Psi}{\Psi_e}\right)^{-1/b} \qquad \Psi<\Psi_e \qquad (1.1.30)$$

The time averaged matrix flux potential Φ is given by

$$\theta=\theta_s \qquad \Psi\geq\Psi_e \qquad (1.1.31)$$

$$\Phi=\eta\Phi^{t+\Delta t}+(1-\eta)\Phi^{t} \qquad 1\geq\eta\geq 0 \qquad (1.1.32)$$

Redinger *et al*. (1984) report that with non-linear flow problems, a backward differencing scheme gives the best results; i.e. $\eta = 1$.

The difference equation derived is similar to the one used by Redinger *et al.* (1984). This form of equation can be used if the soil profile to be modelled is isotropic. If, however, soil variation is to be taken into account, an approach like that of Ross and Bristow (1990) needs to be taken because matrix flux potential, like water content, is not continuous across textural discontinuities. In the one-dimensional model of Ross and Bristow (1990) nodes were placed at textural discontinuities and two matric flux potentials were calculated for each node. The matric flux potential, and also volumetric water content and hydraulic conductivity would depend on the soil properties of the element and the potential at the node. This is illustrated in Figure 1.7 for element [i, j].

The four-quarter elements surrounding a node can be seen as a control volume to which the continuity equation is applied. Taking two-dimensional soil variation into account results in eight flux equations, which are illustrated in Figure 1.8.

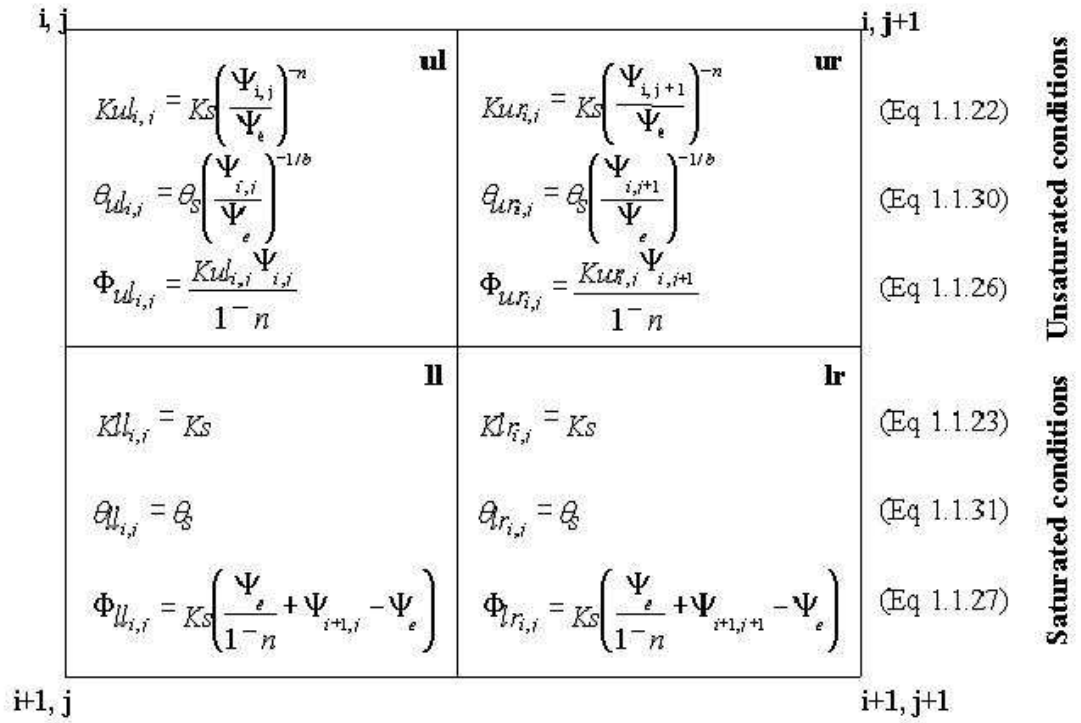

Figure 1.7. Detail of element [i, j] (see Figure 2.5), with K, θ and Φ calculated for each quarter (ul, ur, ll and ul). For demonstration purposes, nodes [i, j] and [i, j+1] are below Ψ_e whilst nodes [i+1, j] and [i+1, j+1] are above Ψ_e.

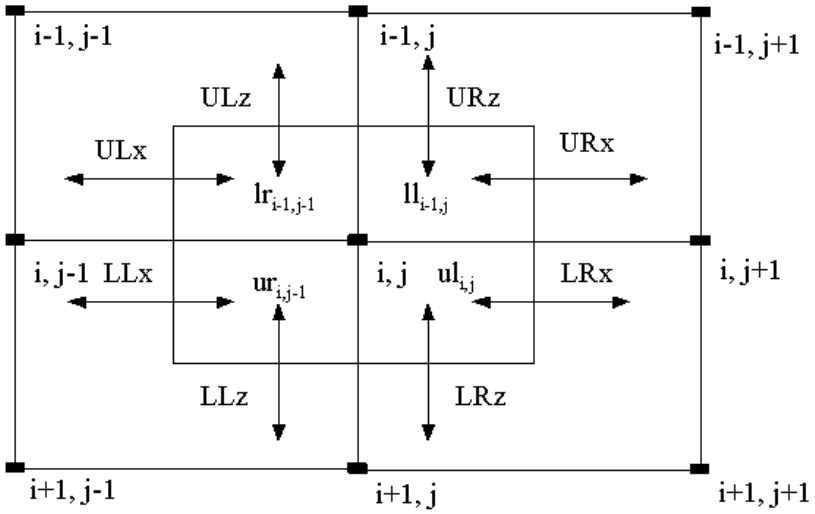

Figure 1.8. Control volume [i, j] illustrating the eight water fluxes.

The fluxes have been named upper right (UR) x and z, upper left (UL) x and z, lower right (LR) x and z and lower left (LL) x and z. The difference form of these equations follows with positive values representing fluxes into the control volume.

$$URx = \frac{\left(\Phi lr_{i-1,j} - \Phi ll_{i-1,j}\right)\left(Z_i - Z_{i-1}\right)}{2\left(X_{j+1} - X_j\right)} \qquad (1.1.33)$$

$$LRx = \frac{\left(\Phi ur_{i,j} - \Phi ul_{i,j}\right)\left(Z_{i+1} - Z_i\right)}{2\left(X_{j+1} - X_j\right)} \qquad (1.1.34)$$

$$ULx = \frac{\left(\Phi ll_{i-1,j-1} - \Phi lr_{i-1,j-1}\right)\left(Z_i - Z_{i-1}\right)}{2\left(X_j - X_{j-1}\right)} \qquad (1.1.35)$$

$$LLx = \frac{\left(\Phi ul_{i,j-1} - \Phi ur_{i,j-1}\right)\left(Z_{i+1} - Z_i\right)}{2\left(X_j - X_{j-1}\right)} \qquad (1.1.36)$$

$$URz = \frac{\left(\Phi ul_{i-1,j} - \Phi ll_{i-1,j}\right)\left(X_{i+1} - X_j\right)}{2\left(Z_i - Z_{i-1}\right)} + \frac{g \quad Kul_{i-1,j}\left(X_{j+1} - X_j\right)}{2} \qquad (1.1.37)$$

$$LRz = \frac{\left(\Phi ll_{i,j} - \Phi ul_{i,j}\right)\left(X_{j+1} - X_j\right)}{2\left(Z_{i+1} - Z_i\right)} - \frac{g \quad Kul_{i,j}\left(X_{j+1} - X_j\right)}{2} \qquad (1.1.38)$$

$$ULz = \frac{\left(\Phi ur_{i-1,j-1} - \Phi lr_{i-1,j-1}\right)\left(X_j - X_{j-1}\right)}{2\left(Z_i - Z_{i-1}\right)} + \frac{g \quad Kur_{i-1,j-1}\left(X_j - X_{j-1}\right)}{2} \qquad (1.1.39)$$

$$LLz = \frac{\left(\Phi lr_{i,j-1} - \Phi ur_{i,j-1}\right)\left(X_j - X_{j-1}\right)}{2\left(Z_{i+1} - Z_i\right)} - \frac{g \quad Kur_{i,j-1}\left(X_j - X_{j-1}\right)}{2} \qquad (1.1.40)$$

$$\Delta S = \frac{\rho_w\left(\theta_{i,j}^{t+\Delta t} - \theta_{i,j}^{t}\right)\left(X_{j+1} - X_{j-1}\right)\left(Z_{i+1} - Z_{i-1}\right)}{4\Delta t} \qquad (1.1.41)$$

Note that the vertical fluxes include gravitational components. The change in storage ΔS, is given in difference form since the volumetric water content $\theta_{i,j}$, is the weighted average water content for the control volume [i, j]:

$$\theta_{i,j} = \frac{\left(\theta lr_{i-1,j-1} \frac{(X_j - X_{j-1})(Z_i - Z_{i-1})}{4} + \theta ll_{i-1,j} \frac{(X_{j+1} - X_j)(Z_i - Z_{i-1})}{4} + \theta ur_{i,j-1} \frac{(X_j - X_{j-1})(Z_{i+1} - Z_i)}{4} + \theta ul_{i,j} \frac{(X_{j+1} - X_j)(Z_{i+1} - Z_i)}{4} \right)}{\left(\frac{(X_{j+1} - X_{j-1})(Z_{i+1} - Z_{i-1})}{4} \right)} \quad (1.1.42)$$

The mass balance error MBE is given by:

$$MBE = URx + LRx + ULx + LLx + URz + LRz + ULz + LLz - \Delta S + I - E - T \quad (1.1.43)$$

Infiltration (I) and evaporation (E) will be discussed later. Plant water uptake (i.e. transpiration, T) depends on canopy radiation interception, atmospheric evaporative demand, and root weighted matric potential. The mechanistic, supply- or demand- limited approach is explained in detail by Annandale *et al*. (2000). The aim is to find the matric potentials that will cause the mass balance error to be negligible. This is done using the Newton-Raphson procedure as described in Campbell (1985). This requires taking the derivatives of all the terms in Eq. (1.1.43) with respect to matric potential. These derivatives follow:

$$\frac{\partial URx}{\partial \Psi_{i,j}} = \frac{-Kll_{i-1,j}(Z_i - Z_{i-1})}{2(X_{j+1} - X_j)} \quad (1.1.44)$$

$$\frac{\partial LRx}{\partial \Psi_{i,j}} = \frac{-Kul_{i,j}(Z_{i+1} - Z_i)}{2(X_{j+1} - X_j)} \quad (1.1.45)$$

$$\frac{\partial ULx}{\partial \Psi_{i,j}} = \frac{-Klr_{i-1,j-1}(Z_i - Z_{i-1})}{2(X_j - X_{j-1})} \quad (1.1.46)$$

$$\frac{\partial LLx}{\partial \Psi_{i,j}} = \frac{-Kur_{i,j-1}(Z_{i+1} - Z_i)}{2(X_j - X_{j-1})} \quad (1.1.47)$$

$$\frac{\partial URz}{\partial \Psi_{i,j}} = \frac{-Kll_{i-1,j}(X_{j+1} - X_j)}{2(Z_i - Z_{i-1})} \quad (1.1.48)$$

$$\frac{\partial LRz}{\partial \Psi_{i,j}} = \frac{-Kul_{i,j}(X_{j+1} - X_j)}{2(Z_{i+1} - Z_i)} - \frac{g(X_{j+1} - X_j)}{2} \frac{\partial Kul_{i,j}}{\partial \Psi_{i,j}} \quad (1.1.49)$$

$$\frac{\partial ULz}{\partial \Psi_{i,j}} = \frac{-Klr_{i-1,j-1}\left(X_j - X_{j-1}\right)}{2\left(Z_i - Z_{i-1}\right)} \qquad (1.1.50)$$

$$\frac{\partial LLz}{\partial \Psi_{i,j}} = \frac{-Kur_{i,j-1}\left(X_j - X_{j-1}\right)}{2\left(Z_{i+1} - Z_i\right)} - \frac{g\left(X_j - X_{j-1}\right)}{2} \frac{\partial Kur_{i,j-1}}{\partial \Psi_{i,j}} \qquad (1.1.51)$$

$$\frac{\partial S}{\partial \Psi_{i,j}} = \rho_w \frac{\partial \Theta_{i,j}^{t+\Delta t}}{\partial \Psi_{i,j}} \left(\frac{\left(X_{j+1} - X_{j-1}\right)\left(Z_{i+1} - Z_{i-1}\right)}{4\Delta t} \right) \qquad (1.1.52)$$

The derivative of the hydraulic conductivity is:

$$\frac{\partial K}{\partial \Psi} = \frac{-nK}{\Psi} \qquad \text{when} \qquad \Psi < \Psi_e \qquad (1.1.53)$$

$$\frac{\partial K}{\partial \Psi} = 0 \qquad \text{when} \qquad \Psi \geq \Psi_e \qquad (1.1.54)$$

While the differential water capacity is:

$$\frac{\partial \theta}{\partial \Psi} = \frac{-\theta}{b\Psi} \qquad \text{when} \qquad \Psi < \Psi_e \qquad (1.1.55)$$

$$\frac{\partial \theta}{\partial \Psi} = 0 \qquad \text{when} \qquad \Psi \geq \Psi_e \qquad (1.1.56)$$

The control volume differential water capacity is also calculated as a weighted average. The derivatives of the sink terms will be discussed later. The sum of all the derivatives at node i, j is $\partial MBE_{i,j} / \partial \Psi_{i,j}$ and this is used to improve the estimate of $\Psi_{i,j}$ in the Newton-Raphson procedure using:

$$\Delta \Psi_{i,j} = \frac{MBE_{i,j}}{\partial MBE_{i,j} / \partial \Psi_{i,j}} \qquad (1.1.57)$$

with $\Delta\Psi$ to be subtracted from $\Psi_{i,j}$. Ross and Bristow (1990) found the slopes $\partial MBE_{i,j} / \partial \Psi$ far from the solution so gave poor estimates of the changes in potential actually needed. They suggest restricting the value of $\Delta\Psi$ to 0.8 $\Psi_{i,j}$ for values of $\Psi_{i,j}$ below an arbitrary cut off value of -0.1 J kg^{-1}. The cut off value is necessary to avoid the limit for change approaching zero as $\Psi_{i,j}$ approaches zero. The cut off value was set to -0.01 J kg^{-1} in this model.

1.1.3.3. Upper boundary condition

The soil surface loses water to the atmosphere by evaporation and gains water by infiltration.

Infiltration

A precipitation or irrigation in mm is converted to a flux in kg m^{-1} s^{-1} by dividing by the time step and multiplying by the horizontal distance, x, over which the water fell. The infiltration does not have to be uniform over the surface.

Non-uniform infiltration is especially important in very coarse soils where lateral redistribution is likely to be limited, or in the case of micro-irrigation.

Evaporation

As with the infiltration flux, it is necessary to multiply the evaporation by the horizontal distance over which it occurs (Surface) in order to get an evaporative flux in kg m^{-1} s^{-1}.

$$E = PE\frac{(h_s - h_c)}{(1 - h_c)}\,Surface \qquad (1.1.58)$$

where h_s is the soil surface humidity and h_c is the canopy humidity. The two-dimensional radiation interception model enables the distribution of energy at the surface.

The surface humidity depends on the soil water potential $\Psi_{i,j}$ (J kg^{-1}) at the surface and is calculated after Campbell (1977) as

$$h_s = \exp\left(\frac{M\Psi}{RT}\right) \qquad (1.1.59)$$

with M the molar mass of water (0.018 kg mol^{-1}), R the gas constant (8.314 J K^{-1} mol^{-1}) and T the Kelvin temperature.

The derivative of this flux with respect to water potential $\partial E/\partial\Psi$ is needed for the Newton Raphson solution and is calculated as

$$\frac{\partial E}{\partial \Psi} = PE\frac{Mh_s/(RT)}{(1 - h_c)}\,Surface \qquad (1.1.60)$$

1.1.3.4. Lower boundary condition

Two lower boundary conditions can be chosen in the model:

i) A gravity drainage lower profile condition is created by setting the lower matric flux potentials of the bottom elements equal to the upper matric flux potentials. The only driving force for downward movement of water is then gravity. This condition is typical for well-drained soil.

ii) A zero-flux lower boundary can be established by setting the upper conductivities (Kur and Kul) of the bottom element to zero. This would simulate an impermeable layer.

These two boundary conditions can be used to test the model. Infiltration and evaporation can be excluded and redistribution of water in a wet profile simulated. The no-flow lower boundary condition should result in water collecting at the bottom of the profile and a unit gradient in matric potential Ψ_m developing (i.e. 0.1 J kg^{-1} decrease in potential per cm increase in height above the bottom). The gravity drainage lower boundary condition should result in a fairly uniform matric potential with depth, with Ψ_m decreasing over time. The horizontal fluxes can be tested by wetting one side of the profile and monitoring redistribution with gravity set to zero. A uniform wetting front should be seen to be moving across the profile with no vertical movement of water.

1.1.3.5. Model stability

In the calculation of soil water redistribution, the aim is to solve the Richards' equation (Eq. 1.1.21) with the Newton-Raphson iterative procedure for each control volume, and assign new values of equilibrated soil water potentials to each node in the grid. The acceptable solution to Richards' equation is the one that causes the mass balance error of the soil water balance to be negligible (Eq. 1.1.43). In SWB-2D, equilibrium in soil water potentials is assumed to occur when MBE $\cong$ 0.0000003. However, conditions may occur when equilibrium in soil water potentials cannot be achieved. The simulation is then interrupted and a warning message appears, which indicates that the maximum number of iterations has been reached. The maximum number of iterations is 20000. The simulation can be resumed by the operator, but this may cause considerable mass balance errors.

Two specific causes of non-convergence can be singled out:

i) The horizontal (∂x) or vertical (∂z) distances between nodes are too big. This may cause large differences in soil water potential at adjacent nodes and equilibrium conditions may not be reached, in particular if nodes have different soil water retention and hydraulic characteristics. The model calculates unsaturated hydraulic conductivity as a function of soil matric potential (Eq. 1.1.22), and uses the arithmetic average hydraulic conductivity between two adjacent nodes to calculate the soil water flux between the two nodes (Eq. 1.1.25). Due to the non-linearity of Eq. 1.1.22, the use of average conductivity could cause large errors if the distances between nodes and the differences in nodal water potentials are large, in which case a weighted average unsaturated hydraulic conductivity would be more suitable. This problem can be overcome if the operator selects smaller distances between nodes.

ii) The time step (∂t) is too big. Large upper boundary fluxes (infiltration or evaporation) could cause large differences in soil water potential at adjacent nodes and equilibrium conditions may not be reached. This problem cannot be overcome by the operator. The model could be improved by including an hourly time step, where smaller upper boundary fluxes over shorter time periods could be used as input.

It would be interesting to carry out a sensitivity analysis to determine the effect of ∂x, ∂z and ∂t on soil water redistribution. It would also be interesting to assess the effect of assuming the arithmetic mean hydraulic conductivity between two adjacent nodes. The model could be made more user-friendly by including a warning system to indicate to the operator the cause of non-convergence (node distance ∂x and ∂z, or time step ∂t).

1.1.4 Link between the two-dimensional radiation and soil water balance model

SWB-2D simulates canopy radiation interception across the row, as well as the two-dimensional soil water balance in widely spaced, micro-irrigated row crops on a daily time step.

Potential transpiration from the trees is calculated as follows. Potential evapotranspiration (PET) is partitioned between potential evaporation (from the soil) and potential transpiration (from the canopy). PET is calculated from weather data using the Penman-Monteith equation (Allen *et al.*, 1998) and the maximum crop factor after rainfall occurs (Jovanovic and Annandale, 1999), as described in Section 1.2.1. Local potential evaporation calculated at each radiation node (PE_j, calculation described in Section 1.1.2) are weighted by the

surface the node represents and accumulated over the whole soil surface to calculate overall potential evaporation (PE). Potential transpiration is taken as the difference between PET and PE. Crop water uptake (transpiration) can either be limited by atmospheric demand or soil-root water supply (Annandale *et al.*, 2000). Root densities at different soil depths are accounted for in the calculation of root water uptake using the approach of Campbell and Diaz (1988). Root depth and the root fraction in the wetted and non-wetted volume of soil can also be entered by the user. In effect, PET is partitioned at the soil surface into potential evaporation and potential transpiration depending on solar orientation, row direction and canopy size, shape and leaf area density (LAD).

1.1.5. Required inputs

Required inputs for the two-dimensional soil water balance model are: starting and planting dates, altitude, rainfall and irrigation water amounts, as well as maximum and minimum daily temperature. For seasonal simulations, the “planting date” is generally taken at bud burst for deciduous trees and at some arbitrary chosen date after harvest and before flowering for evergreen trees, which should correspond to the beginning of the initial stage of the FAO growth curve (Doorenbos and Pruitt, 1977). For convenience, the starting date of the simulation is selected to coincide with the planting date, unless soil water measurements prior to “planting date” are made and used as initial water contents.

Two points on the water retention function, (namely field capacity and permanent wilting point), initial volumetric soil water content and bulk density are required for each soil layer. The field capacity corresponds to the drained upper limit, whilst permanent wilting point is the lower limit of crop water uptake. The principles and methods for the determination of the upper and lower limits of crop water uptake were discussed by Hillel (1998). Soil saturated hydraulic conductivities are estimated by the model using the water retention curve according to the procedure described by Campbell (1985) (Eq. 1.1.20). Row spacing, wetted diameter of micro-jets or drippers, fraction of roots in the wetted volume of soil as well as distance of the nodes from the tree row are also required as input.

A flow diagram of the two-dimensional soil water balance model for hedgerow fruit trees is shown in Figure 1.9. The source code of the finite difference soil water balance model is written in Delphi and can be found in WRC Report No 945/1/02 (Annandale *et al.* 2002).

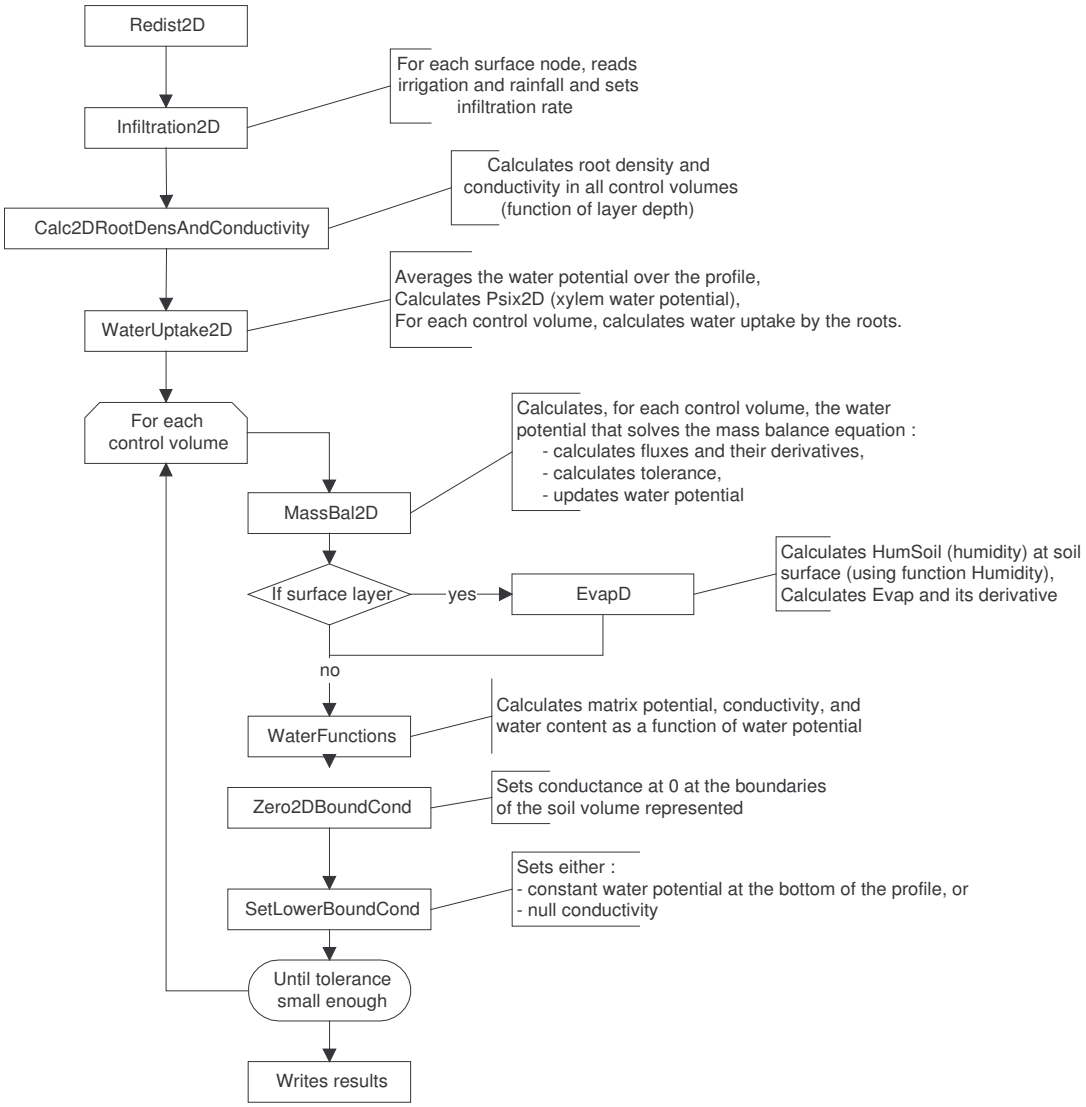

Figure 1.9. Flow diagram of the two-dimensional soil water balance model for hedgerow fruit trees.

1.2 FAO-based crop factor model

The Food and Agriculture Organization (FAO) of the United Nations recommended a semi-empirical approach for calculating crop water requirements, based on the fact that crop yield depends on climatic conditions, genetic potential of the crop and irrigation water management (Doorenbos and Pruitt, 1977). The FAO approach was used to develop the crop water requirement models CROPWAT (Smith, 1992a) and, in South Africa, SAPWAT (Crosby, 1996). Doorenbos and Pruitt (1977) give a comprehensive database of FAO crop

coefficients (Kc) for different climatic conditions and phenological stages (initial, mid-season and late-season stages). They also stressed the need to collect local data on growing season and rate of crop development of irrigated crops. Green (1985a and b) reviewed Kc values empirically related to pan evaporation and growth periods for crops grown in South Africa.

The Kc's published by the FAO represent mean values for a given irrigation cycle and strongly depend on wetting frequency, wetted area and soil type. Allen *et al*. (1996) defined Kc as the sum of the basal crop coefficient (Kcb) and the time-averaged effects of evaporation from the soil surface layer. They also reported Kcb values and maximum crop height (Hc_{max}) for a wide range of species.

Due to the very limited number of specific crop growth parameters for trees available in literature for the purpose of mechanistic modelling, the authors decided to make use of the already published FAO database of Kcb's and growth periods.

An FAO-based crop factor procedure has therefore been developed and combined with the mechanistic SWB model, thereby still allowing evaporation and transpiration to be modelled separately as supply and demand limited processes. The crop factor model does not grow the canopy mechanistically and therefore the effect of water stress on canopy size is not simulated. The simpler crop factor model should, however, still perform satisfactorily if the estimated canopy cover closely resembles that found in the field.

In the following Sections of this report, the FAO-based crop factor model that was built in SWB is described. In particular, the following improvements to SWB are presented:

i) FAO-type crop factor modification;
ii) Soil water balance with localised (micro- or drip) irrigation; and
iii) Yield predictions with the FAO model.

1.2.1. FAO-type crop factor modification

SWB calculates the grass reference evapotranspiration (ETo) using the revised FAO Penman-Monteith methodology (Smith *et al*., 1996). Potential evapotranspiration is calculated as follows:

$$PET = ETo\ Kc_{max} \qquad (1.2.1)$$

Kc_{max} represents the maximum value for Kc following rain or irrigation. It is selected as the maximum of the following two expressions (Allen *et al*., 1996):

$$Kc_{max} = 1.2 + [0.04\ (U_2 - 2) - 0.004\ (RH_{min} - 45)]\ (Hc/3)^{0.3} \qquad (1.2.2)$$

$$Kc_{max} = Kcb + 0.05 \quad (1.2.3)$$

where

U_2 - Mean daily wind speed at 2 m height (m s^{-1})

RH_{min} - Daily minimum relative humidity (%)

Hc - Crop height (m)

The upper limit of Kc_{max} is set at 1.45.

SWB partitions PET into potential crop transpiration (PT) and potential evaporation (PE), and estimates FI_{evap} using the following equations:

$$PT = Kcb\ ETo \quad (1.2.4)$$

(Allen et al., 1996)

$$FI_{evap} = PT/PET \quad (1.2.5)$$

$$PE = (1 - FI_{evap})\ PET \quad (1.2.6)$$

SWB assumes Kcb, Hc and root depth (RD) are equal to the initial values during the initial stage. During the crop development stage, they increase linearly from the end of the initial stage until the beginning of the mid-stage, when they attain maximum values. They remain constant at this maximum during the mid-stage. During the late stage, Kcb decreases linearly until harvest when it reaches the value for the late stage, whilst RD and Hc remain constant at their maximum value. The following crop parameters need therefore to be known: Kcb for the initial, mid and late stages, crop growth periods in days for initial, development, mid and late stages, initial and maximum *RD*, as well as initial Hc and Hc_{max}.

The following input parameters are required to run the FAO-type crop factor model: planting date, latitude, altitude, as well as maximum and minimum daily air temperatures. In the absence of measured data, SWB estimates solar radiation, vapour pressure and wind speed according to the FAO recommendations (Smith, 1992b; Smith *et al.*, 1996). It is, however, recommended that these be measured.

Caution should be exercised against blind acceptance of the FAO parameters taken from literature, as local conditions, management and cultivars are likely to influence crop growth periods and Kcb's. A simple methodology used to generate a database of Kcb values from limited available data, has therefore been developed. Daily Kcb can be calculated from FI_{evap}, Hc and weather data using the following equation:

$$Kcb = FI_{evap}\ PET/ETo \quad (1.2.7)$$

ETo is calculated from weather data. Weather data and crop height are used to calculate crop PET, whilst FI_{evap} can be easily measured in the field. The procedure can be easily and cheaply applied to determine FAO-type crop factors for any species. Evaluation of the model with independent data sets is always recommended.

A flow diagram of the FAO-type crop factor model included in SWB is shown in Figure 1.10.

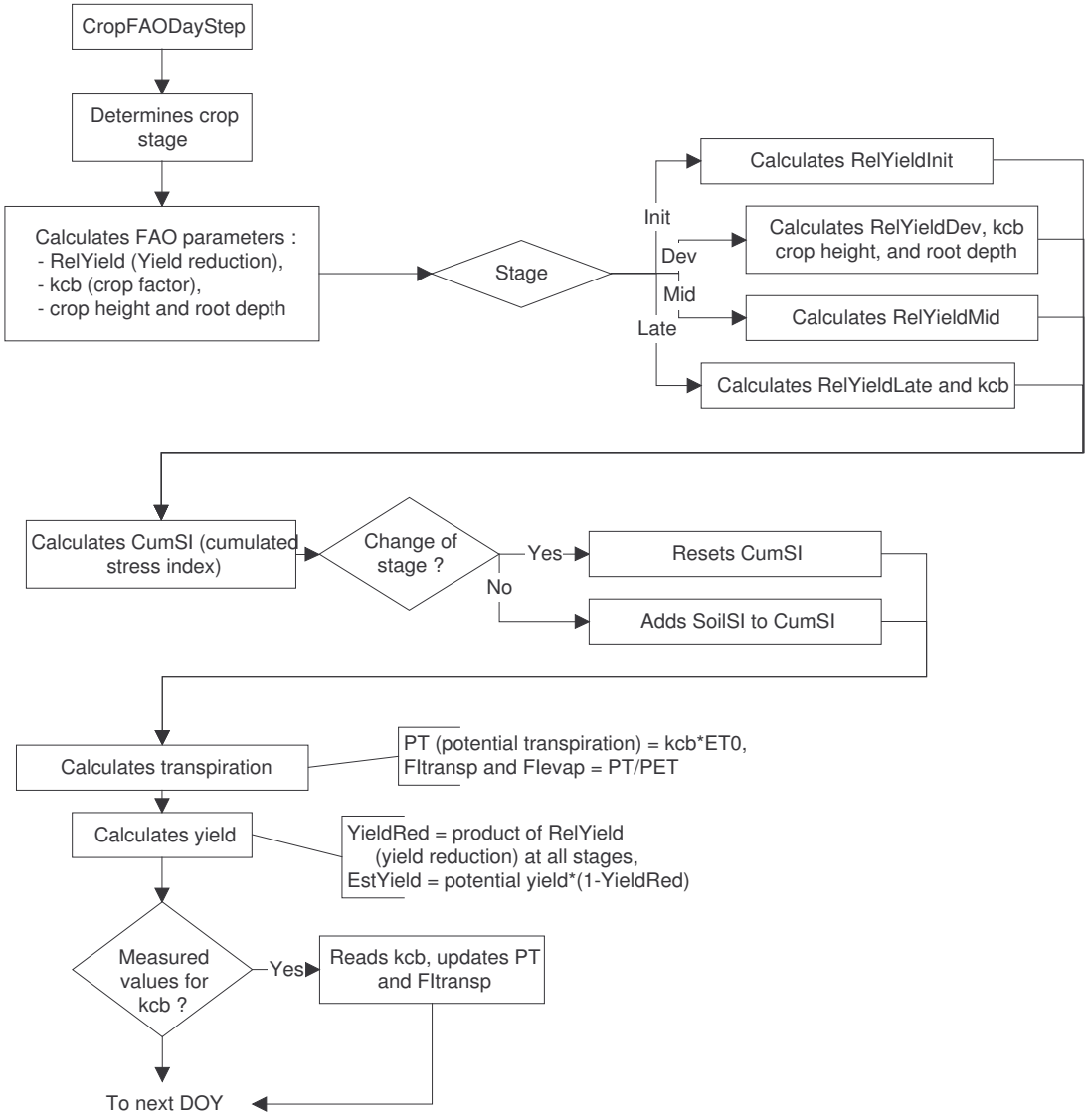

Figure 1.10. Flow diagram of the FAO-type crop factor model.

1.2.2. Soil water balance with localised irrigation

An option for the calculation of the soil water balance under localised irrigation was included in SWB (drip or micro-irrigation). When this option is selected, the model uses a simplified procedure for the calculation of non-uniform wetting of the soil surface, evaporation and transpiration.

In this quasi two-dimensional procedure, a cascading water balance is calculated for both the wetted and non-wetted portion of the profile. Daily soil water contents per soil layer are calculated for both the wetted and non-wetted volumes of soil. The output of soil water deficit is based on the soil water contents in the wetted volume of soil only, as this is the part of the profile managed by the irrigator.

1.2.2.1. Water redistribution

Interception of water by the crop canopy is calculated only when rainfall occurs, as the canopy is not wetted by micro-jets or drippers. Micro- or drip irrigation, commonly used in orchards, only wets a limited area under the canopy of the trees.

Runoff, infiltration and drainage are then calculated as done in the one-dimensional cascading model (Annandale *et al.*, 1999), but for both the wetted and non-wetted portions of the soil. Runoff and drainage for the wetted and non-wetted portions of the soil are weighted by the fraction of the surface irrigated (FI_{irrig}). Total runoff and drainage are calculated as the sum of the components from the wetted and non-wetted portions.

1.2.2.2. Evaporation

Evaporation from the soil surface is also not uniform under micro- or drip irrigation. Two possible cases are simulated when drip or micro irrigations are performed:

i) If the canopy cover fraction is larger than the irrigated surface fraction ($FI_{evap} > FI_{irrig}$), evaporation is simulated only from the non-irrigated portion of the ground.

ii) If the canopy cover is less than the irrigated surface fraction (i.e. $FI_{evap} < FI_{irrig}$), evaporation from the non-irrigated surface fraction ($1 - FI_{irrig}$) and from the non-shaded area ($FI_{irrig} – FI_{trans}$) are calculated separately and added to determine total evaporation.

The procedure used to calculate water loss by evaporation in the cascading model was described in Annandale *et al.* (1999).

1.2.2.3. Transpiration

No root water uptake is calculated for the uppermost soil layer. SWB assumes layer water uptake is weighted by root density when soil water potential is uniform (Campbell and Diaz, 1988). Water loss by crop transpiration is calculated as a function of maximum transpiration rate (T_{max}) and leaf water potential at T_{max} (Ψ_{lm}) (Campbell, 1985; Annandale *et al.*, 2000). It represents the lesser of root water uptake or maximum loss rate. T_{max} and Ψ_{lm} are input parameters that can be easily estimated from one's experience with the crop. In this way, a mechanistic supply and demand limited water uptake calculation was linked to an FAO crop factor approach with a minimal addition of crop input parameters required.

The user can input the fraction of roots in the wetted volume of soil. Daily transpiration is then calculated as the sum of water losses from the wetted and non-wetted volumes of soil, weighted for root fraction and matric potential.

The input data required to run the two-dimensional cascading model are rainfall and irrigation amounts, volumetric soil water content at field capacity and permanent wilting point, as well as initial volumetric soil water content for each soil layer. Row spacing, wetted diameter, distance between micro-jets or drippers, and the fraction of roots in the wetted volume of soil are also required.

A flow diagram of the cascading soil water balance for tree crops under localised irrigation is shown in Figure 1.11.

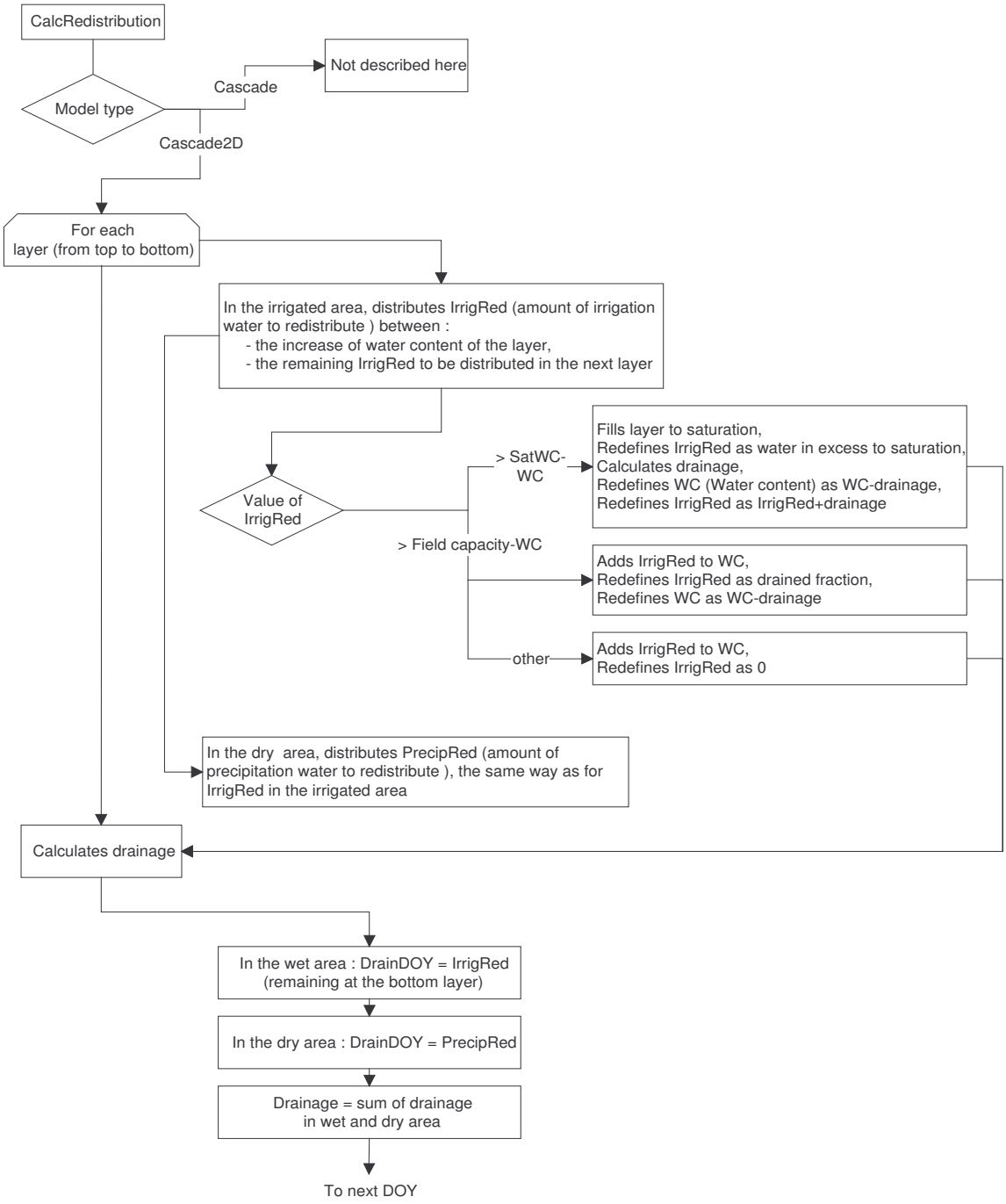

Figure 1.11. Flow diagram of the cascading soil water balance for tree crops under localized irrigation.

1.2.3. Yield predictions with the FAO model

A subroutine for the estimation of yield with the FAO model under conditions of water stress, was included in SWB. The procedure recommended by the FAO was used to compile this procedure (Smith, 1992a). The estimated yield (*Y,* in t ha^{-1}) is calculated as follows

$$Y = Y_{pot}\ (1 - Y_{red}) \qquad (1.2.8)$$

where

Y_{pot} is the Potential yield (t ha^{-1})

Y_{red} is the Fractional yield reduction (%)

Y_{pot} is a specific crop input parameter. Y_{red} is calculated as follows:

$$Y_{red} = (1 - Y_{rel(Init)}\ Y_{rel(Dev)}\ Y_{rel(Mid)}\ Y_{rel(Late)}) \qquad (1.2.9)$$

where

$Y_{rel(Init)}$ is the Fractional yield for initial stage

$Y_{rel(Dev)}$ is the Fractional yield for development stage

$Y_{rel(Mid)}$ is the Fractional yield for mid-season stage

$Y_{rel(Late)}$ is the Fractional yield for late-season stage

Relative yield for each stage (Y_{rel}) is calculated as a function of the stress factor (*Ky*) for that particular stage and a stress index (SI):

$$Y_{rel} = 1 - \frac{Ky}{N} \sum_{d=1}^{d=N} (1 - SI_d) \qquad (1.2.10)$$

Ky for each stage and the duration of the stage in days (*N*) are crop specific input parameters. The subscript of SI indicates the day of the stage. SWB calculates SI on a daily basis as follows:

$$SI = T / (FI_{evap}\ PET) \qquad (1.2.11)$$

where

T is the Actual crop transpiration (mm)

SI therefore represents the relative transpiration of the crop (ratio of actual and potential crop transpiration). The CROPWAT model of the FAO (Smith, 1992a) uses the ratio of actual and potential evapotranspiration instead of SI, as it does not calculate soil water supply limited root uptake.

SWB calculates and outputs estimated yield (Y) and Y_{red} on a daily basis, assuming that no water stress (SI = 1) will occur from that particular day until the end of the growing season.

Required input data for yield prediction with the FAO model are: FAO stress factors for growing stages (initial, development, mid-season and late-season stages) and potential yield.

CHAPTER 2

MATERIALS AND METHODS

In order to evaluate the SWB model, field data had to be collected and compared to model simulations. For this purpose, two field trials were set up. The first trial was established in a peach orchard (deciduous trees) on the lysimeter facilities of Pretoria University's experimental farm in Hatfield. The second trial was established in a citrus orchard (evergreen trees) at the Syferkuil experimental farm of the University of the North. Field data were also collected in Brits from commercial farms and from rows of Leucaena fodder trees on the Hatfield experimental farm.

The sites at the Hatfield and Syferkuil experimental farms were selected because suitable facilities were available. These sites were used to collect data for the evaluation of the model as examples for deciduous and evergreen fruit trees. The data collected in the field trials in Brits and on Leucaena rows in Hatfield were used to support the evaluation of the energy interception subroutine of the model. Although these plantings are not strictly representative of hedgerow orchards, if the model was applicable in these situations, it should then give good predictions of the energy and soil water balance for a wide range of orchards and conditions, provided that correct input parameters are used.

In this Chapter, materials and methods used for data collection in the field trials are described.

2.1 Experimental set-up at the University of Pretoria

2.1.1 Location and environmental characteristics

The field trial at the Hatfield experimental farm (University of Pretoria) was located 120 m West of RSA weather station No. 513465 (25°45'S, 28°16'E, alt. 1372 m). This is a summer rainfall region with an average of *ca* 670 mm a^{-1} (October - March). The rainfall occurs as high intensity short duration events with sunny periods between rains. The monthly average maximum temperature is 30 °C (January), with a monthly minimum average of 1.5 °C (July). Frost occurs during the winter. Even though the frost severity is less than experienced in typical highveld climates, it is sufficient for the low chilling requirement deciduous fruit cultivars commercially propagated in Gauteng and the Northern Province.

The soil in the trial site is a clay loam (30% clay, 16% silt and 54% sand) Hutton (Soil classification working group, 1991) or Ferralsol (FAO, 1998). Soil depth is generally in excess of 1.2 m (a small portion having scattered hard plinthic formations at 1.1 m). Soil

analysis revealed adequate P (120 mg kg^{-1}), pH(H_2O) being 6.4 and sufficient Ca, Mg and K (580, 140 and 160 mg kg^{-1} respectively).

2.1.2 Orchard lay-out, irrigation and cultivation practices

Since it was expedient to develop a reasonable tree canopy as soon as possible, an early maturing vigorous deciduous tree was used in this trial. Young grafted peach trees (*Prunus persica* cv Transvaalia) were planted on 6 September 1996 (DOY 250) in a high density 4.5 x 1 m hedgerow pattern. The tree row orientation was in a E-SE to W-NW axis (110° - 290°). At planting the trees were cut back to 250 mm above the soil surface. As the trees developed during the growing period, steps were taken to promote the central leader growth pattern and develop lower horizontal branches. During winter of 1997 (2 to 15 July) the trees were cut back to a height of 2 m and pruned to a central leader system. By 7 August 1997 (DOY 219) trees were at 80% blossom and reached full bloom on 12 August 1997 (DOY 224). From this date the canopy developed throughout the summer. The fruitlets were counted on 15 September 1997 (DOY 258) to establish the extent of fruit removal, which was done on 25 September 1997 (DOY 268). It is interesting to note that the first fruit was harvested on 17 and 18 November 1997 (DOY 321 and 322) but, since the objective of the research was to evaluate the water and energy balance, and yields for deciduous fruit is influenced primarily by fruit thinning practices, the yield results were not handled in this study.

During the establishment period (first 3 weeks) the trees were basin irrigated manually with a hose pipe daily (first week), and subsequently reducing the irrigation frequency to once per week by the third week. On 2 October 1996 (DOY 276) a low pressure irrigation system (DT-Rotator micro sprayer; Vetsak) capable of delivering 14 l h^{-1} $tree^{-1}$ in a 1.2 m wide band in the tree row was installed. With this irrigation system it was possible to monitor the irrigation volumes by flowmeter measurement. Initially this system worked very well but as the trees developed and created an environment favourable for insects, spiders set up homestead in the rotators and rendered them useless. The rotators were replaced during January 1997 by micro-jets (DT-Spreader 360°/12 stream) having the same delivery rate but covering a slightly larger area (1.3 m band) under the trees. This reduced the insect blocking problem but did not eliminate it. From 8 October 1997 (DOY 281) the irrigation pressure was increased to 3 bar which increased the wetting area to a 2 m band under the tree canopy. The 2 m band was selected to correspond to the dimensions of the lysimeters. Field measurements confirmed that during irrigations, negligible water was applied beyond a 1 m radius, i.e. the lysimeter readings gave an accurate measurement of irrigation applications.

At planting, 57 g super phosphate (10.5% P) per tree was incorporated in the planting hole. Nitrogen was supplied monthly at a rate of 20, 30, 40 and 50 g LAN (28% N) tree^{-1} during October, November, December 1996 and January 1997 with irrigation. Trees were monitored for visual signs of trace element deficiencies (Zn and Mn). Where necessary, light cover (0.2 l tree^{-1}) foliar sprays containing ZnO, $MnSO_4$ plus spray urea were applied to counteract any deficiency. In subsequent years the orchard cultivation practices, i.e. pruning, herbicide, pest control and fertilization programs were done under the guidance of the horticultural section that ensured that these aspects were adequately addressed.

2.1.3 Lysimeter characteristics

The pair of lysimeters had been installed in the 70's as mechanical weighing lysimeters. The surface dimensions are 2 x 2 m. The depth is 0.9 m. Each lysimeter has two trees.

At some stage, load cells coupled to a Campbell Scientific CR10 data-logger, were attached within the lever mechanism to automate recording mass changes. Before planting, tests with trial masses (sand bags of known mass) revealed that there was tremendous variability in the readings and it was necessary to use long measuring periods (one to two hours) to determine average mass for a specific period. By moving the load cell attachment locations to the recording arm of the weighing mechanism, and removing the counter balance weights, it was possible to damp the oscillations ("*see-saw effect*") and thus reduce variability in the readings. This modification enabled the system to give accurate values within a period of 2 to 3 minutes. The programme use to control this data-logger is presented in Appendix A.3.

Each load cell was supplied with an independent constant voltage source. This voltage was supplied through a transformer which converts 220 V AC to 16 V DC, which was used to charge a 12 V, 6.5 Ah lead acid motorcycle battery as an emergency supply, should there be a power failure. From the 12 V DC battery the power passed through an electronic voltage stabilising circuit designed and fabricated by personnel of the UP Engineering Faculty electronics workshop. As a precaution, the voltage supplied to each load cell was monitored hourly with a data-logger.

Once the best location for the load cell attachment had been identified, and the trees planted, the lysimeters were calibrated with sand-bags of known mass. The best input voltage to the load cell of the eastern lysimeter was 9.34±0.03 V while a voltage of 9.21±0.03 V gave the best readings for the western lysimeter. The voltage output from each load cell was recorded as an equivalent depth of water on the basis that one litre (i.e. 1 kg) per m^2 is equivalent to 1 mm. Calibration curves for both lysimeters are presented in Figure 2.1. This calibration was done on 27 August 1996. It is seen that the lysimeters gave

a linear response to changes in mass and that the SE of the recorded mm value was 0.14 mm for the eastern lysimeter (*LyEast*) and 0.138 mm for the western lysimeter (*LyWest*).

At the base of each lysimeter there were drainage pipes that allowing free water that had percolated through the soil in the lysimeter to be removed. These pipes were fitted with thin walled flexible tubing that directed any water that had drained out of the lysimeters onto a mechanism similar to that used in tipping bucket rain gauges. Thus it was possible to monitor the drainage from each lysimeter. The thin walled tubing was very flexible so it had no effect on the free movement of the lysimeter and thus did not detrimentally influence any mass measurement or change. This drainage system was also fitted with shut-off stop cocks that could be closed if one did not want any free drainage to occur from the lysimeters.

To get an indication of the water holding capacities of the lysimeters the following procedures were followed. To begin with, there are no records of the mass of the soil in the lysimeter and the mass of the lysimeter bin. Also, as the trees grew, the dry mass of the lysimeters increased. However, these values are irrelevant since one is primarily interested in the daily changes in mass and not specifically in the absolute beginning and end mass. Since there were no activities that would change the soil mass (e.g. digging or mechanical cultivation) the change in soil mass would be negligible. It was also accepted that the daily dry matter accumulation would be negligible when compared to the mass of water lost or gained. Thus any change in daily mass was attributed to change in water content. To get an indication of the wilting point (WP) of each lysimeter, they were allowed to dry out until mass changes were minimal (during conditions when there was no foliage on the trees) or when early morning wilting was noticed on the foliage. To get an indication of field capacity each lysimeter was given a steady irrigation until drainage from the base of the lysimeter occurred. Irrigation was stopped and the surface was covered with heavy duty plastic to eliminate surface evaporation. Once free drainage had stopped, the plastic was removed and the values recorded were taken as field capacity (FC). As the daily mass of each lysimeter changed this value (in mm) was recorded and summed to give the soil water deficit (SWD in mm).

2.1.4 Calculation of evapotranspiration and crop coefficient from lysimeter data

Once the trees had been planted the lysimeters were calibrated with sand bags of known mass as previously described. The data-logger was programmed to read at 10 s intervals and average these values every 15 min. At a specific time of the day e.g. 0h15 (day i +1) the 15 min average was taken as the lysimeters water status ($Ly_{(i)}$), in mm, for the previous day, i.e. day i. This was done for both lysimeters (*LyEast* and *LyWest*). The water loss for each lysimeter for day i (in mm) was then taken as:

$$\Delta LyEast_{(i)} = LyEast_{(i)} - LyEast_{(i+1)} \quad (2.1.1)$$

$$\Delta LyWest_{(i)} = LyWest_{(i)} - LyWest_{(i+1)} \quad (2.1.2)$$

In the event of there being large unexplainable differences between $LyEast_{(i)}$ and $LyWest_{(i)}$ the values for that day were discarded.

The average of these values was used to reflect daily water loss:

$$\Delta Ly_{(i)} = (\Delta LyEast_{(i)} + \Delta LyWest_{(i)}) / 2 \quad (2.1.3)$$

A gross evapotranspiration for the day was determined by including rain (R), irrigation (Ir) and drainage (D) values as follows:

$$ET_{Gross} = \Delta Ly_{(i)} + R + Ir - D \quad (2.1.4)$$

On the infrequent occasion of ET_{Gross} being negative or inexplicably large for a particular day, the value was disregarded.

It must be remembered that the lysimeters only covered 2 m of the 4.5 m row spacing and thus did not account for 2.5 m of the inter-row, which is normally dry and thus has low evaporative losses. Thus to make a valid comparison with the grass reference evapotranspiration, ETo, which reflects the total area (4.5 m wide rows), the following correction, which assumed no contribution to evaporation from the area outside the lysimeters, was applied:

$$ET_{lys} = ET_{Gross} * Lysimeter\ width / Row\ width = ET_{Gross} * 2 / 4.5 = ET_{Gross} * 0.444 \quad (2.1.5)$$

The daily crop coefficient, Kc, was then determined by:

$$Kc = ET_{lys} / ETo \quad (2.1.6)$$

To determine transpiration rates, the lysimeters were irrigated to field capacity overnight and the surface of the lysimeters was covered with a heavy duty plastic early the next morning. During these measurements, the drainage taps were closed to eliminate any drainage loss being considered. After these measurement periods, the lysimeters were uncovered and allowed to dry out so that the profile could be aerated. This was done to counteract the negative effects of any anaerobic conditions, which could develop while the lysimeters were at a high water content and with the surface sealed.

2.1.5 Weather monitoring

An automatic weather station was installed in the Hatfield weather station enclosure on 24 September 1996 (DOY 268) to give comprehensive weather data from DOY 269. The following weather data was monitored and recorded hourly by a CR10 data-logger:

- Temperature and relative humidity (RH) with an HMP35C sensor;
- Wind speed with an R.M. Young cup anemometer;
- Solar radiation with an LI 200X pyranometer; and
- Rainfall with a Rimco R/TBR tipping bucket rain gauge.

The data-logger was programmed to automatically calculate hourly average saturation vapour pressure (SVP), vapour pressure (VP) and vapour pressure deficit (VPD). These values were calculated following the procedures described by (Tetens, 1930; Annandale, Jovanovic Benade and Allen, 2002). The programme used to control the weather station is presented in Appendix A.1.

The logged daily data was regularly downloaded using a lap-top computer to calculate daily short grass reference evapotranspiration (ETo) according to the FAO 56 procedures as described by Allen *et al*. (1996).

2.1.6 Soil measurements

During winter 1998, two cross-sectional trenches were dug across the rows between two trees to install intensive soil water monitoring sites. Time-domain reflectometry (TDR) probes and heat dissipation sensors (HDS) were installed, on both sides of the row, at depths of 0.06, 0.26, 0.56 and 0.86 m, at distances of 2, 1 and 0 m from the tree trunk, to form a vertical grid across the row as depicted in Figure 2.2. This was done for two tree rows, the one on bare soil, the other with grass sod. During this process, profile characterisation samples were collected, and penetrometer resistance measurements were taken at corresponding sites.

A complete description of soil measurements performed during the course of the trial follows and relevant information is presented in Figures 2.3 to 2.8.

2.1.6.1 Soil physical properties

Profile description

The soil profile is characterised as having a uniform red colour and apedal structure typical of a Hutton profile (Soil Classification Working Group 1991). The orthic A horizon can be taken as being 15 cm deep and having a gradual transition into the Red Apedal B horizon which reaches a depth of 1 m.

Texture

There is very little variation in soil texture across the tree row (Figure 2.3) with the average silt, clay and sand percentages being 16, 30 and 54 % respectively. This classifies the soil as a clay loam. With depth (Figure 2.4), the clay content increases from 24 to 35 % with a corresponding decrease from 62 to 48 % in the sand fraction. The silt content shows only a slight increase from 14 to 18 % with depth.

Bulk density

Between the depths of 20 to 80 cm, the bulk density of the soil was 1.41 ± 0.11 g cm^{-3} (CV 8%) for the southern tree row and 1.37 ± 0.08 g cm^{-3} (CV 6 %) for the northern tree row. One could not identify any consistent trends in bulk density either across the rows or down the profile.

Penetrometer resistance

Penetrometer resistance was measured by Dr T Fyfield (Agricultural Research Council - Institute of Soil, Climate and Water, Pretoria) using a Bush Recording Soil Penetrometer. This instrument records cone resistance at 35 mm depth intervals to a maximum depth of penetration of 525 mm. With a 12.9 mm diameter 30° cone fitted, the maximum recordable force is 50 kg or 3.81 MPa. A mean value was determined from three measurements made at each position. As can be seen in Figure 2.5, there is negligible difference in resistance to penetration between the two rows (southern row having grass sod inter-row and the northern row being clean cultivated). The apparent higher resistance nearer to the soil surface is due to the soil being dryer than the subsoil. The influence of soil water content on penetration resistance is depicted in Figure 2.6.

2.1.6.2 Soil matric potential

Heat dissipation sensors

Soil matric potential (ψ_m) was measured with CS 229 heat dissipation sensors (HDS). Heat dissipation sensors rely on the effect of the water content of a porous block in equilibrium with soil water, on thermal conductivity and heat capacity. Heat dissipation is determined by applying a heat pulse to a heater within the soil and monitoring the temperature at the centre of the block before and during heating. The temperature rise is a function of the thermal

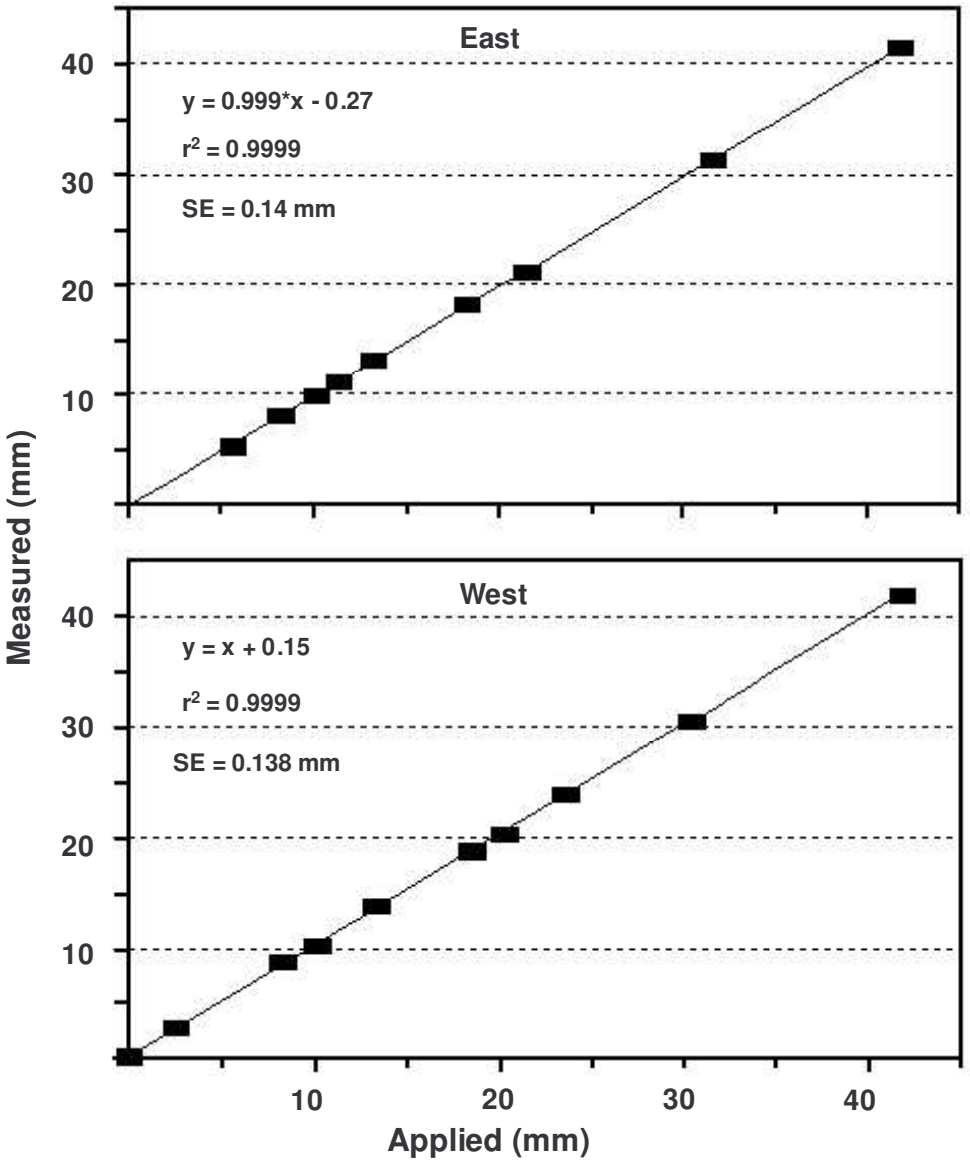

Figure 2.1: Calibration curves of the lysimeters (east and west).

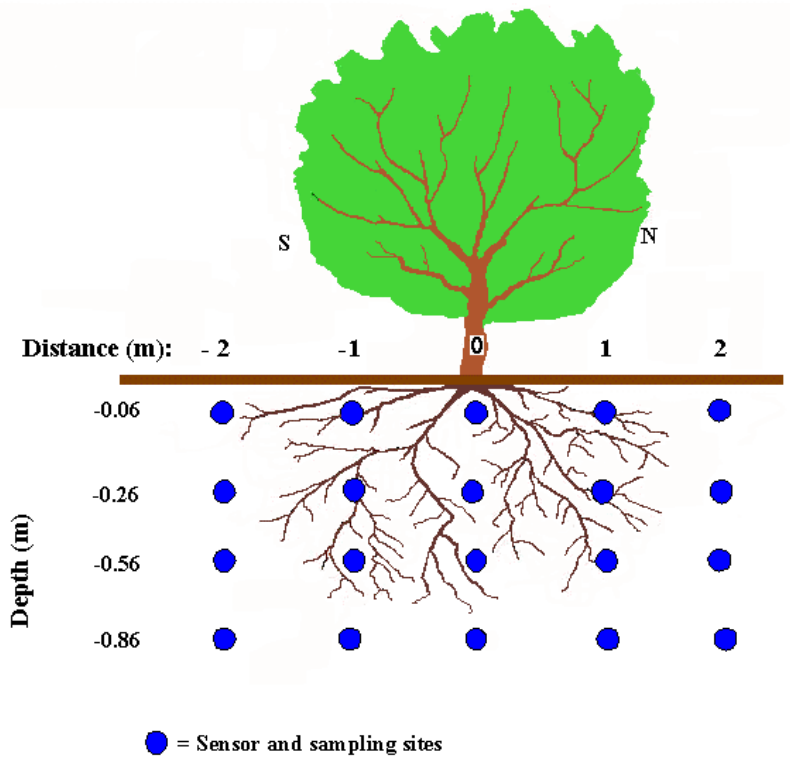

Figure 2.2. Diagrammatic grid indicating monitoring and soil sampling locations in the soil profile for the Hatfield and Syferkuil hedgerow system.

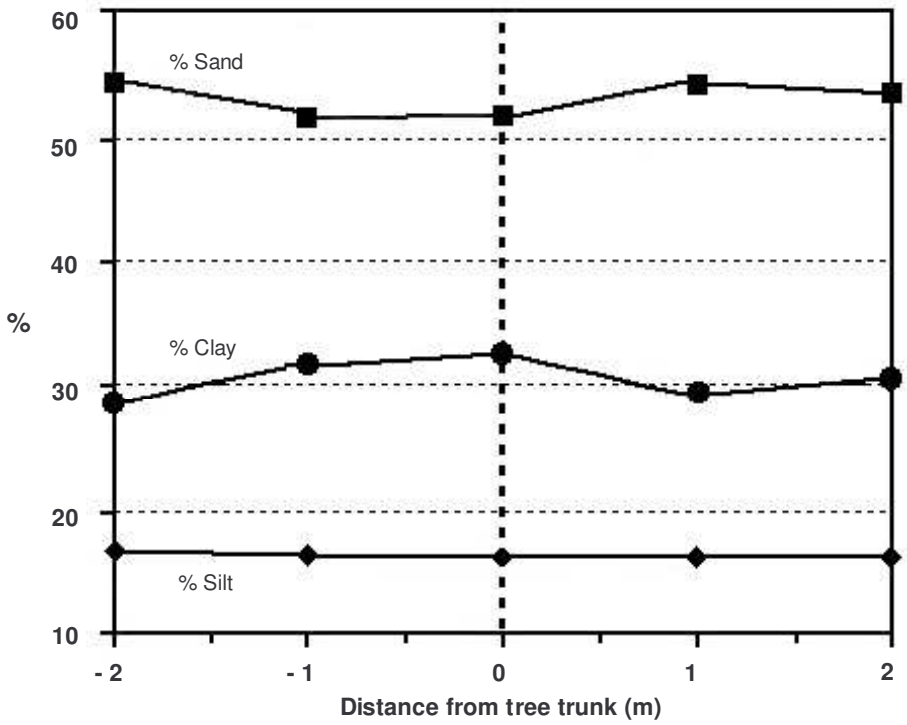

Figure 2.3. Variation of soil texture of B horizon (~ 0.4 m depth) across tree row

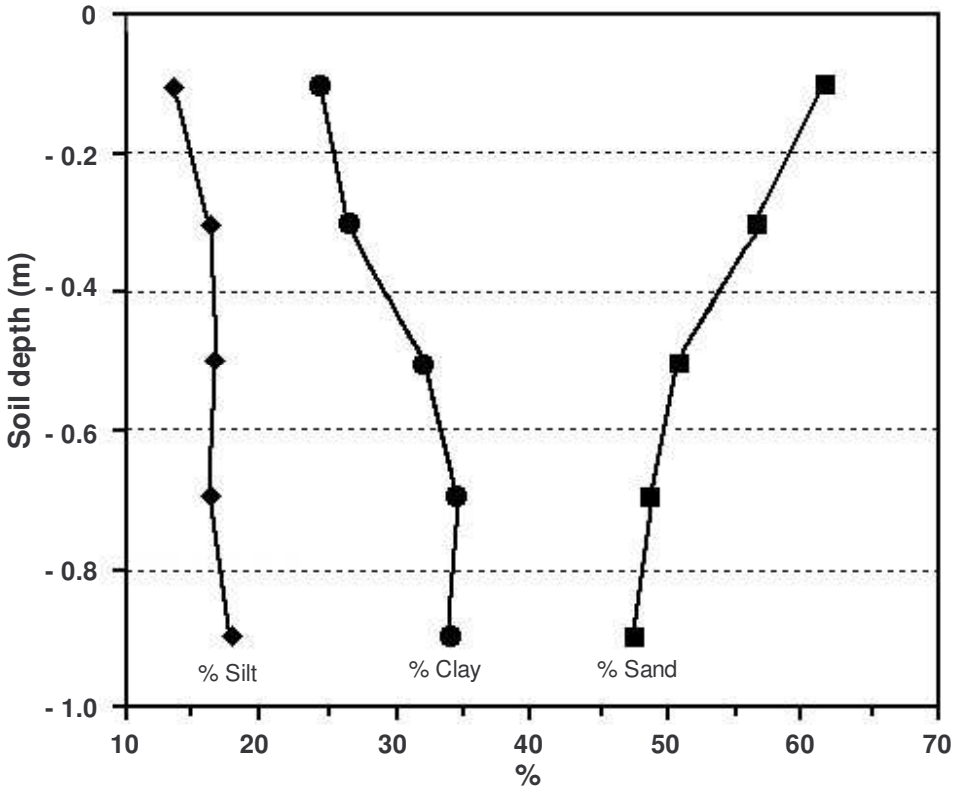

Figure 2.4. Variation of soil texture (mean for row width) with depth.

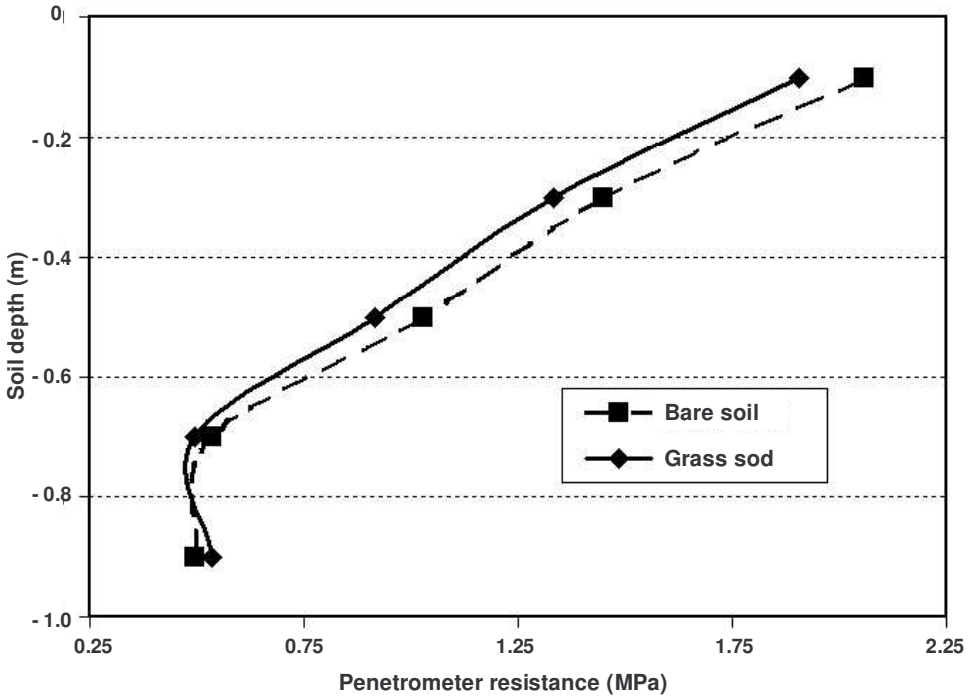

Figure 2.5. Variation of soil penetration resistance with depth.

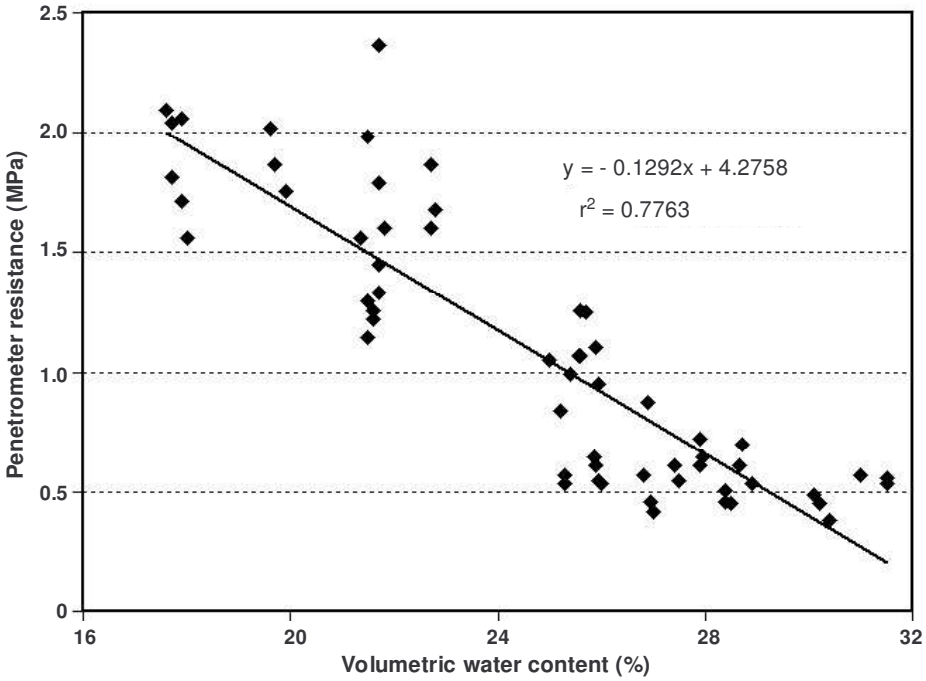

Figure 2.6. Effect of soil water content on soil penetration resistance.

Figure 2.7. View of tube solarimeters and LQS installed under the peach hedgerow to record solar irradiance under a developing canopy.

diffusivity, and therefore of the water content of the block. Transient heat-pulse theory was discussed by Jackson and Taylor (1986), and Campbell *et al*. (1991). The heat dissipation technique for the estimation of ψ_m was also described in the literature by Campbell and Gee (1986), Bristow *et al*. (1993), and Jovanovic and Annandale (1997).

The system used in the peach field trial, consisted of the following components:

i) Two Campbell Scientific data-loggers for controlling the system, as well as recording and storing data.
ii) Two AM416 relay multiplexers, used to increase the number of input channels for the differential measurement of temperature.
iii) Five CE8 eight-channel current excitation modules, used to increase the number of excitation channels.
iv) Forty CS 229 heat dissipation sensors, used to determine soil matric potential.

A scheme of the heat dissipation sensor system is shown in Figure 2.9. Since each current excitation modules (CE8) had eight channels, the system was connected so that the first 16 HDS were controlled by the first data-logger (S row) and the remaining 24 were controlled through the second data-logger (N row). The programmes to control these units are presented in Appendix A.5 and A.6.

Each data-logger was powered by a 12 V battery. The site of each sensor is shown schematically in Figure 2.2. Soil temperature was recorded. Thereafter a 20 s heat pulse was applied to the sensors and the difference in block temperature (ΔT), 20 s and 1 s after heating commenced, was recorded. The output readings were processed using the normalisation procedure of Campbell *et al*. (2001), which simplifies calibration of individual sensors using the dimensionless temperature rise and corrects the reading for actual soil temperature, to the value it would have at 20°C. For this purpose, a user-friendly Delphi program (HDS calculator) was developed by Dr Nebo Jovanovic. This is described in detail in Appendix D of the WRC Report No 945/1/02 (Annandale *et. al.* 2002).

The interval between subsequent heat dissipation measurements should be long enough to permit the heat pulse to dissipate without affecting the following reading. A minimum of 3 min was recommended between readings in order to permit block temperature to re-equilibrate (Jovanovic and Annandale, 1997). In the peach field trial, sample readings were taken every hour.

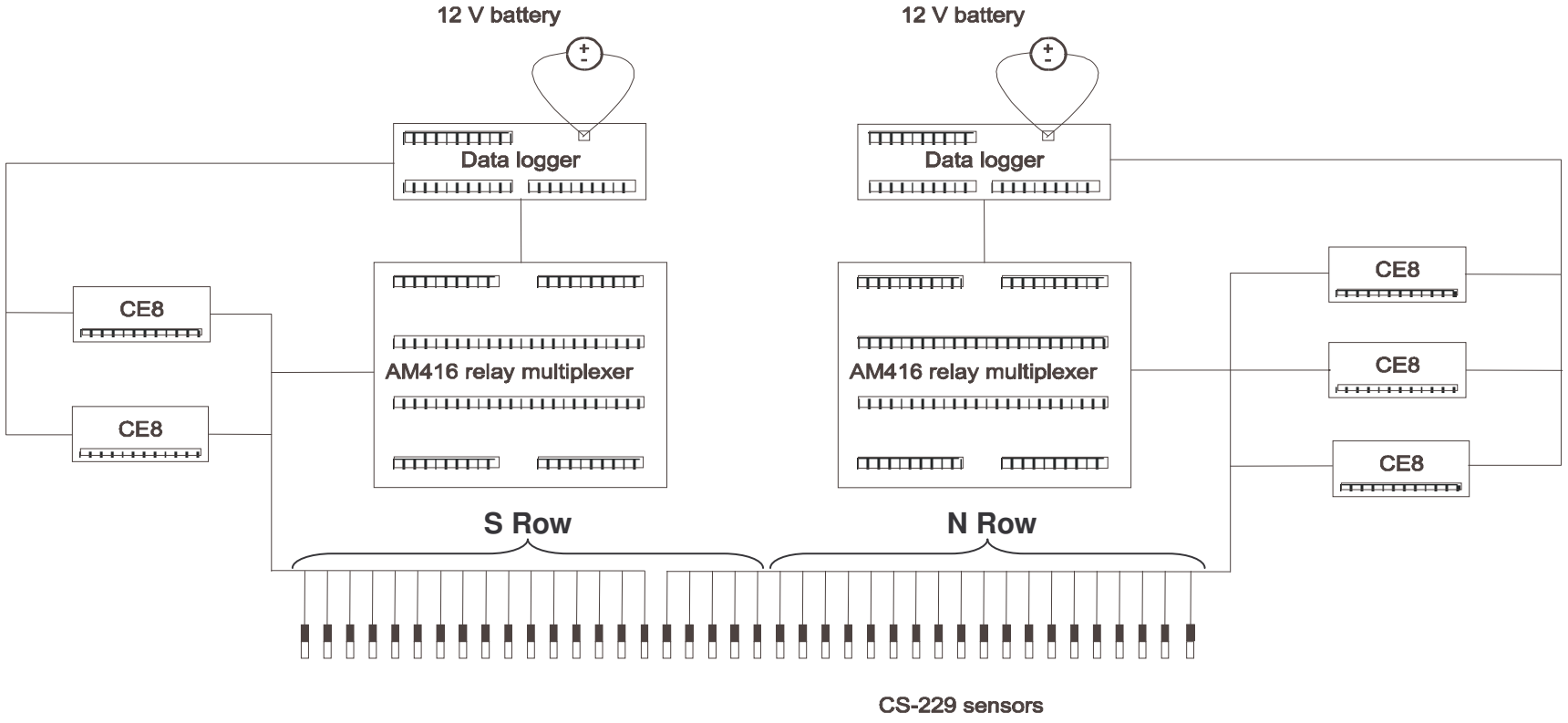

Figure 2.8. Diagrammatic representation of the Heat Dissipation Sensor (HDS) system used in the Hatfield field trial.

2.1.6.3 Soil water content

Neutron water meter

On 18 October 1996, black PVC access tubes for neutron water meter (NWM) measurements were installed in the lysimeters. In two sites in the portion of the orchard surrounding the lysimeters, sets of 12 similar access tubes were installed in a row at right angles to the tree row in such a manner that the soil water content (SWC) across the whole area could be monitored. During winter 1997 a further two sets of 12 tubes were installed. Thus it was possible to monitor the SWC across the tree rows in four sites surrounding the lysimeters. Soil water content was measured with a NWM, model 503DR CPN Hydroprobe which had been calibrated for the site. Initially, readings were taken daily when a series of other measurements were made to monitor the water status of the trees. From February 1997, the SWC was monitored twice weekly.

To determine soil water content (θ) with the NWM a series of standard counts were done in the orchard with the NWM placed on top of the NWM carrying case. The mean (Ct_{Std}) of these readings was determined and used as the denominator to establish a count ratio (Cr_{di}) for each depth interval (Δd_i) at which NWM readings were taken. These count ratios were then converted to the soil water content (θ_{di}) per depth interval and profile water content (θ_p) for each access tube (t_j) using the following equations:

$$Cr_{di} = \frac{Ct_{di}}{Ct_{Std}} \qquad (2.1.7)$$

$$\theta_{di} = \frac{\{(0.194 * Cr_{di}) + 0.015\}}{\Delta d_i} \qquad (2.1.8)$$

$$\theta_p = \sum_{1}^{i} \theta_{di} \qquad (2.1.9)$$

The value of the slope (0.194 m m^{-1}) and constant (0.015 m m^{-1}) in equation 2.1.8 were determined by calibration using test sites close to the trial. The water contents were determined by destructive sampling of the calibration sites and gravimetric determinations. The depth intervals (Δd_i), position of NWM counts and basic scheme used to determine θ for each NWM access tube is depicted in Figure 2.9. In this case, Δd = 0.2m.

The water deficit (θ_{Di}) for each Δd_i was determined and these values summed to establish the soil water deficit (SWD) using the following equations:

$$\theta_{Di} = \frac{\theta fc_{di} - \theta_{di}}{\Delta d_i} \qquad (2.1.10)$$

$$SWD = \sum_{1}^{i} \theta_{Di} \qquad (2.1.11)$$

Where θ_{fcdi} is the FC for each depth interval and are given in Table 2.1.

Table 2.1 Field capacity water content per depth interval for soil at Hatfield peach trial site

Depth interval	Depth (m)	Field Capacity (m m^{-1})
Δd_1	0 to 0.2	0.179
Δd_2	0.2 to 0.4	0.210
Δd_3	0.4 to 0.6	0.216
Δd_4	0.6 to 0.8	0.218
Δd_5	0.8 to 1.0	0.220
Δd_6	1.0 to 1.2	0.224

Since the access tubes were not installed equidistantly across the row, values for each tube represents differing soil volumes and thus differing water reserves. So when determining the water status for the whole row, the value for each access tube must have a weighting factor so that it contributes the correct proportion to the whole row. The scheme used to calculate these weighting factors for each tube (wt_j) is presented in Figure 2.10. Based on this figure, the weighting factor (wt_j) for tube j is:

$$wt_j = \frac{\left[\{(l_j - l_{j-1}) * 0.5\} + \{(l_{j+1} - l) * 0.5\}\right]}{l_r} \qquad (2.1.12)$$

Where l is the distance from the tree trunk to the access tube t_j and l_r is width of the whole row, in this case 4.5 m. When l_{j+1} is the centre of the inter-row, i.e. $l_{j+1} = 0.5 * l_r$, then the following equation is used:

$$wt_j = \frac{\left[\{(l_j - l_{j-1}) * 0.5\} + \{(l_{j+1} - l)\}\right]}{l_r} \qquad (2.1.13)$$

The respective weighting factors and access tube distance (l_j) from the tree trunk for the different access tubes are presented in Table 2.2.

Table 2.2 Weighting factors used in calculate respective NWM access tube contribution to the water status of the whole row at Hatfield peach trial site

NWM Access tube	Distance from trunk (m)	Weighting factor
wt_0	0	0.073
wt_1	0.33	0.074
wt_2	0.66	0.074
wt_3	1.0	0.092
wt_4	1.5	0.111
wt_5	2	0.113

Soil water content was also measured at two locations outside the experimental plot. One neutron probe access tube was set up about 10 m on the North side, the other about 10 m on the South side outside the plot. This was done to monitor possible lateral movement of water from and towards the experimental plot. Measurements from these points indicated negligible lateral movement into the trial site since they consistently recorded much lower water contents.

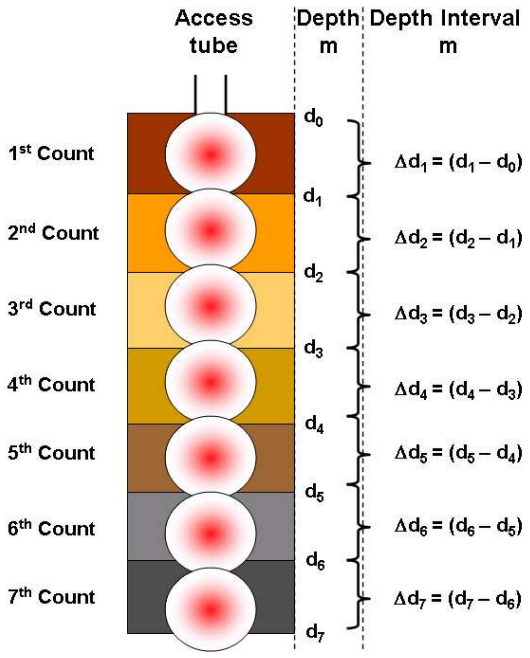

Figure 2.9. Dimensions used to determine profile volumetric water (θ) content from NWM measurements.

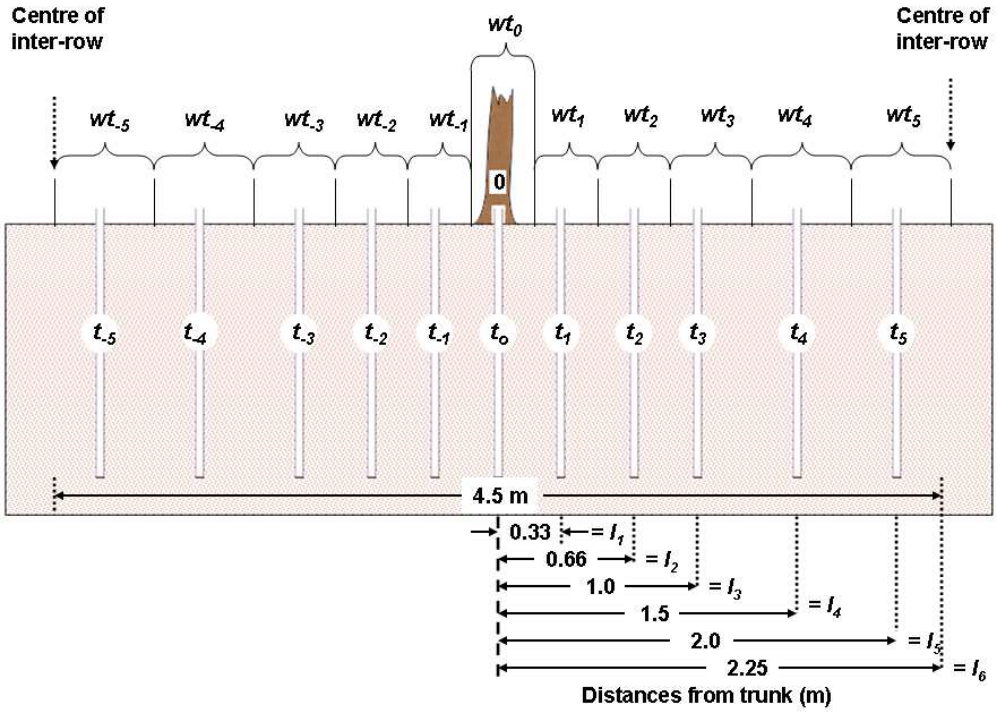

Figure 2.10. Dimensions used to establish weighting factors (wt_j) for each NWM access tube (t_j) to correctly establish water status for the whole row having a width of 4.5 m.

Time-domain reflectometry

Volumetric soil water content in two dimensions was also measured with a time-domain reflectometry system (Topp *et al.*, 1980). This is a relatively new technique that has been successfully employed in similar applications. Initially, the system set up at the Hatfield experimental farm, consisted of the following components:

i) The Tektronix 1502C metallic cable tester is a reflectometer used as a source to send very short time-rise electromagnetic pulses to the probes, and to collect a signal (waveform), which is a reflection of the applied pulse.

ii) Six SDMX50 eight to one, 50 ohm, coax multiplexers with BNC connectors. These multiplexers are used to connect additional multiplexers or probes to the 1502C cable tester.

iii) Forty 30 cm three-rod (unbalanced design) CS605 soil probes. A BNC connector on the RG-58 coax cable of the probe attaches directly to the SDMX50.

iv) TDR 50 ohm RG-8 coax cables with BNC connectors. These cables are used for connecting cable tester and multiplexers.

v) WinTDR 98 v. 4.0 software (Or, Fischer, Hubner and Wrath. 1998) for controlling the measurement sequence, applying algorithms for calculating water content and storing the resulting data.

vi) A computer with the software WinTDR 98 v. 4.0 used for controlling the system, analysing waveforms and storing data.

A scheme of the TDR system used is shown in Figure 2.13.

The cable tester, multiplexers and computer require a power supply. The 1502C and computer with software were housed together in an enclosure, and supplied with 220 V AC through an extension cable. Each SDMX50 multiplexer had its own enclosure. The multiplexers were powered with a 12 V battery serially.

The 1502C was connected to, and controlled by the computer with a 25 to 9 pin cable. The computer software was the WinTDR 98 v. 4.0. This is a Windows 3.1x / Windows 95 based program used to measure the volumetric water content and electrical conductivity of soils by controlling the Tektronix 1502B or 1502C time-domain reflectometry cable tester, and multiplexers if present. Minimum requirements for the computer are 66 MHz 486 processor, VGA display, 5 Mb of hard disk space, and a Windows environment. The software was developed by Or *et al*. (1998), and it was downloaded from the Utah State University Web Site (USU Soil Physics Group) along with the user's guide.

The SDMX50 multiplexers include eight multiplexed coaxial connections and one common. The eight multiplexed connections were used to connect additional higher level multiplexers or probes, whilst the common connection was used to connect to the 1502C or to lower level multiplexers. The SDMX50 multiplexers are Synchronous Devices for Measurement (SDM). The computer communicates with these devices via a parallel port. Addresses set in the multiplexers allowed the 1502C-computer system to communicate with the correct device. The allocation of the correct address was done by positioning jumpers (hardware switches) on the circuit board. There are two jumpers for each multiplexer. The jumpers are labelled MSD for Most Significant Digit and LSD for Least Significant Digit. Each jumper has four pairs of pins. Depending which pair of pins is connected to the jumper, the digit can have the value of 0, 1, 2, or 3. A summary of the SDMX50 address allocation for the system used, is given in Figure 2.13. The 1502C and the computer are labelled level 0. The multiplexer with its input connected to the coax cable from the 1502C is level 1, and level 2 multiplexers (five of them) are connected to the level 1 multiplexer. The computer is connected to the control ports of the level 1 multiplexer with a communication cable carrying address and data information. The other multiplexers are wired serially. The communication cable is linked according to the set-up given by Or *et al*. (1998) (Figure 2.13). Particular care was employed

with this set-up, as multiplexers and computer parallel ports could be damaged due to incorrect wiring.

The pulse generated by the 1502C and its reflection are subject to distortion during travel between the 1502C and TDR probe. Connectors, coax cables and multiplexers connecting the probes to the reflectometer have a characteristic impedance resulting in both resistive and reactive losses. Distortion of the waveform caused by this impedance can introduce error into the water content determination. The TDR system used in this trial was designed to ensure correct probe impedance giving robust reflections. This was done by minimising cable length and by using low attenuation RG-8 coax cable. The SDMX50 multiplexers and CS605 probes are designed to minimise signal attenuation, interference and delay in order to optimise accuracy of measurement. An RG-8 coax cable connected the 1502C and the common connection of the level 1 SDMX50 multiplexer. Five RG-8 coax cables were used to connect the level 1 SDMX50 to the five level 2 SDMX50 multiplexers (Figure 2.13).

The CS605 probes are the sensors of the system. They are made of a block of epoxy, which holds three rods rigidly spaced. The probes act as a wave guide extension on the end of coaxial cable and provide a reflection that is related to the change in impedance. The impedance value is related to the geometrical configuration of the probe (size and spacing of rods), and also inversely related to the dielectric constant of the surrounding material. A change in volumetric water content of the medium surrounding the probe causes a change in the dielectric constant. This is seen as a change in probe impedance, which affects the shape of the reflection. The shape of the reflection contains information used to determine water content with WinTDR 98 v. 4.0. The probes were labelled, and pressed into the soil with the rods at the same depth. The site of each probe is shown schematically in Figure 2.2. The BNC connector of the 50 ohm RG-58 coax cable of the probes connected directly to the level 2 SDMX50 multiplexers (Figure 2.13).

Measurements were taken twice weekly. The output included dielectric constant of the medium and the volumetric soil water content obtained by analysing the waveform of each probe with WinTDR 98 v. 4.0. As surface waves propagate along TDR probes buried in soil, the signal energy is attenuated in proportion to the electrical conductivity along the travel path. This proportional reduction in signal voltage serves as a basis for the measurement of bulk soil electrical conductivity that is largely determined by soil water content. A laboratory calibration for impedance is, however, required for each probe separately in order to accurately estimate the electrical conductivity of the soil solution. However, since the measurement of electrical conductivity was not essential for the purpose of this study, the probes were not calibrated for impedance before being installed in the soil.

From September 2000, the TDR system was changed. Volumetric soil water content data were recorded at four hourly intervals by making use of a CR10X data-logger (Campbell Scientific Inc., Utah, Logan, USA), a Tektronix 1502C cable tester and SDMX50 multiplexers.

Figure 2.11. Installing HDS and TDR sensors in clementine hedgerow at Syferkuil.

Figure 2.12. Completed installation of HDS and TDR sensors and control units in the clementine hedgerow at Syferkuil.

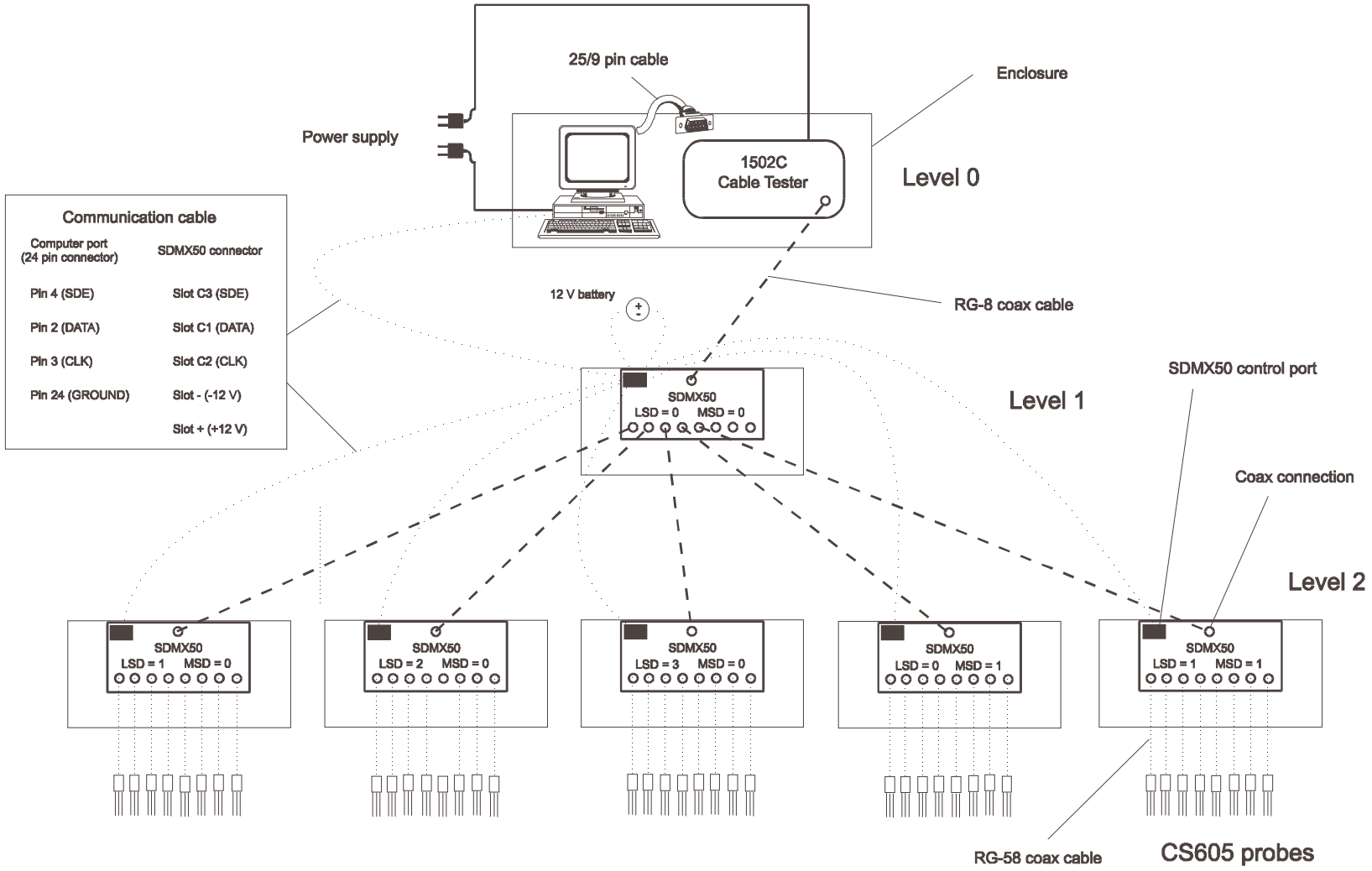

Figure 2.13. Diagrammatic representation of the Time Domain Reflectometry (TDR) system used in the field trial.

2.1.7 Plant measurements

The following plant measurements were made:

- Root distribution by taking soil core samples and washing out roots to determine root length;
- Canopy solar radiation interception with tube solarimeters;
- Leaf area index and density; and
- Canopy size and row orientation.

2.1.7.1 Root distribution

During the winter dormant period, when the soil water measurement instrumentation was installed, core samples were taken at regular intervals across the tree row/inter-row and at specific depths for root length density determinations. These samples were analysed by Dr T Fyfield (Agriculture Research Council - Institute of Soil, Climate and Water, Pretoria).

Roots were washed out of the soil cores using ARC-ISCW's root washing facility at Roodeplaat. After collection in a fine mesh sieve, the debris and obvious weed and dead tree roots were removed and the remaining tree roots were air-dried. Root length was then determined using a Geotron WLM1 Root Length Meter. Root length density was calculated per 200 mm depth layer by dividing the total root length by the volume of the soil core.

2.1.7.2 Canopy radiation interception

Seven Delta-T tube solarimeters (Delta-T Devices Ltd, Burwell, Cambridge, England) were installed across the tree row to measure solar radiation penetration through the canopy at different distances from the row. The tube solarimeters were set up parallel to the tree row. This was done at different times during the course of the trial in order to collect data for the evaluation of the two-dimensional canopy radiant interception model. The tube solarimeters were connected to a CR10X data-logger and used to record total solar radiation at specified time intervals. The programme used to control these sensors is presented in Appendix A.4.

The Delta-T tube solarimeters were regularly serviced during the course of the trial. This involved dismantling some and cleaning glass tubes, repainting checker bar if required, and then reassembly. Others just required exterior cleaning of glass tubes. Where required, some were re-charged with dry air. This involved connecting the solarimeters to an air-drying column filled with dry silica gel and flushing the solarimeters with dry air for 48 hours. All the solarimeters were regularly re-calibrated against a Precision Eppley thermopile pyranometer. The programme used to calibrate these sensors is presented in Appendix A.13.

2.1.7.3 Leaf area index and density

Leaf area index (LAI) was measured using an LAI-2000 plant canopy analyser (LI-COR Inc., Lincoln, Nebraska, USA). This measurement was done by activating detector rings 2, 3 and 4 (i.e. switching off rings 1 and 5). Ring 1 is excluded to reduce effects of solid objects immediately above the fish eye, whilst excluding ring 5 reduces the influence of the tree trunk and open spaces under the canopy. While taking measurements, the LAI-2000 optical sensor was fitted with a 45° view cap (i.e. black-out 315º) to restrict the field-of-view within the tree row. The field-of-view was aimed at measuring the LAI of only the canopy portion of the tree row and excluding the inter-row region. Figure 2.19 shows how the unit is positioned to take under-canopy readings. Measurements were only taken under conditions of diffuse radiation, i.e. before sunrise, after sunset or when uniform cloud cover blocked out direct solar radiation.

Leaf area density (LAD) was determined by converting leaf area index values to leaf area (LAb, m^2 leaf) per canopy base unit area (Acb, m^2 soil surface) as follows:

$$LAb = LAI * Acb \ (m^2 \text{ leaf } m^{-2} \text{ soil surface}) \qquad (2.1.14)$$

The canopy base unit area (Acb*)* is the measured width of the tree row canopy multiplied by a unit row length of 1 m. Once the LA per m of canopy length is known, it is converted to LAD by:

$$LAD = LAb / Vc \ (m^2 \text{ leaf } m^{-3} \text{ canopy}) \qquad (2.1.15)$$

The canopy unit volume (Vc) is the cross-sectional area of the hedge-row canopy multiplied by a unit row length of 1 m. The cross-sectional area of the canopy can either be determined using the formula for the area of an ellipse ($A = \pi a c$; a = half the width and c = half the height) or summation of calculated areas of trigonometric sub-units of the cross-section.

2.1.7.4 Canopy size and row orientation

Canopy dimensions (height and width) were measured with a calibrated 2 m rod and tape measure. These measurements were done as and when required to reflect the changes in canopy dimensions through the growing season. In the case of the deciduous hedgerow canopy that increased its dimensions quickly it was necessary to do frequent measurements (weekly) while the citrus canopy developed much slower so the canopy dimensions were valid for longer periods (monthly). Row orientation was determined with a compass. The reading of the compass was corrected by 15°E to account for magnetic declination from true North.

2.1.8 Leucaena trial

An additional field trial was carried out at the Hatfield experimental station on Leuceaena (*Leucaena leucocephela*) trees, in order to test the two-dimensional radiant interception model for different environmental conditions (tree size and shape as well as row orientation).

Two single rows of leucaena were used with spacing between trees ~ 0.5 m. The row orientation was in an N to S axis (10° - 190°) (Figure 2.15) and E to W axis (10° - 280°) (Figure 2.16). Refer to the end of section 1.1.1 for the convention with respect to characterizing row orientation within the model.

Canopy interception for total solar radiation was measured with tube solarimeters installed at different distances from the row, on both sides of the row. The tube solarimeters were set up parallel to the tree row. This was done for one week for each row.

Leaf area index and density, canopy size as well as row orientation were measured adopting the same method used in the peach trial at Hatfield.

2.2 Experimental set-up at the University of the North

2.2.1 Location and environmental characteristics

The field trial at Syferkuil experimental farm (University of the North) was located 30 km East of Pietersburg (23°51' S; 29°40' E; alt. 1250 m), in the summer rainfall region.

The soil in the trial site is a 1 m deep sandy loam Hutton (Soil classification working group, 1991) or Ferralsol (FAO, 1998). Hard plinthic formations are found below 1 m.

2.2.2 Orchard lay-out, irrigation and cultivation practices

Clementine trees (*Citrus reticulata* cv. *Nules Clementine*) on Swingle citromelo (*Poncirus trifoliate* x *Citrus paradisi*) rootstock were planted in 1985, in a 7.5 x 3.5 m hedgerow pattern. The tree row orientation is in a SE to NW axis (135° - 315°). Grass in the inter-row spacing was mowed regularly to maintain a 3.5 m wide grass sod (10 to 20 cm tall). Herbicides used to control any weed growth under the canopy (~ 4 m width) as and when necessary. Fertilisation and irrigation were applied as required until the beginning of the trial so the trees were healthy with no nutritional or other stress. The irrigation system made use of micro-jets with a wetted diameter of 1.5 m. No insecticide was applied as the orchard was under biological control.

Figure 2.14. View of Clementine hedgerow and tube solarimeter in inter-row. Note the jagged shade line.

Figure 2.15. View of Leucaena N-S axis hedgerow and tube solarimeters. This is with full canopy (LAD = 1.55 m^2 m^{-3}) with afternoon sunshine.

Figure 2.16. View of Leucaena E-W axis hedgerow and tube solarimeters. This is with totally stripped canopy (LAD = 0.39 m^2 m^{-3}) with late afternoon sunshine.

Figure 2.17. View of valencia tramline hedgerow with tube solarimeter and AWS in middle of tramline.

Figure 2.18. View of valencia tramline hedgerow and tube solarimeters installed under canopy to record solar irradiance under tramline canopy.

Figure 2.19. View of LAI-2000 Plant Canopy Analyser (PCA) optical sensor with 45º view cap to blank out 315º field-of-view.

2.2.3 Weather monitoring

An automatic weather station was set up, similar to that installed at the Hatfield experimental farm. Air temperature, relative humidity, solar radiation, wind speed and rainfall were monitored and recorded hourly with a CR10X data-logger. The programme used to control these sensors is presented in Appendix A.2.

2.2.4 Soil measurements

An intensive monitoring site was established, similar to those set up at the Hatfield experimental station. Equipment for measurement of volumetric soil water content and potential was installed on 13 to14 October 1999. Twenty-eight heat dissipation sensors (HDS) and time domain reflectometry (TDR) probes were buried in the soil at nodes located on a grid across the row (similar to that depicted in Figure 2.2). The installation procedure is shown in Figure 2.11 and the final installation is shown in Figure 2.12. The depths were 0.06, 0.26, 0.56 and 0.86 m, i.e at the same depths as at Hatfield. Sensors and probes were installed in the row between two trees, and at distances of 1.25, 2.5 and 3.75 m from the row, on both sides of the row. These distances are not the same as Hatfield as the hedgerow spacing was 7.5 m wide compared to 4.5 m used in the peach hedgerows at Hatfield. The TDR probes were pressed into the soil with the rods parallel to the surface.

Soil temperature and matric potential data from heat dissipation sensors were collected and stored with AM416 multiplexers and CR10X loggers. Soil water content data from TDR probes were collected and stored with SDMX50 coax multiplexers, a data-logger and a 1502C Tektronix cable tester. HDS sensors and TDR probes were installed at a few centimetres from each other. This enabled the determination of soil water retention functions from measurement of matric potential and water content. The programmes used to control these sensors are presented in Appendix A.7 (HDS) and A.10 (TDR).

During the installation of HDS and TDR sensors, soil samples were collected at the same node depths and distances from the tree row. The samples were used to determine bulk density, texture characteristics, as well as nutritional properties.

2.2.5 Plant measurements

During the installation of the intensive monitoring site, core samples were taken at regular intervals across the tree row/inter-row and at specific depths for root length density determinations. These samples were analysed by Dr T Fyfield (Agriculture Research Council - Institute of Soil, Climate and Water, Pretoria). The same method was used as for the core samples taken at the Hatfield experimental farm.

Canopy interception of total solar radiation was measured with tube solarimeters installed across the row between two trees, and at distances of 1.25, 2.5 and 3.75 m from the row, on both sides of the row (Figure 2.14). The tube solarimeters were set up parallel to the tree row. This was done at different times during the course of the trial in order to collect data for evaluation of the two-dimensional canopy radiant interception model. At the same site and time, line quantum sensors were installed to measure canopy interception of photosynthetically active radiation. The instruments were connected to a CR10X data-logger and used to record total solar radiation and photosynthetically active radiation at specified time intervals. The sensors were regularly serviced and calibrated. Leaf area density was measured with an LAI-2000 plant canopy analyzer.

2.3 Field trial at Brits

In order to test the two-dimensional radiant interception model for different environmental conditions (tree size and shape as well as row orientation), field trials were carried out on two commercial farms 15 km north of Brits (25°00'S, 27°46'E, alt. 1107 m).

On the first farm, Empress Mandarin (*Citrus reticulata* cv. *Empress*) were grown in hedgerows with a planting density of 4 x 4 m and row orientation in a SE to NW axis (145° - 325°). The second farm had Delta Valencia (*Citrus sinensis* [L.] cv. Osbeck) grown in a tramline pattern. The spacing was two rows 4 x 4 m with an 8 m gap and row orientation in a SE to NW axis (135° - 315°).

Canopy interception of total solar radiation was measured with tube solarimeters installed at different distances from the row, on both sides of the row. The tube solarimeters were set up parallel to the tree row. This was done for two weeks in each orchard. Figures 2.17 and 2.18 show the installed solarimeters under the tramline canopy while Figure 2.20 is a diagrammatic presentation of the cross-section of the tramline planting indicating the positioning the solarimeters and dimensions of the canopy.

The standard weather data (air temperature, relative humidity, solar radiation, wind speed and rainfall) were monitored and recorded hourly with an automatic weather station set-up in a short grass open area along-side the orchards. (Note: The AWS shown in Figure 2.17 was only a temporary set-up) This open area satisfied the requirements for a weather station site, i.e. sufficient fetch, short mowed grass and no interference from high tress etc.

Leaf area index and density, canopy size as well as row orientation were measured adopting the same method used in the field trial at Hatfield.

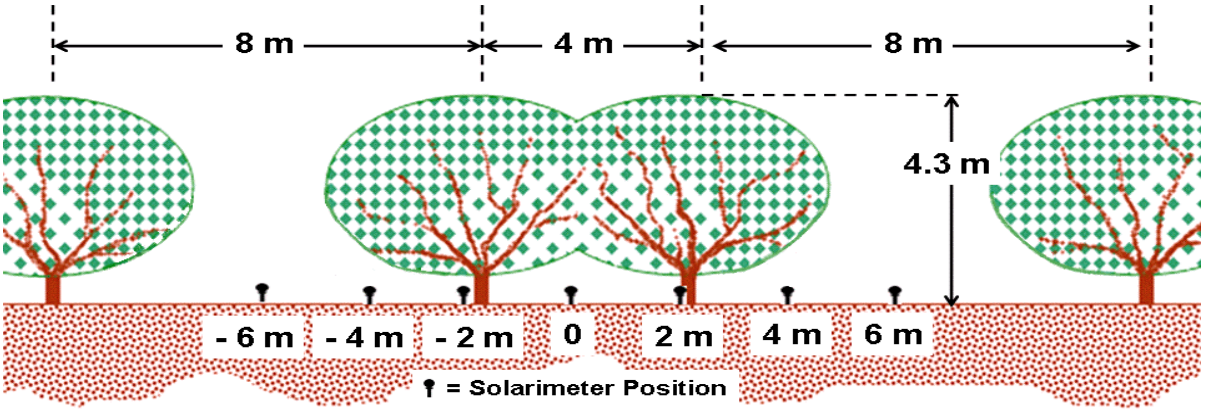

Figure 2.20. Diagrammatic representation of dimensions of the valencia tramline hedgerow at Brits showing the positioning of the solarimeters.

CHAPTER 3

MODELLING

3.1 Evaluation of the SWB model

The SWB model was tested according to the guidelines provided by CAMASE (1995). The verification of the model, *i.e.*:

i) inspection of the internal consistency of the model;
ii) software implementation;
iii) checking units used in the computer program;
iv) detection of violation of natural ranges of parameters and variables;
v) inspection of qualitative behaviour of the model and its implementation by checking whether the response of model output to changing values of a single parameter conforms to theoretical insights;
vi) on-line checks on mass conservation;

was reported in Annandale *et al.* (2002).

In this Chapter, comparison of model output with independent data sets of real world observations and sensitivity analysis are presented. An example of calibration of the simple quasi-2D FAO-based cascading model is presented for peaches (Section 3.2). This was done by adjusting some FAO crop factors such that the model prediction of soil water deficit was consistent with field measurements. The most important observations gathered in the field trials at Hatfield and Syferkuil, and relevant to the development of the SWB model, are also presented.

The two-dimensional energy interception sub-model was evaluated using independent data sets (Sections 3.3). The two-dimensional soil evaporation model evaluation was presented in Annandale *et al*. (2002) and is not included in this thesis. The two-dimensional soil water balance model integrates the interactions of the various components, as it uses the 2D energy interception and 2D soil evaporation sub-models to split evaporation and transpiration. The functionality of the entire model was then evaluated by comparing the output obtained with the two-dimensional soil water balance model to independent field measurement data (Section 3.4).

Scenario simulations were carried out to perform sensitivity analyses (Section 3.5). Scenarios were simulated by varying one input parameter and retaining the same values for the other inputs. Logical sensitivity analyses were performed to establish by inspection of output results whether the model is sensitive at all to changes in an input (factor screening).

This could indicate which input parameters need to be accurately measured or estimated. The sensitivity analyses also provided estimates of scenario effects in order to recommend the most suitable practices for improved water use efficiency under different environmental conditions. One should, however, be aware that the sensitivity to an input may depend on the particular set of values used for other inputs.

3.2 Calibration of the FAO-type model and field observations

The simple, quasi two-dimensional, cascading soil water balance model was calibrated using data from the peach trial at the Hatfield experimental station. In the process, FAO basal crop coefficients (Kcb) were determined for first and second leaf peach trees.

FAO basal crop coefficients were determined by plotting daily Kc values over time for the first two growing seasons of peach trees (Figures 4.1 and 4.2). The daily Kc value was calculated using evapotranspiration measurements from the lysimeters and the grass reference evapotranspiration calculated from weather data. The Kcb values for the various growth stages were determined by fitting an appropriate line through the lower values of Kcb, which are taken to reflect the conditions where the soil surface is dry (negligible evaporation from soil surface) and there is sufficient water not to restrict transpiration. The longer development period during the first season can be expected since it is necessary to develop the tree structure. The drop in actual evapotranspiration measured with lysimeters during the late stage of the first season was caused by water stress (Figure 3.1). The Kcb line during this late stage was estimated.

Simulations of soil water deficit (SWD) with the SWB model were then carried out and compared to measurements obtained with the neutron water meter (Figures 3.3a and 3.3b). The Kcb factors in Figures 3.1 and 3.2 were refined by fitting the simulations of soil water deficit to measured data points (Figures 3.3a and 3.3b).

The initial period of the first season was not well evaluated as too few measurements with the NWM were taken (Figure 3.3) while the experimental procedures were being developed. Thereafter, more measurements were available, which enabled a better evaluation of model predictions. Generally, there was good agreement between predicted and measured soil water balance. This should be expected since the calibration data came from the trial. A section of trees (20 m row length) was stressed in the period from 10 January 1997 to 20 February 1997 in order to check the reliability of SWB under limited water supply. Each of these sections included neutron water meter (NWM) measurement site facilities to monitor soil water status. Comparing the results from the NWM measurements and the SWB

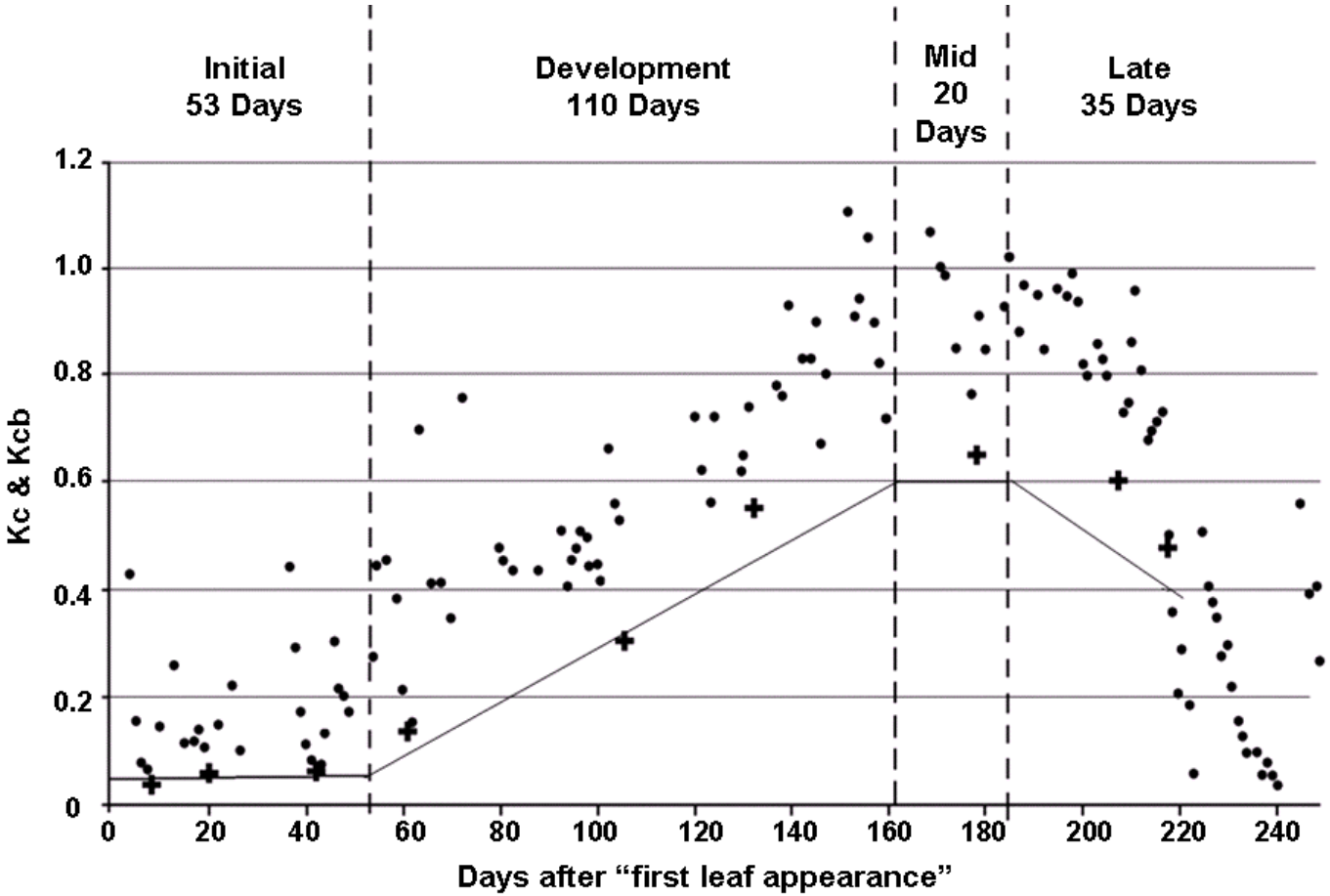

Figure 3.1. Daily Kc (dots) and Kcb (+ and line), as well as growth periods for first leaf season of peaches.

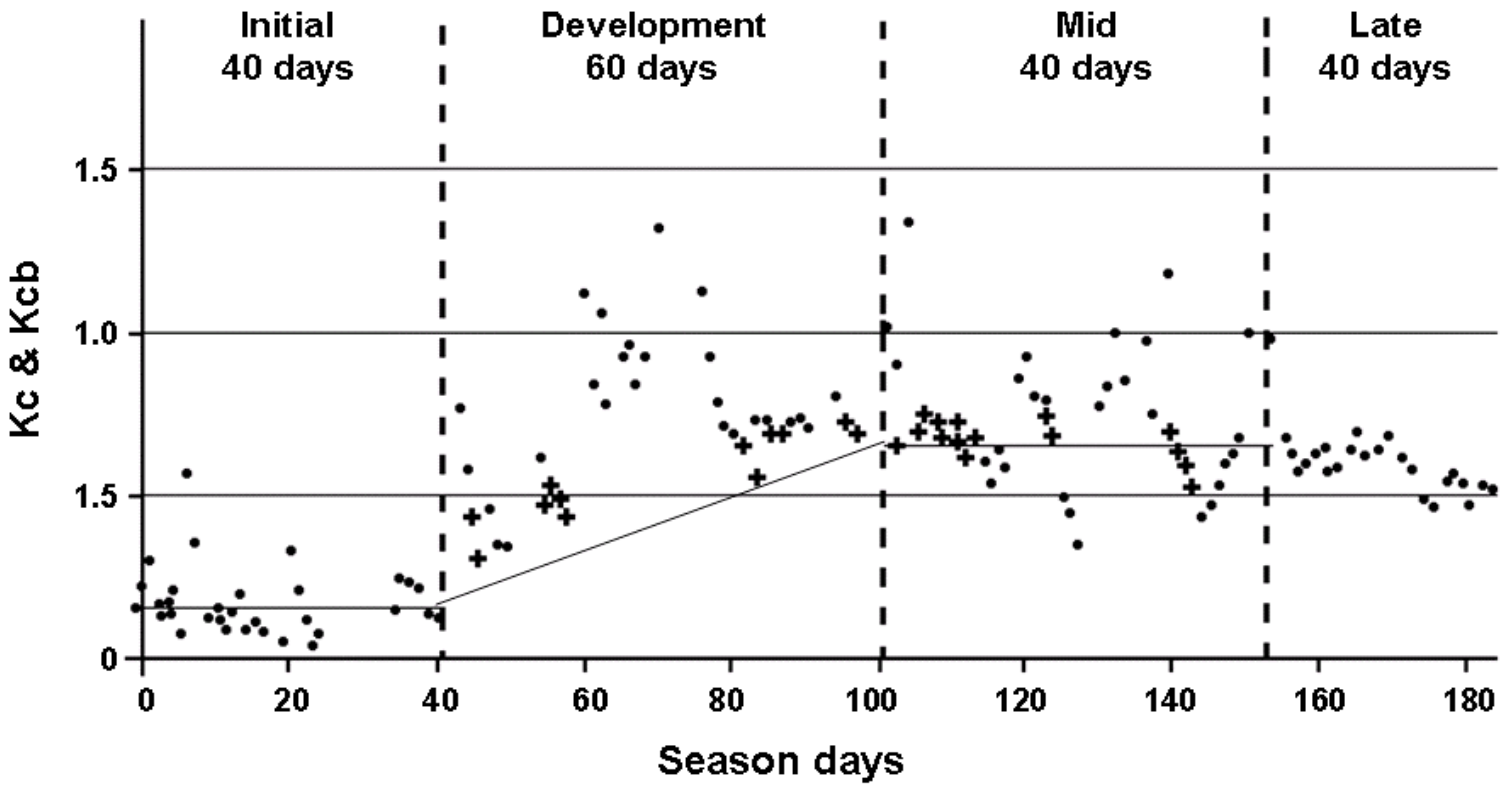

Figure 3.2. Daily Kc (dots) and Kcb (+ and Line), as well as growth periods for second leaf season of peaches.

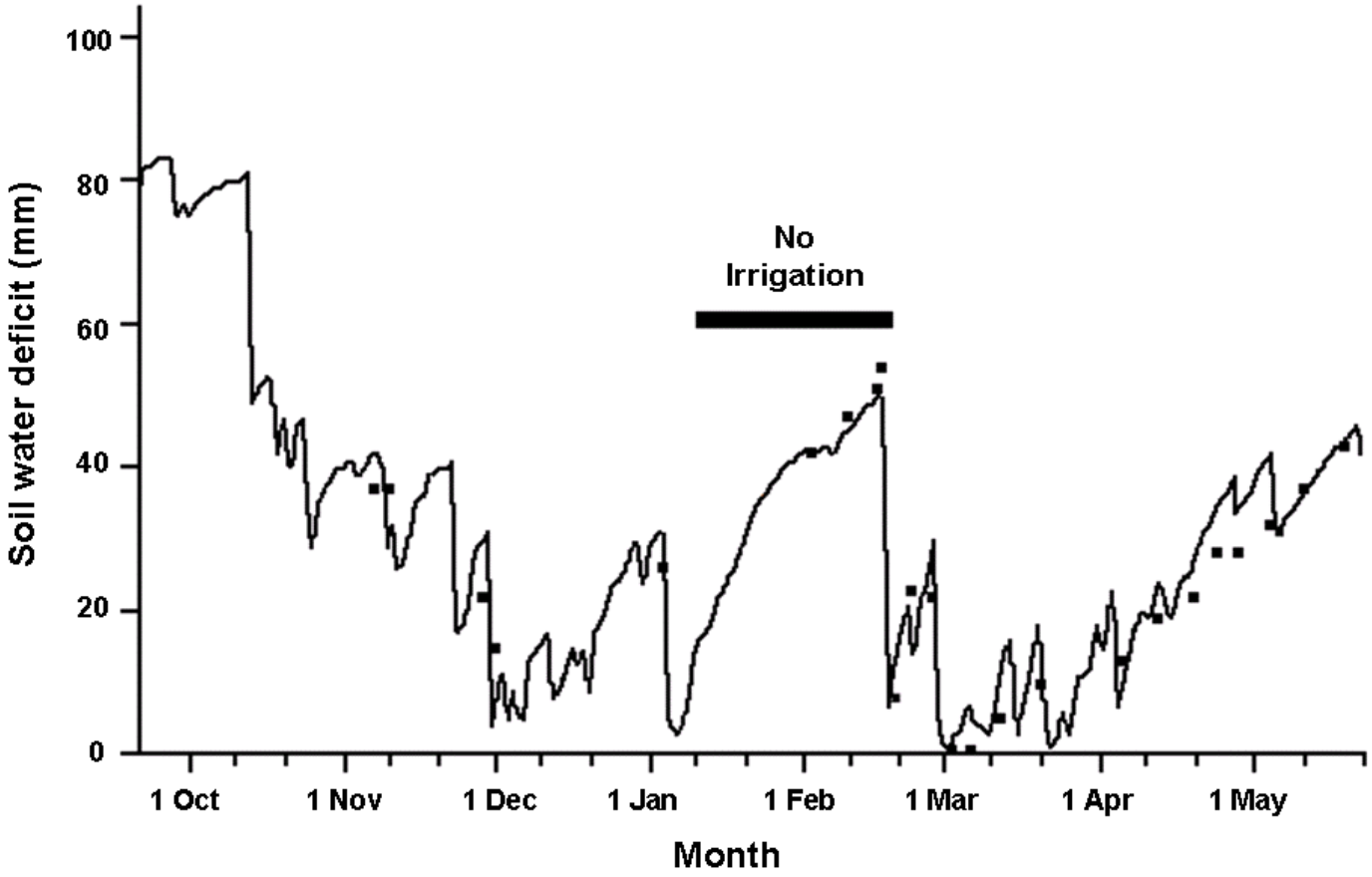

Figure 3.3a. Predicted (solid line) and measured (squares) soil water deficit for first leaf season of peaches (stress treatment).

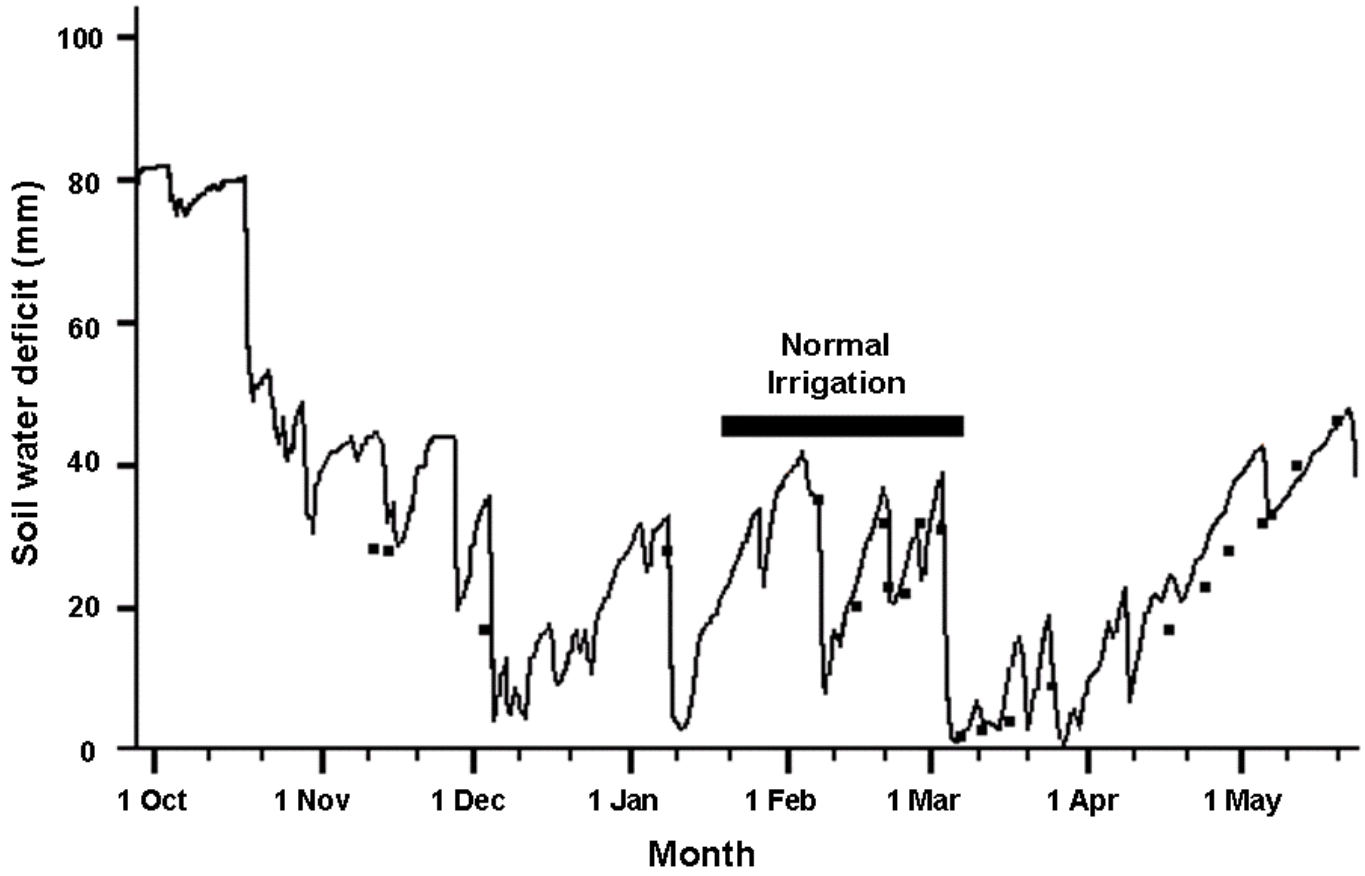

Figure 3.3b. Predicted (solid line) and measured (squares) soil water deficit for first leaf season of peaches (non-stressed treatment).

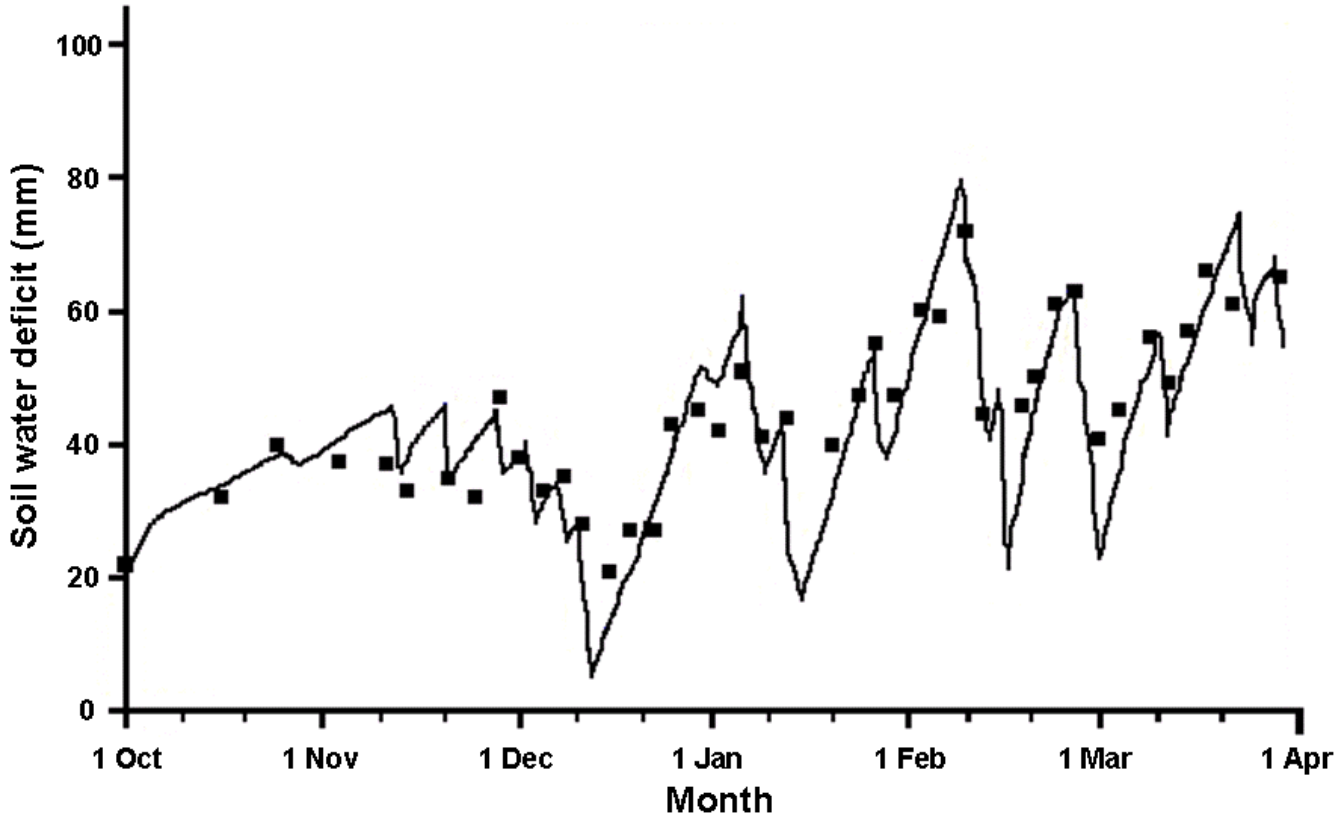

Figure 3.4. Predicted (solid line) and measured (squares) soil water deficit for second leaf season of peaches.

predictions it is seen that the model adequately predicted soil water deficit (SWD) for the stressed (Figure 3.3a) and non-stressed treatments (Figure 3.3b).

The accuracy of the predictions of SWD was evaluated by comparison with SWD determined from NWM measurements. When measured SWD for the whole area (tree row and inter-row) is used, the agreement between predicted and measured SWD is good (r^2 = 0.79) (Figure 3.5a). However, if measured SWD is taken only at the tree row centre (0 m from tree, Figure 3.5c) the agreement decreases (R^2 = 0.53). When one considers SWD measured at the inter-row centre (2 m from tree, Figure 3.5b) there is little agreement (r^2 = 0.33). The reduction in agreement between SWB predictions and actual values is due to the fact that irrigation is applied only under the tree canopy (i.e. near tree trunk) as well as a differing energy balance occurring in the inter-row region. It is thus vitally important to realise that in hedgerow plantings the whole area must be borne in mind when assessing soil water content. The practice of using single or restricted locality measurements, as utilised in agronomic crops, can be misleading in orchards. Orchardists that use single point measurements (e.g. only one tensiometer or NWM access tube arbitrarily placed under tree canopy) could be making large errors in their assessment of the water status of the hedgerow.

The reason for this is obviously the effect of the irrigation distribution, particularly when it is applied only under the tree canopy as illustrated in Figure 3.6. Soil water distribution is also effected by interception of rain by the canopy. Figure 3.7 shows how the percentage rainfall penetration differed for 5 separate rain events. For two of the five events the soil surface between – 1 and 0 m on the southern side of the hedgerow received ~140% of the rain while the corresponding distances on the northern side received only 80 % of the rainfall; a difference of 60 %!, In addition, with changes in canopy characteristics as the season progresses, there are changes in radiation interception by the canopy and the irradiance reaching the soil surface. Figures 3.8 and 3.9 highlight the variation in canopy radiation interception across the row as the season progresses. It is seen that in winter (4 July; DOY 185), when there is no tree canopy, the irradiance across the tree row is around 10 MJ $m^{-2}.d^{-1}$. Two months later (4 September; DOY 247), with the onset of spring, the daily irradiance has increased to around 17 MJ $m^{-2}.d^{-1}$ on the northern side of the hedge-row, whilst on the southern side, due to canopy development, soil irradiance has increased to only about 15 MJ $m^{-2}.d^{-1}$. In mid-summer (28 December, DOY 362), the irradiance in the inter-row region reaches 22.5 MJ $m^{-2}.d^{-1}$, whilst under the canopy the irradiance has decreased to about 2.5 MJ $m^{-2}.d^{-1}$. Figures 3.8 and 3.9 also show how the position of the shadow moves from ~ 1.3 m (Figure 3.8; DOY 185) to virtually under the tree on DOY 362 (Figure 3.9) as the sun elevation increases into summer.

University of Pretoria etd – Du Sautoy, N (2005)

A common assumption with tree crops is that rooting volume is of a similar magnitude to canopy volume. It was therefore interesting to investigate root length densities of peaches at Hatfield and of clementines at Syferkuil. As can be expected, the root length density decreased with depth both in the case of peaches and clementines (Figures 3.10 and 3.11). It was interesting to note the root length density across the tree row (Figures 3.10 and 3.11). There are at least as many, if not more roots in the inter-row region (i.e. in the 1 to 2 m distance from the tree trunk) than in the canopy drip area (0 to 1 m from tree trunk), in particular for peaches. It is common practice in hedgerow plantings to irrigate only under the tree canopy and not irrigate in the inter-row region at all. It must be noted that there are significant amounts of roots in the inter-row region, at least in areas receiving rainfall during the growing season, and thus this portion of the rooting volume must not be disregarded when assessing the contribution of rain to the water balance.

The resultant effect of the root length densities on the profile SWD across the hedgerow into the inter-row is depicted in Figure 3.12 for peaches with grass sod and bare soil in the inter-row area. This Figure depicts the change in SWD through one drying cycle during the development period. It is apparent that, during the 36 h after irrigation, most water was used from the wetted area. The presence or absence of a grass sod also had minimal influence on profile SWD which is to be expected since no irrigation water was applied in the inter-row.

The same effect was observed by analysing data of soil matric potential obtained with heat dissipation sensors. For example, in Figure 3.13, matric potential values decreased (became more negative) at two depths in the soil profile of peaches during a drying cycle after rain. This occurred both for grass sod and bare soil in the inter-row area. It is interesting to note that the top soil (6 cm depth) was wetter than the deeper layer (26 cm depth), as the rain was light and the wetting front did not reach 26 cm soil depth.

Figure 3.14. shows the volumetric soil water content across the row for different depths during a drying cycle of clementines at Syferkuil. The drying cycle started after the soil was wetted by heavy rain. It is evident that root water uptake occurred both from the wetted and non-wetted portion of the soil, due to an evenly distributed root system across the row (Figure 3.11). It is also interesting to note that even though the 56cm depth the matric potential is decreasing much slower than the upper layers, the matric potential is decreasing throughout the entire profile, not just the top layers.

The effect of the canopy absorbing solar energy is highlighted in the diurnal variation of soil temperature at a depth of 6 cm during summer is depicted in Figure 3.15 for peaches. It is seen that under the tree, soil temperature is around 19 to 20 ^{o}C at 06h00 and increases to

22 °C at 14h00. However, in the inter-row region, the 06h00 temperature is 24 °C and increases to 31 °C (grass-sod inter-row) and 33 °C (bare soil inter-row) at 14h00.

The above features, i.e. differing water use under differing water regimes and drastically differing soil temperatures, is a very clear indication in the vastly differing energy balances that occur in hedgerow plantings and the necessity to apply a 2-dimensional approach when analysing the energy and water balance for hedgerow plantings.

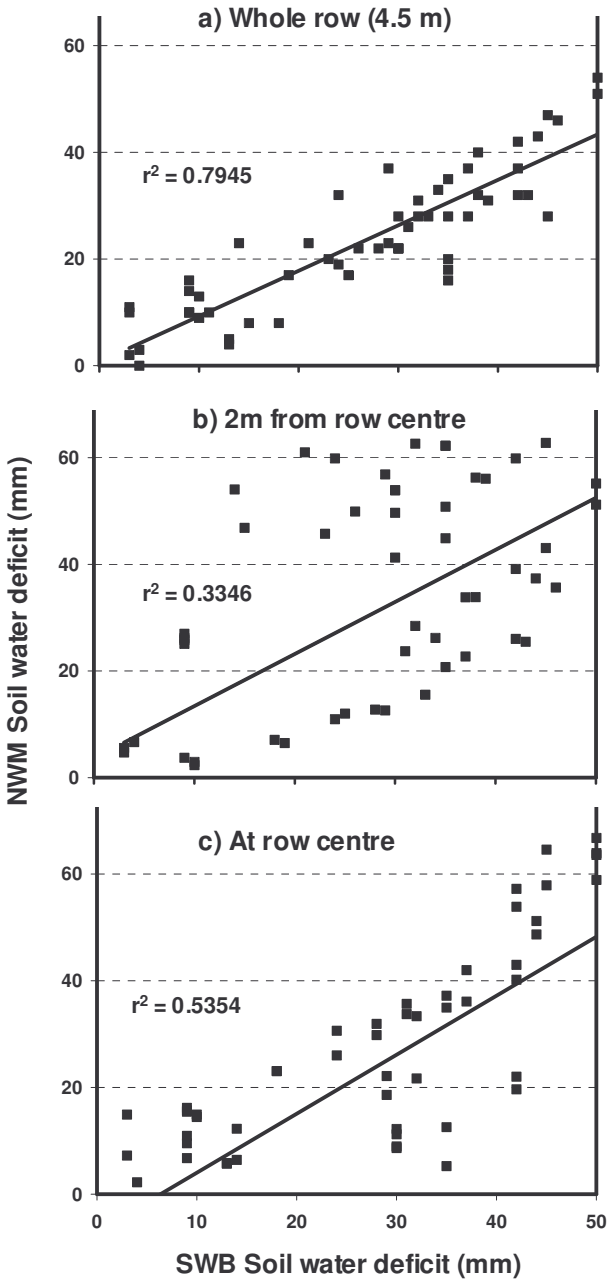

Figure 3.5. Soil water deficit predicted with the SWB model (SWB Soil water deficit) vs. deficit measured with the neutron water meter (NWM Soil water deficit). The comparison was carried out by using NWM measurements for the whole area, 2 m from tree and at the centre of row.

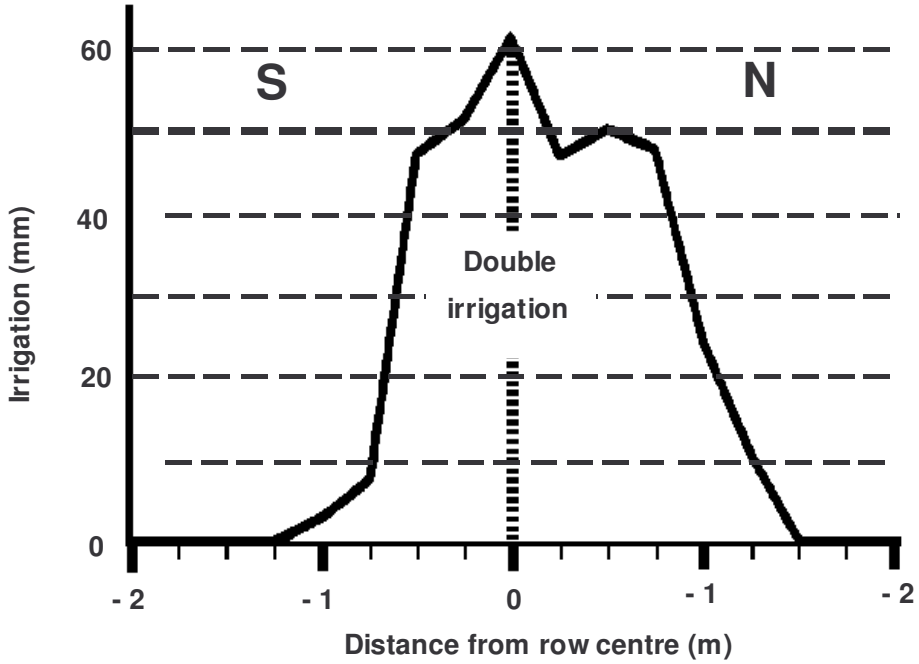

Figure 3.6. Distribution of irrigation application measured with a grid of rain gauges vs. distance from tree row.

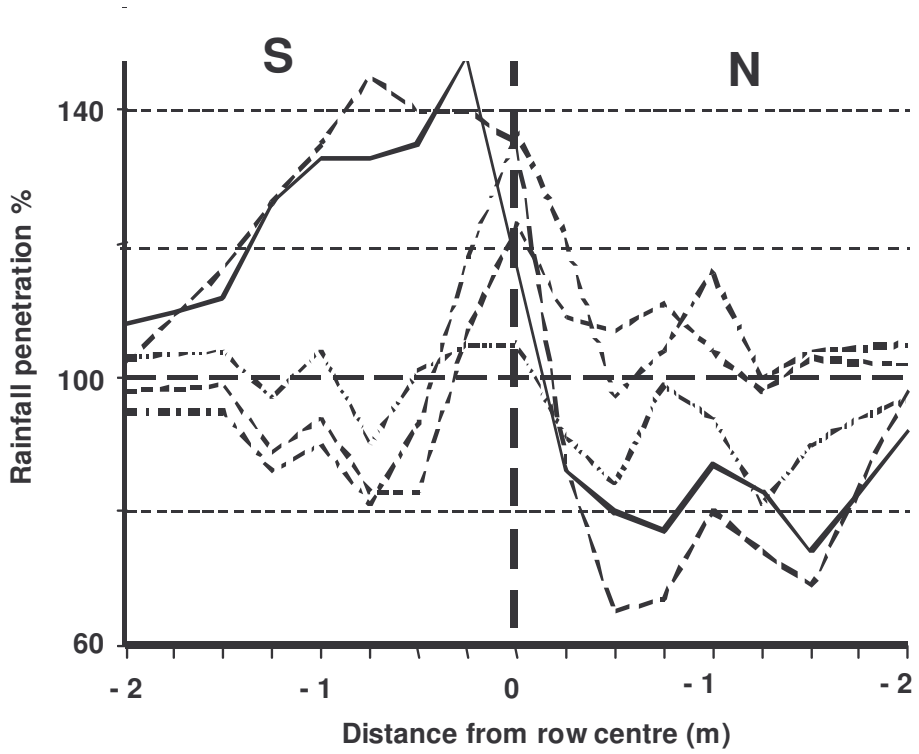

Figure 3.7. Distribution of % penetration of the peach canopy for five rainfall events; measured with a grid of rain gauges and expressed as % of recorded rainfall vs. distance from tree row.

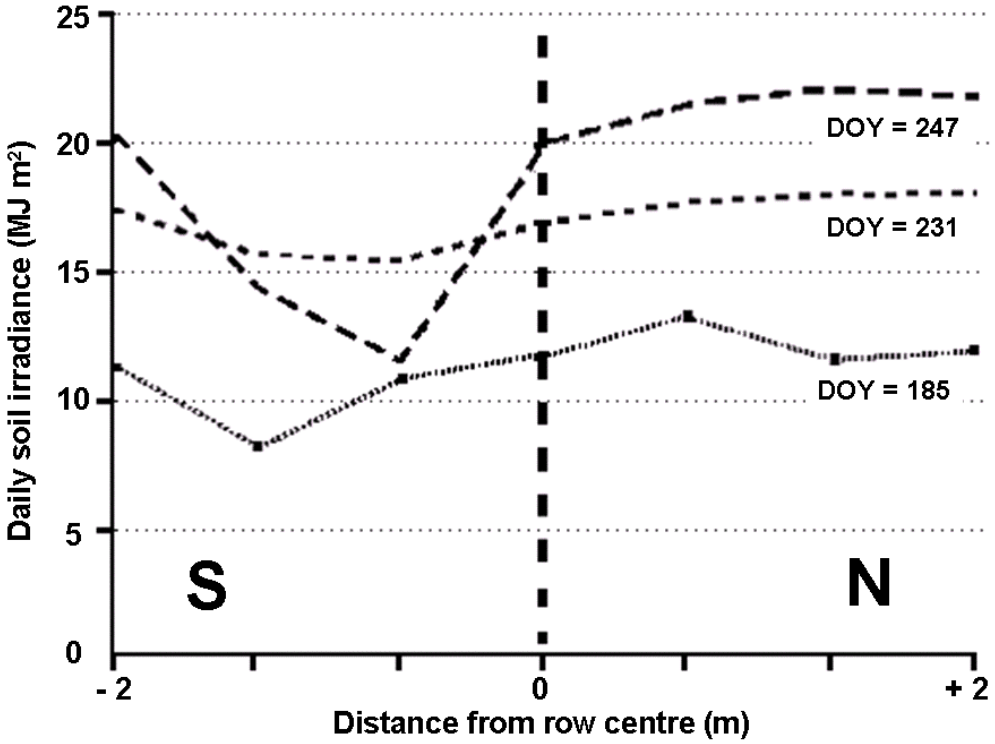

Figure 3.8. Variation of irradiance reaching the soil surface with distance from tree row for three full sunshine days during Spring (second leaf peach tree) (DOY = Day of year).

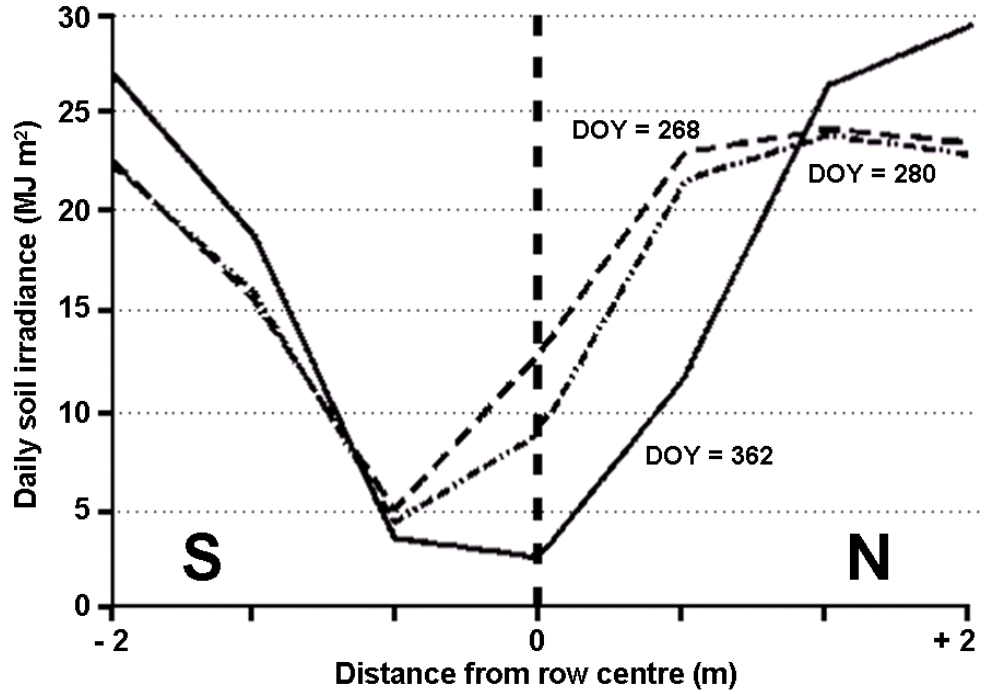

Figure 3.9. Variation of irradiance reaching the soil surface with distance from tree row for three full sunshine days during mid summer (second leaf peach tree) (DOY = Dat of year).

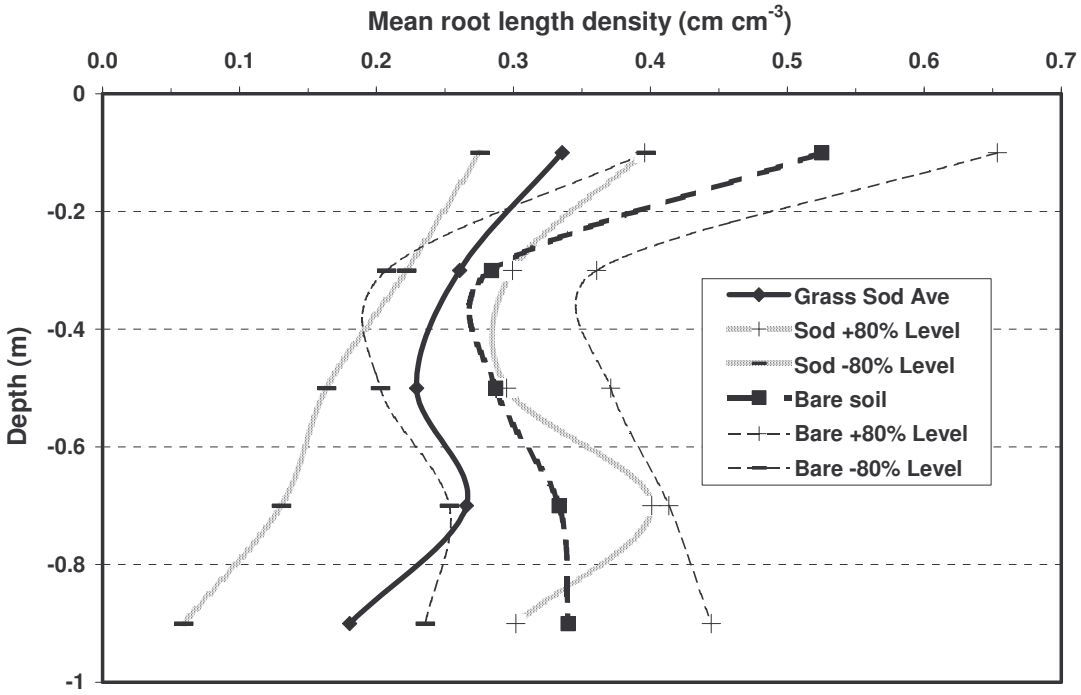

Figure 3.10a. Root length density with soil depth for peaches (Grass sod inter-row is solid lines while Bare soil inter-row is broken lines).

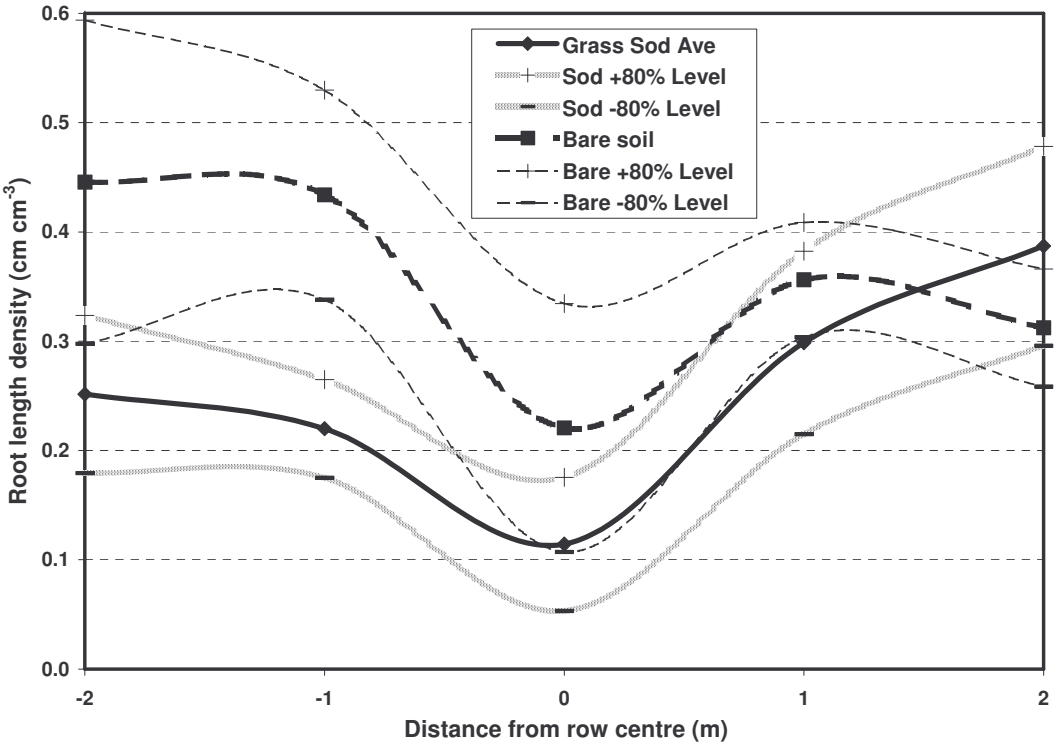

Figure 3.10b. Root length density with distance from the trunk for peaches (Grass sod inter-row is solid lines while Bare soil inter-row is broken lines).

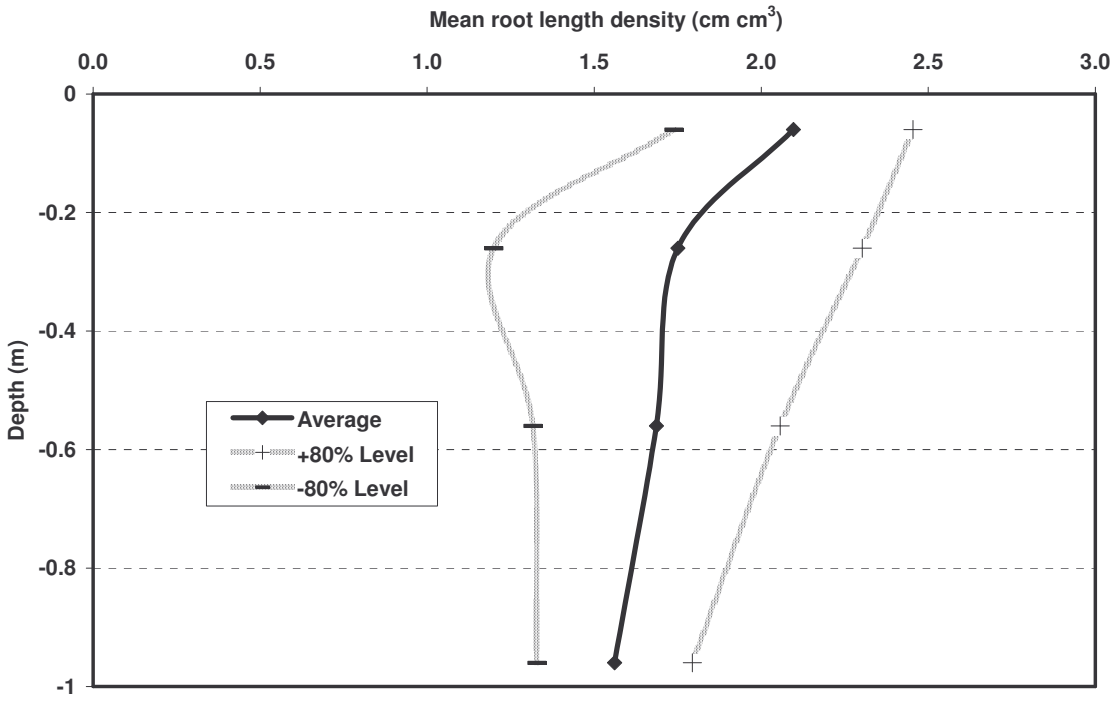

Figure 3.11a. Root length density with soil depth for clementines.

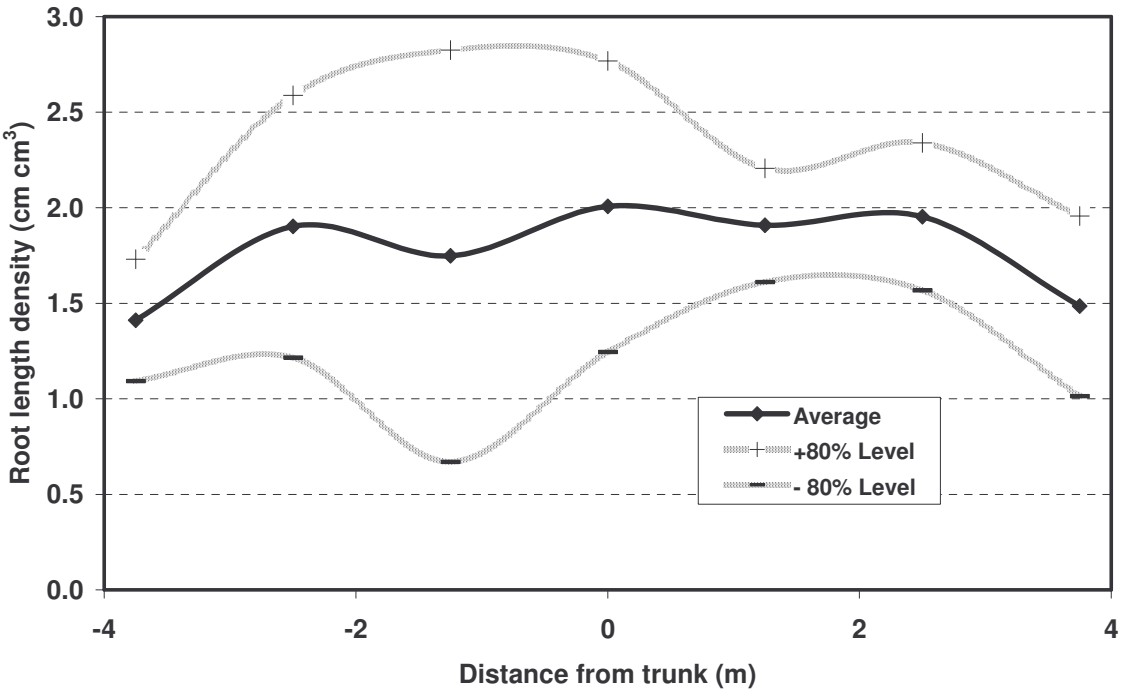

Figure 3.11b. Root length density with distance from the trunk for clementines.

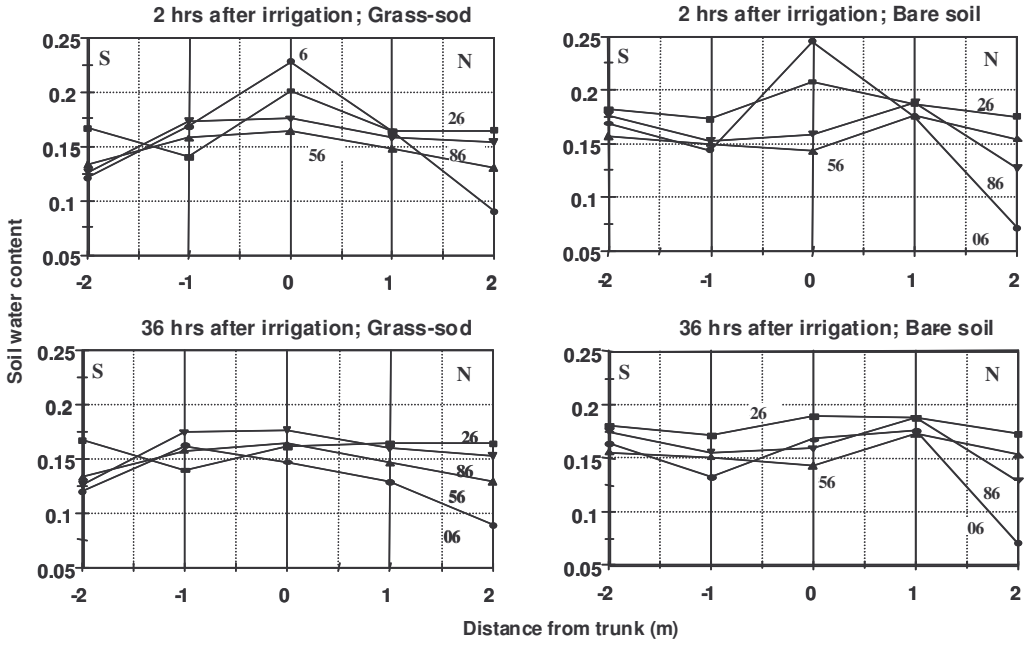

Figure 3.12. Volumetric soil water content across the row at 6, 26, 56 and 86 cm soil depth, and 2 and 36 h after irrigation of peaches (grass sod or bare soil in the inter-row area).

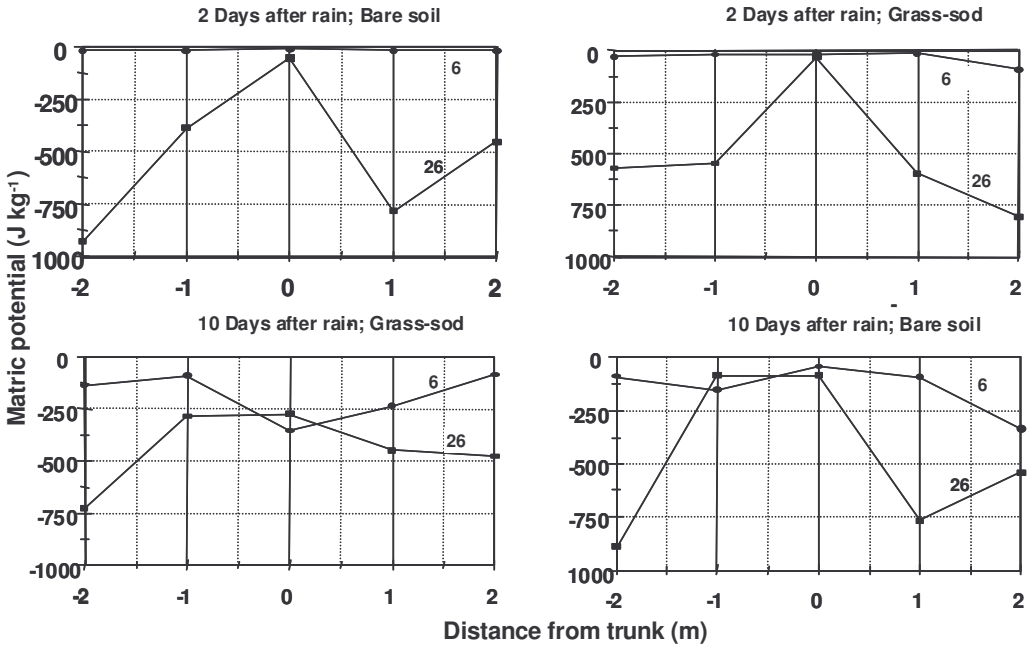

Figure 3.13. Soil matric potential across the row at 6 and 26 cm soil depth, and 2 and 10 days after irrigation of peaches (grass sod or bare soil in the inter-row area).

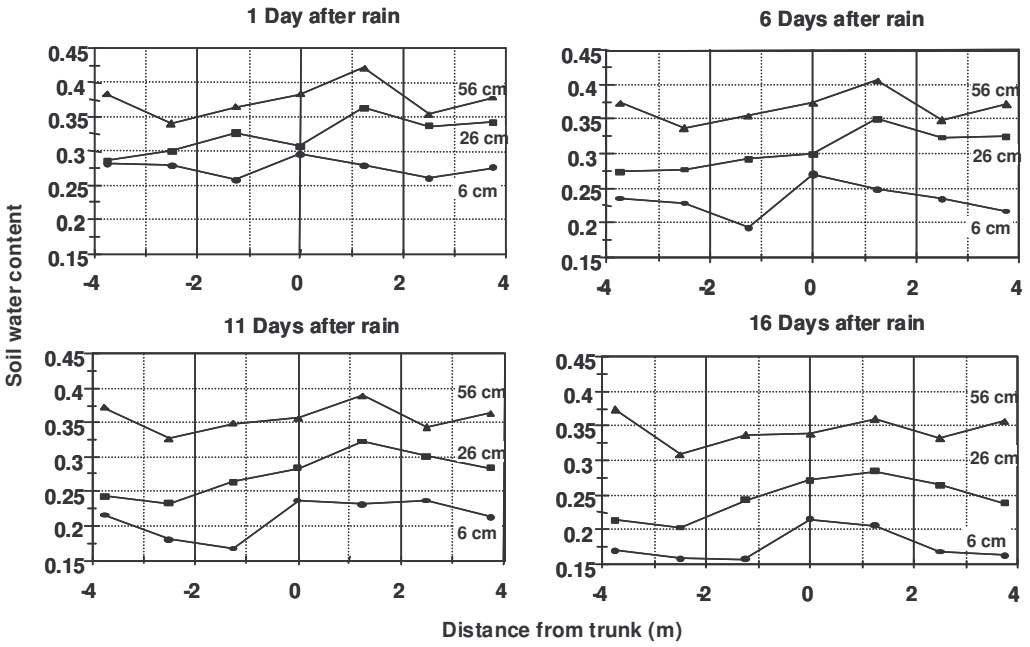

Figure 3.14. Volumetric soil water content across the row at 6, 26 and 56 cm soil depth, and 1, 6, 11 and 16 days after irrigation of clementines.

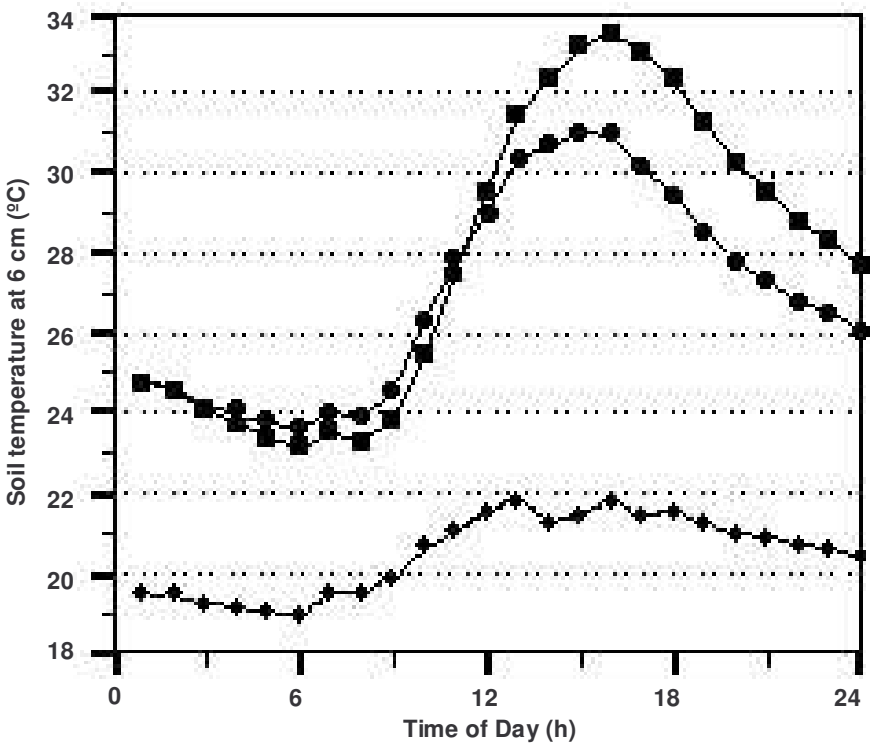

Figure 3.15. Variations in soil temperature measured at 6 cm during a summer day in the peach orchard at Hatfield (Squares indicates Bare soil; Dots indicates Grass sod and Diamonds indicates under tree).

3.3 Evaluation of the two-dimensional energy interception model

3.3.1 Overview of the field trials

The radiant interception model was tested in orchards with differing tree sizes, leaf area densities, shapes and row orientations. Data collected in the peach and Leucaena orchards were used to evaluate the two-dimensional energy interception model for deciduous fruit trees, whilst data obtained from citrus orchards in Syferkuil and Brits were used to evaluate the model for evergreen fruit trees. For the benefit of the reader of this thesis, locality and orchard planting specifications are summarised in Table 3.1.

There are 11 horizontal surface nodes simulated in the model, one at the centre line of the canopy and five on either side of the row, but only seven tube solarimeters were available. Solar radiation interception by the canopy was therefore determined with the use of seven tube solarimeters positioned under the canopy and in the inter-row region. Soil irradiance measurements were taken next to the trunk and on each side of the centre of the row. This arrangement created a symmetrical and equidistant pattern of soil surface irradiance assessment. The solarimeter positions for each canopy are presented in Table 3.2. In the case of the tramline Valencia orchard in Brits (Table 3.1), the position midway between two adjacent tree rows was taken as the centre of the canopy for the simulation (Table 3.2, tube solarimeter No 4). The dimensions of the set-up is presented in Figure 3.11.

The solarimeters were coupled to a CR10 data-logger through an AM416 multiplexer. Milli-volt readings were taken every 10 s for each solarimeter, converted to solar radiation values (W m^{-2}) with the appropriate calibration, and these values were averaged over one hour intervals. Above canopy radiation was measured at automatic weather stations erected in a nearby open area. The AWS was equipped with a CR10X data-logger coupled to a LI 200X pyranometer to measure solar radiation. The data-logger was programmed to take readings every 10 s and automatically calculate and record hourly averages. The logged data was regularly downloaded using a laptop computer.

Radiation data were collected from the various sites during the second half of 1999 and collection details are summarised in Table 3.3. In the case of the Leuceaena hedgerows, leaves were stripped from the canopy in a uniform manner to give a range of leaf area densities. The peach hedgerow was measured at the beginning of the season when the canopy was in the initial period, approximately a month later during the development period and then when the canopy was fully developed at fruit harvest.

The required parameter values are also presented in Table 3.3. These, as well as the respective values in Tables 3.1 and 3.2, were used as the defining parameters for the

hedgerow canopies used in simulating the radiant transmittance. As can be seen in the Tables, a considerable range was covered. Not only were the measurements done from the end of May to early December (i.e. including a good sample of different solar elevations and direct flux densities), the LAI ranged from negligible (0.45) to substantial (5.5). These differences contributed to a range in LAD from 0.3 to 2.16 m^2 leaves m^{-3} canopy. It must also be pointed out that there were also differences in canopy structure; *viz*. a typical "lollipop" (dense ball stuck on a stem) structure as typified by the clementine orchard to the multiple stem scraggy hedge growth found in the Leuceaena. There were also differences in leaf type in that the citrus and peach had simple leaves while the Leuceaena has compound leaves. The orchard canopies also varied tremendously in that the Empress mandarin orchard was a relatively dense planting which approximated a one-dimensional system since little direct radiation penetrated to the soil. On the other extreme were the peach trees during the initial stage (i.e. soon after bud-break) when the foliage was sparse. The single row Leuceaena site was also very open. The clementine, Valencia and mature peach hedgerows formed distinct two-dimensional systems with a dense high hedgerow canopy and a distinct inter-row region. Leaf absorptivity and the canopy extinction coefficient were assumed to be 0.5 for all simulations of total solar radiation transmission (see Section 1.1).

3.3.2 Peach trial (Hatfield)

Figures 3.16 to 3.23 show measured and simulated radiant transmittance at various positions under the canopy of peaches grown in Hatfield for various growth stages and canopy development. The measured radiant transmittance is represented with symbols (blocks), whilst the solid lines are SWB simulations. Next to each graph, the calculated parameters of the statistical analysis between measured and simulated data can be seen. This allows quick, efficient and quantitative evaluation of model performance. The parameters of the statistical analysis are:

i) Number of observations (N);
ii) Coefficient of determination (r^2);
iii) Index of agreement of Willmott (1982) (D);
iv) Root mean square error (RMSE); and
v) Mean absolute error (MAE).

These were recommended by de Jager (1994) to assess model accuracy. He also recommended as model prediction reliability criteria that r^2 and D should be > 0.8, whilst MAE should be < 20%.

The simulations were done for initial, development and mid-stages during the fourth season of growth. The growth stages were associated with different leaf area densities (Table 3.3).

This gave the opportunity to test the model under different conditions of canopy size and density as well as for differing solar paths (elevation & azimuth)

Data for the initial stage (DOY 252 to 260 or 9 to 17 September; early Spring) are shown in Figures 3.16 to 3.19. Figure 3.16 represents simulated and measured daily solar radiation in MJ m^{-2} d^{-1}. This is the total solar energy striking the soil surface at a specific point for the 24hr period of that specific day. During the initial stage, i.e. soon after bud break when there is little canopy development, the solar radiation reaching the soil surface is very well predicted. Five out of the seven nodes assessed had very good agreement (r^2 and D values well above 0.8). The two nodes (0.64 and 1.28 m from the tree row on the Southern side), where the measured daily solar radiation is slightly less than the predicted values can be attributed to two factors. The first factor is that at this growth stage, the canopy comprises mainly of woody material (scaffold branches) instead of leaves. Also, the branches are not uniformly/evenly distributed in the canopy but are localized solid bodies that cast very definite shadows compared to leaves. What most probably happened here is that for a portion of the day a branch could have been casting a shadow on the solarimeter and causing lower readings. The second factor is that at this stage, the canopy has a cross-sectional shape more like a triangle having a higher apex than the oval shape used in the model. So, in practice the shadow cast is longer than estimated by the model. Figure 3.17 shows simulated and measured hourly solar radiation in W m^{-2} intercepted at the soil surface. These figures indicate how the solar energy striking the soil surface changes throughout the day for a period of 10 daily cycles at the specified nodes. Once again, the agreement between the model predictions and measured values show excellent agreement with all seven nodes recording r^2 and D values above 0.9. The measured solar radiation at 0.64 m on the southern side of the tree row appears to be lower than the predicted value at midday. This could most likely be due to a single shadow cast by a branch reducing the solarimeter reading. This will also explain the lower total daily value recorded for this node in Figure 3.16, since the midday radiation is when the solar radiation is at a maximum. The radiant transmittance across the row for a typical day during the initial stage of the crop can be seen in Figure 3.18 for 12/09/1999 and in Figure 3.19 for the same day at 13h00. The predicted high soil irradiance in the northern inter-row area, predicted lower soil irradiance under the tree as well as on the southern, shaded, inter-row area, was in agreement with the previous comments. Considering the variability in the actual canopy properties (i.e. non-uniform foliage distribution as well as not having a truly oval cross-section) the agreement between measured and predicted values is very good.

A month later (DOY 286 to 291, 13 to 19 October), during the development stage of the crop, the measurements and simulations were repeated. Once again good agreement

(r^2 and D values of the order of 0.78 to 0.90 for all but two data sets) was observed between measurements and simulations for both daily (Figure 3.20) and hourly solar radiation (Figure 3.21).

Data were also collected during the stage of full canopy development (around harvest, Figures 3.22 and 3.23). Once again, the agreement between measured and predicted values was very good for most of the nodes monitored. When differences were recorded, the discrepancies were due to the natural deviances in canopy shape from the idealized oval shape used in the model. For example, the cross-sectional shape of the canopy was not perfectly elliptical; it would be better approximated by a triangle. Secondly, and most probably more importantly, the long axis of the canopy ellipse was not normal to the soil surface. Instead of this axis being vertical, it was inclined towards the south due to prevailing wind. In other-words, the hedgerow canopy was not symmetrical but lent to the south. Coupled to this was the fact that there was not a completely uniform distribution of leaves within the canopy. However, when all these factors are considered, the measured and predicted values for the solar irradiance striking the soil at the nodes assessed showed excellent agreement.

.

Table 3.1. List of tree crops monitored and their locality specifications.

Crop	Locality	Latitude	Longitude	Altitude (m)	Planting pattern	Spacing (m)	Row axis
Peach (*Prunus persica* cv. Transvaalia)	Hatfield Experimental Farm, Pretoria	25°45'S	28°16'E	1371	Hedgerow	4.5 x 1.0	E-W (110°-290°)
Leuceaena *(Leucaena leucocephela)*	Hatfield Experimental Farm, Pretoria	25°45'S	28°16'E	1372	Single row	0.3 to 0.4	N-S (10°-190°) E-W (100°-280°)
Clementine (*Citrus reticulata cv. Nules Clementine*)	Syferkuil Experimental Farm, Sovenga	23°51'S	29°40'E	1250	Hedgerow	7.5 x 3.5	NW-SE (135°-315°)
Valencia Delta (*Citrus sinesis* [L.] cv. Osbeck)	Commercial orchard, 15 km North of Brits	25°00'S	27°46'E	1107	Tramline	Two rows 4.0 x 4.0 with 8.0 m gap	NW-SE (135°-315°)
Empress mandarin (*Citrus reticulata* cv. *Empress*)	Commercial orchard, 15 km North of Brits	25°00'S	27°46'E	1107	Hedgerow	4.0 x 2.0	NW-SE (135°-315°)

Table 3.2. Distances (m) from the centre-line of the canopies for tube solarimeters (No. 1 to 7) installed in different hedge-rows.

Crop	No. 4	No. 1 & 7	No. 2 & 6	No. 3 & 5
Peach	At tree trunk	+2 & -2	+1.32 & -1.32	+0.66 & -0.66
Leuceaena	At tree trunk	+2.25 & -2.25	+1.5 & -1.5	+0.75 & -0.75
Clementine	At tree trunk	+3.75 & -3.75	+2.5 & -2.5	+1.25 & -1.25
Valencia Delta	Centre of tramline	+6 & -6	+4 & -4	+2 & -2
Empress mandarin	At tree trunk	+2 & -2	+1.32 & -1.32	+0.66 & -0.66

Table 3.3. Radiation data collection programme and canopy parameters for crops monitored.

Crop	Time period (year 1999)		Canopy status	Tree height (m)	Canopy width (m)	Stem height (m)	Leaf area index (m^2 m^{-2})	Leaf area density (m^2 m^{-3})
	Date	Day of year						
Peach	9 Sep. to 19 Sep.	252 to 262	Initial canopy	3.0	1.8	0.3	0.45	0.30
	5 Oct. to 31 Oct.	278 to 304	Developing canopy	3.2	2.1	0.3	1.92	0.95
	4 Nov. to 22 Nov.	308 to 326	Full canopy	3.3	2.6	0.4	4.05	1.75
Leuceaena	30 May	150	Full canopy (N-S)	2.8	2.8	0	3.39	1.55
	31 May	151	1st Strip (N-S)	2.8	2.8	0	2.67	1.22
	1 June	152	2nd Strip (N-S)	2.8	2.8	0	1.00	0.46
	2 June to 3 June	153 - 154	No leaves (N-S)	2.8	2.8	0	0.51	0.23
	5 June to 9 June	156 -160	Full canopy (E-W)	2.8	3.2	0	3.18	1.40
	10 June	161	1st Strip (E-W)	2.8	3.2	0	2.32	1.00
	11 June	162	No leaves (E-W)	2.8	3.2	0	0.89	0.39
Clementine	3 Dec. to 11 Dec.	337 to 345	Full canopy	3.1	4.0	0.3	5.5	2.16
Valencia Delta	6 July to 20 July	187 to 201	Full canopy	4.3	8.0	0	4.18	1.26
Empress mandarin	20 July to 5 Aug	201 to 217	Full canopy	4.0	2.8	0.4	4.17	1.50

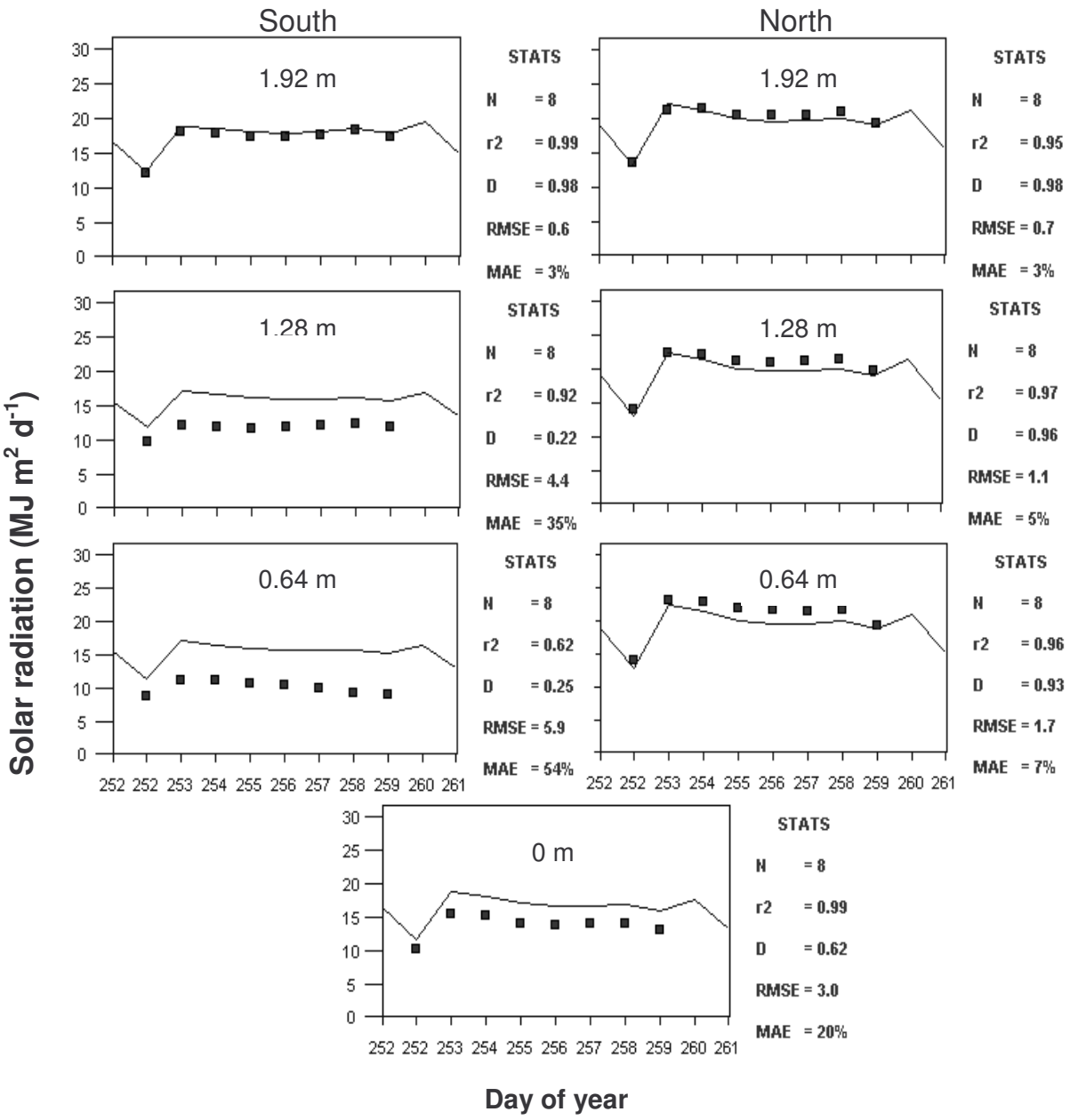

Figure 3.16. Measured (symbols) and simulated (lines) daily solar radiation at different sides and distances from the tree row in a hedgerow peach orchard for period 9 to 17 September 1999 (initial stage of the crop).

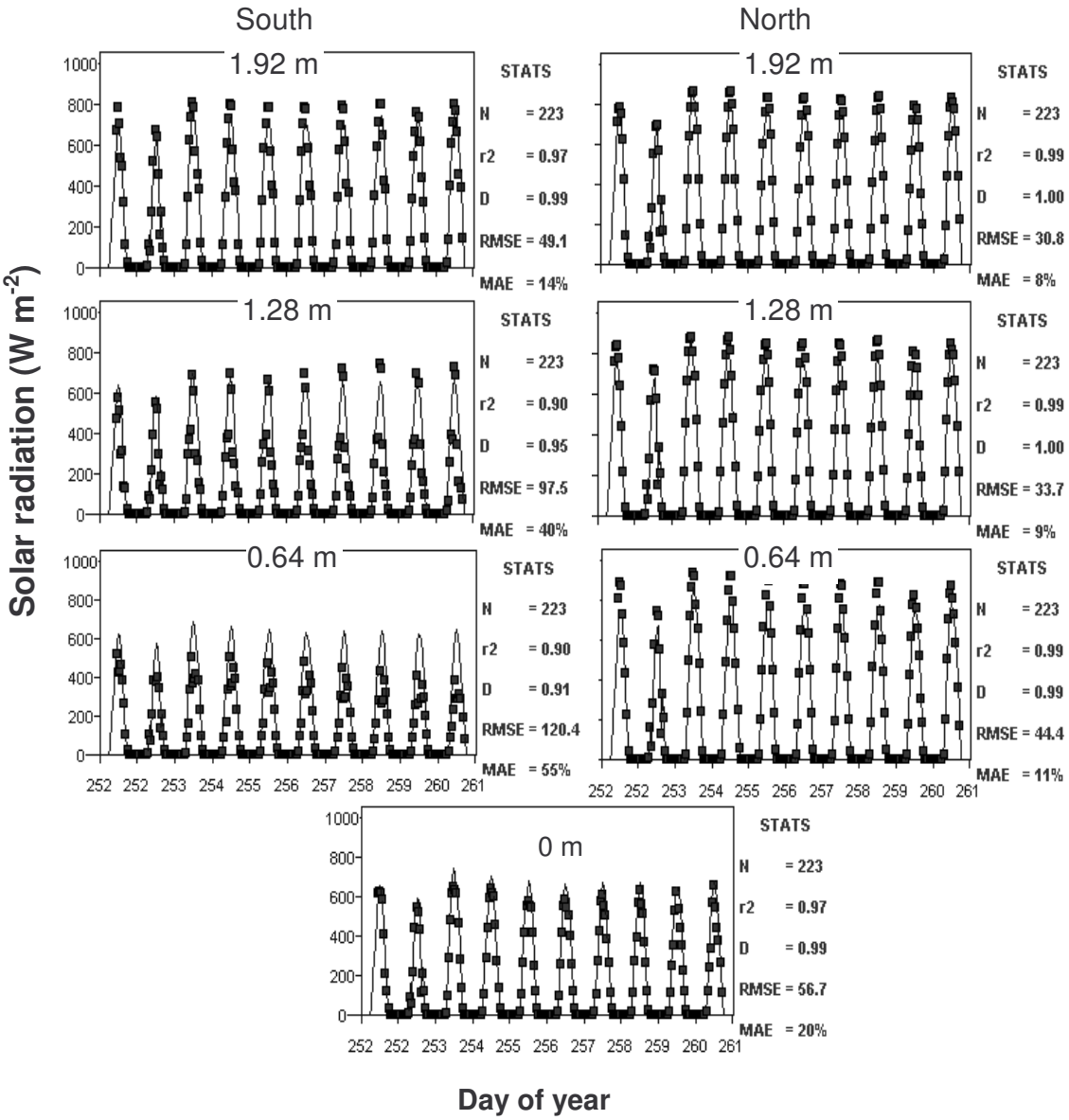

Figure 3.17. Measured (symbols) and simulated (lines) hourly solar radiation at different sides and distances from the tree row in a hedgerow peach orchard for period 9 to 17 September 1999 (initial stage of the crop).

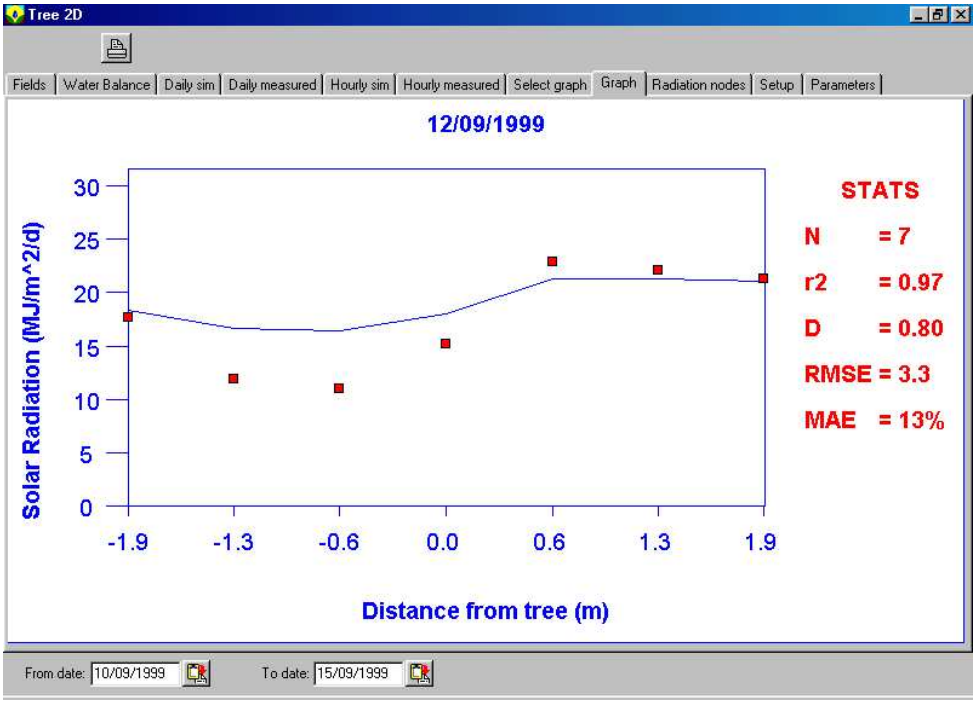

Figure 3.18. Measured (symbols) and simulated (lines) daily solar radiation across the peach hedgerow on 12 September 1999 (initial stage of the crop).

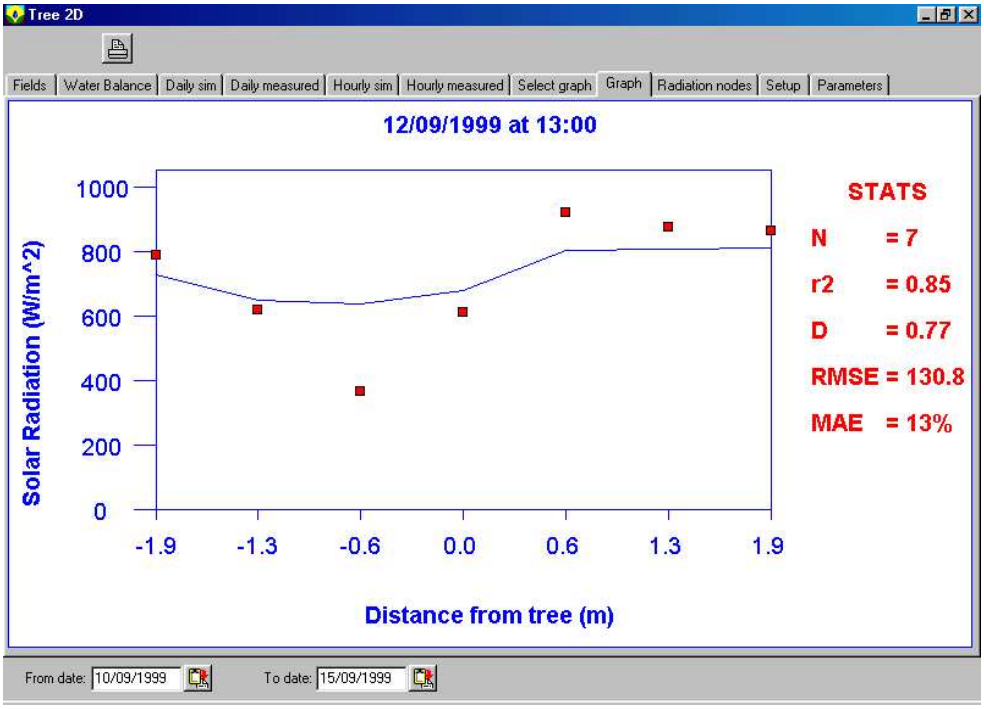

Figure 3.19. Measured (symbols) and simulated (lines) hourly solar radiation across the peach hedgerow on 12 September 1999 at 13h00 (initial stage of the crop).

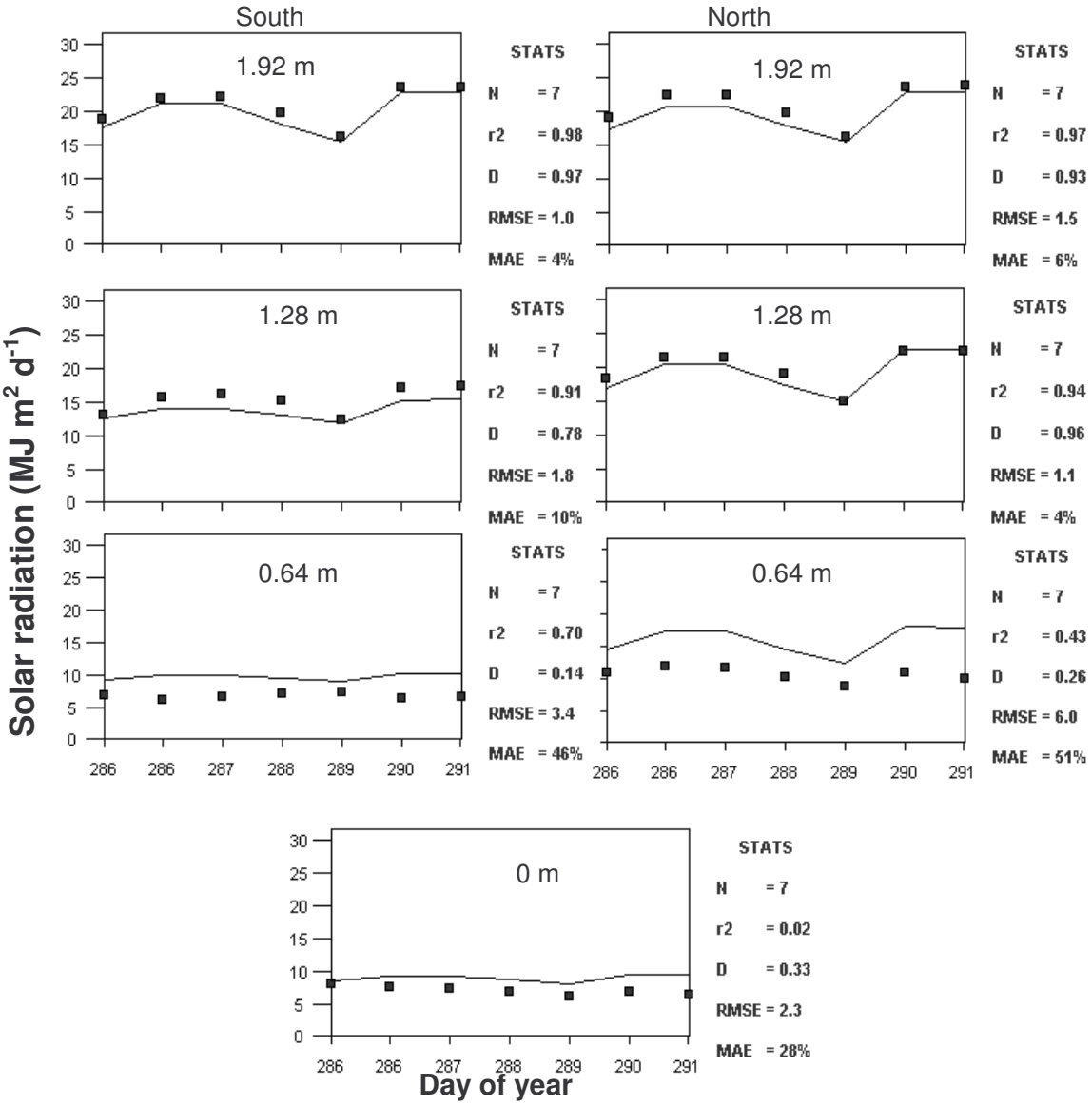

Figure 3.20. Measured (symbols) and simulated (lines) daily solar radiation at different sides and distances from the tree row in a hedgerow peach orchard for period 13 to 19 October 1999 (development stage of the crop).

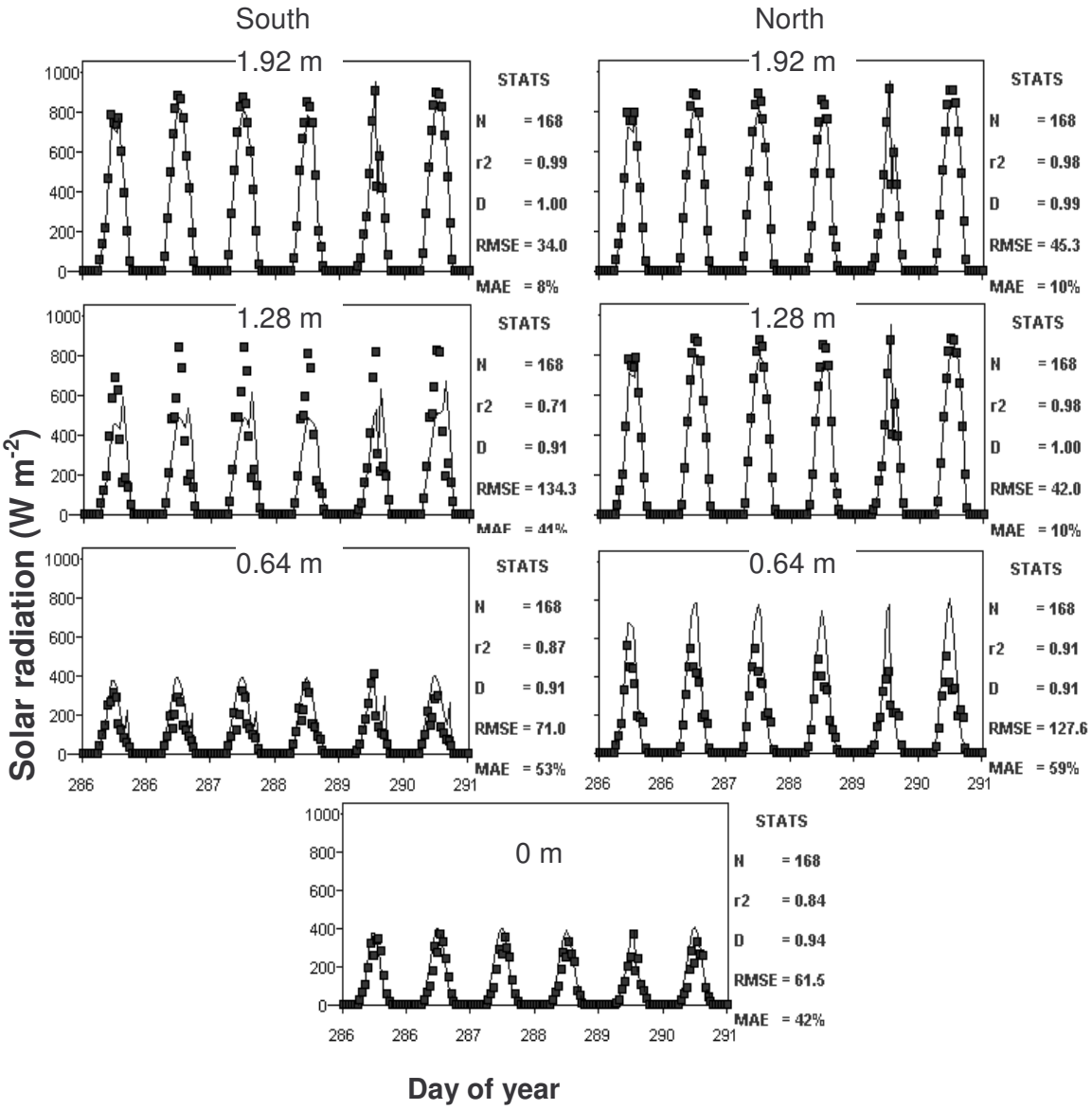

Figure 3.21. Measured (symbols) and simulated (lines) hourly solar radiation at different sides and distances from the tree row in a hedgerow peach orchard for period 13 to 19 October 1999 (development stage of the crop).

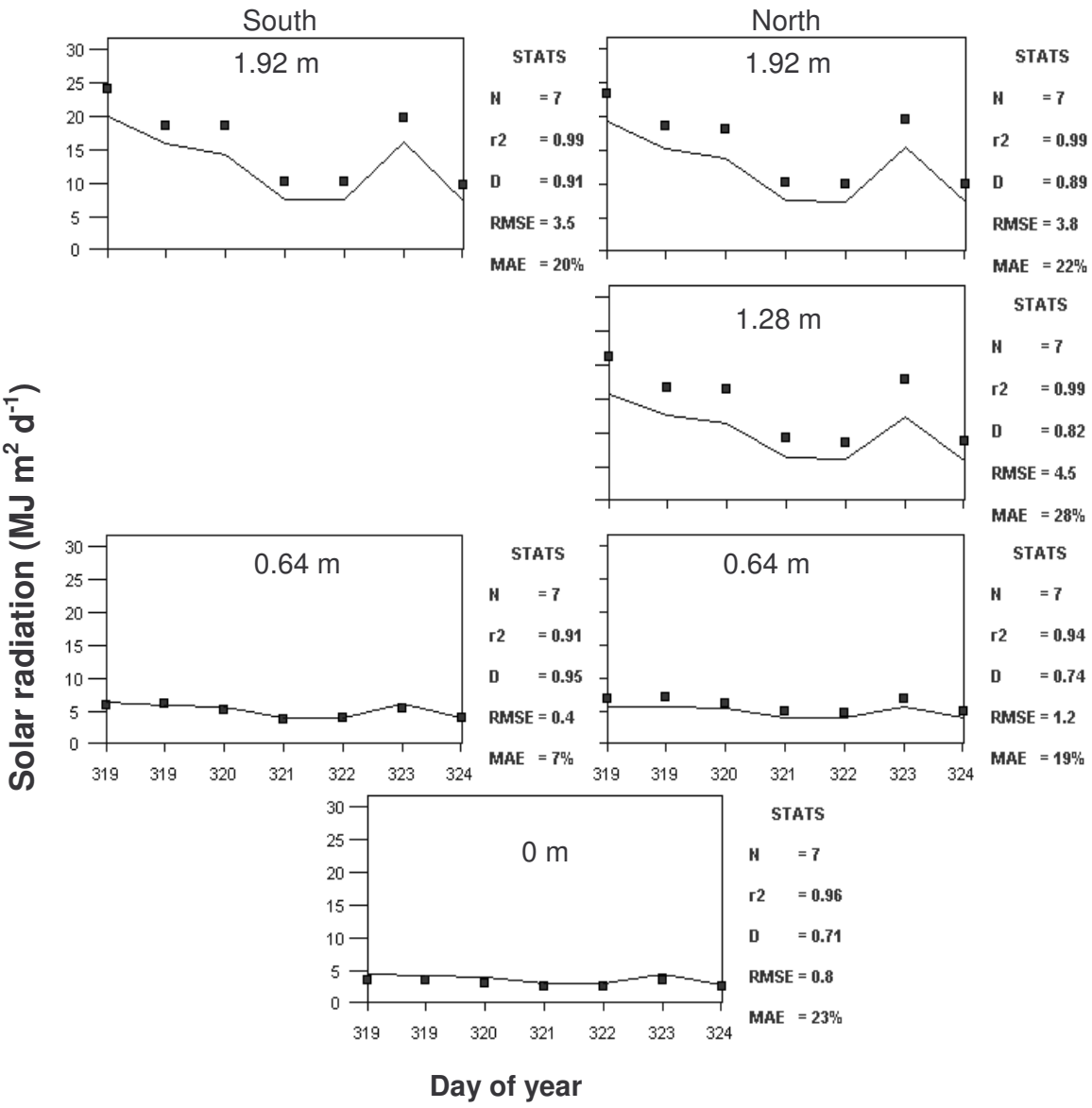

Figure 3.22. Measured (symbols) and simulated (lines) daily solar radiation at different sides and distances from the tree row in a hedgerow peach orchard for period 15 to 21 November 1999 (at harvest).

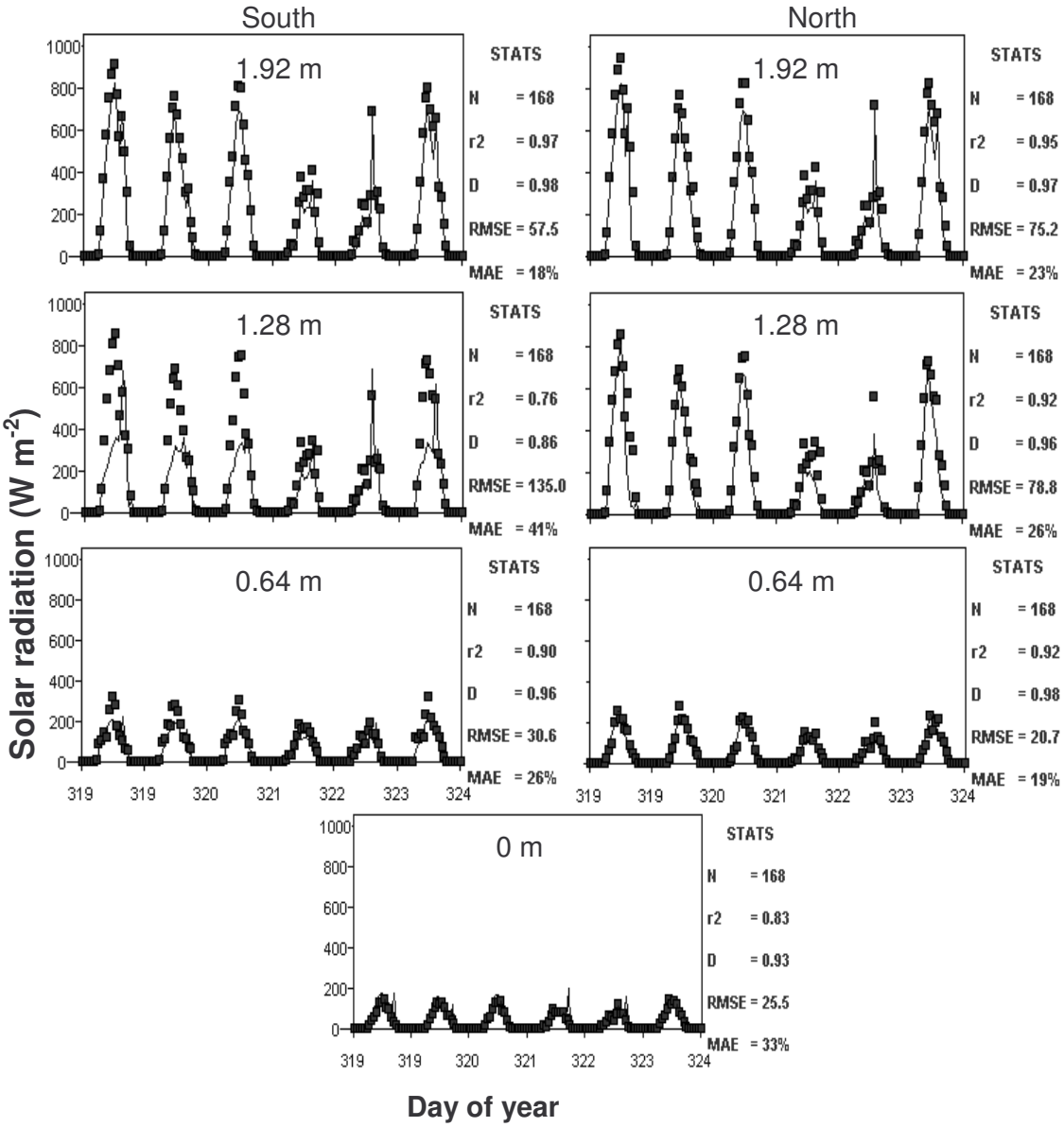

Figure 3.23. Measured (symbols) and simulated (lines) hourly solar radiation at different sides and distances from the tree row in a hedgerow peach orchard for period 15 to 21 November 1999 (at harvest).

3.3.3 Leucaena trial (Hatfield)

Figures 3.25 to 3.31 show measured and simulated hourly radiant transmittance at various positions under the canopy of Leucaena (*Leucaena leucocephela*) grown in Hatfield. This woody perennial had been planted in a single row at 0.3 to 0.4 m spacing within the row. The bushes had been cut back to ground level annually and had formed a coppice of multiple woody stems each having basal diameters ranging from 2 to 5 cm and tapering uniformly to a diameter of < 0.5 cm at a length of 2 to 3 m. The foliage of this hedgerow were small compound leaves with each leaflet having a length of ~0.7 cm and maximum breadth of 0.25 cm. The concentration of woody stems at the base of the plant with extending shoots carrying small sized compound leaves creates a canopy structure similar to a "feather duster", i.e. a dense base with "feathers" extending to the periphery of the canopy. The canopy shape and dimensions as well as the positions of the solarimeters are presented in Figure 3.24. Thus, this canopy is in fact very divergent from the idealized "ellipsoid canopy, having uniformly distributed foliage" on which the radiation interception model is based. In addition, the prevalence of these multiple woody stems and small compound leaves also clash with the principles on which the LAI-2000 PCA (Plant Canopy Analyser) operates and thus the leaf area measurements taken with this instrument could be misleading. The value of this extreme canopy is to test the model in the extreme, if the radiation interception model works on these canopies, it should be applicable to virtually any canopy.

The simulations were done for two single tree rows planted in N-S and E-W row axes (Table 3.1) in order to test the model for different row orientations. Also, leaves were uniformly stripped on several occasions during the course of the trial in order to test the model for different leaf area densities (LAD). This stripping involved removing only leaf material; the stem/branch skeleton of the hedgerow was not altered. As can be seen in Table 3.3 the LAD values for these simulations ranged form 1.55 to 0.23 m^2 m^{-3}.

The model predicted radiant transmittance through the canopy at different distances from the tree row very well when the row orientation was on a N-S axis for all the canopy densities. Figures 3.25 to 3.28 show very good agreement between predicted and measured under canopy irradiance for LAD ranging from 1.55, 1.22, 0.46 and 0.23 m^2 m^{-3}. In all cases the r^2 values are regularly of the order of 0.78 to 0.98, D values exceed 0.82 and RSME are generally acceptable with most of the values being above 60. Of particular interest are days 153, a sunny day and day 154, rainy low solar radiation day (Figure 3.28). These two days, that are markedly different in radiant intensity, show excellent agreement between predicted and measured values. Under these conditions when the row axis is N-S the sun rises on one side of the canopy and as the day progresses, so the sun moves across the top of the

canopy to shine on the second side of the canopy. So in this situation, the solar elevation and azimuth and canopy shape are not particularly important since throughout the day a relatively uniform canopy density is presented to the solar irradiance. When the E-W row axis is evaluated (Figures 3.29 to 3.31), very interesting and important differences occur between the measured and predicted irradiance values. The first trend to note is that on the shaded side of the canopy, i.e. southern side in this case, the predicted and measured values show good agreement for all LAD conditions. At a LAD of 1.40 m^2 m^{-3} (Figure 3.29) the canopy interception on the southern side is high and the predicted soil irradiance values tend to be higher than the measured values. At an LAD of 1.00 m^2 m^{-3} (Figure 3.30) there is a slight reduction in canopy interception with very good agreement between predicted and measured values on the southern side. In Figure 3.31, with a LAD of 0.39 m^2 m^{-3} the canopy interception has decreased further but there is still good agreement between measured and predicted soil irradiance on the southern side. Here the predicted values tend to be less than the measured values, i.e. a change to the trend identified with higher LAD values. However, on the northern, or sunny side, the measured values are constantly, without exception, markedly higher than the predicted values. The cause of these anomalous results can be got by referring to Figures 2.16 and 3.24. In Figure 2.16 it can be seen that the coppice actually forms an inverted triangle shape and not the ellipsoid on which the model is based. Figure 3.24 is a diagrammatic representation of the actual situation compared to the ellipsoid canopy used in the model. In this diagram it is seen that irrespective of the canopy shape, the solar radiation will pass through a substantial portion of the canopy before irradiating the soil on the southern side. So there is good agreement between theory and actual measurements. But a totally different situation exists on the northern side of the canopy. On this side, due to the coppice structure, the stems are effectively parallel to the suns rays and the canopy also allows a large amount of radiation to pass under the canopy. Thus there is negligible canopy interception of the solar radiation resulting in the measured values having little agreement with the predictions. So in this unique situation, the model does not effectively predict the canopy interception. These discrepancies are undoubtedly due to the radical difference this canopy has to the idealized “ellipsoid canopy with uniformly distributed foliage” used by the model. The “feather duster” shaped canopy having a high proportion of discrete stems is a severe test for the applicability of the model. However, in spite of these radical deviations from an “idealized canopy” the results on one side of the canopy are still excellent when one considers the statistical analysis values recorded where the r^2 and D values are consistently in the 0.75 to 0.95 range.

It must be remembered that the LAI 2000 PCA was developed for use in canopies with uniform distribution of leaves and where the branch structure formed a relatively minor

portion of the canopy. Further, the software available for use with this instrument is designed for application in either individual free standing trees or in grain crops where the canopy develops uniformly on the horizontal plane in 360º around the point of measurement. No provision is made for using the LAI 2000 canopy analyser in hedgerow orchard plantings. So the accuracy of LAD values derived from the LAI values obtained with the LAI 2000 could have errors. It would be advantageous to do specific calibration work for various tree canopies if the LAI 2000 canopy analyser is used for LAD determinations in hedgerow orchards.

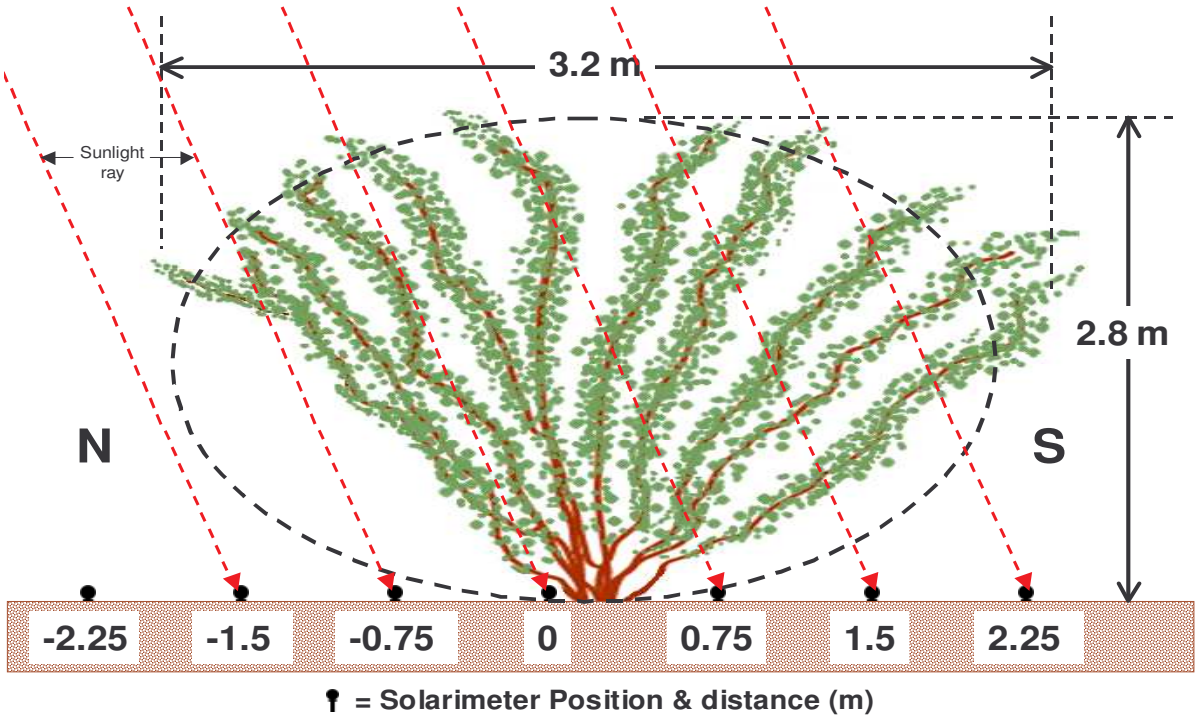

Figure 3.24. Canopy dimensions (m) and shape for the E-W row axis Leuceana hedge-row and the positions of the solarimeters. Note: 1) On the northern side, the coppice stems are virtually parallel to the solar irradiance (dashed arrows) and thus little solar irradiance is intercepted. 2) Due to the “Feather-duster” shape, the solarimeters on the northern side have little foliage interception of solar irradiance. 3) In addition, the canopy is not symmetrical and does not conform to an elliptical shape (dashed outline).

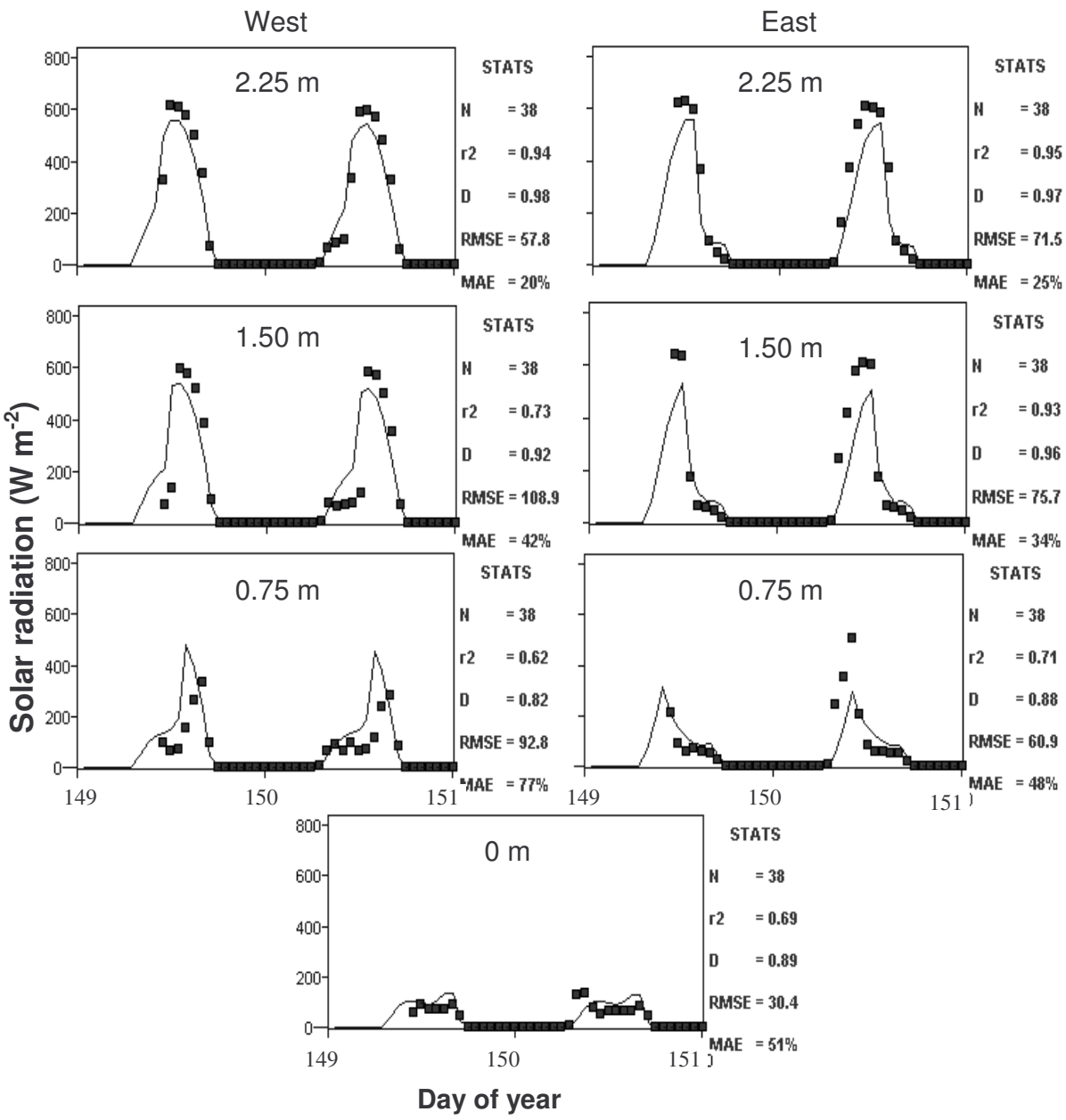

Figure 3.25. Measured (symbols) and simulated (lines) hourly solar radiation at different sides and distances from the tree row in a hedgerow leucaena orchard for period 29 to 30 May 1999 (row axis N-S; LAD = 1.55 m^2 leaf m^{-3} canopy).

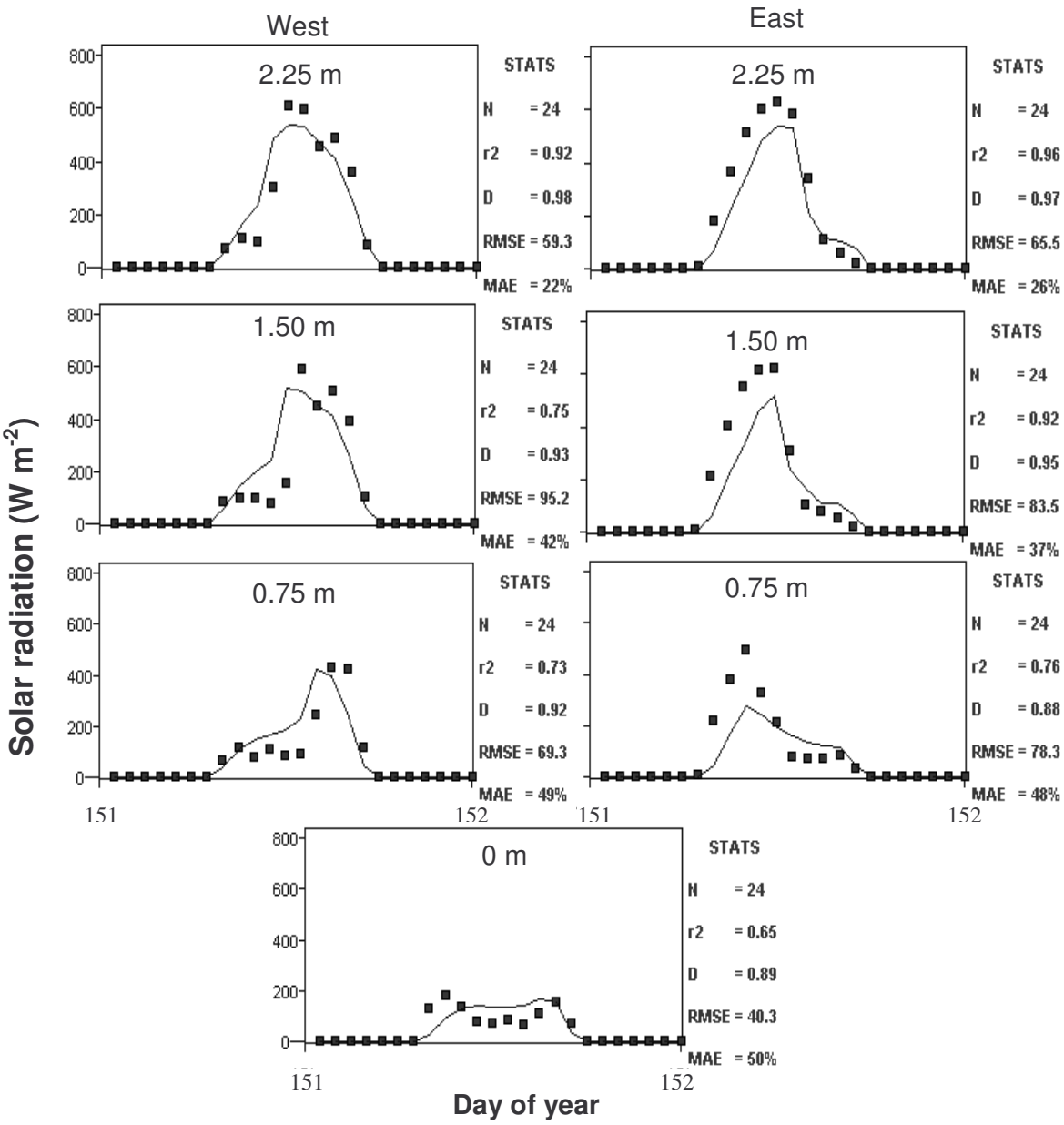

Figure 3.26. Measured (symbols) and simulated (lines) hourly solar radiation at different sides and distances from the tree row in a hedgerow leucaena orchard on 31 May 1999 (row axis N-S; LAD = 1.22 m^2 leaf m^{-3} canopy).

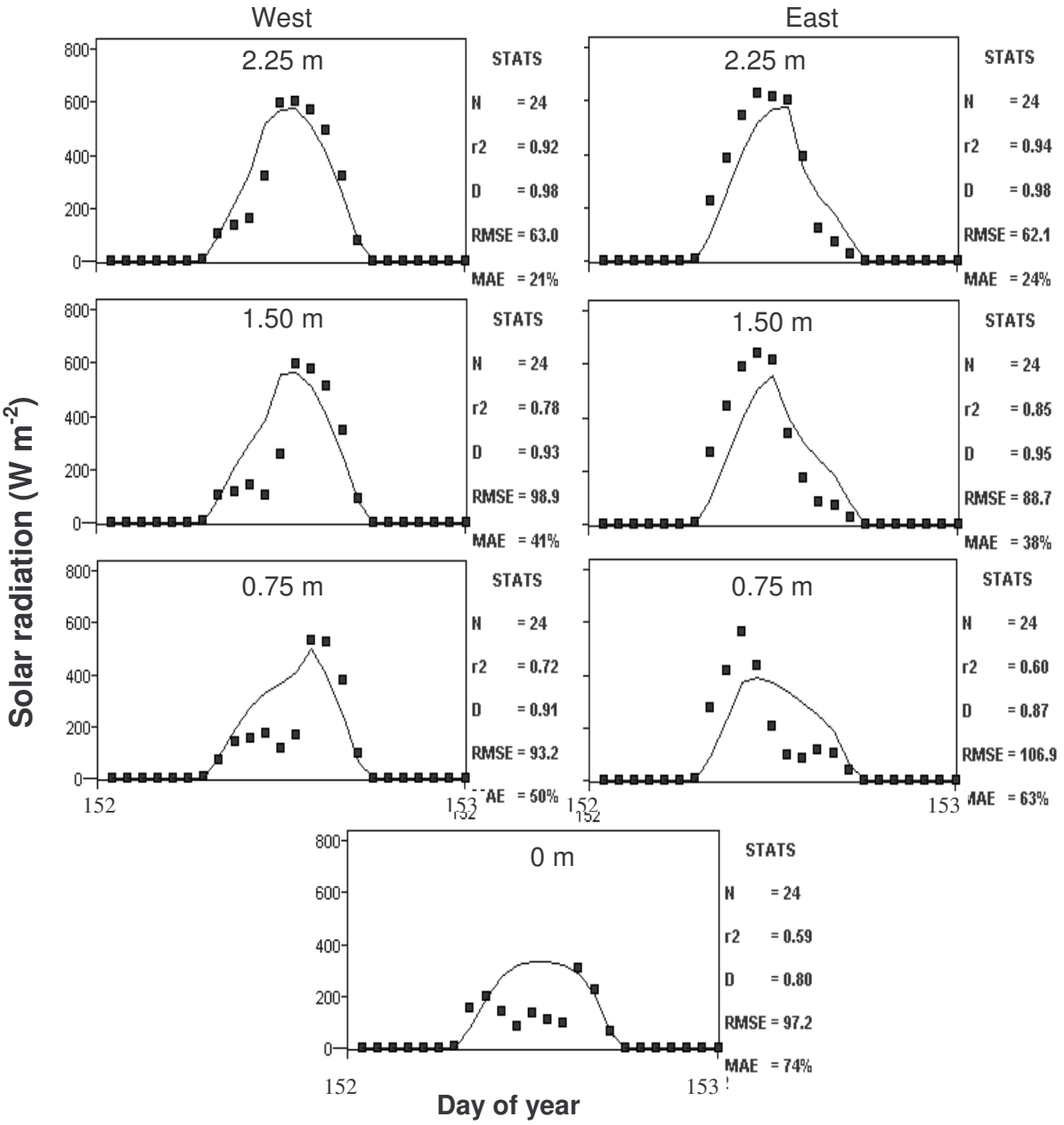

Figure 3.27. Measured (symbols) and simulated (lines) hourly solar radiation at different sides and distances from the tree row in a hedgerow leucaena orchard on 1 June 1999 (row axis N-S; LAD = 0.46 m^2 leaf m^{-3} canopy).

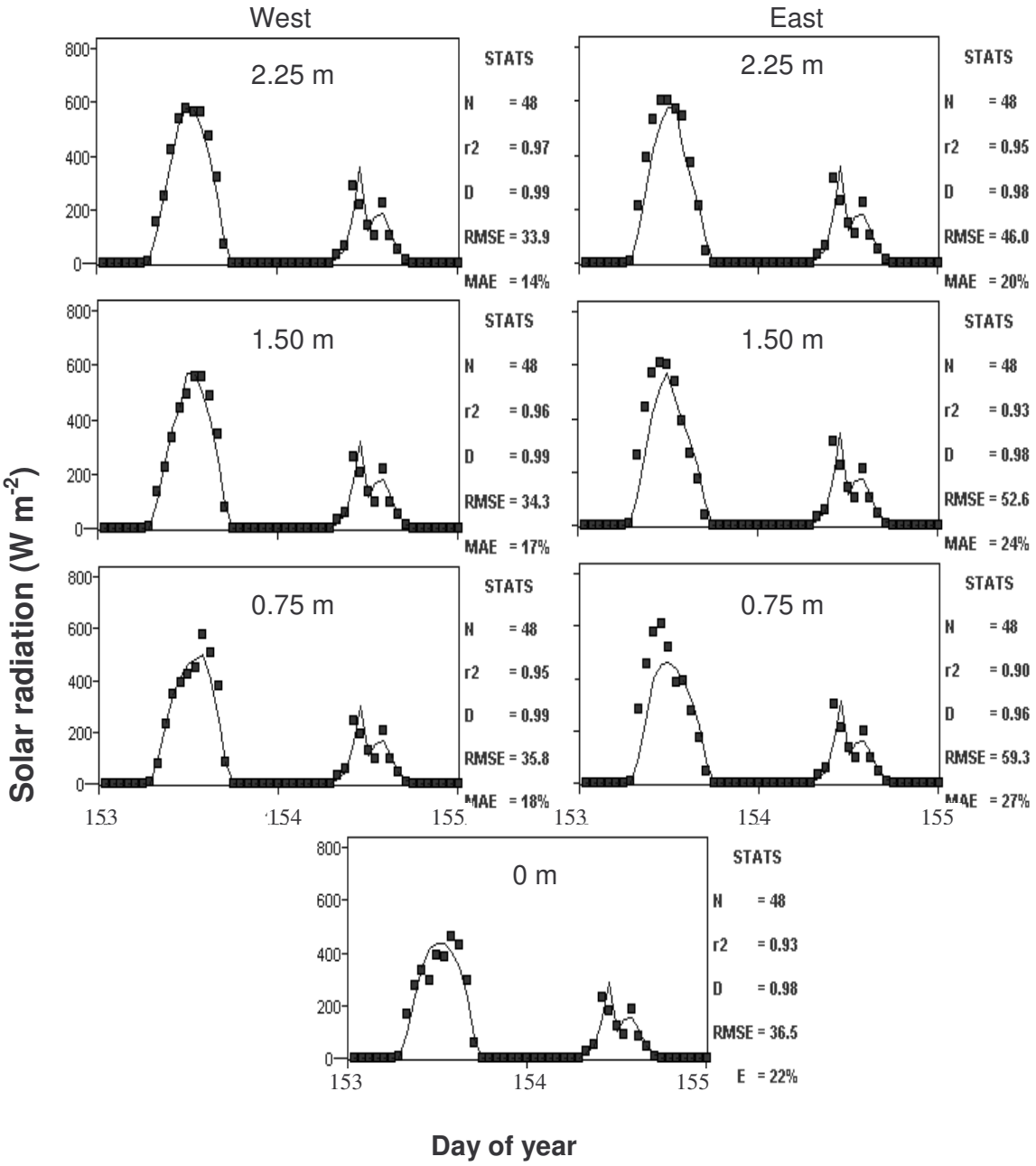

Figure 3.28. Measured (symbols) and simulated (lines) hourly solar radiation at different sides and distances from the tree row in a hedgerow leucaena orchard for period 2 to 3 June 1999 (row axis N-S; LAD = 0.23 m^2 leaf m^{-3} canopy).

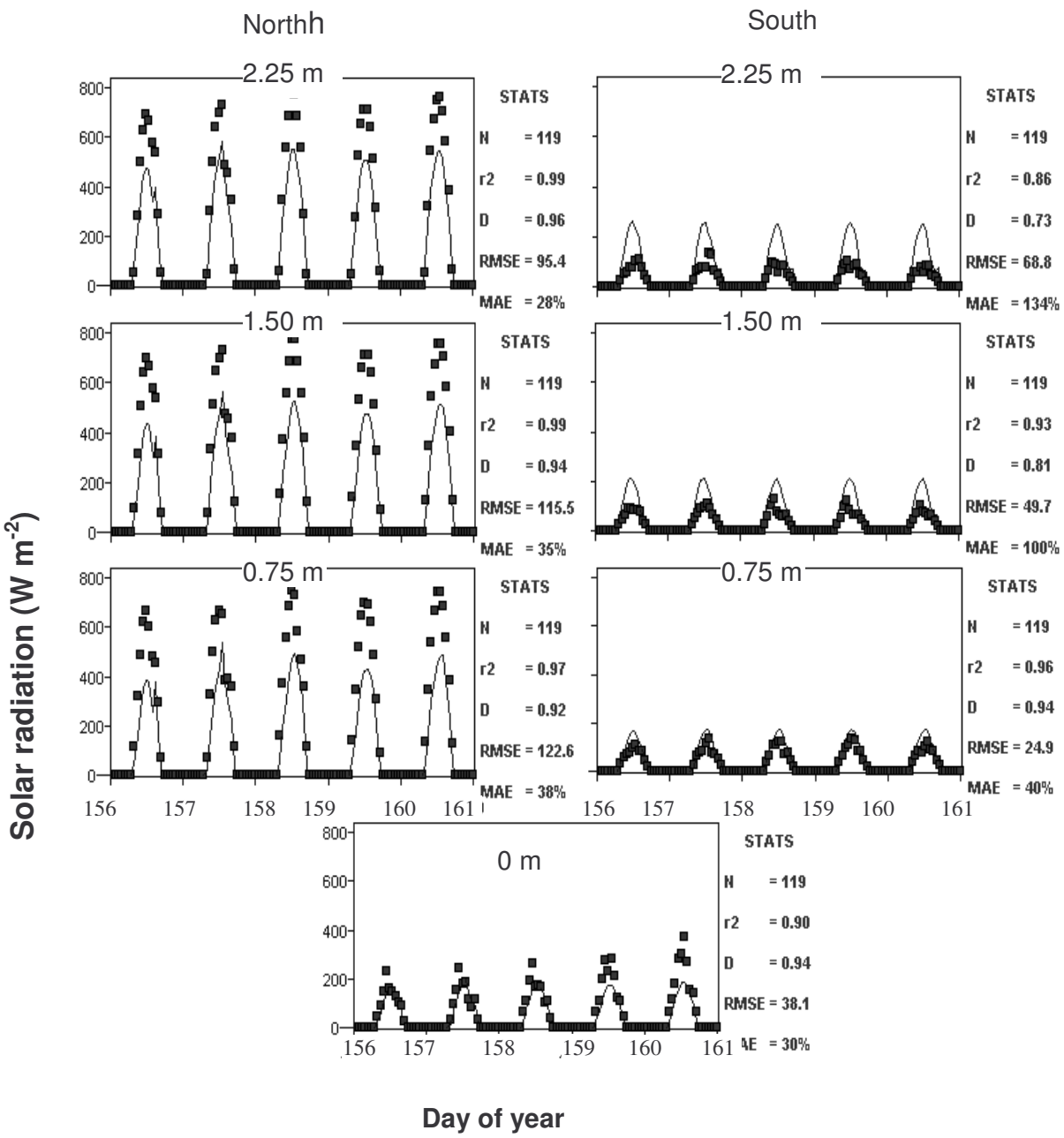

Figure 3.29. Measured (symbols) and simulated (lines) hourly solar radiation at different sides and distances from the tree row in a hedgerow leucaena orchard for period 5 to 9 June 1999 (row axis E-W; LAD = 1.40 m^2 leaf m^{-3} canopy).

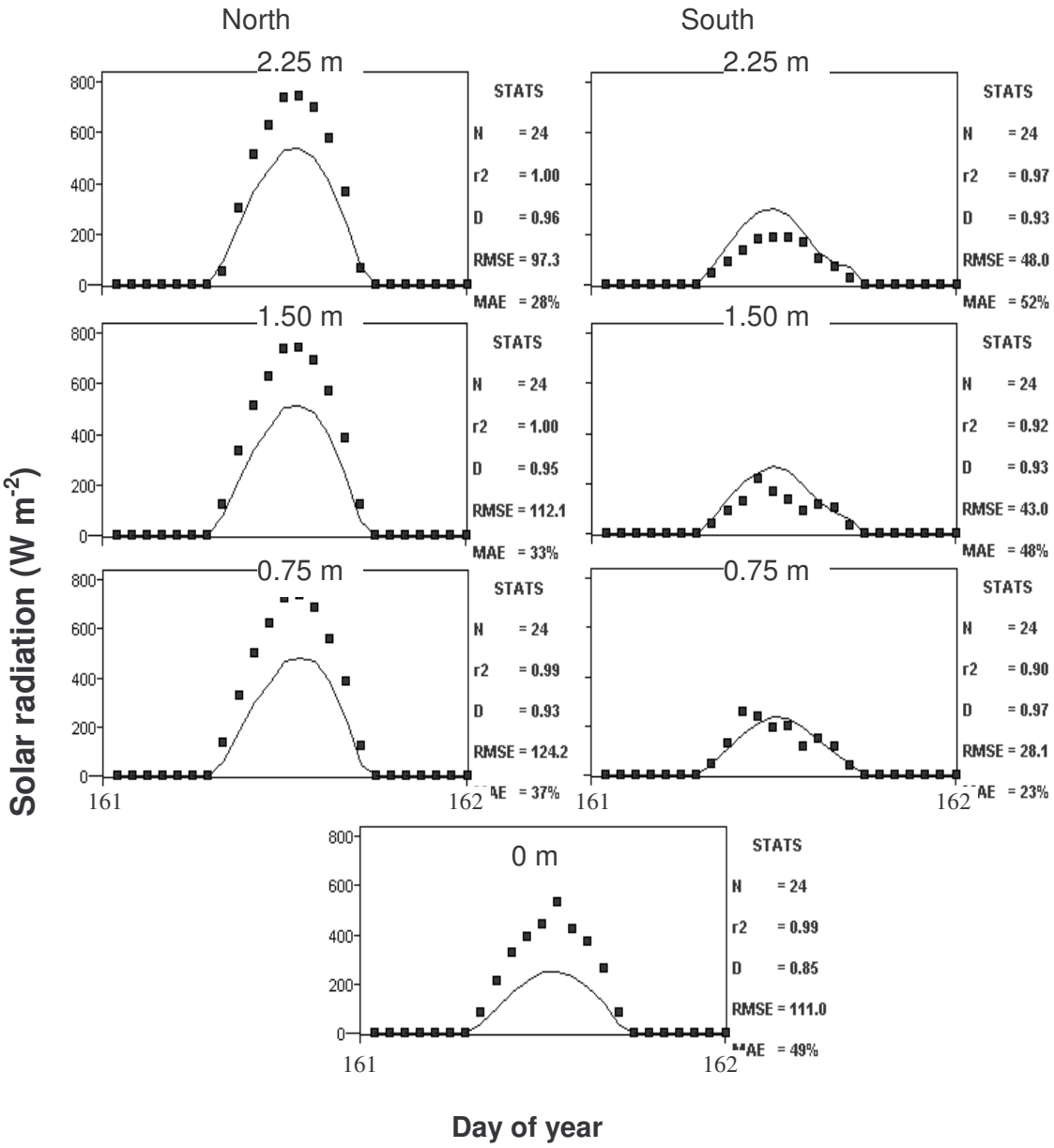

Figure 3.30. Measured (symbols) and simulated (lines) hourly solar radiation at different sides and distances from the tree row in a hedgerow leucaena orchard on 10 June 1999 (row axis E-W; LAD = 1.00 m^2 leaf m^{-3} canopy).

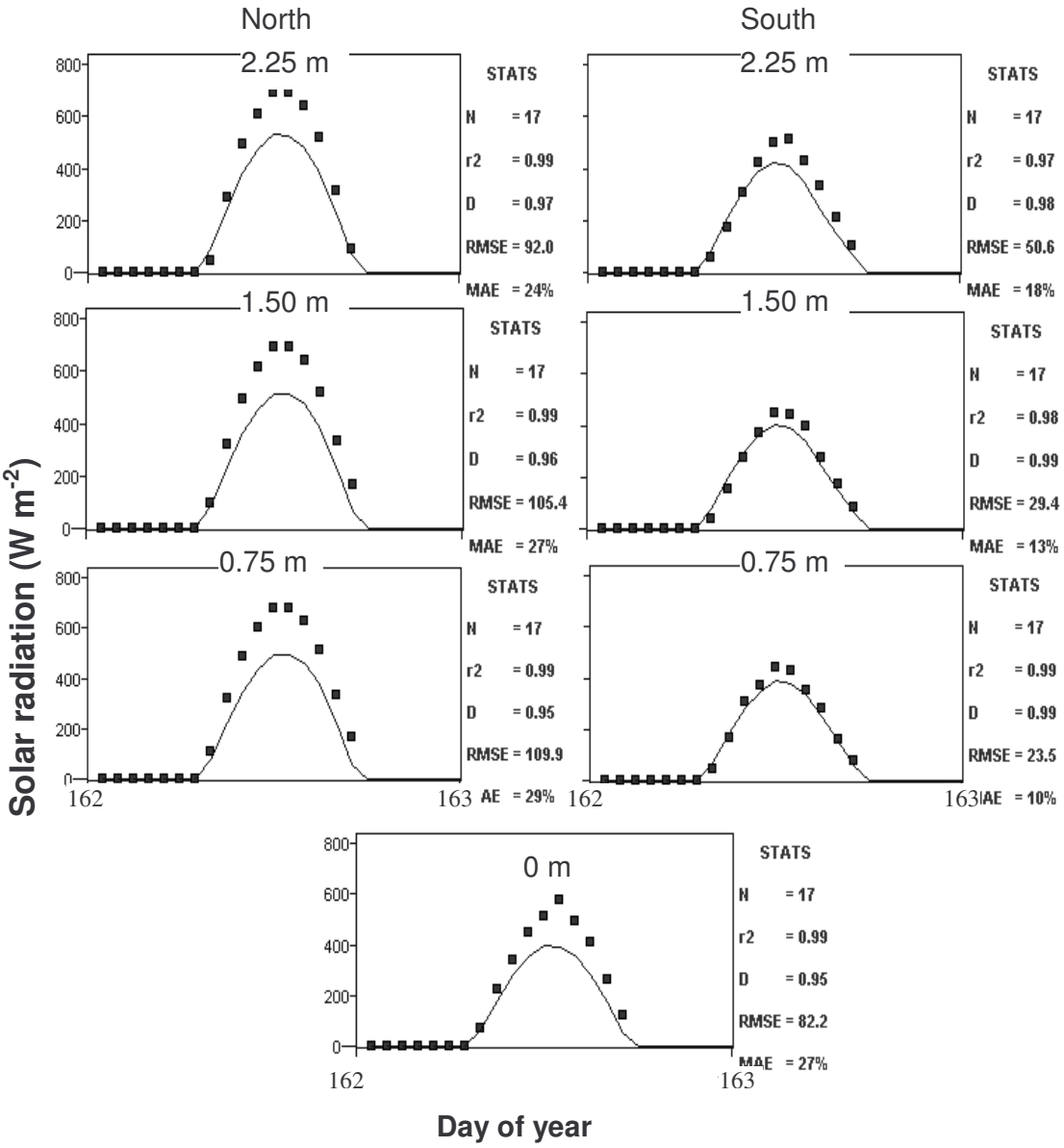

Figure 3.31. Measured (symbols) and simulated (lines) hourly solar radiation at different sides and distances from the tree row in a hedgerow leucaena orchard on 11 June 1999 (row axis E-W; LAD = 0.39 m^2 leaf m^{-3} canopy).

3.3.4 Citrus trial (Syferkuil)

Figures 3.32 and 3.33 depict daily and hourly radiant transmittance in the clementine hedgerow orchard at Syferkuil. Very good agreement between simulated and measured values was observed for all positions under the canopy. Once again the r^2 and D values were generally in the 0.75 to 0.95 range with only a few incidences where these values were unacceptable. The MAE was higher then the reliability criteria of 20% at the tree row and at 1.25 m on either side of the tree row. However, the measured and simulated values at these positions were generally so small that large mean absolute errors were calculated for small discrepancies between measurements and simulations.

An additional simulation was carried out to test the model prediction of transmittance of photosynthetically active radiation (*PAR*). *PAR* was measured with line quantum sensors placed adjacent to the tube solarimeters. Leaf absorptivity for *PAR* was assumed to be 0.8 (Goudriaan, 1977). The canopy extinction coefficient for *PAR* (K_{PAR}) was calculated to be 0.71 using the procedure described by Jovanovic and Annandale (1998), where:

$$k_{PAR} = k\,(\alpha_p\,\alpha_s)^{0.5} \qquad (3.3.1)$$

where k is the canopy extinction coefficient for total solar radiation, α_p is leaf absorptivity for *PAR* and α_s the leaf absorptivity for total solar radiation. k was assumed to be 0.5 (see Section 1.1), α_p is 0.8 (Goudriaan, 1977) and α_s was calculated as the geometric mean of absorptivities in the *PAR* and near-infrared range (α_n):

$$\alpha_s = (\alpha_p\,\alpha_n)^{0.5} \qquad (3.3.2)$$

where leaf absorptivity in the near-infrared range (α_n) is equal to 0.2 (Goudriaan, 1977).

Simulated and measured values of *PAR* (in mol cm^{-2} s^{-1}) are compared in Figure 3.34 for different distances from the tree row. The model predicted *PAR* generally well.

In the case of the simulations at Syferkuil, the major reason for discrepancies between measured and simulated data for both total solar radiation and *PAR*, can be identified by referring to Figure 2.14. It is seen that the shadow cast by the trees was jagged. This shadow outline is caused since the individual trees had a dense spherical shape. Thus, instead of having the idealized ellipsoid “sausage”, the hedgerow canopy shape could better be described as a “row of tennis balls”. So, when considering the variability that actually existed in the hedgerow shape, and the agreement between the predicted and measured soil irradiance, one can safely conclude that the two-dimensional energy interception model worked very well in this evergreen hedgerow.

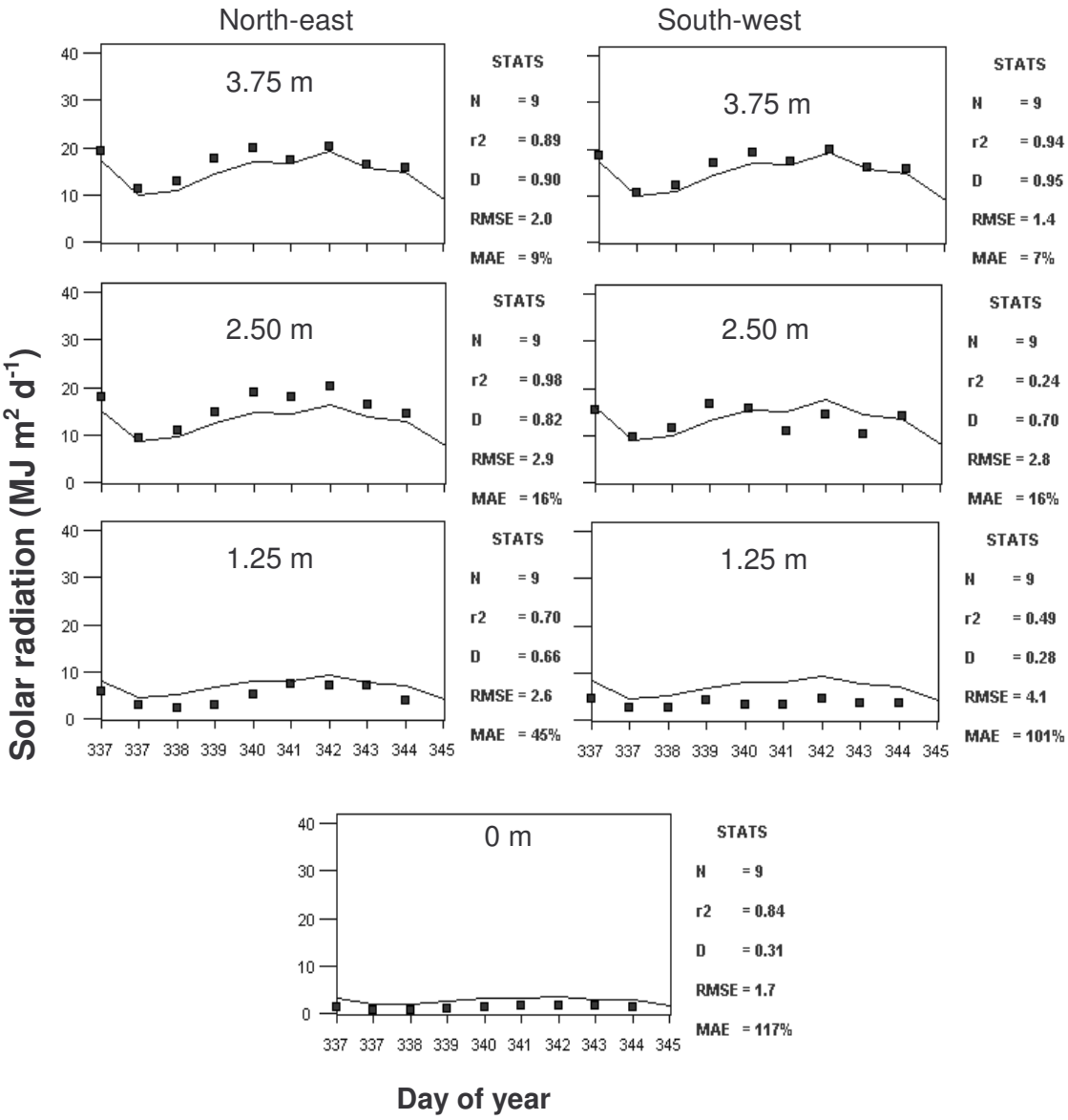

Figure 3.32. Measured (symbols) and simulated (lines) daily solar radiation at different sides and distances from the tree row in a hedgerow clementine orchard for the period 3 to 11 December to 1999.

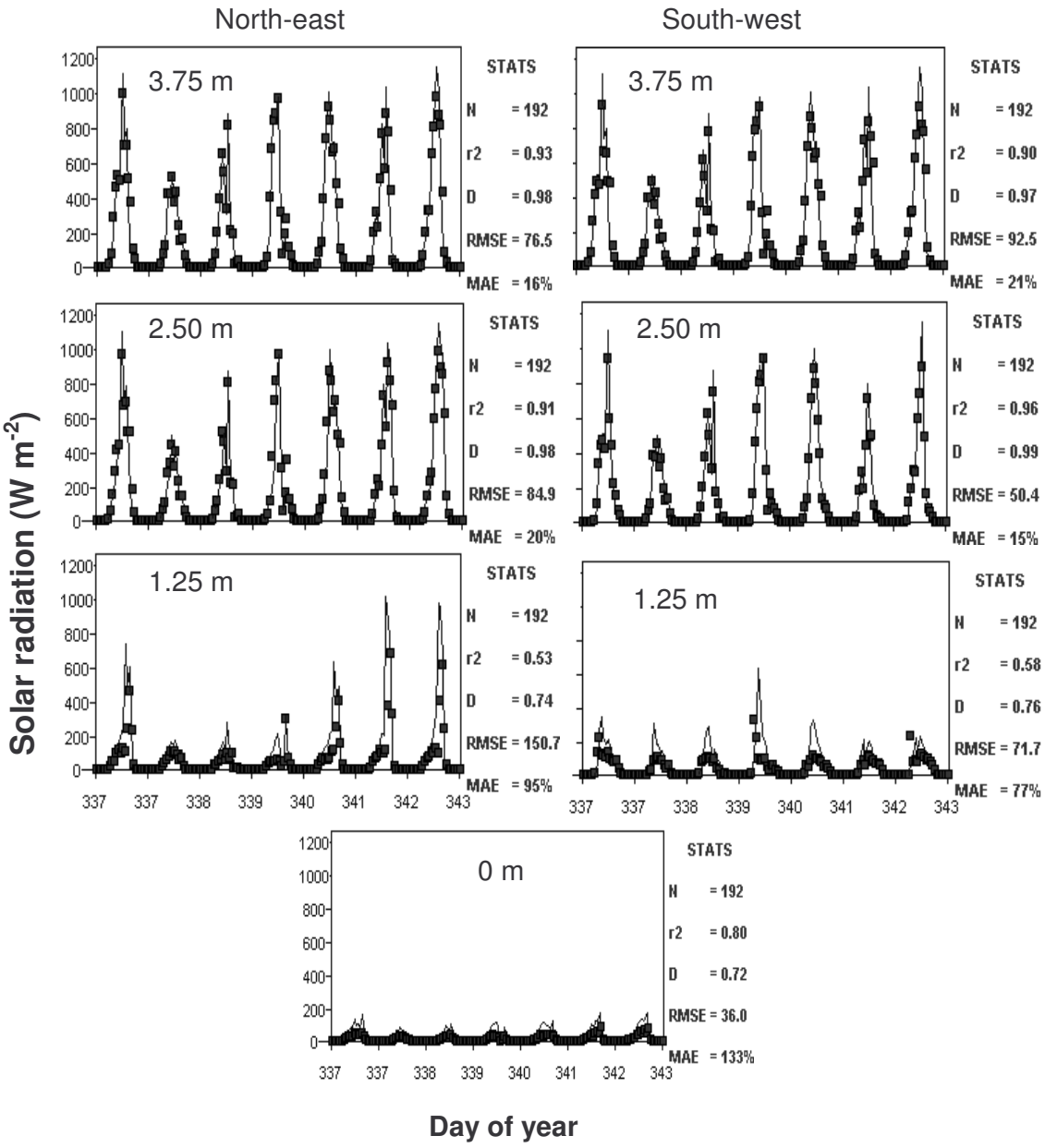

Figure 3.33. Measured (symbols) and simulated (lines) hourly solar radiation at different sides and distances from the tree row in a hedgerow clementine orchard for the period 3 to 9 December 1999.

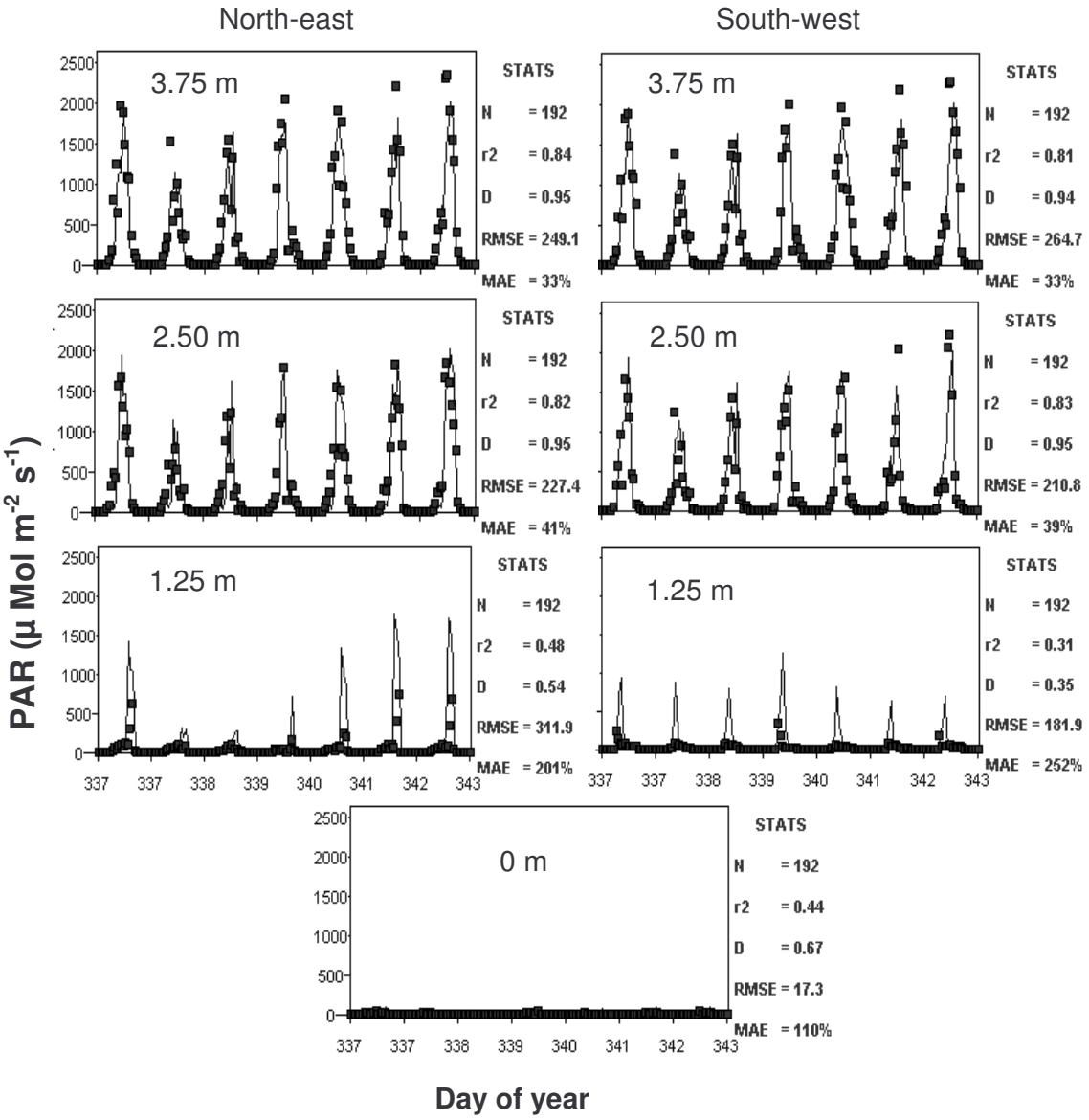

Figure 3.34. Measured (symbols) and simulated (lines) photosynthetically active radiation (PAR) at different sides and distances from the tree row in a hedgerow clementine orchard for the period 3 to 9 December 1999.

3.3.5 Citrus trial (Brits)

Two radiation evaluations were carried out in Brits in order to test the two-dimensional radiation interception model at a third combination of latitude and longitude as well as for a further row orientation. These two orchards also had very differing canopy dimensions and characteristics when compared to the previous orchards investigated. The details of these canopies are summarized in (Table 3.1). In this evaluation the canopy dimensions and LAD was measured, the solar penetration recorded and the model run. So this is an independent data set and thus a true evaluation of the model.

The Delta Valencia plantings were originally planted in a square at a spacing of 4 X 4 m. But, when the lack of light (solar radiation) penetration into the orchard became a problem, every third row was removed. This created the situation where there were two rows of trees planted on a 4 X 4 m spacing, then, with a row being removed, there was an 8 m gap before the next two rows occurred. This orchard pattern is referred to as a "tram-line" planting. A good indication of these features can be seen in Figures 2.17, 2.18 and 2.20. These trees reached a height of 4.25 m and the breadth of the canopy formed by the two rows was 8.2 m. Even though these trees had a good amount of leaf, due to the large canopy cross section, the LAD was actually relatively low at 1.26 m^2 m^{-3}. However, there was a distinct broad hedgerow canopy having a width of 8.2 m with an open inter-row having an average gap of 3.8 m. For this exercise, the middle of the hedgerow was taken at the middle of the "tramline", i.e. between the 4 X 4 m double row (Figure 2.17, 2.18 and 2.20).

The Empress Mandarin orchard was planted on a 4 X 2 m spacing. The mandarin tree has an upright and narrow shape and thus these trees formed a hedgerow having a height of 4 m, width of 2.8 m and an open inter-row space of 1.2 m. The LAD of this hedgerow was 1.5 m^2 m^{-3}. Due to the narrow spacing and height of these hedgerows, direct sunlight penetration to the soil occurred only when the sun was virtually at its maximum elevation angle.

The results from the hourly observations and simulations in the tramline Valencia hedgerow orchard are presented in Figure 3.35. There was reasonable agreement between the predicted and measured values with most of the r^2 and D values being above 0.70. However, as with the other sites, some anomalies did occur. The occurrence of these anomalies could easily be caused by the occurrence of a bulge or indentation of the actual canopy.

The results for the Empress Mandarin hedgerow are presented in Figure 3.36 for hourly radiant transmittance. The canopy development of this orchard was extensive. The canopy base was covering 2.8 m of the 4 m row spacing, which gave a canopy cover of 70%.

Coupled to this is a canopy height of 4 m. This created a situation where very low soil irradiance values were measured. The model overestimated soil irradiance in the inter-row area (1.32 m and 2 m from the tree row) on both sides of the tree row in the middle hours of the day, i.e. noon.

In both the Valencia and the Mandarin orchards, the actual measured soil irradiance in the inter-row area during the middle of the day was less than the predicted irradiance. This was attributed to irregular branches and foliage that shaded the tube solarimeters during these periods of the day. However, considering the heterogeneity of the canopy density, the radical difference that the actual canopies had compared to the idealized ellipsoid “sausage” that the model is based on, the two-dimensional energy interception model performed well.

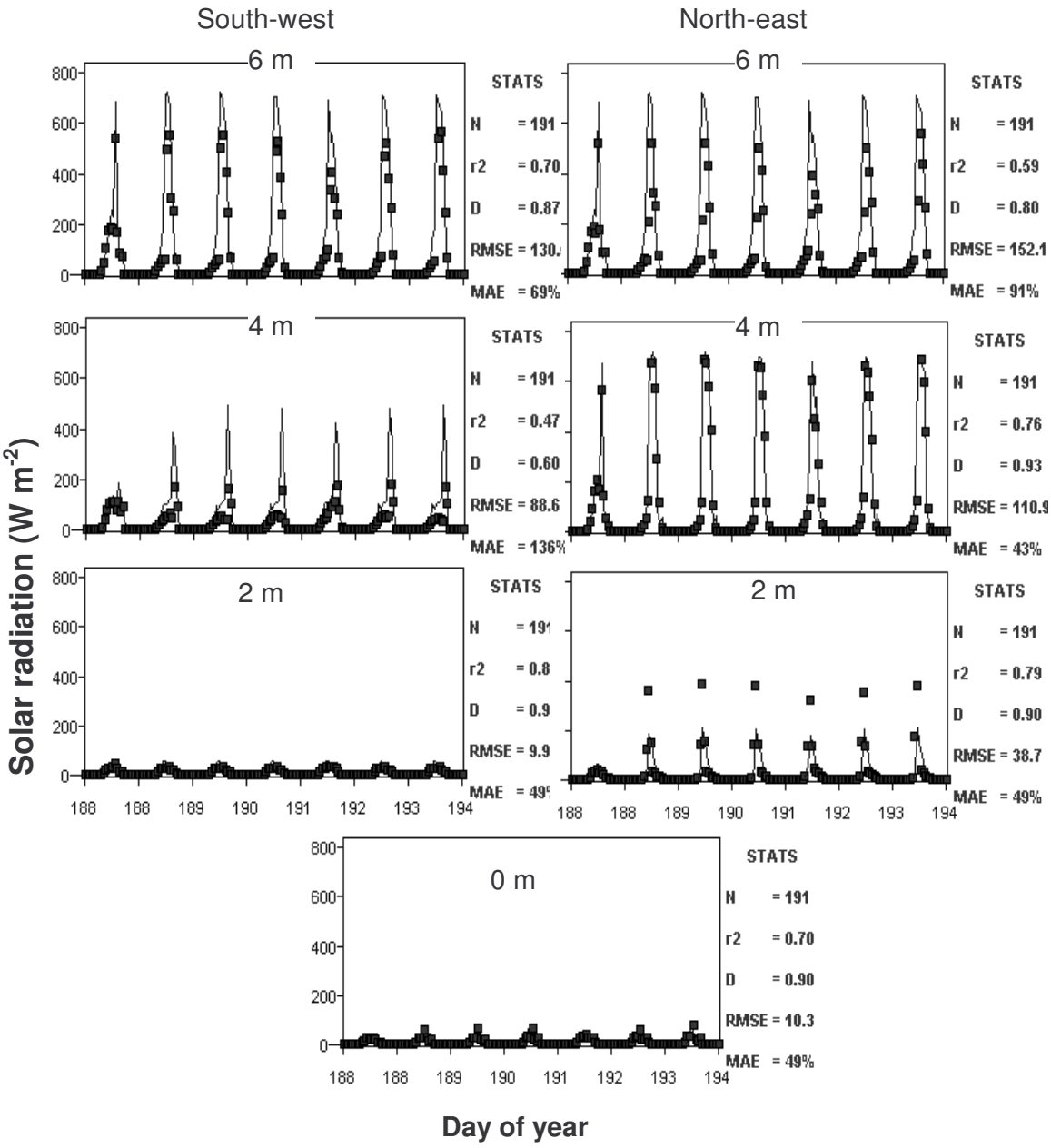

Figure 3.35. Measured (symbols) and simulated (lines) hourly solar radiation at different sides and distances from the tree row in a hedgerow valencia orchard for period 7 to 13 July 1999.

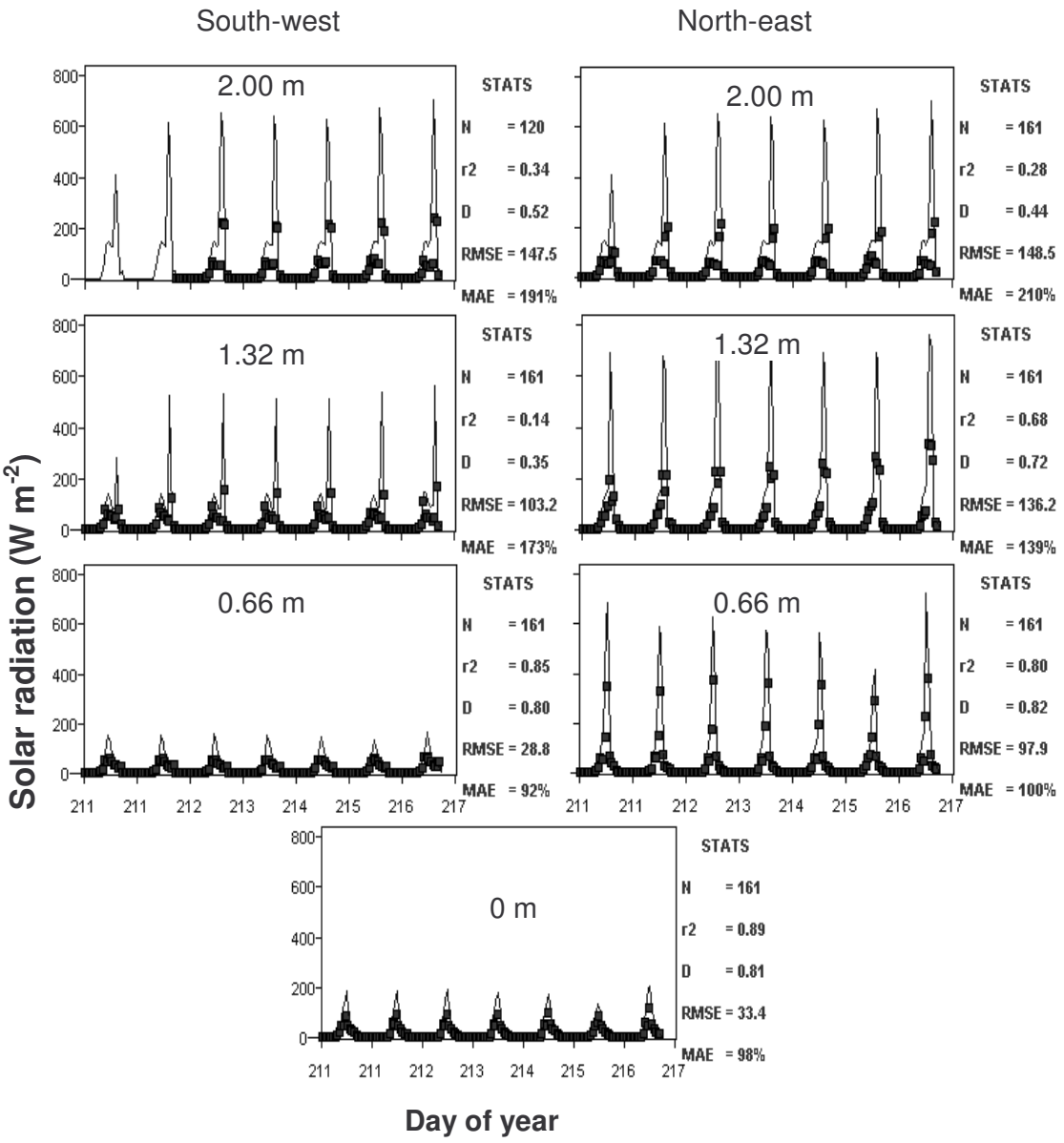

Figure 3.36. Measured (symbols) and simulated (lines) hourly solar radiation at different sides and distances from the tree row in a hedgerow mandarin orchard for the period 30 July to 5 August 1999.

3.4 Evaluation of the two-dimensional water balance model

The two-dimensional soil water balance model uses the energy interception model to allocate energy striking the soil surface for evaporation and the energy absorbed by the canopy for transpiration. The evaluation of the soil evaporation sub-model was not part of this research and the details of that verification can be obtained in the Water Research Commission Report No. 945/1/02. (Annandale *et al.*, 2002). In this section, the volumetric soil water content obtained with the two-dimensional soil water balance model was compared to independent field measurement data in order to evaluate the full SWB two-dimensional model.

Volumetric soil water content data collected with the TDR system in the peach and citrus orchards were compared to SWB simulations. In these simulations, it was assumed that the root distribution across the row was uniform, based on the measurements of root density shown in Figures 3.10a, 3.10b, 3.11a and 3.11b.

Results of model simulations for drying cycles of the peaches and clementines revealed similar trends, so only results for clementine are presented. It must be noted that the summer period for 1999/2000 recorded frequent rain and thus the drying cycles were short. Figures 3.37 to 3.39 deal with the period 13 to 23 February 2000. In Figure 3.37, comparisons are made for the 6 cm depth; the solid line indicating the model predicted volumetric soil water content while the blocks show actual measured values. For the most part there was very good agreement with the mean absolute error (MAE) being ~7% for two comparisons (2.5 and 0 m nodes) and ~17% for the 3.75 and 1.25 m nodes. Similar agreement was recorded for the 26 cm depth in Figure 3.38. At the 90 cm depth (Figure 3.39), MAE was greater, ranging from 14 to 22%. Overall results show that the surface layer (6 cm) predictions were generally very accurate. This indicates that the procedure used to determine the distribution of solar radiation at the surface, used to calculate evaporation, works well. However, it was noted that where differences occurred, the general trend was for the model to predict drier soil than the measurements indicated. This could have been as a result of the very high rainfall causing the surrounding soil to have a high water content and there could thus have been an inflow of subsurface water that was not accounted for in the model predictions for the summer of 1999/2000.

During the 2000/01 summer it was possible to monitor more wetting and drying cycles and the comparisons between measured and simulated volumetric SWC are presented in Figures 3.40 to 3.43 for the Clementine hedgerow orchard. In the “a” portion of these figures the comparisons between the measured (blocks) and SWB predicted (line) values for the

north-western side of the row are presented. The extreme left column of graphs depicts the comparisons for the nodes at 3.75 m starting at the top with the 6 cm depth, then the 26 cm depth comparison just below, followed by the 56 cm depth and finally at the bottom the values for the 86 cm depth. As one moves to the right, so the 2.5 m, then the 1.25 m and finally the nodes at the row centre are depicted. In the "b" portion of Figures 3.40 to 3.43 the comparisons for the north-eastern side of the row are presented. In these figures the nodes at the row centre are on the left with the 1.25, 2.5 and 3.75 m comparisons presented sequentially as one moves to the right. The comparisons for the upper soil depth, i.e. 6 cm, are presented in the top horizontal row of graphics with 26, 56 and 86 cm depths being depicted sequentially as one moves down the figures. In this manner, it is possible to graphically present the spatial and daily comparisons of measured and predicted volumetric SWC on each side of the tree row.

Figure 3.40 presents the comparison between measured and predicted daily SWC for a period just before, during and after a heavy under-canopy irrigation. The time period is 9 to 17 February 2001 and the irrigation applied was ~100 mm across a three metre wide band under the tree canopy. If this water had been applied to the whole surface area it would have been equivalent to a 40 mm irrigation. It is seen in Figures 3.40a and b that the nodes at 3.75 and 2.5 m from the row centre show no change in SWC as would be expected since they did not receive any water. The predicted and measured SWC values for these nodes also show close agreement except for the 86 cm deep node at 3.75 m from the row centre in Figure 3.40a. The nodes 1.25 m from the row centre and at the row centre show excellent agreement in absolute value and trends in the values between measured and SWB predicted SWC at the 6 and 26 cm depths. At the 56 cm depth the trends between measured and SWB predicted values are similar but it appears that the SWB predicted SWC increases sooner than the measured values and then it decreases more quickly. At the 86 cm deep nodes the trends in the predicted and measured SWC are similar but the SWB predicted SWC again tends to increase a bit early. At this depth, the measured SWC is also much higher than the predicted SWC. This trend that the actual/measured SWC at the lower depths is higher than the predicted values could also be due to the citrus roots being less effective at the 56 and 86 cm depths. In Figure 3.11a it is seen that at these depths the mean root length density is less than 1.75 cm cm^{-3}. This value could be regarded as an indication of a threshold value for the rootstock, i.e. when mean root length density is less than 1.75 cm cm^{-3} for the Swingle citromelo rootstock is ineffective for water uptake.

Figure 3.41 shows the comparisons for a rainfall event where 22.6 mm of rain were recorded on 19th February 2001. The comparisons presented are from 18 to 26 February 2001. It is seen that at the 6 cm deep nodes there is excellent agreement in the trends and values of

the SWC for the measured and predicted values. It is also important to note that at distances greater than 1.25 m from the tree, i.e. beyond the canopy, the measured values show a larger increase in SWC after the rainfall event than under the tree canopy. This is due to the interception and canopy storage of rainfall. This aspect of spatially differing canopy interception of rainfall is not being addressed in the model, thus this divergence in the predicted and actual SWC measurements is not surprising. What is surprising is the extent of the canopy interception of rainfall in that with a 22.6 mm rainfall event the soil measurements clearly show these differences. At the 26 cm depth an interesting feature is noted: i.e. the measured SWC values do not reflect any increase while the SWB predictions indicate a noticeable increase in SWC between 19 and 20 February. Apparently, what is happening in practice, is that the wetting front has not penetrated to 26 cm while the model has overestimated the wetting front penetration. At 56 and 86 cm no changes in SWC are measured or predicted. Once again, under the canopy the measured SWC is higher than the predicted values thus supporting the idea that the roots are not effective at these depths. There is good agreement between the measured and predicted SWC at all the 56 cm deep nodes outside the canopy region. In this series of figures the 86 cm nodes show poor agreement between measurements and predictions.

Comparisons for measured and SWB predicted SWC for a good rainfall event, i.e. 34.9 mm on 1 March 2001, are recorded in Figure 3.42. These comparisons run from 26 February to 11 March. Once again there is excellent agreement between the predicted and measured SWC at the 6 cm nodes across the whole row and the effect of canopy interception and storage is clearly shown in the measured values, i.e. for the 6 cm depth at 0 m showing a small increase in SWC in-spite of a heavy rainfall event of 34.9 mm. At the 26 cm deep nodes the model predicted that the wetting front would arrive one day too early (i.e. virtually immediate penetration). This is due to a technicality associated with the daily time step used in the model. The model predicted that the wetting front would reach the TDR sensors on the day of the rainfall, i.e. in a 24 hour time unit. However, since the rain only fell in the late evening the wetting front could only reach the TDR sensors the following day. At the 56 cm depth the measurements show that there is no change in SWC while the SWB predictions indicate that the wetting front would penetrate to that depth. The 86 cm nodes show negligible change in SWC resulting from the rainfall event with good agreement in trends and values on the S-W side but large differences in SWC values on the N-E side.

The last series of comparisons in Figure 3.43 are for a light rainfall event of 8.3 mm on 19 March 2001. The period considered begins on 18 and ends on 29 March 2001. Looking at the measured values it is noted that only at 2.5 m on the south-western side (Figure 4.43a) and at 3.75 m on the north-eastern side (Figure 3.43b) is there a slight response in SWC at

6 cm depth. The rest of the nodes show no response in SWC. So this rainfall of 8.3 mm must be regarded as ineffective in altering the SWC. The SWB predictions show no response to this rainfall as well.

When all these results are considered, the model does a good job of predicting the soil water balance across the hedgerow plantings for a wide range of irrigation and rainfall events. This is particularly true for the top 6 cm layer. At the 86 cm depth there are unacceptable differences between measured and predicted SWC on various instances. A major feature here is most probably due to the impermeable saprolite/rock base causing lateral water movement in the subsoil.

There could be other causes for these discrepancies, for example spatial variability. It is well recognised that spatial variability is a major factor when point measurements of soil water are made with heat dissipation sensors or TDR probes. Due to the high cost of the equipment used, it was not possible to replicate the measurements in order to account for spatial variability.

Another source of error could have been the soil disturbance during the installation of TDR probes. It is clear that, even if soil water sensors are installed taking the utmost care and precautions to minimize soil disturbance, some disturbance of the soil always occurs. Firstly, to get to a depth of 0.4 to 0.9 m some form of excavation and refilling must be done. In addition, during the insertion of TDR probes in the soil volume to be measured, some compaction occurs that changes soil bulk density and water retention properties around the rods of the probes. This could cause errors in measurement, especially because the effect of the volume of soil adjacent to the rods has the greatest effect on the measurement (Knight, 1992).

It must be remembered that in the two-dimensional simulations presented, there are basically seven profiles that are being evaluated by four single point measurements for each profile. In the model, it is assumed that the initial water contents are all the same, i.e. only one initial SWC is required per soil depth as an input and this value is then allocated to all the nodes at that specific soil depth. In practice the initial SWC for each node in the 2-D situation is rarely the same and one then uses an average as a beginning point. This is the reason why some measured SWC values begin either above or below the SWB predicted SWC. In some cases, particularly at the 86 cm depth these discrepancies can be rather large as can be seen in Figure 3.42b. In addition, the model calculates saturated hydraulic conductivity according to equation 1.1.20 and assigns the same value for all horizontal nodes at similar depths. In a natural, in field situation, this idyllic situation will rarely exist.

The problems encountered in measuring soil water content, related to spatial variability and point measurements, are highlighted in Figure 3.44. This Figure presents the measured volumetric soil water content (SWC) data (solid circles) at four depths across the clementine hedgerow, as well as interpolated isolines for two different days. The first day (14 February 2000) was after 48 mm of rain, while 24 February 2000 reflects the water distribution 10 days later. It is important to note the lack of uniformity in the soil water content at the same depth across the hedgerow even after heavy rain. In spite of the fact that most of the profile was very wet (> 34 %), there was a spur of relatively drier soil penetrating to 900 mm. After ten days, the surface layer (6 cm) dried out from around 30 % to ~20%, while the 34% isoline straightened out at a depth of between 400 and 600 mm. This indicates that mainly above this depth the trees were removing water from across the whole inter-row and not from just under the canopy region. It is also important to note that below 600 mm there was a noticeable equilibration of the water content. The water content at 900 mm showed very little change from the original range of 32 to 50 %. This could have been due to the impervious lithic layer preventing free drainage of the subsoil. The large differences in volumetric soil water content measured across the hedgerow at 900 mm soil depth, however, are mainly attributed to spatial variability in soil properties and sensor placement. It is clear that TDR probes can be used in irrigation scheduling to determine crop water use over certain periods. Caution should, however, be exercised in the interpretation of absolute values of volumetric soil water content obtained from the probes.

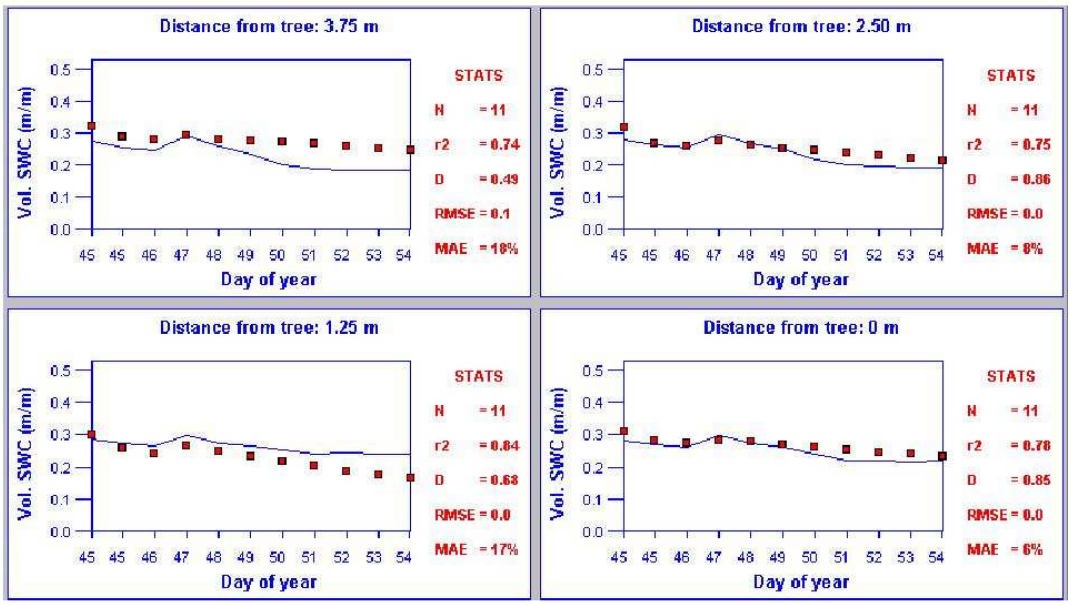

Figure 3.37. Simulated (line) and measured (squares) volumetric soil water content at 6 cm depth, 3.75; 2.5 and 1.25 m on the NE side of the trunk, as well as directly under the tree, for the clementine hedgerow for the period 13 to 23 February 2000.

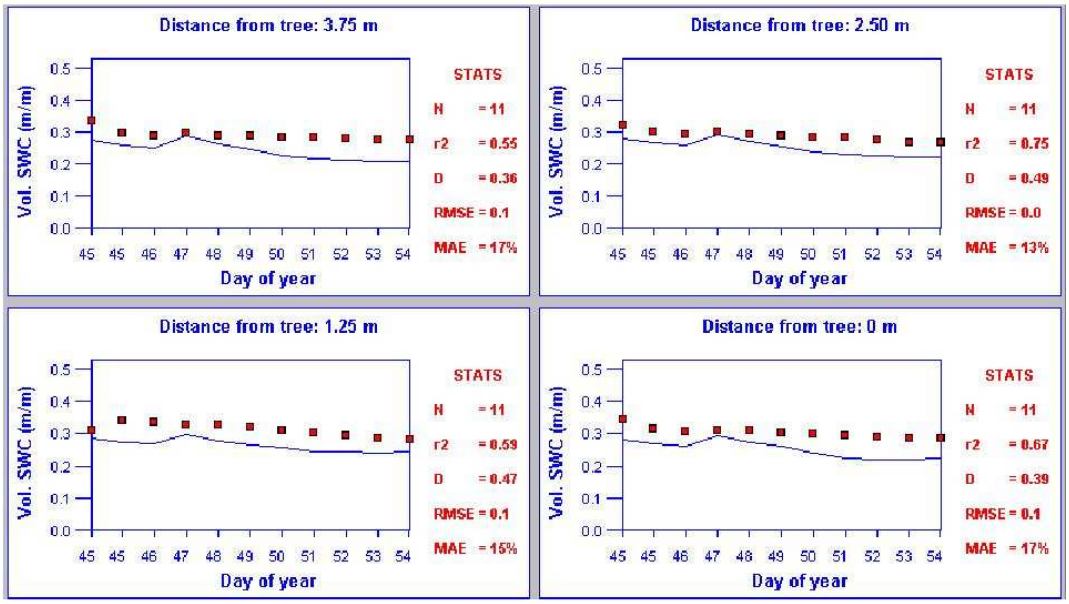

Figure 3.38. Simulated (line) and measured (squares) volumetric soil water content at 26 cm depth, 3.75; 2.5 and 1.25 m on the NE side of the trunk, as well as directly under the tree, for the clementine hedgerow for the period 13 to 23 February 2000.

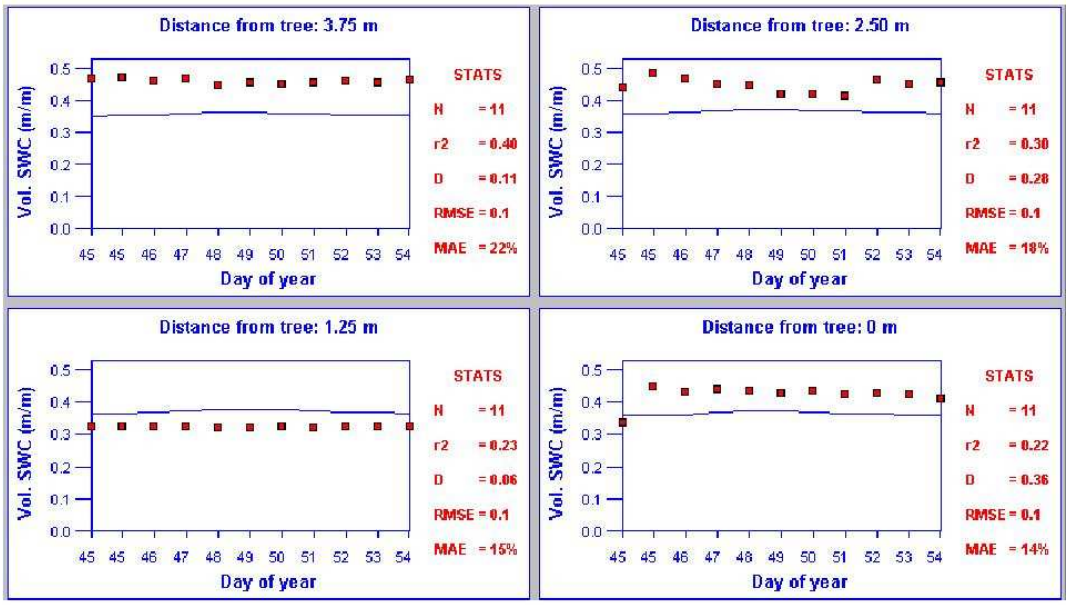

Figure 3.39. Simulated (line) and measured (squares) volumetric soil water content at 90 cm depth, 3.75; 2.5 and 1.25 m on the NE side of the trunk, as well as directly under the tree, for the clementine hedgerow for the period 13 to 23 February 2000.

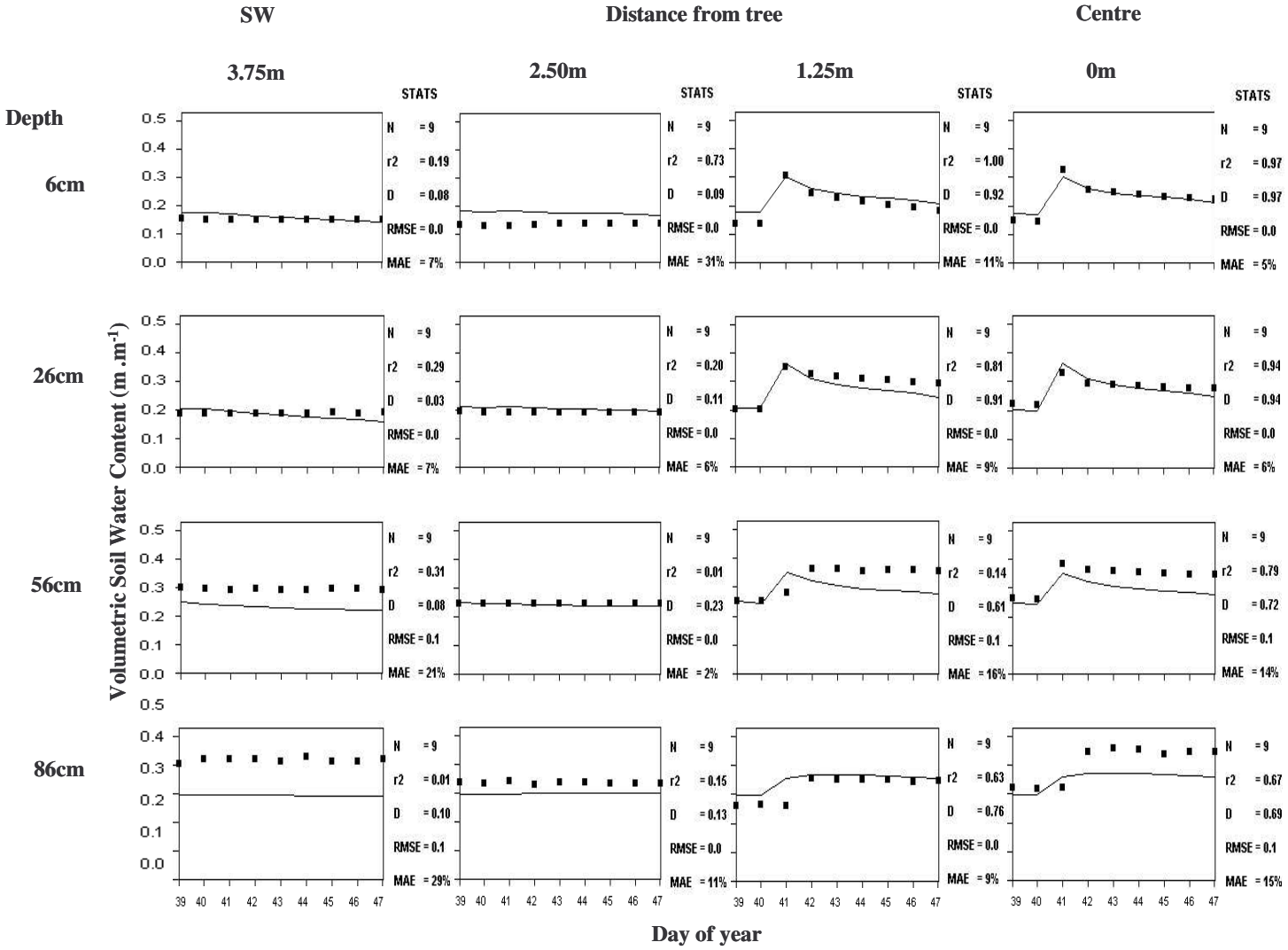

Figure 3.40a. Simulated (line) and measured (squares) volumetric soil water content on the SW side of the clementine hedgerow at 6, 26, 56, and 86 cm depths for the period 9 to 17 February, i.e. during a heavy irrigation event.

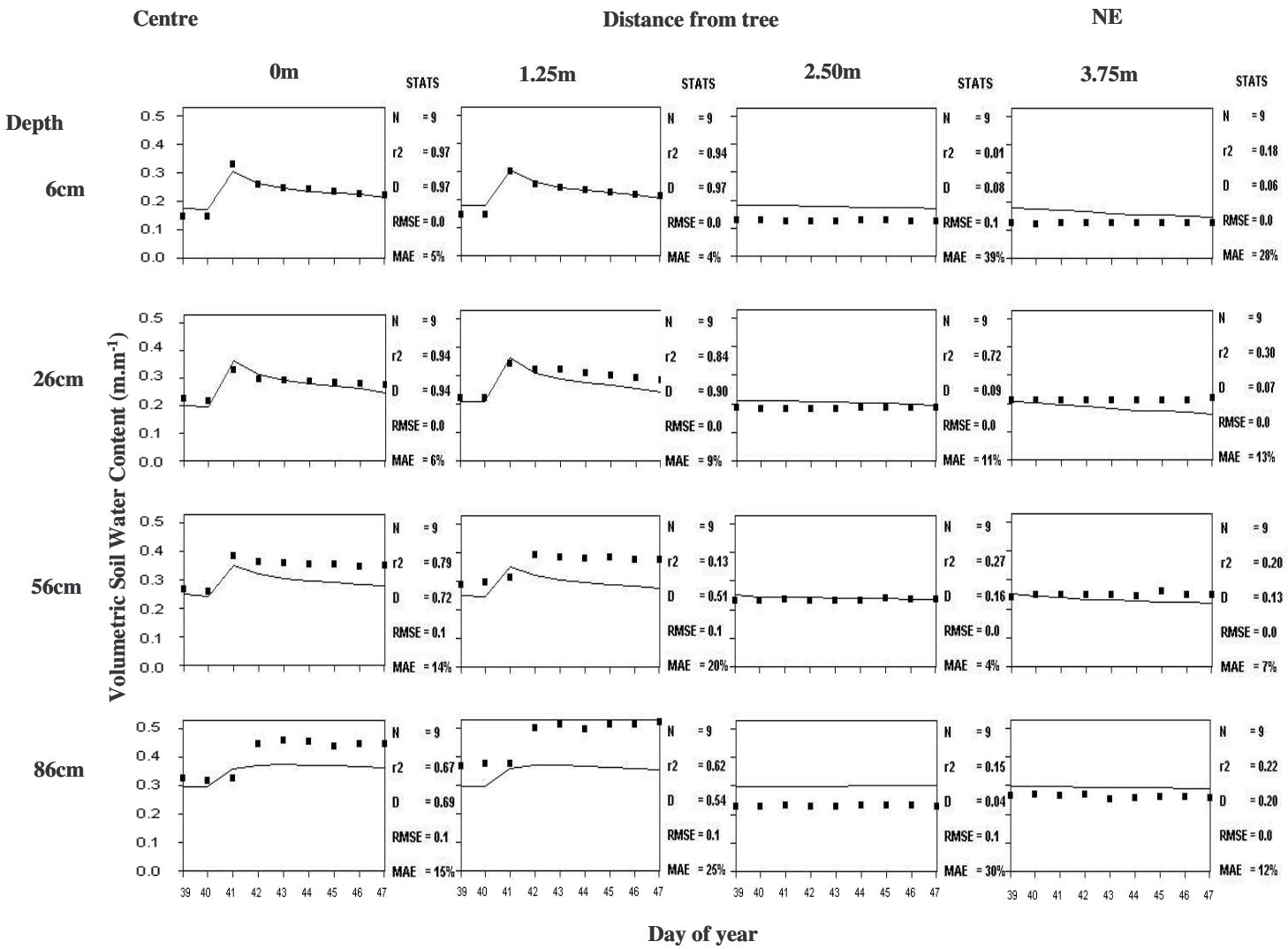

Figure 3.40b. Simulated (line) and measured (squares) volumetric soil water content on the NE side of the clementine hedgerow at 6, 26, 56, and 86 cm depths for the period 9 to 17 February, i.e. during a heavy irrigation event.

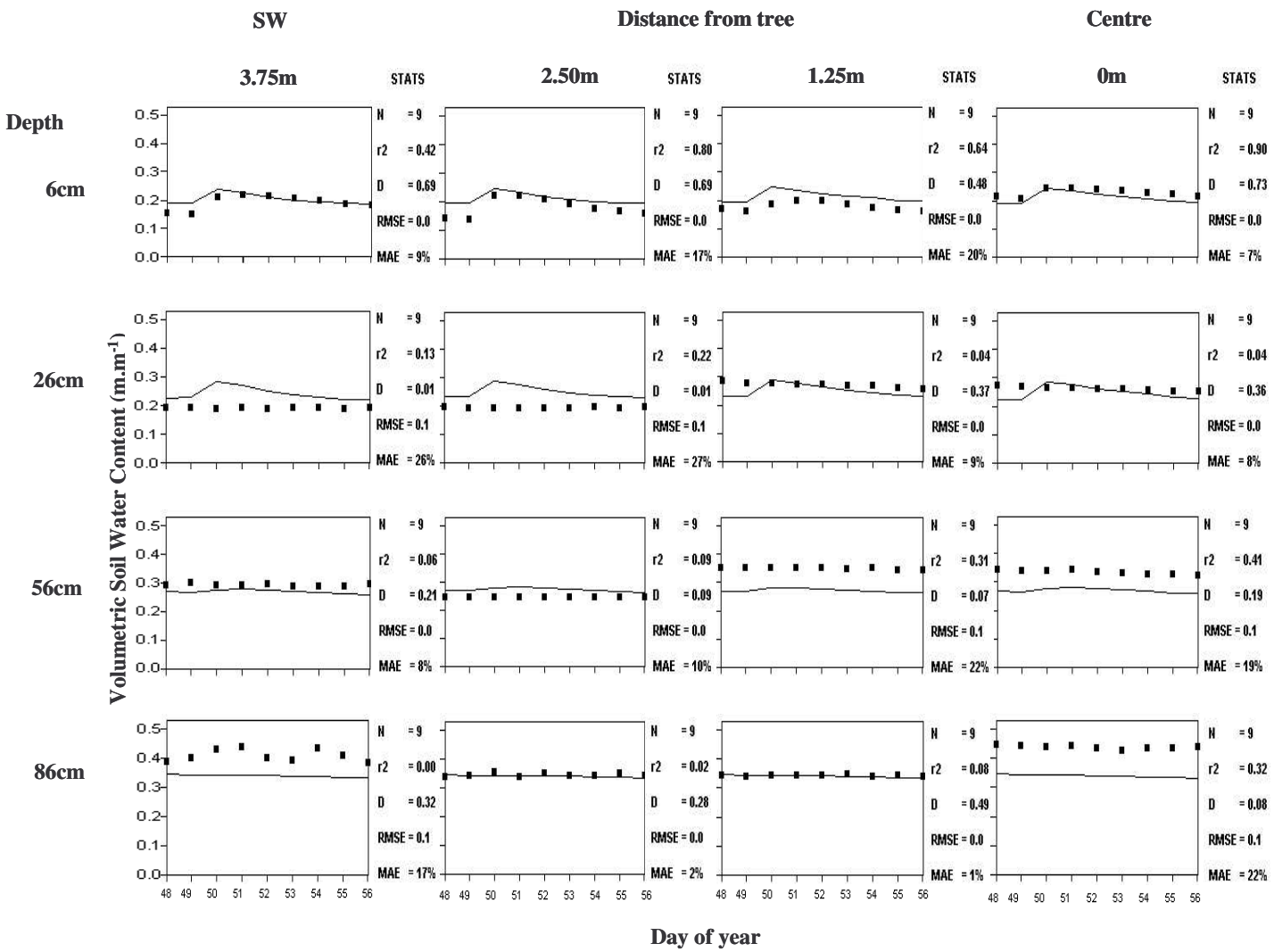

Figure 3.41a. Simulated (line) and measured (squares) volumetric soil water content on the SW side of the clementine hedgerow at 6, 26, 56, and 86 cm depths for the period 18 to 26 February, i.e. during a 22.6 mm rainfall event.

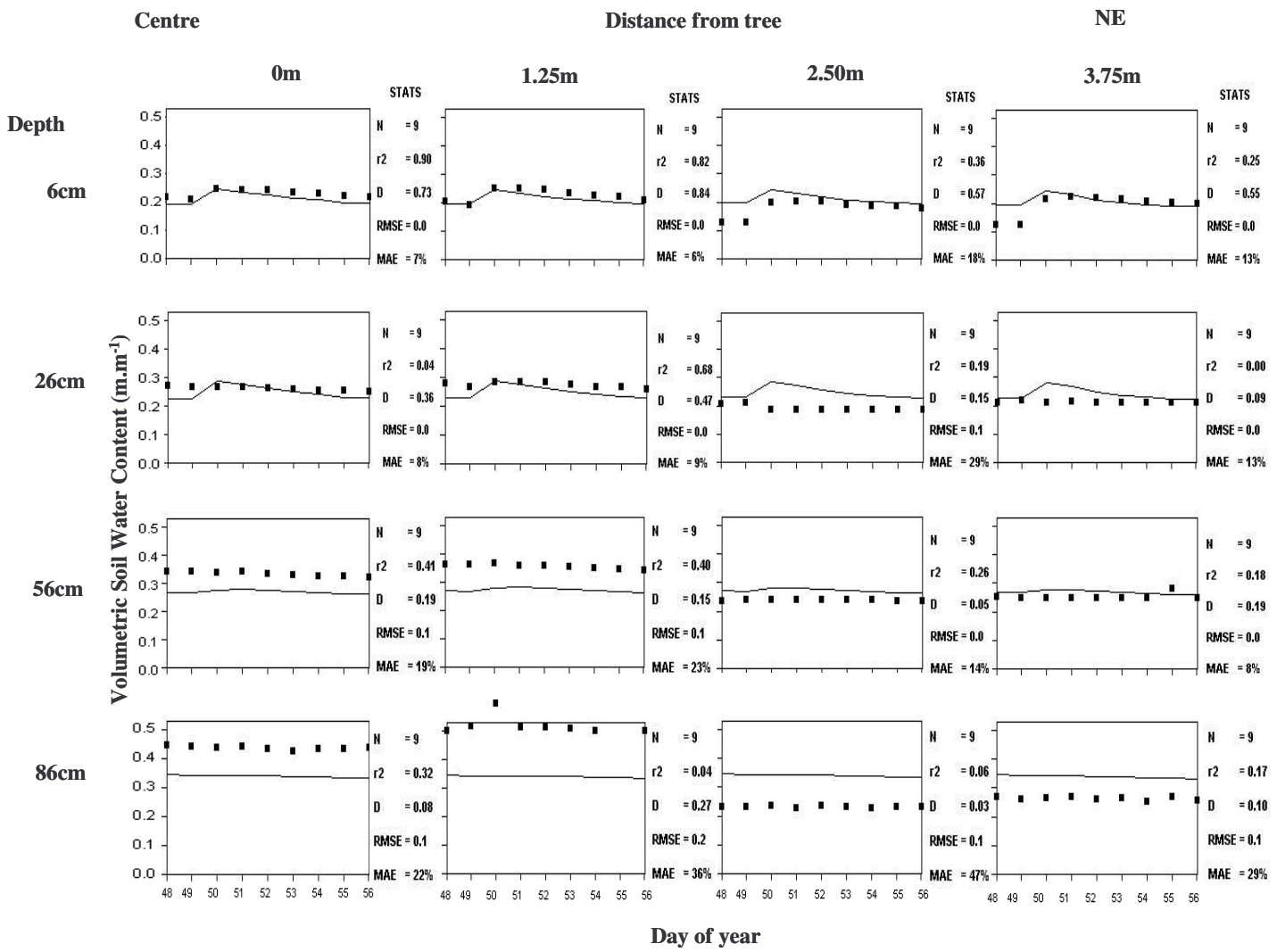

Figure 3.41b. Simulated (line) and measured (squares) volumetric soil water content on the NE side of the clementine hedgerow at 6, 26, 56, and 86 cm depths for the period 9 to 17 February, i.e. during a 22.6 mm rainfall event.

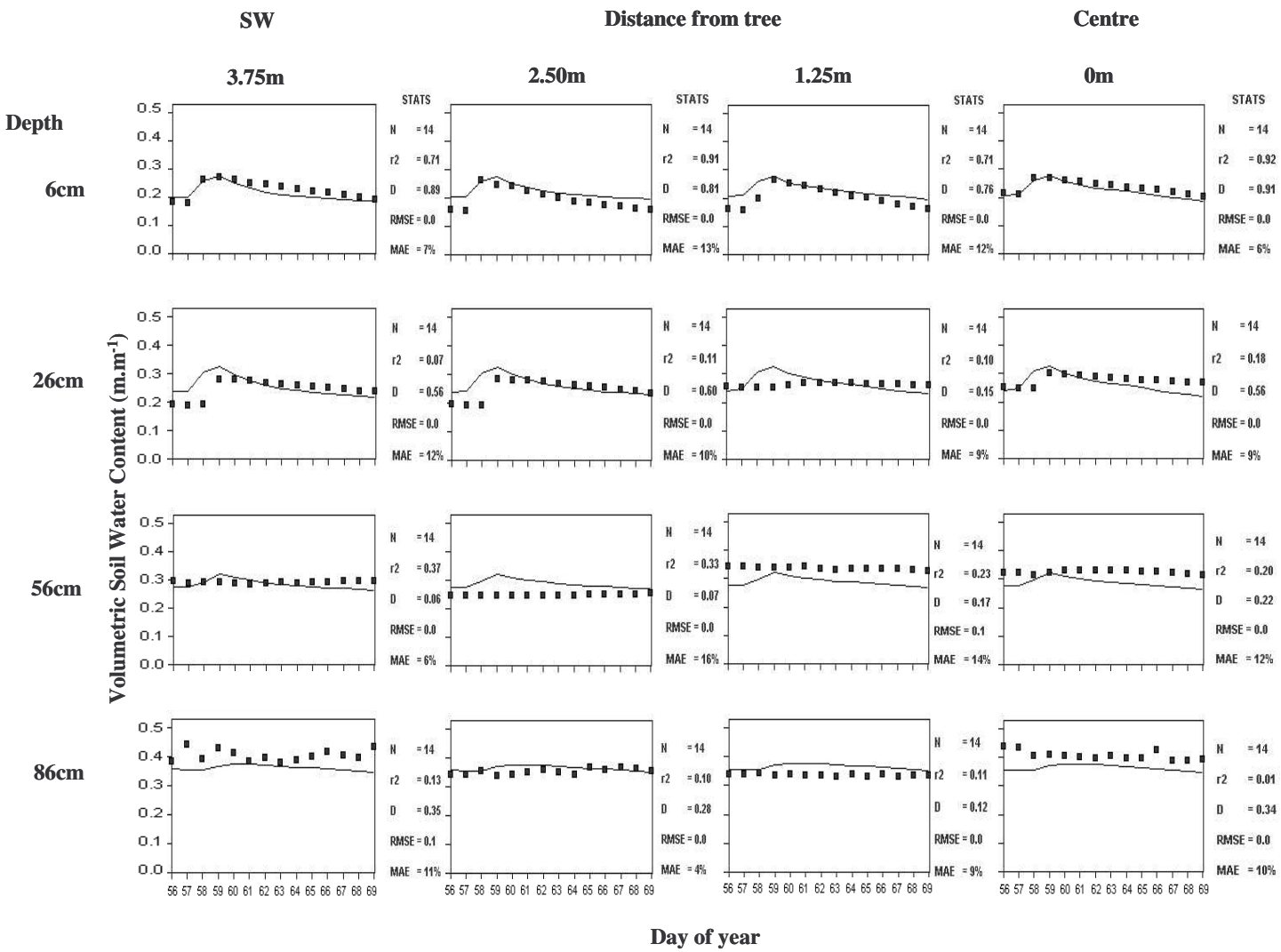

Figure 3.42a. Simulated (line) and measured (squares) volumetric soil water content on the SW side of the clementine hedgerow at 6, 26, 56, and 86 cm depths for the period 26 February to 11 March, i.e. during a heavy rainfall (34.9 mm) event.

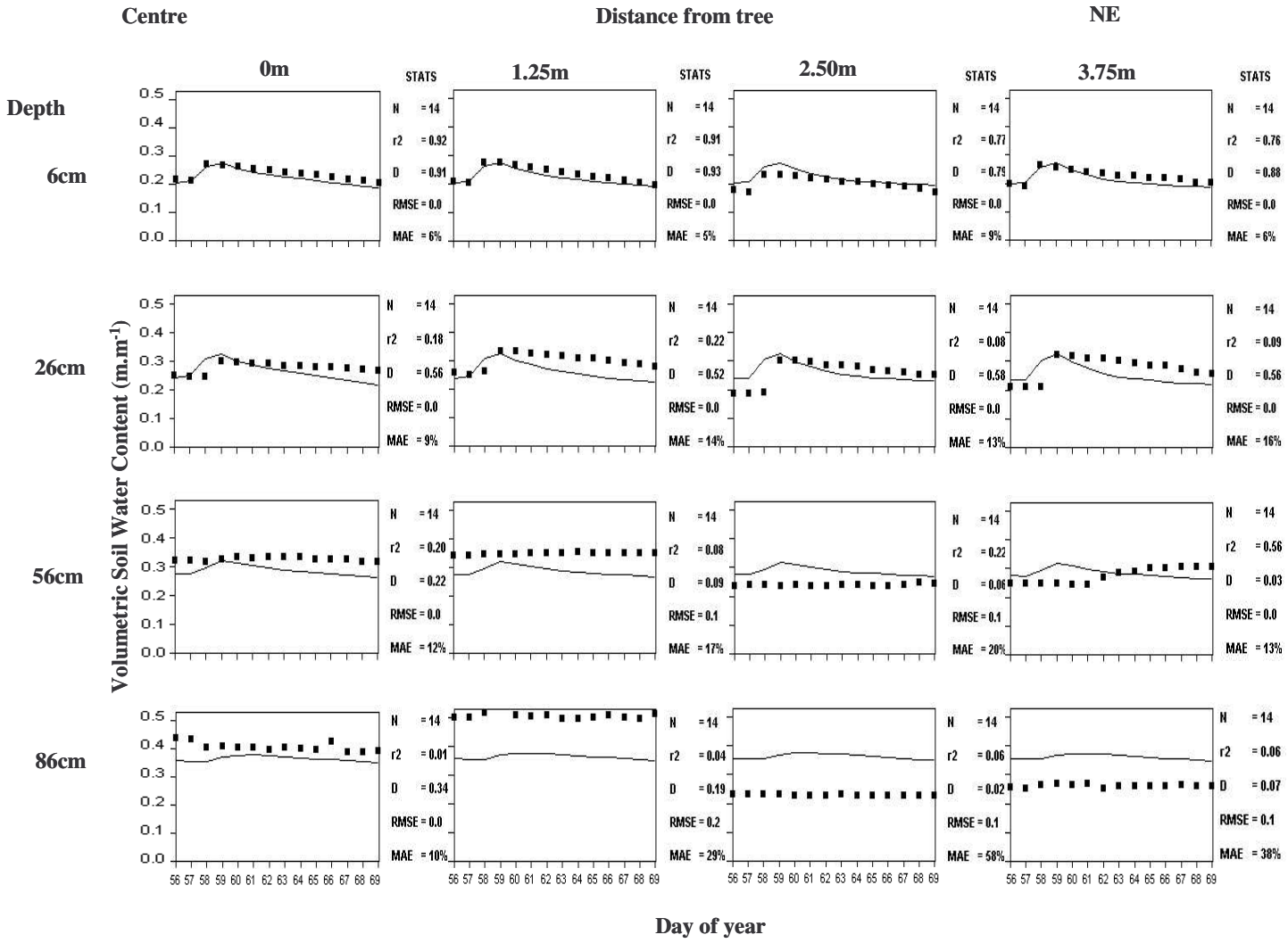

Figure 3.42b. Simulated (line) and measured (squares) volumetric soil water content on the NE side of the clementine hedgerow at 6, 26, 56, and 86 cm depths for the period 26 February to 11 March, i.e. during a heavy rainfall (34.9 mm) event.

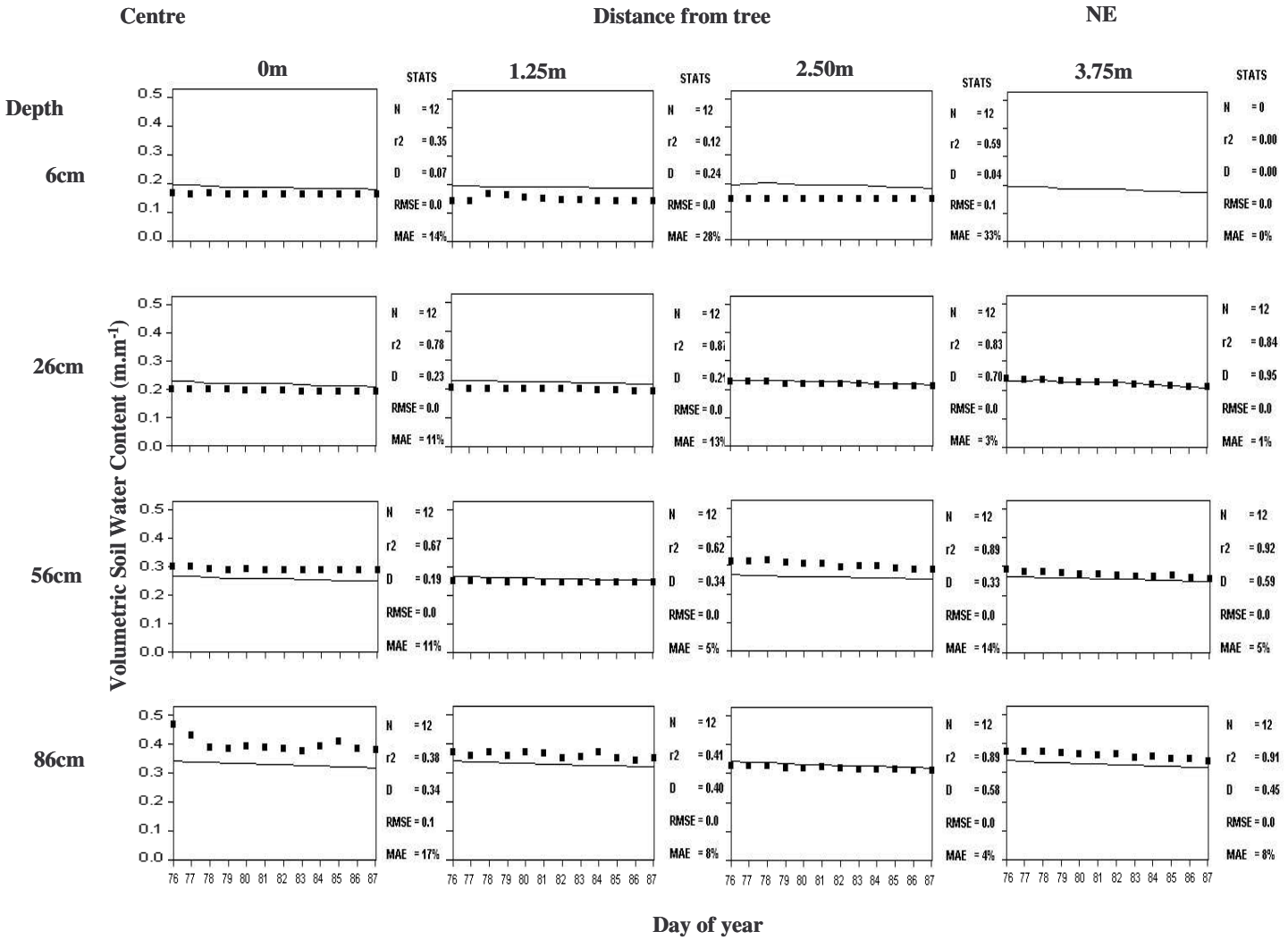

Figure 3.43a. Simulated (line) and measured (squares) volumetric soil water content on the SW side of the clementine hedgerow at 6, 26, 56, and 86 cm depths for the period 18 to 29 March, i.e. during a light rainfall (8.3 mm) event.

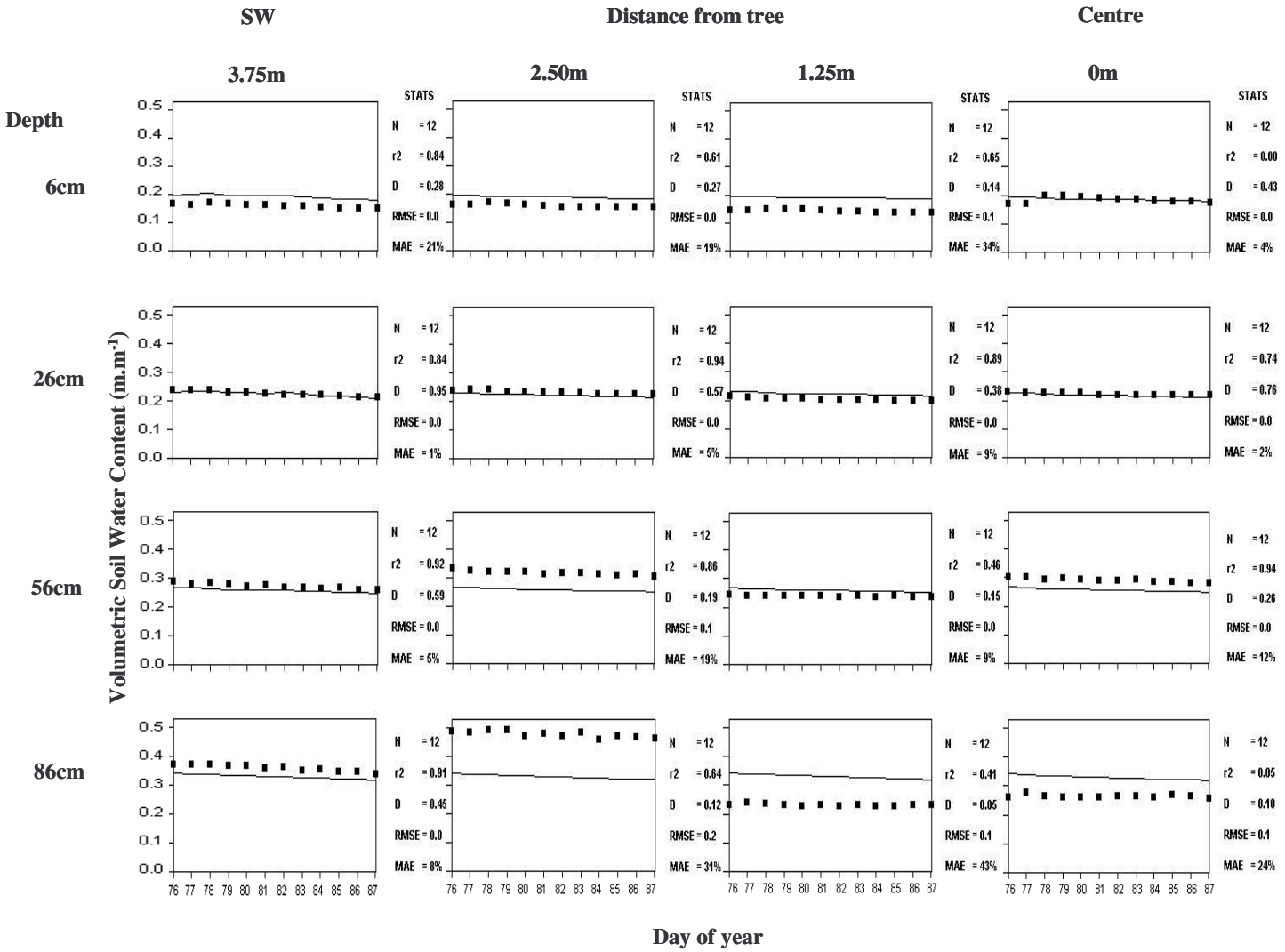

Figure 3.43b. Simulated (line) and measured (squares) volumetric soil water content on the NE side of the clementine hedgerow at 6, 26, 56, and 86 cm depths for the period 18 to 29 March, i.e. during a light rainfall (8.3 mm) event

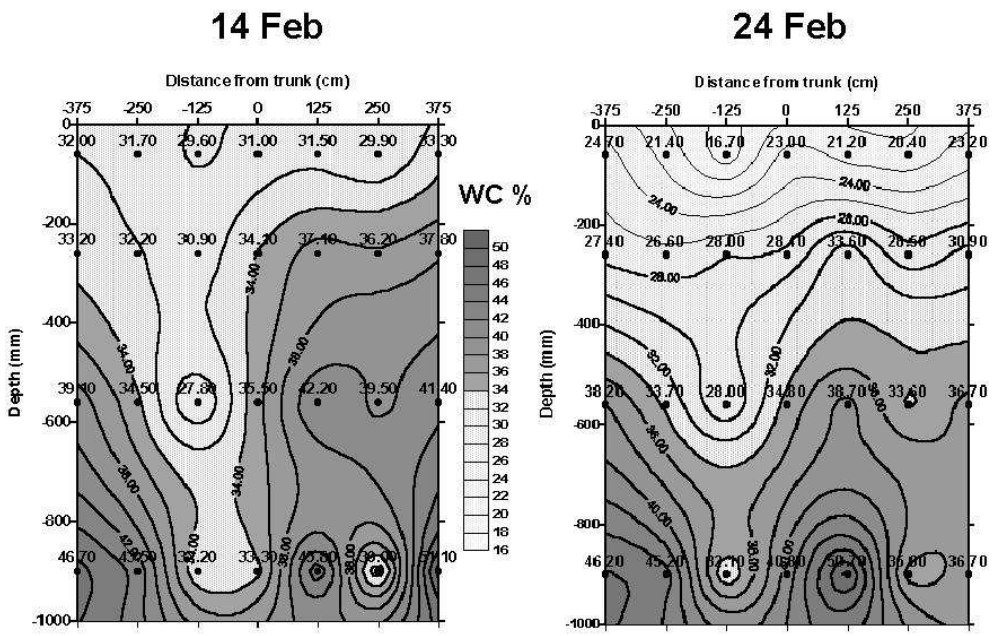

Figure 3.44. Variation in measured volumetric soil water content (WC %) with depth across the clementine hedgerow one day after a 48 mm rainfall (14 February 2000) and 10 days later (24 February 2000). Negative distances on the x-axis are for the SW side of the row, and positive values are for the NE side.

3.5 Scenario modelling and sensitivity analysis

Although the two-dimensional SWB was mainly developed as a tool for real-time irrigation scheduling, it can also be used for planning purposes. In this Section, scenario modelling and sensitivity analyses were carried out varying some input parameters (row orientation, canopy width, wetted diameter and fraction of roots in the wetted volume of soil) and observing variations in certain output variables. The aim of this exercise was to identify the most suitable management practice in order to maximise water use efficiency as well as illustrate another application for this management tool.

Two case studies were considered for two 'virtual" orchards, the one in Kakamas (Northern Cape) and the other in Stellenbosch (Western Cape). The two locations were chosen for comparative purposes, as the latitudes and climates differ considerably. The geographic coordinates of Kakamas are 28º46'S and 20º37'E, altitude is 850 m and the climate is dry and hot with an average annual rainfall of ~ 150 mm, mostly in summer. Stellenbosch (33º54'S; 18º52'E; altitude 146 m) is located in the winter rainfall region (Mediterranean climate) with an average annual rainfall of ~ 800 mm.

In the 'virtual' orchard at Kakamas, field capacity was taken as 0.2 m m^{-1} and permanent wilting point was 0.1 m m^{-1}. At Stellenbosch, field capacity was taken to be 0.15 m m^{-1} and permanent wilting point was 0.08 m m^{-1}. In both orchards, the depth of the soil profile was 1.1 m, the depth of the root system was 1 m and bulk density was 1.5 Mg m^{-3}. Row width was assumed to be 5 m. The irrigation system was assumed to be an under canopy type capable of uniform distribution over the soil surface, most probably micro irrigation.

Weather data sets for the two locations included maximum and minimum temperature, solar radiation, wind speed as well as maximum and minimum relative humidity. The simulations were run from 1 January 1998 until 28 February 1998. This is the period of the year with peak atmospheric evaporative demand at both locations.

The objective of the exercise was to find the row orientation, width of the canopy and width of the irrigated strip that will provide maximum water use efficiency. An additional sensitivity analysis was carried out to investigate the effect of root density in the inter-row area on crop water use.

3.5.1 Row orientation

Scenario simulations were carried out with optimal conditions of soil water supply. Irrigations were simulated daily on a 1 m wide wetted strip to restore daily water losses through evaporation and transpiration. Canopy width was assumed to be 2 m, which is common

practice in the areas considered. Canopy height was 3 m and leaf area density 2 m^2 m^{-3}. Simulations were run varying the row orientation in the two orchards and observing variations in the output results of evaporation and transpiration. The root system was assumed evenly developed in the wetted and non-wetted portions of the profile.

The results are shown in Figure 3.45. Evaporation (E), transpiration (T) and evapotranspiration (ET) were higher in the hot and dry climate of Kakamas compared to Stellenbosch. Transpiration was larger than evaporation at both sites for the specific input data set used. Expressed as % of ET, E was lowest and T was largest at row orientations close to 0º (N-S row axis). Predicted evaporation was highest for N-S row orientations since radiation will reach the soil surface on the eastern side of the canopy during late morning and the soil on the western side during early afternoon. At this time of day the solar irradiance is generally at or near the daily maximum, hence the higher evaporation. However, the benefits from larger increases in transpiration will outweigh the slight increase in evaporation. It is therefore recommended that, at both locations, the orchard be planted in a N-S orientation to maximise canopy interception of solar radiation. If hedgerows are planted on a E-W axis, it would be advantageous to irrigate on the southern, shaded side to minimise water loss through evaporation.

3.5.2 Wetted diameter and canopy width

Scenario simulations were run varying wetted diameter (width of the wetted strip) and canopy width, and observing variations in the output results of evaporation and transpiration. Simulations were run for both case studies with row orientation equal to 0º. Irrigations were simulated daily to restore water losses through evaporation and transpiration. Canopy height was 3 m and leaf area density 2 m^2 m^{-3}. The root system was assumed to be horizontally and evenly developed in the wetted and non-wetted portions of the soil.

Simulated transpiration in mm is shown in Figure 3.46. Transpiration was higher in the hot and dry climate of Kakamas compared to Stellenbosch. It increased by increasing canopy width as well as increasing wetted diameter. This is undoubtedly due to a larger interception of energy by the canopy, and a larger soil water supply. In Figure 3.47, transpiration is expressed as a percent of ET. As canopy width increases so the contribution of T increases. This is due to increased canopy interception and shading of soils reducing the evaporation component. An interesting feature is revealed when considering the effect of increasing wetted diameter, i.e. the transpiration % is reduced due to increased evaporation losses when the wetted area of the soil surface became larger. As a rule of thumb, good water use efficiency can be assumed when more than 70% of the soil water is used for transpiration. In these simulations the 70% T value was achieved only when the canopy width exceeded 2 m

(0.5 m wetted diameter). For the 2.5 m canopy width, 70% T was achieved with a wetted diameter less than 1.5 m. A 3 m wide canopy recorded 70% T with wetted diameters between 1.5 m and 0.5 m. These simulations show how transpiration is influenced by canopy width and wetted diameter, i.e. a too small wetted diameter will restrict transpiration while erring to a large wetted diameter will reduce water use efficiency.

3.5.3 Root density

The SWB model allows the user to choose the fraction of roots in the wetted volume of soil. A sensitivity analysis was carried out for both case studies varying the fraction of roots in the wetted volume of soil, and observing variations in the output results of evaporation and transpiration. Simulations were run for both case studies with row orientation equal to 0º, wetted diameter 2 m and canopy width 2 m. Canopy height was 3 m and leaf area density 2 m^2 m^{-3}. As the first two months of 1998 were very dry at Kakamas and Stellenbosch, 50 mm rains were simulated to occur every 10 days. This yielded a total of 300 mm for the two months.

Figure 3.48 shows simulated evaporation and transpiration as a function of the fraction of roots in the wetted volume of soil. A root fraction of 1 indicates that all roots are assumed to be in the wetted volume of soil, a root fraction of 0.9 indicates that 90% of the roots are in the wetted volume and 10% in the non-wetted volume, and so on. Maximum transpiration was determined for the particular data sets by simulating daily irrigations to restore water losses through evaporation and transpiration.

It was interesting to note the efficiency of rainfall utilisation by crops having different root densities in the wetted and non-wetted portions of the soil (Figure 3.48). Low T and high E was calculated by assuming all roots are in the wetted volume. By decreasing the root fraction in the wetted volume down to 0.5, T increased and E decreased as the roots in the inter-row volume contributed to crop water uptake. By assuming a root fraction of 0.5 (the same amount of roots in the wetted and non-wetted volume, i.e. root system evenly distributed across the row), T was very close to maximum T and evaporation was the lowest. By further decreasing the root fraction in the wetted volume and assuming there were more roots in the non-wetted volume, T decreased and E increased. This occurred as the major contribution to root water uptake originated from the non-wetted volume of soil, where no shading of the soil generally occurred during the day, evaporation was high and less water was available for transpiration. The effect of root density across the row was more pronounced at Kakamas where the atmospheric evaporative demand is higher compared to Stellenbosch.

3.5.4 Interpretation of results

The idea behind doing these simulations is to illustrate one type of application for which this model can be used. These orchard specifications were decided on in a office in Pretoria and could be totally unrealistic. The concept of a ”virtual orchard” could have been applied to Nelspruit and/or Hoedspruit to do a series of “what-if” simulations to give an indication what trends could be expected in that area. This sort of information can be very helpful for planning orchard dimensions and irrigation specifications.

The scenario simulations done for these “virtual orchards” indicate that to maximise water use efficiency, the optimal management for the orchards in Kakamas and Stellenbosch imply row orientation 0º (N-S row axis). These simulations have confirmed that the wetted area does have a important effect on water use efficiency and must be considered. For example, if the wetted area is too small, transpiration is restricted and thus dry matter production, i.e. yield, will be lost. On the other hand, if the wetted area is too large, the evaporation component will be increased thereby reducing water use efficiency. So from the simulations the following guidelines are suggested:

- When the canopy width is 2.0 m the wetted diameter should not exceed 0.5 m.
- A canopy width of 2.5 m would achieve the optimum water use efficiency with a wetted diameter of 1.0 m
- The wetted diameter should be increased to 1.5 m for a 3 m wide canopy.

It must be remembered that for these simulations the profile depth was assumed to be 1.1 m. In other words, a wetted diameter of 0.5 m represents a cross-sectional area of 0.55 m^2 while a wetted diameter of 1 m represents a cross-sectional area of 1.1 m^2. Implicit in this, is an increase in both soil water storage volume as well as root surface area for water uptake with increasing wetted diameter. To meet higher transpiration rates associated with larger canopies there must be a corresponding increase in root surface area available for water uptake, i.e. an increase in the conduit or “plumbing” to supply the increased water flow. These results highlight the important influence root surface area can have on transpiration

In South Africa, a water deficient area, every attempt must be made to make optimal use of any rainfall that occurs. The two example sites selected to illustrate this point are notorious for minimal rainfall during the period that was considered. This is why the rainfall was “cooked” by including “50 mm rains simulated to occur every 10 days”. By doing this it is possible to show the value of rainfall in the inter-row contributing to the water balance. Thus, from these simulations, it is seen that if the region under consideration does experience rainfall, then it is important to create conditions that promotes root development in the inter-

row so that this water can be utilized by the trees. According to these simulations the optimum would be that roots are uniformly distributed across the row, i.e. 50% under the canopy & 50% in the inter-row (root density fraction = 0.5). This information shows that root distribution is an important factor and thus orchardists will have to take notice. An accurate estimate of the root fraction in the wetted and non-wetted volume can be obtained by digging a trench across the row, taking soil samples and determining root densities. Even though this is a labourious task, it is recommended that this practice be applied.

It must be borne in mind that the examples presented in this study are case specific. Different results are to be expected for different conditions and if different input data sets are used. The results of the scenario simulations were obtained assuming the orchard is situated on a level area. It can be expected that under conditions where the orchard surface slopes giving a different aspect, under differing hedgerow orientations as well as at different latitudes, the relative importance of transpiration to evaporation would differ. These variables should be accounted for when planting an orchard.

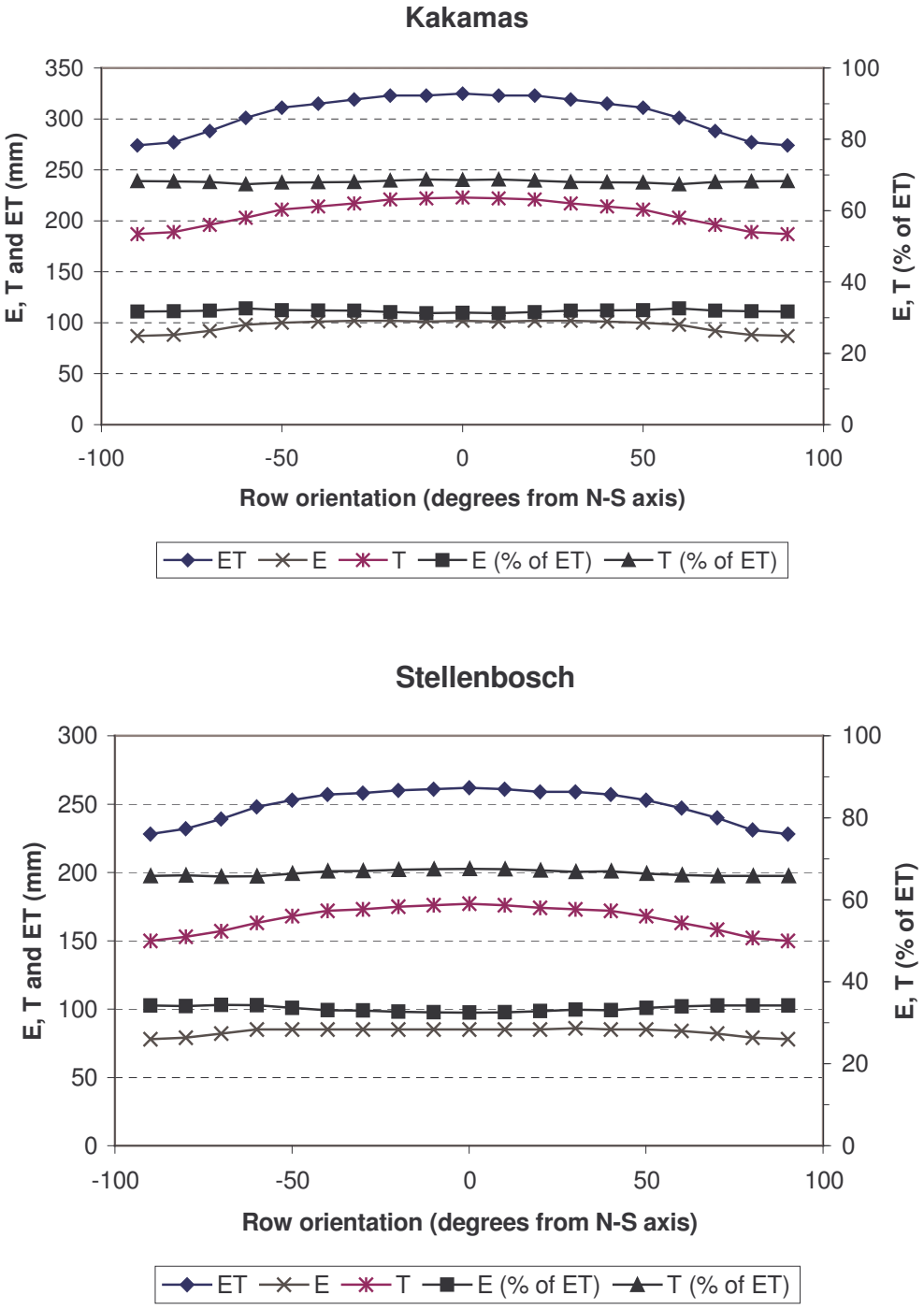

Figure 3.45. Simulated evaporation (E), transpiration (T) and evapotranspiration (ET) as a function of row orientation for two orchards at Kakamas and Stellenbosch for period 1 January to 28 February 1998.

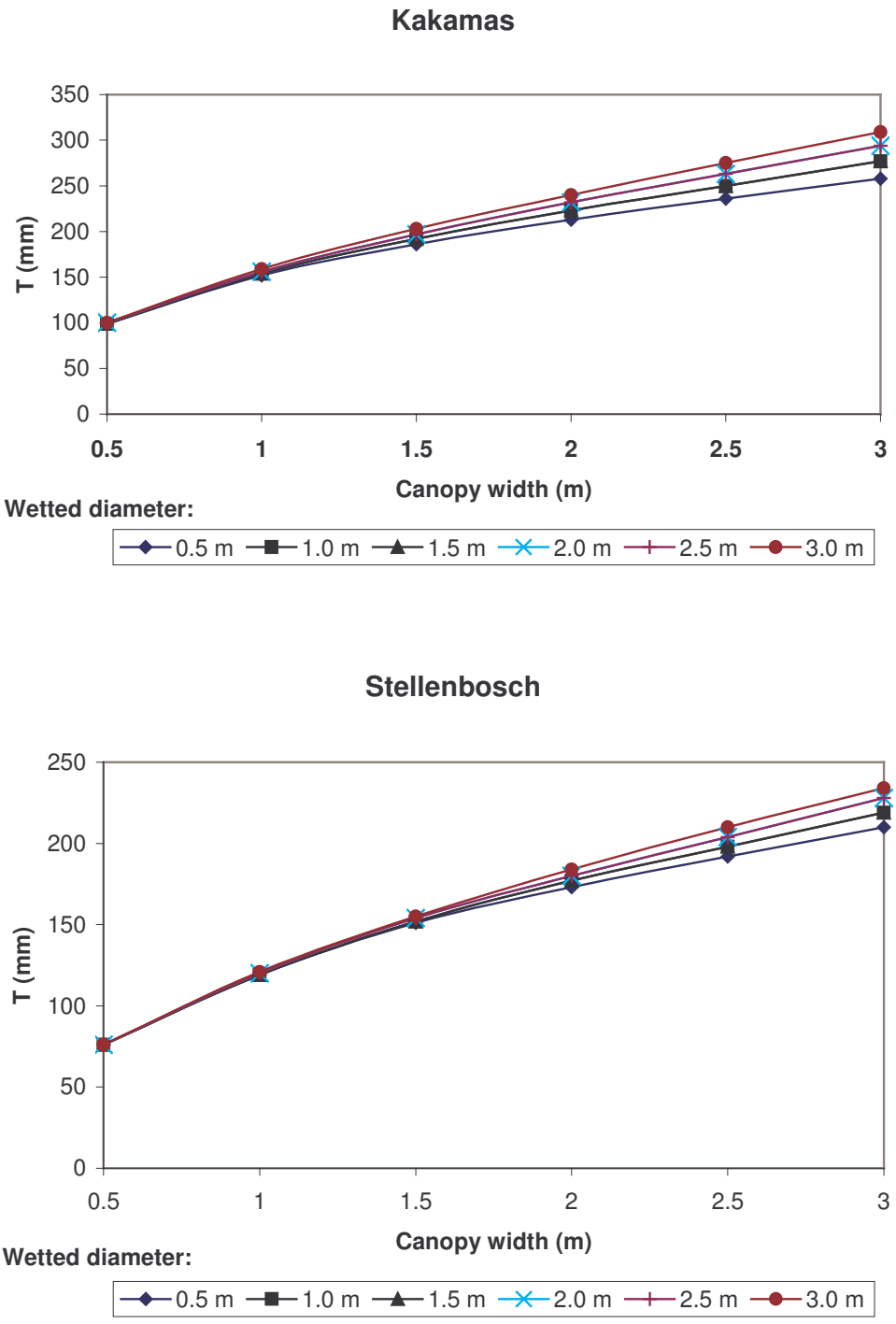

Figure 3.46. Simulated transpiration (T) as a function of canopy width and wetted diameter for two orchards at Kakamas and Stellenbosch for period 1 January to 28 February 1998.

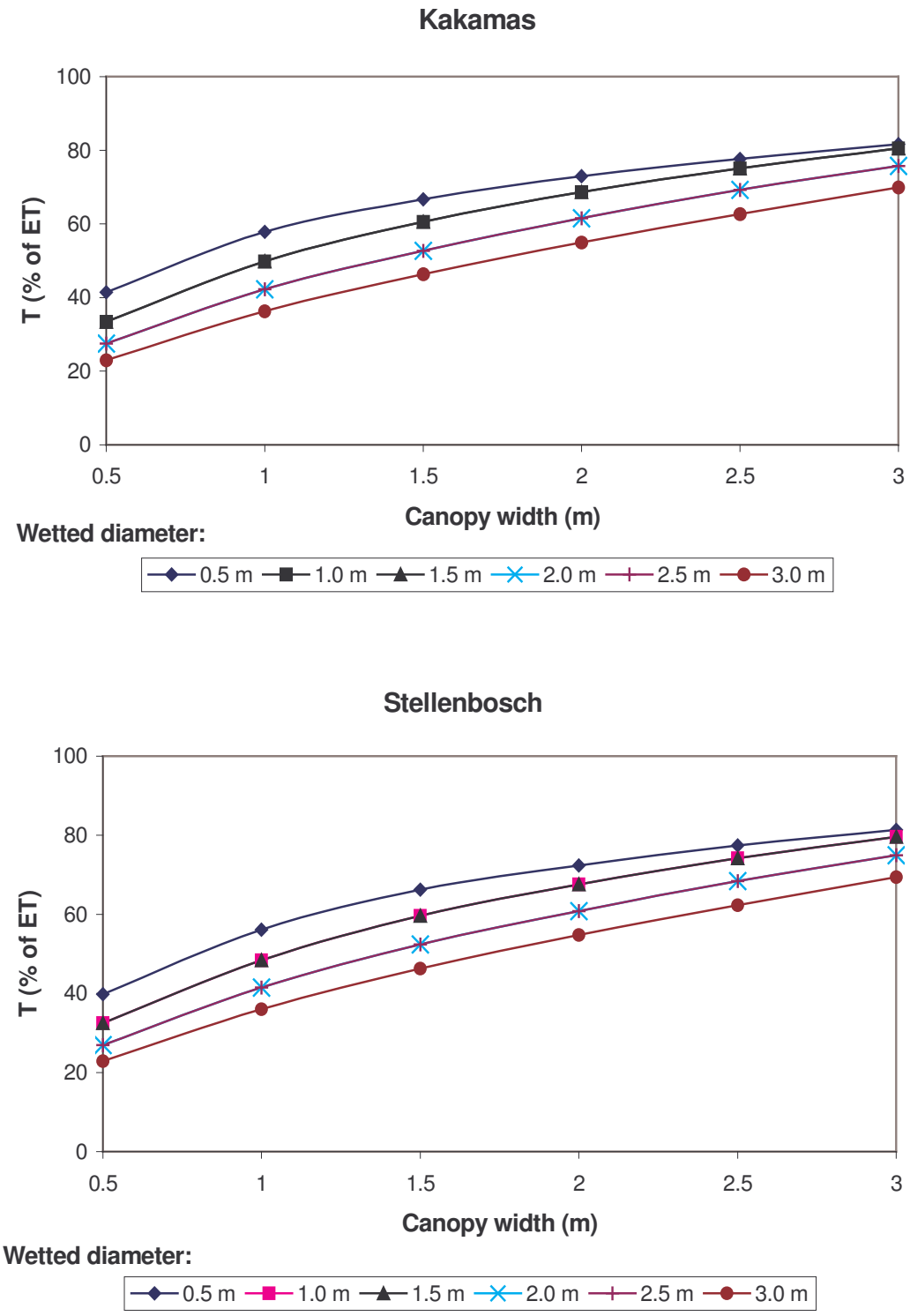

Figure 3.47. Simulated transpiration (T) in % of evapotranspiration (ET) as a function of canopy width and wetted diameter for two orchards at Kakamas and Stellenbosch for period 1 January to 28 February 1998.

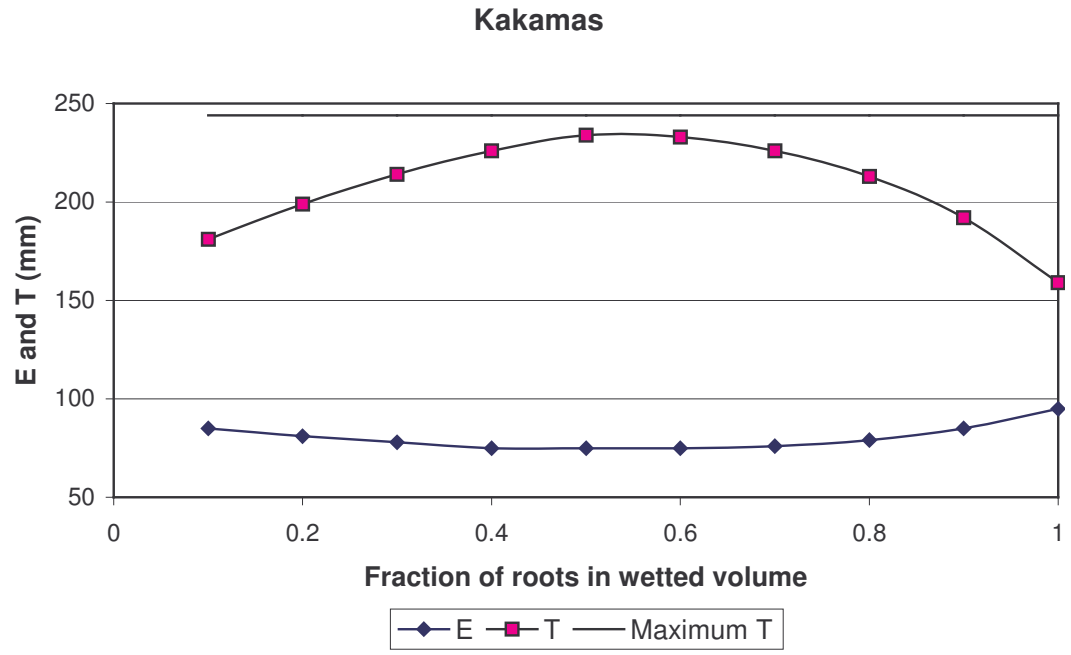

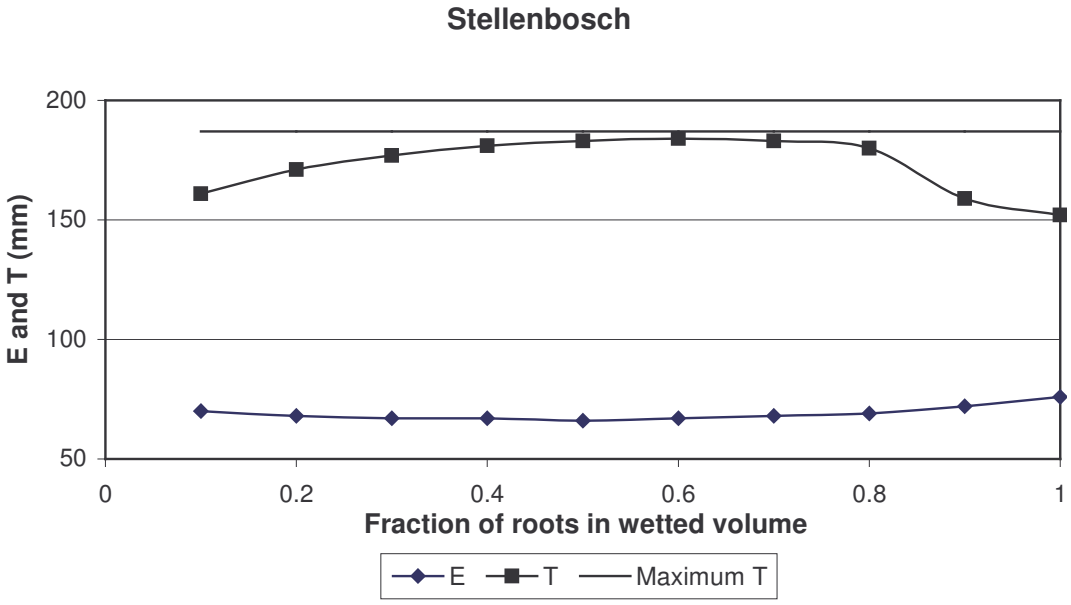

Figure 3.48. Simulated transpiration (T) and evaporation (E) as a function of the fraction of roots in the wetted volume of soil for two orchards at Kakamas and Stellenbosch for period 1 January to 28 February 1998.

CHAPTER 4

CONCLUSIONS AND RECOMMENDATIONS

The objectives of this study have been successfully achieved.

The two-dimensional energy interception model that was developed by the research team was fully evaluated for deciduous orchards using data obtained in field trials on peaches and Leucaena (Hatfield experimental station, University of Pretoria). This model calculates the two-dimensional energy interception for hedgerow fruit trees, based on solar and row orientation, tree size and shape, as well as leaf area density. For model evaluation in evergreen citrus orchards, data obtained in field trials set up at the Syferkuil experimental station (University of the North) and on two commercial farms in Brits were used. The data presented showed that in virtually all instances where solar radiation interception was measured the SWB simulated values corresponded adequately with actual measured values. In the cases where discrepancies occurred there were valid explanations that could be accounted for due to natural variation that is to be expected in nature.

Once the it was shown that the two dimensional energy interception model worked effectively. the two soil water balance models that were included in SWB in order to facilitate irrigation scheduling of hedgerow fruit tree crops were also fully evaluated. Initially a simpler model, based on the FAO crop factor approach and a cascading soil water balance was used. In the latter stages of the study a two-dimensional soil water redistribution model using a finite difference solution had been developed. Evaluating the SWB predictions to actual volumetric soil water content measurements showed that the model simulations give realistic results. Both these models can be used to predict crop water requirements. The advantage of the simpler FAO crop factor approach is that it requires less crop input data than the finite difference model.

The SWB-2D model predicted soil water contents to an acceptable degree at the different soil depths in the trials and accounted for localized irrigation, different rainfall events, varying canopy densities and shapes that can be expected in hedgerow plantings. Root length density is also not always uniform across the row and the SWB model makes provision for this through an input variable, which is defined as the fraction of roots in the wetted volume of soil. In addition, the two-dimensional energy interception model accounts for variations in soil irradiance across the row, and makes provision for shapes of tree canopies that resemble an ellipse with the bottom part cut off to accommodate certain pruning practices. The major difficulties encountered in testing the soil water balance were assumed to be due to spatial variability of the soil properties across the row. In particular, initial soil water

content and hydraulic conductivity since the model assumes homogeneous soil properties for the specified horizontal layers. Canopy interception of rainfall across the row is a variable not accounted for in the model and was shown to have an effect in the dense Clementine canopy.

The FAO-based model and the cascading soil water balance were calibrated for first leaf and second leaf peaches.

The two-dimensional energy interception model was evaluated for different conditions (latitude, row orientation, size of the canopy and leaf area density). It is fair to say that hourly spatial and temporal variations of radiant transmittance were generally well simulated by the radiant interception model presented in this study. The results obtained show that when one deals with a symmetrical and elliptical canopy having a uniform leaf distribution, for example the Syferkuil clementine hedgerow, the model follows the diurnal cycle of radiant transmittance exceptionally well. In the case where the canopy is non-symmetric and/or has non-uniform leaf distribution, as can be expected, errors in predictions of solar radiation transmittance will occur.

Irregular trunks and branches could cause inaccuracies in predictions of the energy balance. At low leaf area densities, the shade from trunks and branches is not accounted for in the SWB model. Thus a method should be developed to take this into account when determining leaf area densities. The current results indicate that a non-symmetric canopy shape and non-uniform leaf distribution are not critical, particularly when the hedgerow has a N-S axis. When a canopy has a markedly different canopy shape, i.e. a coppice as encountered with the Leucaena hedgerow, errors could occur with E-W axis hedgerows.

Simulations of solar radiation interception by the two-dimensional SWB model were in good agreement with observations, though the tree dimensions for which the model gave the best predictions were slightly different from those measured in the orchard. The two-dimensional energy and soil water balance model was evaluated using data from the citrus trial at Syferkuil. The model predicted the soil water content at different depths in the soil profile and distances from the tree row reasonably well. The major difficulties encountered in the evaluation of the soil water balance were due to spatial variability of soil properties and disturbance of the soil when the water measurement sensors were installed.

Careful installation is therefore recommended for soil water sensors that give point measurements like those used in this study (heat dissipation sensors and TDR probes). The TDR probes can be used in irrigation scheduling to determine crop water use over certain periods. Caution should, however, be exercised in the interpretation of absolute values of volumetric soil water content obtained as output reading from the probes.

The successful evaluation of the two-dimensional energy interception and soil water balance model opens the opportunity to develop a useful yield predictor and productivity efficiency measure if one knows the canopy to fruit ratio. This information could also be useful for fruit colour and internal quality research. An ultimate objective should be to use this model for yield estimations and to be able to do "what if" analyses for varying irrigation-yield interactions. The initial step, i.e. getting the energy and water balance working has been achieved. In addition the methodology for soil water and energy monitoring has been established. The logical step would be to take this work to the next level, i.e. energy-water-yield balance. This could be of tremendous benefit to the fruit industry.

As demonstrated with data from the peach trial at Hatfield, bare soil as opposed to cover crops between rows can also have a large effect on the efficient use of rainfall, and this should be further investigated.

It is common practice on commercial farms to irrigate orchards with drip irrigation systems and apply irrigations several times during the day. This implies the need for an hourly time step model in order to accurately predict the soil water balance. The hourly Penman-Monteith reference evapotranspiration procedure has recently been finalised and appears in the Irrigation and Drainage Bulletin No. 56 published by the FAO (Allen *et al.*, 1998). This could also be included in the SWB model for hourly predictions of crop water requirements.

The two-dimensional energy and soil water balance model is primarily meant to be a real-time, irrigation scheduling tool for commercial orchards. It does work but it is a bit too complicated for the average farmer. For a big farming operation that has the technical personnel, it can be very useful. Results from the application of this model should guide irrigation scheduling consultants, extension officers and farmers to more efficiently use scarce water resources on high value tree crops. The two-dimensional model, however, can also be used for planning purposes as demonstrated in the scenario simulations. The mechanistic canopy radiation interception routine which has been shown to be very accurate will make it possible to evaluate the effect of row orientation and spacing as well as the effect of wetted diameter and pruning practices on water use. An optimisation program could be built in SWB in order to optimise all input parameters at the same time. This would facilitate the choice of optimal management without having to run simulations by trial and error. Computer software that could be adapted for use with SWB is PEST – ASP (Model-Independent Parameter ESTimation) developed by John Doherty and Watermark Numerical Computing (Australia).

The biggest contribution of this model is likely to be the quantification of the contribution that rainfall can make to crop water use by taking the non-irrigated inter-row soil reservoir into

account. Scenario simulations proved that crop water uptake from the inter-row volume of soil can be high and this needs to be accounted for in irrigation management in order to maximise rainfall use efficiency. It is recommended to accurately estimate the root fraction in the wetted and non-wetted volume of soil by digging a trench across the row, taking soil samples and determining root density.

With the growing importance of precision farming applications, this model could also be effectively used in maize crops with wide row spacing. These rows actually fit the ellipsoid canopy shape that is the basis of the 2-D energy interception very well. Since water management is crucial to the successful production of maize in the dryer south western portion of the SA maize production areas this tool could prove very useful.

The two-dimensional energy interception and finite difference soil water balance model is expected to be more accurate than the cascading soil water balance, due to the sound physical principles on which it is based. The mechanistic detailed approach could give guidance with respect to the magnitude of errors made by using simpler, more empirical approaches. However, the two-dimensional model will also require more input parameters compared to the simpler cascading model. In particular, the most difficult parameters to determine will be the leaf area density for the radiant energy part due to the cost of the instrumentation, and the hydraulic conductivity for the soil part due to the specialised knowledge and scientific equipment required. On the other hand, the cascading model requires calibrated FAO crop factors in order to reasonably partition E and T.

REFERENCES

ALLEN RG, SMITH M, PRUITT WO and PEREIRA LS (1996) Modifications to the FAO crop coefficient approach. *Proc. of the Int. Conf. on Evapotranspiration and Irrigation Scheduling*, San Antonio, Texas, USA. 124-132.

ALLEN RG, PEREIRA LS, RAES D and SMITH M (1998) *Crop evapotranspiration. Guidelines for computing crop water requirements.* Irrigation and Drainage Paper No. 56. FAO, Rome, Italy.

ANNANDALE JG, BENADÉ N, JOVANOVIC NZ, STEYN JM and DU SAUTOY N (1999) Facilitating Irrigation Scheduling by Means of the Soil Water Balance Model. Water Research Commission Report No. 753/1/99, Pretoria, South Africa.

ANNANDALE JG, JOVANOVIC NZ, BENADĒ N and ALLEN RG (2002) Software for missing data error analysis of Penman-Monteith reference evapotranspiration. *Irrig Sci.* 21: 57 – 67.

ANNANDALE JG, JOVANOVIC NZ, MPANDELI NZ, LOBIT P and DU SAUTOY N (2002) Two Dimensional Energy Interception and Water Balance Model for Hedgerow Tree Crops. Water Research Commission Report No. 945/1/02, Pretoria, South Africa.

ANNANDALE JG, CAMPBELL GS, OLIVIER FC and JOVANOVIC NZ (2000) Predicting crop water uptake under full and deficit irrigation: An example using pea (*Pisum sativum* L. cv. Puget). *Irrig. Sci.* 19 65-72.

BENNIE ATP, COETZEE MJ, VAN ANTWERPEN R, VAN RENSBURG LD and DU T. BURGER R (1988) 'n Waterbalansmodel vir besproeiing gebaseer op profielwatervoorsieningstempo en gewaswaterbehoeftes. Waternavorsingskommissie Verslag No. 144/1/88, Pretoria, South Africa.

BRISTOW KL, CAMPBELL GS and CALISSENDORFF K (1993) Test of a heat-pulse probe for measuring changes in soil water content. *Soil Sci. Soc. Am. J.* 57 930-934.

CAMASE (1995) Newsletter of Agro-ecosystems modelling. Extra edition. AB-DLO Publisher, November 1995, Wageningen, The Netherlands, 8 pp.

CAMPBELL GS (1977) *An Introduction to Environmental Biophysics.* Springer, New York.

CAMPBELL GS (1985) *Soil physics with Basic*. Elsevier Science, Amsterdam.

CAMPBELL GS and DIAZ R (1988) Simplified soil-water balance models to predict crop transpiration. In: Bidinger FR and Johansen C (eds.) *Drought research priorities for the dryland tropics*. ICRISAT, India. 15-26.

CAMPBELL GS and GEE GW (1986) Water potential: Miscellaneous methods. In: Klute A (ed.) *Methods of Soil Analysis. Part 1.* Agronomy monograph No. 9. American Society of Agronomy, Soil Science Society of America, Madison, Wisconsin. 619-633.

CAMPBELL GS and NORMAN JM (1998) *An introduction to environmental biophysics.* 2nd ed. Springer, New York.

CAMPBELL GS and STOCKLE CO (1993) Prediction and simulation of water use in agricultural systems. In: *International Crop Science I.* Crop Sci. Soc. of Am., 677 S. Segoe Rd., Madison, WI 53711, USA.

CAMPBELL GS, CALISSENDORFF K and WILLIAMS JH (1991) Probe for measuring soil specific heat using a heat-pulse method. *Soil Sci. Soc. Am. J.* 55 291-293.

CAMPBELL GS, FLINT AL, BILSKIE J and CALISSENDORFF C (2001) Calibration and temperature correction of heat dissipation matric potential sensors. Unpublished.

CHARLES-EDWARDS DA and THORNLEY HM (1973) Light interception by an isolated plant. A simple model. *Ann. Bot.* 37 919-928

CHARLES-EDWARDS DA and THORPE MR (1976) Interception of diffuse and direct-beam radiation by a hedgerow apple orchard. *Ann. Bot.* 40 603-613.

CROSBY CT (1996) SAPWAT 1.0 - A computer program for estimating irrigation requirements in Southern Africa. Water Research Commission Report No. 379/1/96, Pretoria, South Africa.

DE JAGER JM (1994) Accuracy of vegetation evaporation ratio formulae for estimating final wheat yield. *Water SA* 20(4) 307-315.

DOORENBOS J and PRUITT WO (1977) *Crop water requirements*. FAO Irrigation and Drainage Paper No. 24. FAO, Rome, Italy.

FAO (1998) *World Reference Base for Soil Resources.* World Soil Resources Report No. 84. FAO, Rome, Italy.

GREEN GC (1985a) *Estimated irrigation requirements of crops in South Africa. Part 1*. Dept of Agric. and Water Supply, Pretoria, South Africa.

GREEN GC (1985b) *Estimated irrigation requirements of crops in South Africa. Part 2*. Dept of Agric. and Water Supply, Pretoria, South Africa.

GOUDRIAAN J (1977) Crop micrometeorology: a simulation study. Simulation monographs, Pudoc, Wagenningen.

HANKS RJ and RITCHIE JT (1991) *Modeling plant and soil systems.* Agronomy Monograph No. 31, ASA-CSSA-SSSA, 677 S. Segoe Rd., Madison, WI 53711. 545 pp.

HILLEL D (1998) Environmental Soil Physics. Academic Press, San Diego

HODGES T and RITCHIE JT (1991) The CERES-wheat phenology model. In: Hodges T (ed.) *Predicting crop phenology*. CRC Press, Boston.

JACKSON RD and TAYLOR SA (1986) Thermal conductivity and diffusivity. In: Klute A (ed.) *Methods of Soil Analysis. Part 1.* Agronomy monograph No. 9. American Society of Agronomy, Soil Science Society of America, Madison, Wisconsin. 945-956.

JOVANOVIC NZ and ANNANDALE JG (1997) A laboratory evaluation of Watermark electrical resistance and Campbell Scientific 229 heat dissipation matric potential sensors. *Water SA* 23(3) 227-232.

JOVANOVIC NZ and ANNANDALE JG (1998) Measurement of radiant interception of crop canopies with the LAI-2000 plant canopy analyzer. *SA J. Plant and Soil* 15(1) 6-13.

JOVANOVIC NZ and ANNANDALE JG (1999) An FAO type crop factor modification to SWB for inclusion of crops with limited data: Examples for vegetable crops. *Water SA* 25(2) 181-189.

KNIGHT JH (1992) Sensitivity of time domain reflectometry measurements to lateral variations in soil water content. *Water Resour. Res*. 28(9) 2345-2352.

MONTEITH JL (1977) Climate and efficiency of crop production in Britain. *Philos. Trans. R. Soc. London, Ser. B* 281 277-294.

NORMAN JM and WELLES (1983) Radiative transfer in an array of canopies. *Agron. J.* 75 481-488.

OR D, FISHER B, HUBSCHER RA and WRAITH J (1998) WinTDR 98 v. 4.0. Users Guide. Utah State University, Plant, Soils and Biometeorology, Logan, Utah, May 1998.

REDINGER GJ, CAMPBELL GS, SAXTON KE and PAPENDICK RI (1984) Infiltration rate of slot mulches: measurement and numerical simulation. *Soil Sci. Soc. Am. J.* 48 982-986.

RITCHIE JT (1972) Model for predicting evaporation from a row crop with incomplete cover. *Water Resour. Res.* 8 1204-1213.

ROSS PJ and BRISTOW KL (1990) Simulating water movement in layered and gradational soils using the Kirchhoff transform. *Soil Sci. Soc. Am. J.* 54 1519-1524.

SINCLAIR TR and SELIGMAN NG (1996) Crop modeling: from infancy to maturity. *Agron. J.* 88 698-704.

SINGELS A and DE JAGER JM (1991a) Refinement and validation of PUTU wheat crop growth model. 1. Phenology. *S. A. Plant Soil* 8(2) 59-66.

SINGELS A and DE JAGER JM (1991b) Refinement and validation of PUTU wheat crop growth model. 2. Leaf area expansion. *S. A. Plant Soil* 8(2) 67-72.

SINGELS A and DE JAGER JM (1991c) Refinement and validation of PUTU wheat crop growth model. 3. Grain growth. *S. A. Plant Soil* 8(2) 73-77.

SMITH M (1992a) *CROPWAT - A computer program for irrigation planning and management.* FAO Irrigation and Drainage Paper No. 46. FAO, Rome, Italy.

SMITH M (1992b) Expert consultation on revision of FAO methodologies for crop water requirements. FAO, Rome, Italy, 28-31 May 1990.

SMITH M, ALLEN RG and PEREIRA LS (1996) Revised FAO methodology for crop water requirements. *Proc. of the Int. Conf. on Evapotranspiration and Irrigation Scheduling*, San Antonio, Texas, USA. 133-140.

SOIL CLASSIFICATION WORKING GROUP (1991) *Soil classification. A taxonomic system for South Africa.* Soil and Irrigation Research Institute, Dept of Agricultural Development, Pretoria, South Africa.

TANNER CB (1960) Energy balance approach to evapotranspiration from crops. *Soil. Sci. Soc. Am. Proc*. 24 1-9.

TANNER CB and JURY WA (1976) Estimating evaporation and transpiration from a row crop during incomplete cover. *Agron. J*. 68 239-243.

TETENS O (1930) Uber einige meteorologische Begriffe. *Z. Geophys.* 6 297-309.

TOPP GC, DAVIS JL and ANNAN AP (1980) Electromagnetic determination of soil water content: measurements in coaxial transmission lines. *Water Resour. Res.* 16(3) 574-582.

WHISLER FD, ACOCK B, BAKER DN, FYE RE, HODGES HF, LAMBERT JR, LEMMON HE, MCKINION JM and REDDY VR (1986) Crop simulation models in agronomic systems. *Adv. Agron.* 40 141-208.

WILLMOTT CJ (1982) Some comments on the evaluation of model performance. *Bull. Am. Met. Soc.* 63 1309-1313.

WEISS A and NORMAN JM (1985) Partitioning solar radiation into direct and diffuse, visible and near-infrared components. *Agric. For. Met.* 34 205-213.

APPENDIX A

PROGRAM CODE USED FOR CAMPELL SCIENTIFIC DATA-LOGGERS

A.1 Hatfield Automatic Weather Station

```
;{CR10}
;Programme for monitoring automatic weather station at Hatfield Exp Farm
;Updated on 29/10/96 to include SVP, VP & VPD
;Updated on 7/11/96 to correct Temp & Rain calibrations with manual
    ;station
;Updated 25/11/96 to correct for overestimation of rain - multiplier
    ;changed from .5598 to .4976
;Updated 26/11/96 to correct for SVP, VP & VPD (ie not give rh_frac
    ;as VP
;Updated with recalibration of Pyranometer and Cup anamometer on 4/7/98

* Table 1 Program
  01:  10 Execution Interval (seconds)

1:  Temp (107) (P11)
 1: 1       Reps
 2: 1       In Chan
 3: 1       Excite all reps w/Exchan 1
 4: 1       Loc [ Temp_C    ]
 5: 1       Mult
 6: .17     Offset

2:  Excite-Delay (SE) (P4)
 1: 1       Reps
 2: 5       2500 mV Slow Range
 3: 2       In Chan
 4: 2       Excite all reps w/Exchan 2
 5: 15      Delay (units 0.01 sec)
 6: 2500    mV Excitation
 7: 2       Loc [ RH        ]
 8: .1028   Mult
 9: 1.42    Offset

3:  Pulse (P3)
 1: 1       Reps
 2: 1       Pulse Input Channel
 3: 22      Switch Closure, Output Hz
 4: 3       Loc [ Wind_mps  ]
 5: .8685   Mult
 6: 0       Offset

4:  Volt (Diff) (P2)
 1: 1       Reps
 2: 33      25 mV 50 Hz Rejection Range
 3: 2       In Chan
 4: 4       Loc [ Rad_Wpm2  ]
 5: 99.944  Mult
 6: 0       Offset

5:  Pulse (P3)
 1: 1       Reps
```

```
 2: 2       Pulse Input Channel
 3: 2       Switch Closure
 4: 5       Loc [ Rain_mm   ]
 5: .4976   Mult
 6: 0.0     Offset

6:  Z=X*F (P37)
 1: 2       X Loc [ RH      ]
 2: .01     F
 3: 7       Z Loc [ rh_frac   ]

7:  Saturation Vapor Pressure (P56)
 1: 1       Temperature Loc [ Temp_C    ]
 2: 8       Loc [ SVP       ]

8:  Z=X*Y (P36)
 1: 8       X Loc [ SVP       ]
 2: 7       Y Loc [ rh_frac   ]
 3: 9       Z Loc [ VP_kPa    ]

9:  Z=X-Y (P35)
 1: 8       X Loc [ SVP       ]
 2: 9       Y Loc [ VP_kPa    ]
 3: 10      Z Loc [ VPD_kPa   ]

10:  Batt Voltage (P10)
 1: 6       Loc [ Batt_V    ]

11:  If time is (P92)
 1: 0000    Minutes (Seconds --) into a
 2: 60      Interval (same units as above)
 3: 10      Set Output Flag High

12:  Real Time (P77)
 1: 1220    Year,Day,Hour/Minute (prev day at midnight, 2400 at midnight)

13:  Average (P71)
 1: 4       Reps
 2: 1       Loc [ Temp_C    ]

14:  Totalize (P72)
 1: 1       Reps
 2: 5       Loc [ Rain_mm   ]

15:  Average (P71)
 1: 3       Reps
 2: 8       Loc [ SVP       ]

16:  If time is (P92)
 1: 0000    Minutes (Seconds --) into a
 2: 1440    Interval (same units as above)
 3: 10      Set Output Flag High

17:  Real Time (P77)
 1: 1200    Year,Day (prev day at midnight)

18:  Totalize (P72)
 1: 1       Reps
 2: 5       Loc [ Rain_mm   ]
```

19: Maximize (P73)
1: 1 Reps
2: 10 Value with Hr-Min
3: 1 Loc [Temp_C]

20: Minimize (P74)
1: 1 Reps
2: 10 Value with Hr-Min
3: 1 Loc [Temp_C]

21: Sample (P70)
1: 1 Reps
2: 6 Loc [Batt_V]

A.2 Mobile Automatic Weather Station at Syferkuil Clementine Orchard

```
;{CR10X}
;SYCALAWS.CSI
;Program drafted to control Mobile AWS on 27 & 28 June 2000
;WIRING:
;  Radiometer (Top): Black to H1; Red to L1
;            (Bot): Blue to H2; Brown to L2
;  Diffuse; to Diff 3
;  HMP 35C:  Orange to H6    Green to L6
;            Black to E1     Yellow to E2
;            Red to V12      Clear + White + Purple to G
;  Cup anemometer:   Red to P1     Green & Black to G
;  Rain Gauge:       White to P2   Black to G
;OUTPUT:
;  Hourly: Code; DOY; Hour; Station_ID; T; RH; Rad (W/m2); Reflect;
;          Diffuse; Wind (m/s); Rain (mm); rh (frac); SVP; VP & VPD (kPa)
;  Daily:  Code; DOY; Hour: Station ID; Tx; Tn; Rad (ave W/m2 for 24hrs)
;          VP (ave kPa); Rain (Tot mm); Wind (m/s); Total Solar

* Table 1 Program
  01:  10Execution Interval (seconds)

1:  Read ID (P117)
 1: 1        Loc [ StationID ]

2:  Z=F (P30)
 1: 1        F
 2: 0        Exponent of 10
 3: 1        Z Loc [ StationID ]

3:  Batt Voltage (P10)
 1: 13       Loc [ V_Batt    ]

4:  Temp (107) (P11)
 1: 1        Reps
 2: 11       SE Channel
 3: 1        Excite all reps w/E1
 4: 2        Loc [ Temp_C    ]
 5: 1        Mult
 6: .08      Offset

5:  Excite-Delay (SE) (P4)
 1: 1        Reps
 2: 5        2500 mV Slow Range
 3: 12       SE Channel
 4: 2        Excite all reps w/Exchan 2
 5: 15       Delay (units 0.01 sec)
 6: 2500     mV Excitation
 7: 3        Loc [ RH        ]
 8: .1026    Mult
 9: 2.0285   Offset

6:  Z=X*F (P37)
 1: 3        X Loc [ RH        ]
 2: .01      F
 3: 9        Z Loc [ rh_frac   ]

7:  Saturation Vapor Pressure (P56)
 1: 2        Temperature Loc [ Temp_C    ]
```

```
 2: 10      Loc [ SVP_kPa   ]

8:  Z=X*Y (P36)
 1: 10      X Loc [ SVP_kPa   ]
 2: 9       Y Loc [ rh_frac   ]
 3: 11      Z Loc [ VP_kPa    ]

9:  Z=X-Y (P35)
 1: 10      X Loc [ SVP_kPa   ]
 2: 11      Y Loc [ VP_kPa    ]
 3: 12      Z Loc [ VPD_kPa   ]

10:  Volt (Diff) (P2)
 1: 1       Reps
 2: 33       25 mV 50 Hz Rejection Range
 3: 1       DIFF Channel
 4: 4       Loc [ Rad_Wm2   ]
 5: 56.635   Mult
 6: 0       Offset
;Measures solar radiation and converts to W/m^2

11:  If (X<=>F) (P89)
 1: 4       X Loc [ Rad_Wm2   ]
 2: 4       <
 3: 0       F
 4: 30       Then Do

12:  Z=F (P30)
 1: 0       F
 2: 0       Exponent of 10
 3: 4       Z Loc [ Rad_Wm2   ]

13:  End (P95)
;Eliminates -ve  Radiation values

14:  Z=X (P31)
 1: 4       X Loc [ Rad_Wm2   ]
 2: 14      Z Loc [ TotSolar  ]

15:  Z=X*F (P37)
 1: 14      X Loc [ TotSolar  ]
 2: .00001   F
 3: 14      Z Loc [ TotSolar  ]


16:  Volt (Diff) (P2)
 1: 1       Reps
 2: 25       2500 mV 60 Hz Rejection Range
 3: 2       DIFF Channel
 4: 5       Loc [ Reflect   ]
 5: 51.143   Mult
 6: 0.0     Offset

17:  If (X<=>F) (P89)
 1: 5       X Loc [ Reflect   ]
 2: 4       <
 3: 0       F
 4: 30       Then Do

18:  Z=F (P30)
```

```
 1: 0       F
 2: 0       Exponent of 10
 3: 5       Z Loc [ Reflect   ]

19:  End (P95)

20:  Volt (Diff) (P2)
 1: 1       Reps
 2: 25      2500 mV 60 Hz Rejection Range
 3: 3       DIFF Channel
 4: 6       Loc [ Diffuse   ]
 5: 119.2   Mult
 6: 0       Offset

21:  If (X<=>F) (P89)
 1: 6       X Loc [ Diffuse   ]
 2: 4       <
 3: 0       F
 4: 30      Then Do

22:  Z=F (P30)
 1: 0       F
 2: 0       Exponent of 10
 3: 6       Z Loc [ Diffuse   ]

23:  End (P95)

24:  Pulse (P3)
 1: 1       Reps
 2: 1       Pulse Channel 1
 3: 21      Low Level AC, Output Hz
 4: 7       Loc [ Wind_ms   ]
 5: .75     Mult
 6: .2      Offset
;Measures wind speed

25:  If (X<=>F) (P89)
 1: 7       X Loc [ Wind_ms   ]
 2: 4       <
 3: 0.20001  F
 4: 30      Then Do

26:  Z=F (P30)
 1: 0       F
 2: 0       Exponent of 10
 3: 7       Z Loc [ Wind_ms   ]

27:  End (P95)
;Corrects for wind speed less than 0.2 m/s

28:  Pulse (P3)
 1: 1       Reps
 2: 2       Pulse Channel 2
 3: 2       Switch Closure, All Counts
 4: 8       Loc [ Rain_mm   ]
 5: .2      Mult
 6: 0.0     Offset

29:  If (X<=>F) (P89)
 1: 8       X Loc [ Rain_mm   ]
```

```
 2: 3       >=
 3: 0.2     F
 4: 30      Then Do

30:  If time is (P92)
 1: 0       Minutes (Seconds --) into a
 2: 1       Interval (same units as above)
 3: 10      Set Output Flag High (Flag 0)

31:  Set Active Storage Area (P80)
 1: 1       Final Storage Area 1
 2: 333     Array ID

32:  Real Time (P77)
 1: 1220    Year,Day,Hour/Minute (midnight = 2400)

33:  Totalize (P72)
 1: 1       Reps
 2: 8       Loc [ Rain_mm   ]

34:  End (P95)
;Records rain at 1 min intervals when it is raining

35:  If time is (P92)
 1: 0       Minutes (Seconds --) into a
 2: 60      Interval (same units as above)
 3: 10      Set Output Flag High (Flag 0)

36:  Set Active Storage Area (P80)
 1: 1       Final Storage Area 1
 2: 111     Array ID

37:  Real Time (P77)
 1: 1220    Year,Day,Hour/Minute (midnight = 2400)

38:  Sample (P70)
 1: 1       Reps
 2: 1       Loc [ StationID ]

39:  Sample (P70)
 1: 1       Reps
 2: 13      Loc [ V_Batt    ]

40:  Average (P71)
 1: 6       Reps
 2: 2       Loc [ Temp_C    ]

41:  Totalize (P72)
 1: 1       Reps
 2: 8       Loc [ Rain_mm   ]

42:  Average (P71)
 1: 4       Reps
 2: 9       Loc [ rh_frac   ]

43:  If time is (P92)
 1: 0       Minutes (Seconds --) into a
 2: 1440    Interval (same units as above)
 3: 10      Set Output Flag High (Flag 0)
```

```
44:  Set Active Storage Area (P80)
 1: 1        Final Storage Area 1
 2: 222      Array ID

45:  Real Time (P77)
 1: 1220     Year,Day,Hour/Minute (midnight = 2400)

46:  Sample (P70)
 1: 1        Reps
 2: 1        Loc [ StationID ]

47:  Maximum (P73)
 1: 1        Reps
 2: 00       Value Only
 3: 2        Loc [ Temp_C    ]

48:  Minimum (P74)
 1: 1        Reps
 2: 00       Time Option
 3: 2        Loc [ Temp_C    ]

49:  Average (P71)
 1: 1        Reps
 2: 4        Loc [ Rad_Wm2   ]

50:  Average (P71)
 1: 1        Reps
 2: 11       Loc [ VP_kPa    ]

51:  Totalize (P72)
 1: 1        Reps
 2: 8        Loc [ Rain_mm   ]

52:  Average (P71)
 1: 1        Reps
 2: 7        Loc [ Wind_ms   ]

53:  Totalize (P72)
 1: 1        Reps
 2: 14       Loc [ TotSolar  ]
```

A.3 Lysimeter and tube solarimeter control program Peach Orchard

```
;{CR10}
;TITLE: LYS15MIN
;{CR10}
;Program for monitoring Lysimeter & Tube Solarimeter data
   ;at 15 min intervals from 8th December 1996
;Drafted and installed on 8/12/96

* Table 1 Program
  01:  10Execution Interval (seconds)

1:  Volt (Diff) (P2)
 1: 1        Reps
 2: 33       25 mV 50 Hz Rejection Range
 3: 1        In Chan
 4: 1        Loc [ East_mm   ]
 5: 221      Mult
 6: -1440    Offset

2:  Volt (Diff) (P2)
 1: 1        Reps
 2: 33       25 mV 50 Hz Rejection Range
 3: 2        In Chan
 4: 2        Loc [ West_mm   ]
 5: 228      Mult
 6: -1520    Offset

3:  Volt (Diff) (P2)
 1: 1        Reps
 2: 35       2500 mV 50 Hz Rejection Range
 3: 3        In Chan
 4: 3        Loc [ ExcitE_V  ]
 5: 0.0055   Mult
 6: 0.0      Offset

4:  Volt (Diff) (P2)
 1: 1        Reps
 2: 35       2500 mV 50 Hz Rejection Range
 3: 4        In Chan
 4: 4        Loc [ ExcitW_V  ]
 5: 0.0054   Mult
 6: 0.0      Offset

5:  Do (P86)
 1: 41       Set Port 1 High

6:  Beginning of Loop (P87)
 1: 0000     Delay
 2: 7        Loop Count

7:  Do (P86)
 1: 72       Pulse Port 2

8:  Volt (Diff) (P2)
 1: 1        Reps
 2: 33       25 mV 50 Hz Rejection Range
 3: 6        In Chan
 4: 7     -- Loc [ Sol_1s    ]
 5: 1.0      Mult
```

```
 6: 0.0      Offset

9:  End (P95)

10:  Do (P86)
 1: 51       Set Port 1 Low

11:  Z=X*F (P37)
 1: 7        X Loc [ Sol_1s    ]
 2: 76.802   F
 3: 7        Z Loc [ Sol_1s    ]

12:  Z=X*F (P37)
 1: 8        X Loc [ Sol_2     ]
 2: 69.505   F
 3: 8        Z Loc [ Sol_2     ]

13:  Z=X*F (P37)
 1: 9        X Loc [ Sol_3     ]
 2: 69.605   F
 3: 9        Z Loc [ Sol_3     ]

14:  Z=X*F (P37)
 1: 10       X Loc [ Sol_4mid  ]
 2: 74.879   F
 3: 10       Z Loc [ Sol_4mid  ]

15:  Z=X*F (P37)
 1: 11       X Loc [ Sol_5     ]
 2: 66.019   F
 3: 11       Z Loc [ Sol_5     ]

16:  Z=X*F (P37)
 1: 12       X Loc [ Sol_6     ]
 2: 70.965   F
 3: 12       Z Loc [ Sol_6     ]

17:  Z=X*F (P37)
 1: 13       X Loc [ Sol_7N    ]
 2: 69.087   F
 3: 13       Z Loc [ Sol_7N    ]

18:  Pulse (P3)
 1: 1        Reps
 2: 1        Pulse Input Channel
 3: 02       Switch Closure
 4: 5        Loc [ DrainE_mm ]
 5: 0.0024   Mult
 6: 0.0      Offset

19:  Pulse (P3)
 1: 1        Reps
 2: 2        Pulse Input Channel
 3: 02       Switch Closure
 4: 6        Loc [ DrainW_mm ]
 5: 0.0026   Mult
 6: 0.0      Offset

20:  Batt Voltage (P10)
 1: 14       Loc [ Batt_V    ]
```

21: If time is (P92)
1: 0 Minutes (Seconds --) into a
2: 15 Interval (same units as above)
3: 10 Set Output Flag High

22: Real Time (P77)
1: 1120 Year,Day,Hour/Minute (2400 at midnight)

23: Resolution (P78)
1: 1 high resolution

24: Average (P71)
1: 2 Reps
2: 1 Loc [East_mm]

25: Resolution (P78)
1: 0 low resolution

26: Totalize (P72)
1: 2 Reps
2: 5 Loc [DrainE_mm]

27: Average (P71)
1: 7 Reps
2: 7 Loc [Sol_1s]

28: Sample (P70)
1: 2 Reps
2: 3 Loc [ExcitE_V]

29: Sample (P70)
1: 1 Reps
2: 14 Loc [Batt_V]

A.4 Program to control tube solarimeters & Line Quantum Sensors

```
;{CR10X}
;TITLE: SOLPEN.CSI
; Program for measurement of light penetration of hedgerow plantings.
; Use HMP35C TEMPERATURE & RH PROBE (S/N 636980) wired as follows:
;    Red = + 12V, Yellow (power control) =  E2 ,
;    Green (RH) = SE 11,    Orange (Temp) = SE 12
;    Black (Temp Excitation) = Switched Excitation = E1,
;    Clear + White + Purple = Ground
; Albedo meter in Diff Channel 1 (Top) & 2 (Bottom)
; Diffuse Radiation Pyranometer in Diff channel 3 (Pyran No 1)
; AM416 to Diff Channels 4 & 5
;    Control port C1 is for RES & Control port C2 is for CLK
;    Tube Solarimeters in Sets 1, 2, 3 & 4H1-L1
;    LQS in Sets 4H2-L2, 5, 6 & 7

* Table 1 Program

1:  Temp (107) (P11)
 1: 1        Reps
 2: 11       SE Channel
 3: 1        Excite all reps w/E1
 4: 1        Loc [ AirTemp   ]
 5: 1.0      Mult
 6: 0.08     Offset

2:  Excite-Delay (SE) (P4)
 1: 1        Reps
 2: 5        2500 mV Slow Range
 3: 12       SE Channel
 4: 2        Excite all reps w/Exchan 2
 5: 15       Delay (units 0.01 sec)
 6: 2500     mV Excitation
 7: 2        Loc [ RH        ]
 8: 1.0256   Mult
 9: 2.0285   Offset
; Calibration for HMP35C (S/N 636980) is RH = 2.02852 + 1.02559X
;    where X is RH calculated by instruction P4.

3:  Volt (Diff) (P2)
 1: 1        Reps
 2: 33       25 mV 50 Hz Rejection Range
 3: 1        DIFF Channel
 4: 3        Loc [ AlbTop    ]
 5: 56.6352  Mult
 6: 0.0      Offset

4:  Volt (Diff) (P2)
 1: 1        Reps
 2: 33       25 mV 50 Hz Rejection Range
 3: 2        DIFF Channel
 4: 4        Loc [ AlbBot    ]
 5: 51.1427  Mult
 6: 0.0      Offset

5:  Volt (Diff) (P2)
 1: 1        Reps
 2: 33       25 mV 50 Hz Rejection Range
 3: 3        DIFF Channel
```

```
 4: 5        Loc [ Diffuse   ]
 5: 119.2    Mult
 6: 0.0      Offset

6:  Do (P86)
 1: 41       Set Port 1 High
; Activate AM416 thru' C1 (RES =C1)

7:  Beginning of Loop (P87)
 1: 0        Delay
 2: 7        Loop Count
;7 loops with 2 Diff sensors per set = 7 x 2 = 14

8:  Do (P86)
 1: 72       Pulse Port 2
; Pulses AM416 thru' C2 (CLK = C2)

9:  Step Loop Index (P90)
 1: 2        Step
; Necessary not to over-write readings

10:  Volt (Diff) (P2)
 1: 2        Reps
 2: 33       25 mV 50 Hz Rejection Range
 3: 4        DIFF Channel
 4: 6     -- Loc [ Sol1      ]
 5: 1        Mult
 6: 0.0      Offset

11:  End (P95)
; Ends loop determining mV readings from sensors
; Readings recorded in Loc 6 to 19 inclusive

12:  Do (P86)
 1: 51       Set Port 1 Low
;Resets AM416 to beginning (Controlled thru' C1)

13:  Z=X*F (P37)
 1: 6        X Loc [ Sol1      ]
 2: 66.681   F
 3: 6        Z Loc [ Sol1      ]

14:  Z=X*F (P37)
 1: 7        X Loc [ Sol2      ]
 2: 65.727   F
 3: 7        Z Loc [ Sol2      ]

15:  Z=X*F (P37)
 1: 8        X Loc [ Sol3      ]
 2: 67.266   F
 3: 8        Z Loc [ Sol3      ]

16:  Z=X*F (P37)
 1: 9        X Loc [ Sol4      ]
 2: 71.336   F
 3: 9        Z Loc [ Sol4      ]

17:  Z=X*F (P37)
 1: 10       X Loc [ Sol5      ]
 2: 65.83    F
```

```
 3: 10      Z Loc [ Sol5     ]

18:  Z=X*F (P37)
 1: 11      X Loc [ Sol6     ]
 2: 65.076  F
 3: 11      Z Loc [ Sol6     ]

19:  Z=X*F (P37)
 1: 12      X Loc [ Sol7     ]
 2: 63.59   F
 3: 12      Z Loc [ Sol7     ]

20:  Z=X*F (P37)
 1: 13      X Loc [ LQS1     ]
 2: 439.062  F
 3: 13      Z Loc [ LQS1     ]

21:  Z=X*F (P37)
 1: 14      X Loc [ LQS2     ]
 2: 311.512  F
 3: 14      Z Loc [ LQS2     ]

22:  Z=X*F (P37)
 1: 15      X Loc [ LQS3     ]
 2: 364.085  F
 3: 15      Z Loc [ LQS3     ]

23:  Z=X*F (P37)
 1: 16      X Loc [ LQS4     ]
 2: 444.295  F
 3: 16      Z Loc [ LQS4     ]

24:  Z=X*F (P37)
 1: 17      X Loc [ LQS5     ]
 2: 405.383  F
 3: 17      Z Loc [ LQS5     ]

25:  Z=X*F (P37)
 1: 18      X Loc [ LQS6     ]
 2: 419.737  F
 3: 18      Z Loc [ LQS6     ]

26:  Z=X*F (P37)
 1: 19      X Loc [ LQS7     ]
 2: 423.338  F
 3: 19      Z Loc [ LQS7     ]

27:  Batt Voltage (P10)
 1: 20      Loc [ Batt_V    ]

28:  If time is (P92)
 1: 0       Minutes (Seconds --) into a
 2: 15      Interval (same units as above)
 3: 10      Set Output Flag High (Flag 0)

29:  Real Time (P77)
 1: 1220    Year,Day,Hour/Minute (midnight = 2400)

30:  Average (P71)
 1: 19      Reps
```

```
 2: 1        Loc [ AirTemp    ]

31:  If time is (P92)
 1: 0        Minutes (Seconds --) into a
 2: 1440     Interval (same units as above)
 3: 10       Set Output Flag High (Flag 0)

32:  Real Time (P77)
 1: 1200     Year,Day (midnight = 2400)

33:  Maximum (P73)
 1: 1        Reps
 2: 10       Value with Hr-Min
 3: 1        Loc [ AirTemp    ]

34:  Minimum (P74)
 1: 1        Reps
 2: 10       Value with Hr-Min
 3: 1        Loc [ AirTemp    ]

35:  Maximum (P73)
 1: 1        Reps
 2: 10       Value with Hr-Min
 3: 2        Loc [ RH         ]

36:  Minimum (P74)
 1: 1        Reps
 2: 10       Value with Hr-Min
 3: 2        Loc [ RH         ]

37:  Sample (P70)
 1: 1        Reps
 2: 20       Loc [ Batt_V     ]
```

A.5 Heat dissipation sensors (HDS) program; 16 Sensors

```
;{CR10}
;HDS16SE.csi

;Program drafted to read 16 Heat Dissipation Sensors using
;    SE Channels 1 to 8 and AM416 multiplexer to SE channels 9 & 10'
;Thermocouple connections:
;    To CR10  => "High" line SE 1 to 8; "Low line AG (8 T/c's)
;    To AM416 => "High" line SET 1 H1 thru to SET 4 H2 (8 T/c's)
;AM416 linked to CR10 thru' SE channel 9 & 10
;    Pulsed thru C4 (CLK) & Reset thru' C5 (RES)
;CR10TCR (Thermistor Reference Temp) connected thru'
;    SE chan 12 (Red lead); Excitation chan 3 (E3, Black lead)
;    & AG (clear lead)
;Two CE8's excited thru' C1 & C2
;Final Draft 19/12/99

* Table 1 Program
            01:         1           Execution Interval (seconds)

1:  If time is (P92)
 1: 0        Minutes (Seconds --) into a
 2: 120      Interval (same units as above)
 3: 11       Set Flag 1 High

2:  If Flag/Port (P91)
 1: 21       Do if Flag 1 is Low
 2: 0        Go to end of Program Table

3:  AC Half Bridge (P5)
 1: 1        Reps
 2: 22       7.5 mV 60 Hz Rejection Range
 3: 12       SE Channel
 4: 3        Excite all reps w/Exchan 3
 5: 2000     mV Excitation
 6: 3        Loc [ TCRT      ]
 7: 800      Mult
 8: 0.0      Offset

4:  Polynomial (P55)
 1: 1        Reps
 2: 3        X Loc [ TCRT      ]
 3: 1        F(X) Loc [ RefTemp   ]
 4: -53.46   C0
 5: 90.807   C1
 6: -83.257  C2
 7: 52.283   C3
 8: -16.723  C4
 9: 2.211    C5

5:  Batt Voltage (P10)
 1: 2        Loc [ Battery   ]
;Record Battery voltage

6:  Do (P86)
 1: 45       Set Port 5 High
;Activate AM416 thru' "Control port 5" (Res = C5)
```

```
7:  Beginning of Loop (P87)
 1: 0        Delay
 2: 8        Loop Count
;8 loops with 2 Diff sensors per set = 8 X 2 = 16

8:  Do (P86)
 1: 74       Pulse Port 4
;Pulses AM416 thru' C4 (CLK = C4)

9:  Step Loop Index (P90)
 1: 2        Step
;Necessary not to over-write readings

10:  Thermocouple Temp (DIFF) (P14)
 1: 2        Reps
 2: 21       2.5 mV 60 Hz Rejection Range
 3: 1        DIFF Channel
 4: 1        Type T (Copper-Constantan)
 5: 1        Ref Temp Loc [ RefTemp    ]
 6: 5     -- Loc [ SoilT_1    ]
 7: 1.0      Mult
 8: 0.0      Offset

11:  End (P95)
;End first round of soil Temp measurements
;Soil Temps recorded in Loc 5 to 20 inclusive.

12:  Do (P86)
 1: 55       Set Port 5 Low
;Resets AM416 to beginning

13:  Do (P86)
 1: 41       Set Port 1 High
;Activate 1st CE8 thru' C1

14:  Do (P86)
 1: 42       Set Port 2 High
; Activates 2nd CE8 thru' C2

15:  Beginning of Loop (P87)
 1: 0        Delay
 2: 2        Loop Count

16:  Excitation with Delay (P22)
 1: 1        Ex Channel
 2: 0        Delay W/Ex (units = 0.01 sec)
 3: 50       Delay After Ex (units = 0.01 sec)
 4: 0        mV Excitation

17:  End (P95)
;Create 1 sec period; i.e. activates two CE8s for 1 sec

18:  Do (P86)
 1: 45       Set Port 5 High
;Activates AM416

19:  Beginning of Loop (P87)
 1: 0        Delay
 2: 8        Loop Count
```

```
20:  Do (P86)
 1: 74       Pulse Port 4

21:  Step Loop Index (P90)
 1: 2        Step

22:  Thermocouple Temp (DIFF) (P14)
 1: 2        Reps
 2: 21       2.5 mV 60 Hz Rejection Range
 3: 1        DIFF Channel
 4: 1        Type T (Copper-Constantan)
 5: 1        Ref Temp Loc [ RefTemp   ]
 6: 21    -- Loc [ Sec1_1    ]
 7: 1.0      Mult
 8: 0.0      Offset

23:  End (P95)

24:  Do (P86)
 1: 55       Set Port 5 Low
;Resets AM416 to beginning
;Complete 16 measurements of Temp after 1 sec heating
;Measurements recorded in Locs 21 to 36 inclusive

25:  Beginning of Loop (P87)
 1: 0        Delay
 2: 40       Loop Count

26:  Excitation with Delay (P22)
 1: 1        Ex Channel
 2: 0        Delay W/Ex (units = 0.01 sec)
 3: 50       Delay After Ex (units = 0.01 sec)
 4: 0        mV Excitation

27:  End (P95)
;Create 20 sec delay; i.e. continue heating for 20 sec.

28:  Do (P86)
 1: 45       Set Port 5 High
;Activate AM416

29:  Beginning of Loop (P87)
 1: 0        Delay
 2: 8        Loop Count

30:  Do (P86)
 1: 74       Pulse Port 4

31:  Step Loop Index (P90)
 1: 2        Step

32:  Thermocouple Temp (DIFF) (P14)
 1: 2        Reps
 2: 21       2.5 mV 60 Hz Rejection Range
 3: 1        DIFF Channel
 4: 1        Type T (Copper-Constantan)
 5: 1        Ref Temp Loc [ RefTemp   ]
 6: 37    -- Loc [ Sc20_1    ]
 7: 1.0      Mult
 8: 0.0      Offset
```

```
33:  End (P95)

34:  Do (P86)
 1: 55       Set Port 5 Low
; Resets AM416 to beginning
;End Temp measurements after 21 sec heating
;Results recorded to Locs 37 to 52 inclusive.

35:  Do (P86)
 1: 51       Set Port 1 Low

36:  Do (P86)
 1: 52       Set Port 2 Low
;Deactivates two CE8s.

37:  Beginning of Loop (P87)
 1: 0        Delay
 2: 16       Loop Count

38:  Z=X-Y (P35)
 1: 37    -- X Loc [ Sc20_1    ]
 2: 21    -- Y Loc [ Sec1_1    ]
 3: 53    -- Z Loc [ dT_1      ]

39:  End (P95)
;Calculates dT for 16 sensors and places results in
;Locs 53 to 68 inclusive.

40:  Z=F (P30)
 1: 4.001    F
 2: 0        Exponent of 10
 3: 69       Z Loc [ Psi_1     ]

41:  Z=X^Y (P47)
 1: 53       X Loc [ dT_1      ]
 2: 69       Y Loc [ Psi_1     ]
 3: 69       Z Loc [ Psi_1     ]

42:  Z=X*F (P37)
 1: 69       X Loc [ Psi_1     ]
 2: 20.64    F
 3: 69       Z Loc [ Psi_1     ]
;Calcs Psi for HDS S/N 4391: 20.64*(dT)^4.001

43:  Z=F (P30)
 1: 6.494    F
 2: 0        Exponent of 10
 3: 70       Z Loc [ Psi_2     ]

44:  Z=X^Y (P47)
 1: 54       X Loc [ dT_2      ]
 2: 70       Y Loc [ Psi_2     ]
 3: 70       Z Loc [ Psi_2     ]

45:  Z=X*F (P37)
 1: 70       X Loc [ Psi_2     ]
 2: 14.075   F
 3: 70       Z Loc [ Psi_2     ]
;Calcs Psi for HDS S/N 4364: 14.075*(dT)^6.494
```

```
46:  Z=F (P30)
 1: 6.383    F
 2: 0        Exponent of 10
 3: 71       Z Loc [ Psi_3     ]

47:  Z=X^Y (P47)
 1: 55       X Loc [ dT_3      ]
 2: 71       Y Loc [ Psi_3     ]
 3: 71       Z Loc [ Psi_3     ]

48:  Z=X*F (P37)
 1: 71       X Loc [ Psi_3     ]
 2: 14.036   F
 3: 71       Z Loc [ Psi_3     ]
;Calcs Psi for HDS S/N 4380: 14.036*(dT)^6.383

49:  Z=F (P30)
 1: 4.75     F
 2: 0        Exponent of 10
 3: 72       Z Loc [ Psi_4     ]

50:  Z=X^Y (P47)
 1: 56       X Loc [ dT_4      ]
 2: 72       Y Loc [ Psi_4     ]
 3: 72       Z Loc [ Psi_4     ]

51:  Z=X*F (P37)
 1: 72       X Loc [ Psi_4     ]
 2: 18.077   F
 3: 72       Z Loc [ Psi_4     ]
;Calcs Psi for HDS S/N 4375: 18.077*(dT)^4.75

52:  Z=F (P30)
 1: 6.2479   F
 2: 0        Exponent of 10
 3: 73       Z Loc [ Psi_5     ]

53:  Z=X^Y (P47)
 1: 57       X Loc [ dT_5      ]
 2: 73       Y Loc [ Psi_5     ]
 3: 73       Z Loc [ Psi_5     ]

54:  Z=X*F (P37)
 1: 73       X Loc [ Psi_5     ]
 2: 13.351   F
 3: 73       Z Loc [ Psi_5     ]
;Calcs PSi for HDS S/N 4625: 13.351*(dT)^6.2479

55:  Z=F (P30)
 1: 6.0652   F
 2: 0        Exponent of 10
 3: 74       Z Loc [ Psi_6     ]

56:  Z=X^Y (P47)
 1: 58       X Loc [ dT_6      ]
 2: 74       Y Loc [ Psi_6     ]
 3: 74       Z Loc [ Psi_6     ]

57:  Z=X*F (P37)
```

```
 1: 74       X Loc [ Psi_6     ]
 2: 16.536   F
 3: 74       Z Loc [ Psi_6     ]
;Calcs Psi for HDS S/N 4382: 16.536*(dT)^6.0652

58:  Z=F (P30)
 1: 6.1381   F
 2: 0        Exponent of 10
 3: 75       Z Loc [ Psi_7     ]

59:  Z=X^Y (P47)
 1: 59       X Loc [ dT_7      ]
 2: 75       Y Loc [ Psi_7     ]
 3: 75       Z Loc [ Psi_7     ]

60:  Z=X*F (P37)
 1: 75       X Loc [ Psi_7     ]
 2: 20.341   F
 3: 75       Z Loc [ Psi_7     ]
;Calcs Psi for HDS S/N 4379: 20.341*(dT)^6.1381

61:  Z=F (P30)
 1: 3.4538   F
 2: 0        Exponent of 10
 3: 76       Z Loc [ Psi_8     ]

62:  Z=X^Y (P47)
 1: 60       X Loc [ dT_8      ]
 2: 76       Y Loc [ Psi_8     ]
 3: 76       Z Loc [ Psi_8     ]

63:  Z=X*F (P37)
 1: 76       X Loc [ Psi_8     ]
 2: 21.684   F
 3: 76       Z Loc [ Psi_8     ]
;Calcs Psi for HDS S/N 4377: 21.684*(dT)^3.4538

64:  Z=F (P30)
 1: 5.555    F
 2: 0        Exponent of 10
 3: 77       Z Loc [ Psi_9     ]

65:  Z=X^Y (P47)
 1: 61       X Loc [ dT_9      ]
 2: 77       Y Loc [ Psi_9     ]
 3: 77       Z Loc [ Psi_9     ]

66:  Z=X*F (P37)
 1: 77       X Loc [ Psi_9     ]
 2: 13.81    F
 3: 77       Z Loc [ Psi_9     ]
;Calcs Psi for HDS S/N 4378: 13.81*(dT)^5.555

67:  Z=F (P30)
 1: 3.7574   F
 2: 0        Exponent of 10
 3: 78       Z Loc [ Psi_10    ]

68:  Z=X^Y (P47)
 1: 62       X Loc [ dT_10     ]
```

```
 2: 78       Y Loc [ Psi_10    ]
 3: 78       Z Loc [ Psi_10    ]

69:  Z=X*F (P37)
 1: 78       X Loc [ Psi_10    ]
 2: 36.046   F
 3: 78       Z Loc [ Psi_10    ]
;Calcs Psi for HDS S/N 1334: 36.046*(dT)^3.7574

70:  Z=F (P30)
 1: 3.9514   F
 2: 0        Exponent of 10
 3: 79       Z Loc [ Psi_11    ]

71:  Z=X^Y (P47)
 1: 63       X Loc [ dT_11     ]
 2: 79       Y Loc [ Psi_11    ]
 3: 79       Z Loc [ Psi_11    ]

72:  Z=X*F (P37)
 1: 79       X Loc [ Psi_11    ]
 2: 25.233   F
 3: 79       Z Loc [ Psi_11    ]
;Calcs Psi for HDS S/N 1351: 25.2335*(dT)^3.9514

73:  Z=F (P30)
 1: 3.9807   F
 2: 0        Exponent of 10
 3: 80       Z Loc [ Psi_12    ]

74:  Z=X^Y (P47)
 1: 64       X Loc [ dT_12     ]
 2: 80       Y Loc [ Psi_12    ]
 3: 80       Z Loc [ Psi_12    ]

75:  Z=X*F (P37)
 1: 80       X Loc [ Psi_12    ]
 2: 33.516   F
 3: 80       Z Loc [ Psi_12    ]
;Calcs Psi for HDS S/N 1358: 33.516*(dT)^3.9807

76:  Z=F (P30)
 1: 6.5528   F
 2: 0        Exponent of 10
 3: 81       Z Loc [ Psi_13    ]

77:  Z=X^Y (P47)
 1: 65       X Loc [ dT_13     ]
 2: 81       Y Loc [ Psi_13    ]
 3: 81       Z Loc [ Psi_13    ]

78:  Z=X*F (P37)
 1: 81       X Loc [ Psi_13    ]
 2: 36.177   F
 3: 81       Z Loc [ Psi_13    ]
;Calcs Psi for HDS S/N 4722: 36.177*(dT)^6.5528

79:  Z=F (P30)
 1: 5.6721   F
 2: 0        Exponent of 10
```

```
 3: 82      Z Loc [ Psi_14    ]

80:  Z=X^Y (P47)
 1: 66      X Loc [ dT_14     ]
 2: 82      Y Loc [ Psi_14    ]
 3: 82      Z Loc [ Psi_14    ]

81:  Z=X*F (P37)
 1: 82      X Loc [ Psi_14    ]
 2: 21.948  F
 3: 82      Z Loc [ Psi_14    ]
;Calcs PSi for HDS S/N 4727: 21.948*(dT)^5.6721

82:  Z=F (P30)
 1: 5.703   F
 2: 0       Exponent of 10
 3: 83      Z Loc [ Psi_15    ]

83:  Z=X^Y (P47)
 1: 67      X Loc [ dT_15     ]
 2: 83      Y Loc [ Psi_15    ]
 3: 83      Z Loc [ Psi_15    ]

84:  Z=X*F (P37)
 1: 83      X Loc [ Psi_15    ]
 2: 21.251  F
 3: 83      Z Loc [ Psi_15    ]
;Calcs Psi for HDS S/N 4721: 21.251*(dT)^5.703

85:  Z=F (P30)
 1: 3.6961  F
 2: 0       Exponent of 10
 3: 84      Z Loc [ Psi_16    ]

86:  Z=X^Y (P47)
 1: 68      X Loc [ dT_16     ]
 2: 84      Y Loc [ Psi_16    ]
 3: 84      Z Loc [ Psi_16    ]

87:  Z=X*F (P37)
 1: 84      X Loc [ Psi_16    ]
 2: 15.968  F
 3: 84      Z Loc [ Psi_16    ]
;Calcs Psi for HDS S/N 4234: 15.9687*(dT)^3.6961

88:  Do (P86)
 1: 10      Set Output Flag High

89:  Set Active Storage Area (P80)
 1: 1       Final Storage Area 1
 2: 111     Array ID

90:  Real Time (P77)
 1: 1220    Year,Day,Hour/Minute (midnight = 2400)

91:  Minimize (P74)
 1: 1       Reps
 2: 0       Value Only
 3: 2       Loc [ Battery   ]
```

```
92:  Average (P71)
 1: 1        Reps
 2: 1        Loc [ RefTemp    ]

93:  Sample (P70)
 1: 16       Reps
 2: 69       Loc [ Psi_1      ]

94:  Do (P86)
 1: 10       Set Output Flag High

95:  Set Active Storage Area (P80)
 1: 1        Final Storage Area 1
 2: 222      Array ID

96:  Real Time (P77)
 1: 1220     Year,Day,Hour/Minute (midnight = 2400)

97:  Sample (P70)
 1: 16       Reps
 2: 53       Loc [ dT_1       ]

98:  Do (P86)
 1: 10       Set Output Flag High

99:  Set Active Storage Area (P80)
 1: 1        Final Storage Area 1
 2: 333      Array ID

100:  Real Time (P77)
 1: 1220     Year,Day,Hour/Minute (midnight = 2400)

101:  Sample (P70)
 1: 16       Reps
 2: 5        Loc [ SoilT_1    ]

102:  Do (P86)
 1: 21       Set Flag 1 Low

* Table 2 Program
        02:         0.0000              Execution Interval (seconds)

* Table 3  Subroutines

End Program
```

A.6 Heat dissipation sensors (HDS) program; 24 Sensors

```
;{CR10X}
;24HDSPSI.CSI
;Program done to read 24 Heat Dissipation Sensors (HDS)
;thru' AM416 multiplexer & excited thru three CE8s.
;AM416 clocked <pulsed) thru C4 & Reset thru C5.
;CE8s activated thru C1, C2 & C6.

* Table 1 Program
  01:  10Execution Interval (seconds)

1:  If time is (P92)
 1: 0        Minutes (Seconds --) into a
 2: 60       Interval (same units as above)
 3: 11       Set Flag 1 High

2:  If Flag/Port (P91)
 1: 21       Do if Flag 1 is Low
 2: 0        Go to end of Program Table

3:  AC Half Bridge (P5)
 1: 1        Reps
 2: 22       7.5 mV 60 Hz Rejection Range
 3: 12       SE Channel
 4: 3        Excite all reps w/Exchan 3
 5: 2000     mV Excitation
 6: 3        Loc [ TCRT      ]
 7: 800      Mult
 8: 0        Offset

4:  Polynomial (P55)
 1: 1        Reps
 2: 3        X Loc [ TCRT      ]
 3: 1        F(X) Loc [ RefTemp   ]
 4: -53.46   C0
 5: 90.807   C1
 6: -83.257  C2
 7: 52.283   C3
 8: -16.723  C4
 9: 2.211    C5

5:  Batt Voltage (P10)
 1: 2        Loc [ Battery   ]

;          MEASUREMENTS FOR 1st 8 T/c's ON CR10X

6:  Thermocouple Temp (SE) (P13)
 1: 8        Reps
 2: 22       7.5 mV 60 Hz Rejection Range
 3: 1        SE Channel
 4: 1        Type T (Copper-Constantan)
 5: 1        Ref Temp (Deg. C) Loc [ RefTemp   ]
 6: 5        Loc [ SoilT_1   ]
 7: 1.0      Mult
 8: 0        Offset
;Det Soil T for 1st 8 T/c's: recorded in Locs 5 to 12

7:  Do (P86)
 1: 41       Set Port 1 High
```

```
;Activates 1st CE8 thru C1

8:  Beginning of Loop (P87)
 1: 0       Delay
 2: 2       Loop Count

9:  Excitation with Delay (P22)
 1: 1       Ex Channel
 2: 0       Delay W/Ex (units = 0.01 sec)
 3: 50      Delay After Ex (units = 0.01 sec)
 4: 0       mV Excitation

10:  End (P95)
;Create 1 sec period (2 X 50 X 0.01 = 1 sec)
;       Activates CE8 No 1 for 1 sec

11:  Thermocouple Temp (SE) (P13)
 1: 8       Reps
 2: 22      7.5 mV 60 Hz Rejection Range
 3: 1       SE Channel
 4: 1       Type T (Copper-Constantan)
 5: 1       Ref Temp (Deg. C) Loc [ RefTemp   ]
 6: 29      Loc [ Sec1_1    ]
 7: 1       Mult
 8: 0       Offset
;Records Temp after 1 sec heating: Locs 29 to 36 inclusive

12:  Beginning of Loop (P87)
 1: 0       Delay
 2: 40      Loop Count

13:  Excitation with Delay (P22)
 1: 1       Ex Channel
 2: 0       Delay W/Ex (units = 0.01 sec)
 3: 50      Delay After Ex (units = 0.01 sec)
 4: 0       mV Excitation

14:  End (P95)
;Creates 20 sec delay, i.e. continue heating for 20 sec

15:  Thermocouple Temp (SE) (P13)
 1: 8       Reps
 2: 22      7.5 mV 60 Hz Rejection Range
 3: 1       SE Channel
 4: 1       Type T (Copper-Constantan)
 5: 1       Ref Temp (Deg. C) Loc [ RefTemp   ]
 6: 53      Loc [ T20s_1    ]
 7: 1       Mult
 8: 0       Offset
;Determine Temp of 1st T/c's after 21 sec heating: Locs 53 to 60 inclusive

16:  Do (P86)
 1: 51      Set Port 1 Low
;Deactivates CE8 No 1
;           COMPLETED MEASUREMENTS FOR 1st 8 T/c's

;           MEASURE SOIL TEMP FOR BALANCE OF T/c's

17:  Do (P86)
 1: 45      Set Port 5 High
```

```
;Actvate AM416 thru' Control port 5 (Res = C5)

18:  Beginning of Loop (P87)
 1: 0        Delay
 2: 8        Loop Count
;8 loops with 2 SE sensors per set: 8 X 2 = 16

19:  Do (P86)
 1: 74       Pulse Port 4
;Pulses AM416 thru' C4 (CLK = C4)

20:  Step Loop Index (P90)
 1: 2        Step
;Necessary not to over-write readings

21:  Thermocouple Temp (SE) (P13)
 1: 2        Reps
 2: 21       2.5 mV 60 Hz Rejection Range
 3: 9        SE Channel
 4: 1        Type T (Copper-Constantan)
 5: 1        Ref Temp (Deg. C) Loc [ RefTemp   ]
 6: 13    -- Loc [ SoilT_9   ]
 7: 1        Mult
 8: 0        Offset

22:  End (P95)
;Ends determ of 16 soil Temp measurements
;Temps recorded in Loc 9 to 24 inclusive.

23:  Do (P86)
 1: 55       Set Port 5 Low
;Resets AM 416 to beginning

;          MEASUREMENTS FOR 2nd GROUP OF T/c's (Heating cycle)

24:  Do (P86)
 1: 42       Set Port 2 High
;Activates 2nd CE8 thru' C2

25:  Beginning of Loop (P87)
 1: 0        Delay
 2: 2        Loop Count

26:  Excitation with Delay (P22)
 1: 1        Ex Channel
 2: 0        Delay W/Ex (units = 0.01 sec)
 3: 50       Delay After Ex (units = 0.01 sec)
 4: 0        mV Excitation

27:  End (P95)
;Create 1 sec period; i.e. activate CE8 No 2 for 1 sec

28:  Do (P86)
 1: 45       Set Port 5 High
;Activates AM416

29:  Beginning of Loop (P87)
 1: 0        Delay
 2: 4        Loop Count
```

```
30:  Do (P86)
 1: 74       Pulse Port 4

31:  Step Loop Index (P90)
 1: 2        Step

32:  Thermocouple Temp (SE) (P13)
 1: 2        Reps
 2: 21       2.5 mV 60 Hz Rejection Range
 3: 9        SE Channel
 4: 1        Type T (Copper-Constantan)
 5: 1        Ref Temp (Deg. C) Loc [ RefTemp   ]
 6: 37    -- Loc [ Sec1_9    ]
 7: 1        Mult
 8: 0        Offset

33:  End (P95)
;Ends 8 T/c measurements after 1 sec heating; Locs 37 to 44 inclusive

34:  Do (P86)
 1: 55       Set Port 5 Low
;Resets AM416

35:  Beginning of Loop (P87)
 1: 0        Delay
 2: 40       Loop Count

36:  Excitation with Delay (P22)
 1: 1        Ex Channel
 2: 0        Delay W/Ex (units = 0.01 sec)
 3: 50       Delay After Ex (units = 0.01 sec)
 4: 0        mV Excitation

37:  End (P95)
;Creates 20 sec delay; i.e. continue heating for 20 sec

38:  Do (P86)
 1: 45       Set Port 5 High
;Activates AM416

39:  Beginning of Loop (P87)
 1: 0        Delay
 2: 4        Loop Count

40:  Do (P86)
 1: 74       Pulse Port 4

41:  Step Loop Index (P90)
 1: 2        Step

42:  Thermocouple Temp (SE) (P13)
 1: 2        Reps
 2: 21       2.5 mV 60 Hz Rejection Range
 3: 9        SE Channel
 4: 1        Type T (Copper-Constantan)
 5: 1        Ref Temp (Deg. C) Loc [ RefTemp   ]
 6: 61    -- Loc [ T20s_9    ]
 7: 1        Mult
 8: 0        Offset
```

```
43:  End (P95)
;Ends Temp measurements after 21 sec heating for 2nd Group of T/c's
;Temp 21 sec (T20s_9) recorded in Locs 61 to 68 inclusive.
;   NNB AM416 is not reset, left at SET 4

44:  Do (P86)
 1: 52       Set Port 2 Low
;Deactivates CE8 No 2

;           MEASUREMENTS FOR 3rd GROUP OF 8 T/c's (Heating cycle)

45:  Do (P86)
 1: 46       Set Port 6 High
;Activates 3rd CE8

46:  Beginning of Loop (P87)
 1: 0        Delay
 2: 2        Loop Count

47:  Excitation with Delay (P22)
 1: 1        Ex Channel
 2: 0        Delay W/Ex (units = 0.01 sec)
 3: 50       Delay After Ex (units = 0.01 sec)
 4: 0        mV Excitation

48:  End (P95)
;Create 1 sec period for 3rd CE8

49:  Beginning of Loop (P87)
 1: 0        Delay
 2: 4        Loop Count

50:  Do (P86)
 1: 74       Pulse Port 4

51:  Step Loop Index (P90)
 1: 2        Step

52:  Thermocouple Temp (SE) (P13)
 1: 2        Reps
 2: 21       2.5 mV 60 Hz Rejection Range
 3: 9        SE Channel
 4: 1        Type T (Copper-Constantan)
 5: 1        Ref Temp (Deg. C) Loc [ RefTemp    ]
 6: 45    -- Loc [ Sec1_17    ]
 7: 1        Mult
 8: 0        Offset

53:  End (P95)

54:  Do (P86)
 1: 55       Set Port 5 Low
;Resets AM416 to channel 1

55:  Do (P86)
 1: 45       Set Port 5 High
;Activates AM416

56:  Beginning of Loop (P87)
 1: 0        Delay
```

```
 2: 4       Loop Count

57:  Do (P86)
 1: 74      Pulse Port 4

58:  Do (P86)
 1: 74      Pulse Port 4

59:  End (P95)
;Steps AM416 thru 8 channels, i.e. to SET 5

60:  Beginning of Loop (P87)
 1: 0       Delay
 2: 40      Loop Count

61:  Excitation with Delay (P22)
 1: 1       Ex Channel
 2: 0       Delay W/Ex (units = 0.01 sec)
 3: 50      Delay After Ex (units = 0.01 sec)
 4: 0       mV Excitation

62:  End (P95)
;20 sec delay

63:  Beginning of Loop (P87)
 1: 0       Delay
 2: 4       Loop Count

64:  Do (P86)
 1: 74      Pulse Port 4

65:  Step Loop Index (P90)
 1: 2       Step

66:  Thermocouple Temp (SE) (P13)
 1: 2       Reps
 2: 21      2.5 mV 60 Hz Rejection Range
 3: 9       SE Channel
 4: 1       Type T (Copper-Constantan)
 5: 1       Ref Temp (Deg. C) Loc [ RefTemp   ]
 6: 69    -- Loc [ T20s_17   ]
 7: 1       Mult
 8: 0       Offset

67:  End (P95)
;Ends Temp 21 sec measurements for 3rd CE8
; recorded in Locs 69 to 76

68:  Do (P86)
 1: 55      Set Port 5 Low
;Resets AM416 to channel 1

69:  Do (P86)
 1: 56      Set Port 6 Low
;Deactivates CE8 No 3
;          ENDS MEASUREMENTS FOR 3rd GROUP OF T/c's

70:  Beginning of Loop (P87)
 1: 0       Delay
 2: 24      Loop Count
```

```
71:  Z=X-Y (P35)
 1: 53    -- X Loc [ T20s_1    ]
 2: 29    -- Y Loc [ Sec1_1    ]
 3: 77    -- Z Loc [ dT_1      ]
;Calculates dT for 24 sensors and places result in
;Locs 77 to 100 inclusive

72:  End (P95)
;Ends dT calc loop

73:  Z=F (P30)
 1: 3.5268   F
 2: 0        Exponent of 10
 3: 101      Z Loc [ Psi_1     ]

74:  Z=X^Y (P47)
 1: 77       X Loc [ dT_1      ]
 2: 101      Y Loc [ Psi_1     ]
 3: 101      Z Loc [ Psi_1     ]

75:  Z=X*F (P37)
 1: 101      X Loc [ Psi_1     ]
 2: -40.043  F
 3: 101      Z Loc [ Psi_1     ]
;Calc  PSi for HDS S/N 1353

76:  Z=F (P30)
 1: 4.4796   F
 2: 0        Exponent of 10
 3: 102      Z Loc [ Psi_2     ]

77:  Z=X^Y (P47)
 1: 78       X Loc [ dT_2      ]
 2: 102      Y Loc [ Psi_2     ]
 3: 102      Z Loc [ Psi_2     ]

78:  Z=X*F (P37)
 1: 102      X Loc [ Psi_2     ]
 2: -21.6616 F
 3: 102      Z Loc [ Psi_2     ]
;Calcs Psi for HDS S/N 1347

79:  Z=F (P30)
 1: 5.3718   F
 2: 0        Exponent of 10
 3: 103      Z Loc [ Psi_3     ]

80:  Z=X^Y (P47)
 1: 79       X Loc [ dT_3      ]
 2: 103      Y Loc [ Psi_3     ]
 3: 103      Z Loc [ Psi_3     ]

81:  Z=X*F (P37)
 1: 103      X Loc [ Psi_3     ]
 2: -16.879  F
 3: 103      Z Loc [ Psi_3     ]
;Calcs Psi for HDS S/N 4724

82:  Z=F (P30)
```

```
 1: 4.1613   F
 2: 0        Exponent of 10
 3: 104      Z Loc [ Psi_4     ]

83:  Z=X^Y (P47)
 1: 80       X Loc [ dT_4      ]
 2: 104      Y Loc [ Psi_4     ]
 3: 104      Z Loc [ Psi_4     ]

84:  Z=X*F (P37)
 1: 104      X Loc [ Psi_4     ]
 2: -14.441  F
 3: 104      Z Loc [ Psi_4     ]
;Calcs Psi for HDS S/N 4725

85:  Z=F (P30)
 1: 6.8064   F
 2: 0        Exponent of 10
 3: 105      Z Loc [ Psi_5     ]

86:  Z=X^Y (P47)
 1: 81       X Loc [ dT_5      ]
 2: 105      Y Loc [ Psi_5     ]
 3: 105      Z Loc [ Psi_5     ]

87:  Z=X*F (P37)
 1: 105      X Loc [ Psi_5     ]
 2: -17.576  F
 3: 105      Z Loc [ Psi_5     ]
;Calcs Psi for HDS S/N 4723

88:  Z=F (P30)
 1: 7.1627   F
 2: 0        Exponent of 10
 3: 106      Z Loc [ Psi_6     ]

89:  Z=X^Y (P47)
 1: 82       X Loc [ dT_6      ]
 2: 106      Y Loc [ Psi_6     ]
 3: 106      Z Loc [ Psi_6     ]

90:  Z=X*F (P37)
 1: 106      X Loc [ Psi_6     ]
 2: -10.032  F
 3: 106      Z Loc [ Psi_6     ]
;Calculates Psi for HDS S/N 4728

91:  Z=F (P30)
 1: 7.4655   F
 2: 0        Exponent of 10
 3: 107      Z Loc [ Psi_7     ]

92:  Z=X^Y (P47)
 1: 83       X Loc [ dT_7      ]
 2: 107      Y Loc [ Psi_7     ]
 3: 107      Z Loc [ Psi_7     ]

93:  Z=X*F (P37)
 1: 107      X Loc [ Psi_7     ]
 2: -11.282  F
```

```
 3: 107      Z Loc [ Psi_7     ]
;Calcs Psi for HDS S/N 4719

94:  Z=F (P30)
 1: 6.3041   F
 2: 0        Exponent of 10
 3: 108      Z Loc [ Psi_8     ]

95:  Z=X^Y (P47)
 1: 84       X Loc [ dT_8      ]
 2: 108      Y Loc [ Psi_8     ]
 3: 108      Z Loc [ Psi_8     ]

96:  Z=X*F (P37)
 1: 108      X Loc [ Psi_8     ]
 2: -22.561  F
 3: 108      Z Loc [ Psi_8     ]
;Calcs Psi for HDS S/N 4720

97:  Z=F (P30)
 1: 5.1654   F
 2: 0        Exponent of 10
 3: 109      Z Loc [ Psi_9     ]

98:  Z=X^Y (P47)
 1: 85       X Loc [ dT_9      ]
 2: 109      Y Loc [ Psi_9     ]
 3: 109      Z Loc [ Psi_9     ]

99:  Z=X*F (P37)
 1: 109      X Loc [ Psi_9     ]
 2: -21.8557 F
 3: 109      Z Loc [ Psi_9     ]
;Calcs Psi for HDS S/N 1329

100:  Z=F (P30)
 1: 2.9517   F
 2: 0        Exponent of 10
 3: 110      Z Loc [ Psi_10    ]

101:  Z=X^Y (P47)
 1: 86       X Loc [ dT_10     ]
 2: 110      Y Loc [ Psi_10    ]
 3: 110      Z Loc [ Psi_10    ]

102:  Z=X*F (P37)
 1: 110      X Loc [ Psi_10    ]
 2: -19.139  F
 3: 110      Z Loc [ Psi_10    ]
;Calcs Psi for HDS S/N 1343

103:  Z=F (P30)
 1: 3.904    F
 2: 0        Exponent of 10
 3: 111      Z Loc [ Psi_11    ]

104:  Z=X^Y (P47)
 1: 87       X Loc [ dT_11     ]
 2: 111      Y Loc [ Psi_11    ]
 3: 111      Z Loc [ Psi_11    ]
```

```
105:  Z=X*F (P37)
 1: 111      X Loc [ Psi_11    ]
 2: -20.2988 F
 3: 111      Z Loc [ Psi_11    ]
;Calcs Psi for HDS S/N 1352

106:  Z=F (P30)
 1: 3.8467   F
 2: 0        Exponent of 10
 3: 112      Z Loc [ Psi_12    ]

107:  Z=X^Y (P47)
 1: 88       X Loc [ dT_12     ]
 2: 112      Y Loc [ Psi_12    ]
 3: 112      Z Loc [ Psi_12    ]

108:  Z=X*F (P37)
 1: 112      X Loc [ Psi_12    ]
 2: -25.316  F
 3: 112      Z Loc [ Psi_12    ]
;Calcs Psi for HDS 4726

109:  Z=F (P30)
 1: 5.297    F
 2: 0        Exponent of 10
 3: 113      Z Loc [ Psi_13    ]

110:  Z=X^Y (P47)
 1: 89       X Loc [ dT_13     ]
 2: 113      Y Loc [ Psi_13    ]
 3: 113      Z Loc [ Psi_13    ]

111:  Z=X*F (P37)
 1: 113      X Loc [ Psi_13    ]
 2: -14.864  F
 3: 113      Z Loc [ Psi_13    ]
;Calcs Psi for HDS S/N 4360

112:  Z=F (P30)
 1: 6.7863   F
 2: 0        Exponent of 10
 3: 114      Z Loc [ Psi_14    ]

113:  Z=X^Y (P47)
 1: 90       X Loc [ dT_14     ]
 2: 114      Y Loc [ Psi_14    ]
 3: 114      Z Loc [ Psi_14    ]

114:  Z=X*F (P37)
 1: 114      X Loc [ Psi_14    ]
 2: -12.595  F
 3: 114      Z Loc [ Psi_14    ]
;Calcs Psi for HDS S/N 4390

115:  Z=F (P30)
 1: 5.3778   F
 2: 0        Exponent of 10
 3: 115      Z Loc [ Psi_15    ]
```

```
116:  Z=X^Y (P47)
 1: 91       X Loc [ dT_15     ]
 2: 115      Y Loc [ Psi_15    ]
 3: 115      Z Loc [ Psi_15    ]

117:  Z=X*F (P37)
 1: 115      X Loc [ Psi_15    ]
 2: -20.325  F
 3: 115      Z Loc [ Psi_15    ]
;Calcs Psi for HDS S/N 4626

118:  Z=F (P30)
 1: 4.1613   F
 2: 0        Exponent of 10
 3: 116      Z Loc [ Psi_16    ]

119:  Z=X^Y (P47)
 1: 92       X Loc [ dT_16     ]
 2: 116      Y Loc [ Psi_16    ]
 3: 116      Z Loc [ Psi_16    ]

120:  Z=X*F (P37)
 1: 116      X Loc [ Psi_16    ]
 2: -25.6447 F
 3: 116      Z Loc [ Psi_16    ]
;Calcs Psi for HDS S/N 1345

121:  Z=F (P30)
 1: 6.0703   F
 2: 0        Exponent of 10
 3: 117      Z Loc [ Psi_17    ]

122:  Z=X^Y (P47)
 1: 93       X Loc [ dT_17     ]
 2: 117      Y Loc [ Psi_17    ]
 3: 117      Z Loc [ Psi_17    ]

123:  Z=X*F (P37)
 1: 117      X Loc [ Psi_17    ]
 2: -16.882  F
 3: 117      Z Loc [ Psi_17    ]
;Calcs Psi for HDS S/N 4367

124:  Z=F (P30)
 1: 5.832    F
 2: 0        Exponent of 10
 3: 118      Z Loc [ Psi_18    ]

125:  Z=X^Y (P47)
 1: 94       X Loc [ dT_18     ]
 2: 118      Y Loc [ Psi_18    ]
 3: 118      Z Loc [ Psi_18    ]

126:  Z=X*F (P37)
 1: 118      X Loc [ Psi_18    ]
 2: -19.189  F
 3: 118      Z Loc [ Psi_18    ]
;Calcs Psi for HDS S/N 4374

127:  Z=F (P30)
```

```
 1: 5.8407   F
 2: 0        Exponent of 10
 3: 119      Z Loc [ Psi_19    ]

128:  Z=X^Y (P47)
 1: 95       X Loc [ dT_19     ]
 2: 119      Y Loc [ Psi_19    ]
 3: 119      Z Loc [ Psi_19    ]

129:  Z=X*F (P37)
 1: 119      X Loc [ Psi_19    ]
 2: -12.842  F
 3: 119      Z Loc [ Psi_19    ]
;Calcs Psi for HDS S/N 4627

130:  Z=F (P30)
 1: 4.9265   F
 2: 0        Exponent of 10
 3: 120      Z Loc [ Psi_20    ]

131:  Z=X^Y (P47)
 1: 96       X Loc [ dT_20     ]
 2: 120      Y Loc [ Psi_20    ]
 3: 120      Z Loc [ Psi_20    ]

132:  Z=X*F (P37)
 1: 120      X Loc [ Psi_20    ]
 2: -16.17   F
 3: 120      Z Loc [ Psi_20    ]
;Calcs Psi for HDS S/N 4381

133:  Z=F (P30)
 1: 1        F
 2: 0        Exponent of 10
 3: 121      Z Loc [ Psi_21    ]
;Psi for "Psi_21"

134:  Z=F (P30)
 1: 5.8008   F
 2: 0        Exponent of 10
 3: 122      Z Loc [ Psi_22    ]

135:  Z=X^Y (P47)
 1: 98       X Loc [ dT_22     ]
 2: 122      Y Loc [ Psi_22    ]
 3: 122      Z Loc [ Psi_22    ]

136:  Z=X*F (P37)
 1: 122      X Loc [ Psi_22    ]
 2: -16.268  F
 3: 122      Z Loc [ Psi_22    ]
;Calcs Psi for HDS S/N 4365

137:  Z=F (P30)
 1: 4.9347   F
 2: 0        Exponent of 10
 3: 123      Z Loc [ Psi_23    ]

138:  Z=X^Y (P47)
 1: 99       X Loc [ dT_23     ]
```

```
 2: 123      Y Loc [ Psi_23    ]
 3: 123      Z Loc [ Psi_23    ]

139:  Z=X*F (P37)
 1: 123      X Loc [ Psi_23    ]
 2: -16.016  F
 3: 123      Z Loc [ Psi_23    ]
;Calcs Psi for HDS S/N 4628

140:  Z=F (P30)
 1: 5.4848   F
 2: 0        Exponent of 10
 3: 124      Z Loc [ Psi_24    ]

141:  Z=X^Y (P47)
 1: 100      X Loc [ dT_24     ]
 2: 124      Y Loc [ Psi_24    ]
 3: 124      Z Loc [ Psi_24    ]

142:  Z=X*F (P37)
 1: 124      X Loc [ Psi_24    ]
 2: -19.324  F
 3: 124      Z Loc [ Psi_24    ]

143:  Do (P86)
 1: 10       Set Output Flag High (Flag 0)

144:  Set Active Storage Area (P80)
 1: 1        Final Storage Area 1
 2: 111      Array ID

145:  Real Time (P77)
 1: 1220     Year,Day,Hour/Minute (midnight = 2400)

146:  Minimize (P74)
 1: 1        Reps
 2: 0        Value Only
 3: 2        Loc [ Battery   ]

147:  Average (P71)
 1: 1        Reps
 2: 1        Loc [ RefTemp   ]

148:  Sample (P70)
 1: 24       Reps
 2: 101      Loc [ Psi_1     ]

149:  Do (P86)
 1: 10       Set Output Flag High (Flag 0)

150:  Set Active Storage Area (P80)
 1: 1        Final Storage Area 1
 2: 222      Array ID

151:  Real Time (P77)
 1: 1220     Year,Day,Hour/Minute (midnight = 2400)

152:  Sample (P70)
 1: 24       Reps
 2: 77       Loc [ dT_1      ]
```

153: Do (P86)
1: 10 Set Output Flag High (Flag 0)

154: Set Active Storage Area (P80)
1: 1 Final Storage Area 1
2: 333 Array ID

155: Real Time (P77)
1: 1220 Year,Day,Hour/Minute (midnight = 2400)

156: Sample (P70)
1: 24 Reps
2: 5 Loc [SoilT_1]

A.7 Heat dissipation sensors (HDS) program; 28 Sensors

```
;{CR10X}
;HDS28CIT.CSI
;Program drafted to read 28 Heat Dissipation Sensors (HDS)
;thru' AM416 multiplexer & excited thru' four CE8s.
;CR10TCR (Thermistor Reference Temperature) connected thru'
;   SE channel 12 (Red lead): Excitation channel 3 (E3, Black lead)
;   & AG (clear lead)
;AM416 clocked <pulsed) thru C5 & Reset thru C6.
;CE8s activated thru C1, C2, C3, & C4.
;OUTPUT: RefT, SoilT, dT & Psi on the Hour.
;Drafted: Begun 19/11/99

* Table 1 Program
          01:        1          Execution Interval (seconds)

1:  If time is (P92)
 1: 0        Minutes (Seconds --) into a
 2: 120      Interval (same units as above)
 3: 11       Set Flag 1 High

2:  If Flag/Port (P91)
 1: 21       Do if Flag 1 is Low
 2: 0        Go to end of Program Table

3:  AC Half Bridge (P5)
 1: 1        Reps
 2: 22       7.5 mV 60 Hz Rejection Range
 3: 12       SE Channel
 4: 3        Excite all reps w/Exchan 3
 5: 2000     mV Excitation
 6: 3        Loc [ TCRT      ]
 7: 800      Mult
 8: 0        Offset

4:  Polynomial (P55)
 1: 1        Reps
 2: 3        X Loc [ TCRT      ]
 3: 1        F(X) Loc [ RefTemp    ]
 4: -53.46   C0
 5: 90.807   C1
 6: -83.257  C2
 7: 52.283   C3
 8: -16.723  C4
 9: 2.211    C5

5:  Batt Voltage (P10)
 1: 2        Loc [ Battery    ]

6:  Do (P86)
 1: 46       Set Port 6 High
;Activate AM416 thru' Control Port 6 (Res = C6)

7:  Beginning of Loop (P87)
 1: 0        Delay
 2: 14       Loop Count
;14 loops with 2 Diff sensors per set: 14 X 2 = 28

8:  Do (P86)
```

```
 1: 75       Pulse Port 5
;Pulses AM416 thru" C5 (CLK = C5)

9:  Step Loop Index (P90)
 1: 2        Step
;Necessary not to over-write readings

10:  Thermocouple Temp (DIFF) (P14)
 1: 2        Reps
 2: 21       2.5 mV 60 Hz Rejection Range
 3: 1        DIFF Channel
 4: 1        Type T (Copper-Constantan)
 5: 1        Ref Temp Loc [ RefTemp    ]
 6: 5     -- Loc [ SoilT_1    ]
 7: 1        Mult
 8: 0        Offset

11:  End (P95)
;Ends first round of 28 soil Temp measurements
;Temps recorded in Loc 5 to 32 inclusive.

12:  Do (P86)
 1: 56       Set Port 6 Low
;Resets AM416 to beginning

13:  Do (P86)
 1: 41       Set Port 1 High
;Activates 1st CE8 thru' C1

14:  Do (P86)
 1: 42       Set Port 2 High
;Activates 2nd CE8 thru' C2

15:  Do (P86)
 1: 43       Set Port 3 High
;Activates 3rd CE8 thru' C3

16:  Do (P86)
 1: 44       Set Port 4 High
;Activates 4th CE8 thru' C4

17:  Beginning of Loop (P87)
 1: 0        Delay
 2: 2        Loop Count

18:  Excitation with Delay (P22)
 1: 1        Ex Channel
 2: 0        Delay W/Ex (units = 0.01 sec)
 3: 50       Delay After Ex (units = 0.01 sec)
 4: 0        mV Excitation

19:  End (P95)
;Create 1 sec period (2 X 50 X 0.01 = 1 sec);
;       i.e. activate CE8's for 1 sec

20:  Do (P86)
 1: 46       Set Port 6 High
;Activates AM416

21:  Beginning of Loop (P87)
```

```
 1: 0       Delay
 2: 14      Loop Count

22:  Do (P86)
 1: 75      Pulse Port 5

23:  Step Loop Index (P90)
 1: 2       Step

24:  Thermocouple Temp (DIFF) (P14)
 1: 2       Reps
 2: 21      2.5 mV 60 Hz Rejection Range
 3: 1       DIFF Channel
 4: 1       Type T (Copper-Constantan)
 5: 1       Ref Temp Loc [ RefTemp   ]
 6: 33    -- Loc [ Sec1_1    ]
 7: 1.0     Mult
 8: 0       Offset

25:  End (P95)

26:  Do (P86)
 1: 56      Set Port 6 Low
;Complete 28 measurements of Temp after 1 sec heating
;Measurements recorded in Locs 33 to 60 inclusive.

27:  Beginning of Loop (P87)
 1: 0       Delay
 2: 40      Loop Count

28:  Excitation with Delay (P22)
 1: 1       Ex Channel
 2: 0       Delay W/Ex (units = 0.01 sec)
 3: 50      Delay After Ex (units = 0.01 sec)
 4: 0       mV Excitation

29:  End (P95)
;Creates 20 sec delay; i.e. continue heating for 20 sec

30:  Do (P86)
 1: 46      Set Port 6 High

31:  Beginning of Loop (P87)
 1: 0       Delay
 2: 14      Loop Count

32:  Do (P86)
 1: 75      Pulse Port 5

33:  Step Loop Index (P90)
 1: 2       Step

34:  Thermocouple Temp (DIFF) (P14)
 1: 2       Reps
 2: 21      2.5 mV 60 Hz Rejection Range
 3: 1       DIFF Channel
 4: 1       Type T (Copper-Constantan)
 5: 1       Ref Temp Loc [ RefTemp   ]
 6: 61    -- Loc [ T20s_1    ]
 7: 1.0     Mult
```

```
 8: 0.0      Offset

35:  End (P95)

36:  Do (P86)
 1: 56       Set Port 6 Low
;Ends Temp measurements after 21 sec heating & resets AM416
;Temp 21 sec (T20s_X) recorded in Locs 61 to 88 inclusive.

37:  Do (P86)
 1: 51       Set Port 1 Low
;Deactivates CE8 No 1

38:  Do (P86)
 1: 52       Set Port 2 Low
;Deactivates CE8 No 2

39:  Do (P86)
 1: 53       Set Port 3 Low
;Deactivates CE8 No 3

40:  Do (P86)
 1: 54       Set Port 4 Low
;Deactivates CE8 No 4

41:  Beginning of Loop (P87)
 1: 0        Delay
 2: 28       Loop Count

42:  Z=X-Y (P35)
 1: 61    -- X Loc [ T20s_1    ]
 2: 33    -- Y Loc [ Sec1_1    ]
 3: 89    -- Z Loc [ dT_1      ]
;Calculates dT for 28 sensors and places result in
;   Locs 89 to 116 inclusive

43:  End (P95)
;Ends dT calc loop

44:  Do (P86)
 1: 10       Set Output Flag High (Flag 0)

45:  Set Active Storage Area (P80)
 1: 1        Final Storage Area 1
 2: 111      Array ID

46:  Real Time (P77)
 1: 1220     Year,Day,Hour/Minute (midnight = 2400)

47:  Minimize (P74)
 1: 1        Reps
 2: 0        Value Only
 3: 2        Loc [ Battery    ]

48:  Average (P71)
 1: 1        Reps
 2: 1        Loc [ RefTemp    ]

49:  Sample (P70)
 1: 28       Reps
```

```
 2: 5        Loc [ SoilT_1    ]

50:  Do (P86)
 1: 10       Set Output Flag High (Flag 0)

51:  Set Active Storage Area (P80)
 1: 1        Final Storage Area 1
 2: 222      Array ID

52:  Real Time (P77)
 1: 1220     Year,Day,Hour/Minute (midnight = 2400)

53:  Sample (P70)
 1: 28       Reps
 2: 89       Loc [ dT_1       ]

54:  Do (P86)
 1: 21       Set Flag 1 Low

* Table 2 Program
            02:         0.0000              Execution Interval (seconds)

* Table 3  Subroutines

End Program
```

A.8 TDR cable length measurement for 28 TDR probes in Clementine Orchard

```
;{CR10X}
;CLEMTDRD.CSI
; Program drafted to measure cable lengths of 28 TDR probes
;   having different lengths.
; Drafted 28/11/99
; SDM1502 Cable Tester DIP switch set at 0000 to give address of 00
; Level 1 SDMX50 coaxial multiplexer MSD = 0 & LSD = 1 to give
;          address of 01
; Level 2 SDMX50 coaxial multiplexers (three off) MSD = 0 & LSD = 2 to
;          give address of 02
; Four probes with cable length of 16ft connected at Level 1
; Eight probes with length of 20 ft connected to Box 6, Level 2
;          via channel 6 in Level 1 Mux
; Eight probes with length of 24 ft connected to Box 7, Level 2
;          via channel 7 in Level 1 Mux
; Eight probes with length of 29 ft connected to Box 8, Level 2
;          via channel 8 in level 1 Mux
; Program activated thru flag 1.

* Table 1 Program
  01: 10 Execution Interval (seconds)

1:  If Flag/Port (P91)
 1: 11       Do if Flag 1 is High
 2: 30       Then Do

2:  Do (P86)
 1: 44       Set Port 4 High

3:  Excitation with Delay (P22)
 1: 1        Ex Channel
 2: 0        Delay W/Ex (units = 0.01 sec)
 3: 500      Delay After Ex (units = 0.01 sec)
 4: 0        mV Excitation

4:  TDR Measurement (P100)
 1: 00       SDM1502 Address
 2: 98       Manual MUX Address Advance
 3: .3       Probe Length (meters)
 4: 0.0      Cable Length (meters)
 5: 7104     MMMP  Mux & Probe Selection
 6: 1        Loc [ W1_06_1   ]
 7: 1        Mult
 8: 0        Offset
;Measure Probes for site W1

5:  TDR Measurement (P100)
 1: 00       SDM1502 Address
 2: 98       Manual MUX Address Advance
 3: .3       Probe Length (meters)
 4: 0.0      Cable Length (meters)
 5: 6104     MMMP  Mux & Probe Selection
 6: 5        Loc [ W2_06_2   ]
 7: 1.0      Mult
 8: 0.0      Offset

6:  TDR Measurement (P100)
 1: 00       SDM1502 Address
```

```
 2: 98      Manual MUX Address Advance
 3: .3      Probe Length (meters)
 4: 0.0     Cable Length (meters)
 5: 1004    MMMP  Mux & Probe Selection
 6: 9       Loc [ W3_06_3   ]
 7: 1.0     Mult
 8: 0.0     Offset

 7:  TDR Measurement (P100)
 1: 00      SDM1502 Address
 2: 98      Manual MUX Address Advance
 3: .3      Probe Length (meters)
 4: 0.0     Cable Length (meters)
 5: 6504    MMMP  Mux & Probe Selection
 6: 13      Loc [ C4_06_4   ]
 7: 1.0     Mult
 8: 0.0     Offset


 8:  TDR Measurement (P100)
 1: 00      SDM1502 Address
 2: 98      Manual MUX Address Advance
 3: .3      Probe Length (meters)
 4: 0.0     Cable Length (meters)
 5: 7504    MMMP  Mux & Probe Selection
 6: 17      Loc [ E5_06_5   ]
 7: 1.0     Mult
 8: 0.0     Offset

 9:  TDR Measurement (P100)
 1: 00      SDM1502 Address
 2: 98      Manual MUX Address Advance
 3: .3      Probe Length (meters)
 4: 0.0     Cable Length (meters)
 5: 8104    MMMP  Mux & Probe Selection
 6: 21      Loc [ E6_06_6   ]
 7: 1.0     Mult
 8: 0.0     Offset

10:  TDR Measurement (P100)
 1: 00      SDM1502 Address
 2: 98      Manual MUX Address Advance
 3: .3      Probe Length (meters)
 4: 0.0     Cable Length (meters)
 5: 8504    MMMP  Mux & Probe Selection
 6: 25      Loc [ E7_06_7   ]
 7: 1.0     Mult
 8: 0.0     Offset

11:  Do (P86)
 1: 54      Set Port 4 Low

12:  Batt Voltage (P10)
 1: 29      Loc [ V_batt    ]

13:  Do (P86)
 1: 10      Set Output Flag High (Flag 0)

14:  Real Time (P77)
 1: 1220    Year,Day,Hour/Minute (midnight = 2400)
```

```
15:  Sample (P70)
 1: 29       Reps
 2: 1        Loc [ W1_06_1   ]

16:  Do (P86)
 1: 21       Set Flag 1 Low

17:  End (P95)
```

A.9 TDR cable length measurement for 40 TDR probes in Peach Orchard

```
;{CR10X}
;HATTDRd.CSI
; Program drafted to measure cable lengths of 40 CS605 TDR probes
; having different lengths
; Drafted 20/10/99
; SDM1502 Cable Tester DIP switch set at 0000 togive address of 00
; Level 1 SDMX50 coaxial multiplexer MSD = 0 & LSD = 1 to give address 01
; Level 2 SDMX50 coaxial multiplexers (five off) MSD = 0 & LSD = 2
;          to give address of 02

* Table 1 Program
  01:  10Execution Interval (seconds)

1:  If Flag/Port (P91)
 1: 15       Do if Flag 5 is High
 2: 30       Then Do

2:  Do (P86)
 1: 44       Set Port 4 High

3:  Excitation with Delay (P22)
 1: 1        Ex Channel
 2: 0        Delay W/Ex (units = 0.01 sec)
 3: 500      Delay After Ex (units = 0.01 sec)
 4: 0        mV Excitation

4:  TDR Measurement (P100)
 1: 00       SDM Address
 2: 98       Manual MUX Address Advance
 3: .3       Probe Length (meters)
 4: 0.0      Cable Length (meters)
 5: 1441     MMMP Mux & Probe Selection
 6: 1        Loc [ S1_06____ ]
 7: 0.1138   Mult
 8: -0.1758  Offset

5:  TDR Measurement (P100)
 1: 00       SDM Address
 2: 98       Manual MUX Address Advance
 3: .3       Probe Length (meters)
 4: 0.0      Cable Length (meters)
 5: 1331     MMMP Mux & Probe Selection
 6: 2        Loc [ S1_26     ]
 7: 0.1138   Mult
 8: -0.1758  Offset

6:  TDR Measurement (P100)
 1: 00       SDM Address
 2: 98       Manual MUX Address Advance
 3: .3       Probe Length (meters)
 4: 0.0      Cable Length (meters)
 5: 1221     MMMP Mux & Probe Selection
 6: 3        Loc [ S1_56     ]
 7: 0.1138   Mult
 8: -0.1758  Offset

7:  TDR Measurement (P100)
 1: 00       SDM Address
```

2: 98 Manual MUX Address Advance
3: .3 Probe Length (meters)
4: 0.0 Cable Length (meters)
5: 1111 MMMP Mux & Probe Selection
6: 4 Loc [S1_86]
7: 0.1138 Mult
8: -0.1758 Offset

8: TDR Measurement (P100)
1: 00 SDM Address
2: 98 Manual MUX Address Advance
3: .3 Probe Length (meters)
4: 0.0 Cable Length (meters)
5: 1881 MMMP Mux & Probe Selection
6: 5 Loc [S3_06]
7: 0.1138 Mult
8: -0.1758 Offset

9: TDR Measurement (P100)
1: 00 SDM Address
2: 98 Manual MUX Address Advance
3: .3 Probe Length (meters)
4: 0.0 Cable Length (meters)
5: 1771 MMMP Mux & Probe Selection
6: 6 Loc [S3_26]
7: 0.1138 Mult
8: -0.1758 Offset

10: TDR Measurement (P100)
1: 00 SDM Address
2: 98 Manual MUX Address Advance
3: .3 Probe Length (meters)
4: 0.0 Cable Length (meters)
5: 1661 MMMP Mux & Probe Selection
6: 7 Loc [S3_56]
7: 0.1138 Mult
8: -0.1758 Offset

11: TDR Measurement (P100)
1: 00 SDM Address
2: 98 Manual MUX Address Advance
3: .3 Probe Length (meters)
4: 0.0 Cable Length (meters)
5: 1551 MMMP Mux & Probe Selection
6: 8 Loc [S3_86]
7: 0.1138 Mult
8: -0.1758 Offset

12: TDR Measurement (P100)
1: 00 SDM Address
2: 98 Manual MUX Address Advance
3: .3 Probe Length (meters)
4: 0.0 Cable Length (meters)
5: 2441 MMMP Mux & Probe Selection
6: 9 Loc [S5_06]
7: 0.1138 Mult
8: -0.1758 Offset

13: TDR Measurement (P100)
1: 00 SDM Address

2: 98 Manual MUX Address Advance
3: .3 Probe Length (meters)
4: 0.0 Cable Length (meters)
5: 2331 MMMP Mux & Probe Selection
6: 10 Loc [S5_26]
7: 0.1138 Mult
8: -0.1758 Offset

14: TDR Measurement (P100)
1: 00 SDM Address
2: 98 Manual MUX Address Advance
3: .3 Probe Length (meters)
4: 0.0 Cable Length (meters)
5: 2221 MMMP Mux & Probe Selection
6: 11 Loc [S5_56]
7: 0.1138 Mult
8: -0.1758 Offset

15: TDR Measurement (P100)
1: 00 SDM Address
2: 98 Manual MUX Address Advance
3: .3 Probe Length (meters)
4: 0.0 Cable Length (meters)
5: 2111 MMMP Mux & Probe Selection
6: 12 Loc [S5_86]
7: 0.1138 Mult
8: -0.1758 Offset

16: TDR Measurement (P100)
1: 00 SDM Address
2: 98 Manual MUX Address Advance
3: .3 Probe Length (meters)
4: 0.0 Cable Length (meters)
5: 2881 MMMP Mux & Probe Selection
6: 13 Loc [S7_06]
7: 0.1138 Mult
8: -0.1758 Offset

17: TDR Measurement (P100)
1: 00 SDM Address
2: 98 Manual MUX Address Advance
3: .3 Probe Length (meters)
4: 0.0 Cable Length (meters)
5: 2771 MMMP Mux & Probe Selection
6: 14 Loc [S7_26]
7: 0.1138 Mult
8: -0.1758 Offset

18: TDR Measurement (P100)
1: 00 SDM Address
2: 98 Manual MUX Address Advance
3: .3 Probe Length (meters)
4: 0.0 Cable Length (meters)
5: 3441 MMMP Mux & Probe Selection
6: 15 Loc [S7_56]
7: 0.1138 Mult
8: -0.1758 Offset

19: TDR Measurement (P100)
1: 00 SDM Address

```
 2: 98      Manual MUX Address Advance
 3: .3      Probe Length (meters)
 4: 0.0     Cable Length (meters)
 5: 3331    MMMP Mux & Probe Selection
 6: 16      Loc [ S7_86    ]
 7: 0.1138  Mult
 8: -0.1758 Offset

20: TDR Measurement (P100)
 1: 00      SDM Address
 2: 98      Manual MUX Address Advance
 3: .3      Probe Length (meters)
 4: 0.0     Cable Length (meters)
 5: 2661    MMMP Mux & Probe Selection
 6: 17      Loc [ S9_06    ]
 7: 0.1138  Mult
 8: -0.1758 Offset

21: TDR Measurement (P100)
 1: 00      SDM Address
 2: 98      Manual MUX Address Advance
 3: .3      Probe Length (meters)
 4: 0.0     Cable Length (meters)
 5: 2551    MMMP Mux & Probe Selection
 6: 18      Loc [ S9_26    ]
 7: 0.1138  Mult
 8: -0.1758 Offset

22: TDR Measurement (P100)
 1: 00      SDM Address
 2: 98      Manual MUX Address Advance
 3: .3      Probe Length (meters)
 4: 0.0     Cable Length (meters)
 5: 3221    MMMP Mux & Probe Selection
 6: 19      Loc [ S9_56    ]
 7: 0.1138  Mult
 8: -0.1758 Offset

23: TDR Measurement (P100)
 1: 00      SDM Address
 2: 98      Manual MUX Address Advance
 3: .3      Probe Length (meters)
 4: 0.0     Cable Length (meters)
 5: 3111    MMMP Mux & Probe Selection
 6: 20      Loc [ S9_86    ]
 7: 0.1138  Mult
 8: -0.1758 Offset

24: TDR Measurement (P100)
 1: 00      SDM Address
 2: 98      Manual MUX Address Advance
 3: .3      Probe Length (meters)
 4: 0.0     Cable Length (meters)
 5: 4221    MMMP Mux & Probe Selection
 6: 21      Loc [ N1_06    ]
 7: 0.1138  Mult
 8: -0.1758 Offset

25: TDR Measurement (P100)
 1: 00      SDM Address
```

2: 98 Manual MUX Address Advance
3: .3 Probe Length (meters)
4: 0.0 Cable Length (meters)
5: 4111 MMMP Mux & Probe Selection
6: 22 Loc [N1_26]
7: 0.1138 Mult
8: -0.1758 Offset

26: TDR Measurement (P100)
1: 00 SDM Address
2: 98 Manual MUX Address Advance
3: .3 Probe Length (meters)
4: 0.0 Cable Length (meters)
5: 3661 MMMP Mux & Probe Selection
6: 23 Loc [N1_56]
7: 0.1138 Mult
8: -0.1758 Offset

27: TDR Measurement (P100)
1: 00 SDM Address
2: 98 Manual MUX Address Advance
3: .3 Probe Length (meters)
4: 0.0 Cable Length (meters)
5: 3551 MMMP Mux & Probe Selection
6: 24 Loc [N1_86]
7: 0.1138 Mult
8: -0.1758 Offset

28: TDR Measurement (P100)
1: 00 SDM Address
2: 98 Manual MUX Address Advance
3: .3 Probe Length (meters)
4: 0.0 Cable Length (meters)
5: 4441 MMMP Mux & Probe Selection
6: 25 Loc [N3_06]
7: 0.1138 Mult
8: -0.1758 Offset

29: TDR Measurement (P100)
1: 00 SDM Address
2: 98 Manual MUX Address Advance
3: .3 Probe Length (meters)
4: 0.0 Cable Length (meters)
5: 4331 MMMP Mux & Probe Selection
6: 26 Loc [N3_26]
7: 0.1138 Mult
8: -0.1758 Offset

30: TDR Measurement (P100)
1: 00 SDM Address
2: 98 Manual MUX Address Advance
3: .3 Probe Length (meters)
4: 0.0 Cable Length (meters)
5: 3881 MMMP Mux & Probe Selection
6: 27 Loc [N3_56]
7: 0.1138 Mult
8: -0.1758 Offset

31: TDR Measurement (P100)
1: 00 SDM Address

2: 98 Manual MUX Address Advance
3: .3 Probe Length (meters)
4: 0.0 Cable Length (meters)
5: 3771 MMMP Mux & Probe Selection
6: 28 Loc [N3_86]
7: 0.1138 Mult
8: -0.1758 Offset

32: TDR Measurement (P100)
1: 00 SDM Address
2: 98 Manual MUX Address Advance
3: .3 Probe Length (meters)
4: 0.0 Cable Length (meters)
5: 4881 MMMP Mux & Probe Selection
6: 29 Loc [N5_06]
7: 0.1138 Mult
8: -0.1758 Offset

33: TDR Measurement (P100)
1: 00 SDM Address
2: 98 Manual MUX Address Advance
3: .3 Probe Length (meters)
4: 0.0 Cable Length (meters)
5: 4771 MMMP Mux & Probe Selection
6: 30 Loc [N5_26]
7: 0.1138 Mult
8: -0.1758 Offset

34: TDR Measurement (P100)
1: 00 SDM Address
2: 98 Manual MUX Address Advance
3: .3 Probe Length (meters)
4: 0.0 Cable Length (meters)
5: 4661 MMMP Mux & Probe Selection
6: 31 Loc [N5_56]
7: 0.1138 Mult
8: -0.1758 Offset

35: TDR Measurement (P100)
1: 00 SDM Address
2: 98 Manual MUX Address Advance
3: .3 Probe Length (meters)
4: 0.0 Cable Length (meters)
5: 4551 MMMP Mux & Probe Selection
6: 32 Loc [N5_86]
7: 0.1138 Mult
8: -0.1758 Offset

36: TDR Measurement (P100)
1: 00 SDM Address
2: 98 Manual MUX Address Advance
3: .3 Probe Length (meters)
4: 0.0 Cable Length (meters)
5: 5441 MMMP Mux & Probe Selection
6: 33 Loc [N7_06]
7: 0.1138 Mult
8: -0.1758 Offset

37: TDR Measurement (P100)
1: 00 SDM Address

2: 98 Manual MUX Address Advance
3: .3 Probe Length (meters)
4: 0.0 Cable Length (meters)
5: 5331 MMMP Mux & Probe Selection
6: 34 Loc [N7_26]
7: 0.1138 Mult
8: -0.1758 Offset

38: TDR Measurement (P100)
1: 00 SDM Address
2: 98 Manual MUX Address Advance
3: .3 Probe Length (meters)
4: 0.0 Cable Length (meters)
5: 5221 MMMP Mux & Probe Selection
6: 35 Loc [N7_56]
7: 0.1138 Mult
8: -0.1758 Offset

39: TDR Measurement (P100)
1: 00 SDM Address
2: 98 Manual MUX Address Advance
3: .3 Probe Length (meters)
4: 0.0 Cable Length (meters)
5: 5111 MMMP Mux & Probe Selection
6: 36 Loc [N7_86]
7: 0.1138 Mult
8: -0.1758 Offset

40: TDR Measurement (P100)
1: 00 SDM Address
2: 98 Manual MUX Address Advance
3: .3 Probe Length (meters)
4: 0.0 Cable Length (meters)
5: 5881 MMMP Mux & Probe Selection
6: 37 Loc [N9_06]
7: 0.1138 Mult
8: -0.1758 Offset

41: TDR Measurement (P100)
1: 00 SDM Address
2: 98 Manual MUX Address Advance
3: .3 Probe Length (meters)
4: 0.0 Cable Length (meters)
5: 5771 MMMP Mux & Probe Selection
6: 38 Loc [N9_26]
7: 0.1138 Mult
8: -0.1758 Offset

42: TDR Measurement (P100)
1: 00 SDM Address
2: 98 Manual MUX Address Advance
3: .3 Probe Length (meters)
4: 0.0 Cable Length (meters)
5: 5661 MMMP Mux & Probe Selection
6: 39 Loc [N9_56]
7: 0.1138 Mult
8: -0.1758 Offset

43: TDR Measurement (P100)
1: 00 SDM Address

```
 2: 98       Manual MUX Address Advance
 3: .3       Probe Length (meters)
 4: 0.0      Cable Length (meters)
 5: 5551     MMMP Mux & Probe Selection
 6: 40       Loc [ N9_86     ]
 7: 0.1138   Mult
 8: -0.1758  Offset

44:  Do (P86)
 1: 54       Set Port 4 Low

45:  Do (P86)
 1: 10       Set Output Flag High (Flag 0)

46:  Real Time (P77)
 1: 110      Day,Hour/Minute (midnight = 0000)

47:  Sample (P70)
 1: 41       Reps
 2: 1        Loc [ S1_06____ ]

48:  Do (P86)
 1: 25       Set Flag 5 Low

49:  End (P95)
```

A.10 TDR Water Content measurement for 28 TDR probes in Clementine Orchard

```
;{CR10X}
;CLEMTDRD.CSI
; Program drafted to measure Water Content of 28 TDR probes
;   having different lengths.
; Drafted 28/11/99
; SDM1502 Cable Tester DIP switch set at 0000 to give address of 00
; Level 1 SDMX50 coaxial multiplexer MSD = 0 & LSD = 1 to give
;          address of 01
; Level 2 SDMX50 coaxial multiplexers (three off) MSD = 0 & LSD = 2 to
;          give address of 02
; Four probes with cable length of 16ft connected at Level 1
; Eight probes with length of 20 ft connected to Box 6, Level 2
;          via channel 6 in Level 1 Mux
; Eight probes with length of 24 ft connected to Box 7, Level 2
;          via channel 7 in Level 1 Mux
; Eight probes with length of 29 ft connected to Box 8, Level 2
;          via channel 8 in level 1 Mux
; Program activated thru flag 1.

* Table 1 Program
  01:  10Execution Interval (seconds)

1:  If time is (P92)
 1: 0        Minutes (Seconds --) into a
 2: 120      Interval (same units as above)
 3: 11       Set Flag 1 High

2:  If Flag/Port (P91)
 1: 11       Do if Flag 1 is High
 2: 30       Then Do

3:  Do (P86)
 1: 44       Set Port 4 High

4:  Excitation with Delay (P22)
 1: 1        Ex Channel
 2: 0        Delay W/Ex (units = 0.01 sec)
 3: 500      Delay After Ex (units = 0.01 sec)
 4: 0        mV Excitation

5:  TDR Measurement (P100)
 1: 00       SDM1502 Address
 2: 4080     La/L with Probe Correction in mm
 3: .3       Probe Length (meters)
 4: 19.0     Cable Length (meters)
 5: 7104     MMMP  Mux & Probe Selection
 6: 1        Loc [ W1_06_1   ]
 7: 0.1138   Mult
 8: -0.1758  Offset
;Measure Probes for site W1

6:  TDR Measurement (P100)
 1: 00       SDM1502 Address
 2: 4080     La/L with Probe Correction in mm
 3: .3       Probe Length (meters)
 4: 18.1     Cable Length (meters)
 5: 6104     MMMP  Mux & Probe Selection
 6: 5        Loc [ W2_06_2   ]
```

```
 7: 0.1138   Mult
 8: -0.1758  Offset
;Measures Probes for site W2

7:  TDR Measurement (P100)
 1: 00       SDM1502 Address
 2: 4080     La/L with Probe Correction in mm
 3: .3       Probe Length (meters)
 4: 10.1     Cable Length (meters)
 5: 1004     MMMP  Mux & Probe Selection
 6: 9        Loc [ W3_06_3   ]
 7: 0.1138   Mult
 8: -0.1758  Offset
;Measures Probes for site W3

8:  TDR Measurement (P100)
 1: 00       SDM1502 Address
 2: 4080     La/L with Probe Correction in mm
 3: .3       Probe Length (meters)
 4: 18.1     Cable Length (meters)
 5: 6504     MMMP  Mux & Probe Selection
 6: 13       Loc [ C4_06_4   ]
 7: 0.1138   Mult
 8: -0.1758  Offset
;Measures Probes for site C4

9:  TDR Measurement (P100)
 1: 00       SDM1502 Address
 2: 4080     La/L with Probe Correction in mm
 3: .3       Probe Length (meters)
 4: 19.0     Cable Length (meters)
 5: 7504     MMMP  Mux & Probe Selection
 6: 17       Loc [ E5_06_5   ]
 7: 0.1138   Mult
 8: -0.1758  Offset

10:  TDR Measurement (P100)
 1: 00       SDM1502 Address
 2: 4080     La/L with Probe Correction in mm
 3: .3       Probe Length (meters)
 4: 21.1     Cable Length (meters)
 5: 8104     MMMP  Mux & Probe Selection
 6: 21       Loc [ E6_06_6   ]
 7: 0.1138   Mult
 8: -0.1758  Offset

11:  TDR Measurement (P100)
 1: 00       SDM1502 Address
 2: 4080     La/L with Probe Correction in mm
 3: .3       Probe Length (meters)
 4: 21.1     Cable Length (meters)
 5: 8504     MMMP  Mux & Probe Selection
 6: 25       Loc [ E7_06_7   ]
 7: 0.1138   Mult
 8: -0.1758  Offset

12:  Do (P86)
 1: 54       Set Port 4 Low

13:  Batt Voltage (P10)
```

```
 1: 29       Loc [ V_batt    ]

14:  Do (P86)
 1: 10       Set Output Flag High (Flag 0)

15:  Real Time (P77)
 1: 1220     Year,Day,Hour/Minute (midnight = 2400)

16:  Sample (P70)
 1: 29       Reps
 2: 1        Loc [ W1_06_1   ]

17:  Do (P86)
 1: 21       Set Flag 1 Low

18:  End (P95)
```

A.11 TDR Water Content measurement for 40 TDR probes in Peach Orchard

```
;{CR10X}
;HATTDRw.CSI
; Program drafted to measure water content of 40 CS605 TDR probes
; having different lenghts
; Drafted 21/10/99
; SDM1502 Cable Tester DIP switch set at 0000 togive address of 00
; Level 1 SDMX50 coaxial multiplexer MSD = 0 & LSD = 1 to give address 01
; Level 2 SDMX50 coaxial multiplexers (five off) MSD = 0 & LSD = 2
;          to give address of 02

* Table 1 Program
01:  10              Execution Interval (seconds)

1:  If time is (P92)
 1: 0        Minutes (Seconds --) into a
 2: 240      Interval (same units as above)
 3: 30       Then Do

2:  Do (P86)
 1: 44       Set Port 4 High

3:  Excitation with Delay (P22)
 1: 1        Ex Channel
 2: 0        Delay W/Ex (units = 0.01 sec)
 3: 500      Delay After Ex (units = 0.01 sec)
 4: 0        mV Excitation

4:  TDR Measurement (P100)
 1: 00       SDM Address
 2: 4080     La/L with Probe Correction in mm
 3: .3       Probe Length (meters)
 4: 13.6     Cable Length (meters)
 5: 1441     MMMP Mux & Probe Selection
 6: 1        Loc [ S1_06____ ]
 7: 0.1138   Mult
 8: -0.1758  Offset

5:  TDR Measurement (P100)
 1: 00       SDM Address
 2: 4080     La/L with Probe Correction in mm
 3: .3       Probe Length (meters)
 4: 14.6     Cable Length (meters)
 5: 1331     MMMP Mux & Probe Selection
 6: 2        Loc [ S1_26     ]
 7: 0.1138   Mult
 8: -0.1758  Offset

6:  TDR Measurement (P100)
 1: 00       SDM Address
 2: 4080     La/L with Probe Correction in mm
 3: .3       Probe Length (meters)
 4: 15.8     Cable Length (meters)
 5: 1221     MMMP Mux & Probe Selection
 6: 3        Loc [ S1_56     ]
 7: 0.1138   Mult
 8: -0.1758  Offset

7:  TDR Measurement (P100)
```

1: 00 SDM Address
2: 4080 La/L with Probe Correction in mm
3: .3 Probe Length (meters)
4: 17.4 Cable Length (meters)
5: 1111 MMMP Mux & Probe Selection
6: 4 Loc [S1_86]
7: 0.1138 Mult
8: -0.1758 Offset

8: TDR Measurement (P100)
1: 00 SDM Address
2: 4080 La/L with Probe Correction in mm
3: .3 Probe Length (meters)
4: 12.5 Cable Length (meters)
5: 1881 MMMP Mux & Probe Selection
6: 5 Loc [S3_06]
7: 0.1138 Mult
8: -0.1758 Offset

9: TDR Measurement (P100)
1: 00 SDM Address
2: 4080 La/L with Probe Correction in mm
3: .3 Probe Length (meters)
4: 13.6 Cable Length (meters)
5: 1771 MMMP Mux & Probe Selection
6: 6 Loc [S3_26]
7: 0.1138 Mult
8: -0.1758 Offset

10: TDR Measurement (P100)
1: 00 SDM Address
2: 4080 La/L with Probe Correction in mm
3: .3 Probe Length (meters)
4: 14.6 Cable Length (meters)
5: 1661 MMMP Mux & Probe Selection
6: 7 Loc [S3_56]
7: 0.1138 Mult
8: -0.1758 Offset

11: TDR Measurement (P100)
1: 00 SDM Address
2: 4080 La/L with Probe Correction in mm
3: .3 Probe Length (meters)
4: 15.8 Cable Length (meters)
5: 1551 MMMP Mux & Probe Selection
6: 8 Loc [S3_86]
7: 0.1138 Mult
8: -0.1758 Offset

12: TDR Measurement (P100)
1: 00 SDM Address
2: 4080 La/L with Probe Correction in mm
3: .3 Probe Length (meters)
4: 11.4 Cable Length (meters)
5: 2441 MMMP Mux & Probe Selection
6: 9 Loc [S5_06]
7: 0.1138 Mult
8: -0.1758 Offset

13: TDR Measurement (P100)

1: 00 SDM Address
2: 4080 La/L with Probe Correction in mm
3: .3 Probe Length (meters)
4: 12.5 Cable Length (meters)
5: 2331 MMMP Mux & Probe Selection
6: 10 Loc [S5_26]
7: 0.1138 Mult
8: -0.1758 Offset

14: TDR Measurement (P100)
1: 00 SDM Address
2: 4008 La/L with Probe Correction in mm
3: .3 Probe Length (meters)
4: 13.5 Cable Length (meters)
5: 2221 MMMP Mux & Probe Selection
6: 11 Loc [S5_56]
7: 0.1138 Mult
8: -0.1758 Offset

15: TDR Measurement (P100)
1: 00 SDM Address
2: 4080 La/L with Probe Correction in mm
3: .3 Probe Length (meters)
4: 14.6 Cable Length (meters)
5: 2111 MMMP Mux & Probe Selection
6: 12 Loc [S5_86]
7: 0.1138 Mult
8: -0.1758 Offset

16: TDR Measurement (P100)
1: 00 SDM Address
2: 4080 La/L with Probe Correction in mm
3: .3 Probe Length (meters)
4: 9.9 Cable Length (meters)
5: 2881 MMMP Mux & Probe Selection
6: 13 Loc [S7_06]
7: 0.1138 Mult
8: -0.1758 Offset

17: TDR Measurement (P100)
1: 00 SDM Address
2: 4080 La/L with Probe Correction in mm
3: .3 Probe Length (meters)
4: 11.4 Cable Length (meters)
5: 2771 MMMP Mux & Probe Selection
6: 14 Loc [S7_26]
7: 0.1138 Mult
8: -0.1758 Offset

18: TDR Measurement (P100)
1: 00 SDM Address
2: 4080 La/L with Probe Correction in mm
3: .3 Probe Length (meters)
4: 12.4 Cable Length (meters)
5: 3441 MMMP Mux & Probe Selection
6: 15 Loc [S7_56]
7: 0.1138 Mult
8: -0.1758 Offset

19: TDR Measurement (P100)

1: 00 SDM Address
2: 4080 La/L with Probe Correction in mm
3: .3 Probe Length (meters)
4: 13.6 Cable Length (meters)
5: 3331 MMMP Mux & Probe Selection
6: 16 Loc [S7_86]
7: 0.1138 Mult
8: -0.1758 Offset

20: TDR Measurement (P100)
1: 00 SDM Address
2: 4080 La/L with Probe Correction in mm
3: .3 Probe Length (meters)
4: 9.9 Cable Length (meters)
5: 2661 MMMP Mux & Probe Selection
6: 17 Loc [S9_06]
7: 0.1138 Mult
8: -0.1758 Offset

21: TDR Measurement (P100)
1: 00 SDM Address
2: 4080 La/L with Probe Correction in mm
3: .3 Probe Length (meters)
4: 9.9 Cable Length (meters)
5: 2551 MMMP Mux & Probe Selection
6: 18 Loc [S9_26]
7: 0.1138 Mult
8: -0.1758 Offset

22: TDR Measurement (P100)
1: 00 SDM Address
2: 4080 La/L with Probe Correction in mm
3: .3 Probe Length (meters)
4: 11.4 Cable Length (meters)
5: 3221 MMMP Mux & Probe Selection
6: 19 Loc [S9_56]
7: 0.1138 Mult
8: -0.1758 Offset

23: TDR Measurement (P100)
1: 00 SDM Address
2: 4080 La/L with Probe Correction in mm
3: .3 Probe Length (meters)
4: 12.4 Cable Length (meters)
5: 3111 MMMP Mux & Probe Selection
6: 20 Loc [S9_86]
7: 0.1138 Mult
8: -0.1758 Offset

24: TDR Measurement (P100)
1: 00 SDM Address
2: 4080 La/L with Probe Correction in mm
3: .3 Probe Length (meters)
4: 14.6 Cable Length (meters)
5: 4221 MMMP Mux & Probe Selection
6: 21 Loc [N1_06]
7: 0.1138 Mult
8: -0.1758 Offset

25: TDR Measurement (P100)

1: 00 SDM Address
2: 4080 La/L with Probe Correction in mm
3: .3 Probe Length (meters)
4: 14.5 Cable Length (meters)
5: 4111 MMMP Mux & Probe Selection
6: 22 Loc [N1_26]
7: 0.1138 Mult
8: -0.1758 Offset

26: TDR Measurement (P100)
1: 00 SDM Address
2: 4080 La/L with Probe Correction in mm
3: .3 Probe Length (meters)
4: 11.3 Cable Length (meters)
5: 3661 MMMP Mux & Probe Selection
6: 23 Loc [N1_56]
7: 0.1138 Mult
8: -0.1758 Offset

27: TDR Measurement (P100)
1: 00 SDM Address
2: 4080 La/L with Probe Correction in mm
3: .3 Probe Length (meters)
4: 12.4 Cable Length (meters)
5: 3551 MMMP Mux & Probe Selection
6: 24 Loc [N1_86]
7: 0.1138 Mult
8: -0.1758 Offset

28: TDR Measurement (P100)
1: 00 SDM Address
2: 4080 La/L with Probe Correction in mm
3: .3 Probe Length (meters)
4: 14.5 Cable Length (meters)
5: 4441 MMMP Mux & Probe Selection
6: 25 Loc [N3_06]
7: 0.1138 Mult
8: -0.1758 Offset

29: TDR Measurement (P100)
1: 00 SDM Address
2: 4080 La/L with Probe Correction in mm
3: .3 Probe Length (meters)
4: 16.0 Cable Length (meters)
5: 4331 MMMP Mux & Probe Selection
6: 26 Loc [N3_26]
7: 0.1138 Mult
8: -0.1758 Offset

30: TDR Measurement (P100)
1: 00 SDM Address
2: 4080 La/L with Probe Correction in mm
3: .3 Probe Length (meters)
4: 12.4 Cable Length (meters)
5: 3881 MMMP Mux & Probe Selection
6: 27 Loc [N3_56]
7: 0.1138 Mult
8: -0.1758 Offset

31: TDR Measurement (P100)

1: 00 SDM Address
2: 4080 La/L with Probe Correction in mm
3: .3 Probe Length (meters)
4: 13.6 Cable Length (meters)
5: 3771 MMMP Mux & Probe Selection
6: 28 Loc [N3_86]
7: 0.1138 Mult
8: -0.1758 Offset

32: TDR Measurement (P100)
1: 00 SDM Address
2: 4080 La/L with Probe Correction in mm
3: .3 Probe Length (meters)
4: 16.1 Cable Length (meters)
5: 4881 MMMP Mux & Probe Selection
6: 29 Loc [N5_06]
7: 0.1138 Mult
8: -0.1758 Offset

33: TDR Measurement (P100)
1: 00 SDM Address
2: 4080 La/L with Probe Correction in mm
3: .3 Probe Length (meters)
4: 17.2 Cable Length (meters)
5: 4771 MMMP Mux & Probe Selection
6: 30 Loc [N5_26]
7: 0.1138 Mult
8: -0.1758 Offset

34: TDR Measurement (P100)
1: 00 SDM Address
2: 4080 La/L with Probe Correction in mm
3: .3 Probe Length (meters)
4: 18.4 Cable Length (meters)
5: 4661 MMMP Mux & Probe Selection
6: 31 Loc [N5_56]
7: 0.1138 Mult
8: -0.1758 Offset

35: TDR Measurement (P100)
1: 00 SDM Address
2: 4080 La/L with Probe Correction in mm
3: .3 Probe Length (meters)
4: 19.4 Cable Length (meters)
5: 4551 MMMP Mux & Probe Selection
6: 32 Loc [N5_86]
7: 0.1138 Mult
8: -0.1758 Offset

36: TDR Measurement (P100)
1: 00 SDM Address
2: 4080 La/L with Probe Correction in mm
3: .3 Probe Length (meters)
4: 17.2 Cable Length (meters)
5: 5441 MMMP Mux & Probe Selection
6: 33 Loc [N7_06]
7: 0.1138 Mult
8: -0.1758 Offset

37: TDR Measurement (P100)

1: 00 SDM Address
2: 4080 La/L with Probe Correction in mm
3: .3 Probe Length (meters)
4: 18.3 Cable Length (meters)
5: 5331 MMMP Mux & Probe Selection
6: 34 Loc [N7_26]
7: 0.1138 Mult
8: -0.1758 Offset

38: TDR Measurement (P100)
1: 00 SDM Address
2: 4080 La/L with Probe Correction in mm
3: .3 Probe Length (meters)
4: 19.3 Cable Length (meters)
5: 5221 MMMP Mux & Probe Selection
6: 35 Loc [N7_56]
7: 0.1138 Mult
8: -0.1758 Offset

39: TDR Measurement (P100)
1: 00 SDM Address
2: 4080 La/L with Probe Correction in mm
3: .3 Probe Length (meters)
4: 20.4 Cable Length (meters)
5: 5111 MMMP Mux & Probe Selection
6: 36 Loc [N7_86]
7: 0.1138 Mult
8: -0.1758 Offset

40: TDR Measurement (P100)
1: 00 SDM Address
2: 4080 La/L with Probe Correction in mm
3: .3 Probe Length (meters)
4: 18.4 Cable Length (meters)
5: 5881 MMMP Mux & Probe Selection
6: 37 Loc [N9_06]
7: 0.1138 Mult
8: -0.1758 Offset

41: TDR Measurement (P100)
1: 00 SDM Address
2: 4080 La/L with Probe Correction in mm
3: .3 Probe Length (meters)
4: 19.4 Cable Length (meters)
5: 5771 MMMP Mux & Probe Selection
6: 38 Loc [N9_26]
7: 0.1138 Mult
8: -0.1758 Offset

42: TDR Measurement (P100)
1: 00 SDM Address
2: 4080 La/L with Probe Correction in mm
3: .3 Probe Length (meters)
4: 20.6 Cable Length (meters)
5: 5661 MMMP Mux & Probe Selection
6: 39 Loc [N9_56]
7: 0.1138 Mult
8: -0.1758 Offset

43: TDR Measurement (P100)

```
 1: 00       SDM Address
 2: 4080     La/L with Probe Correction in mm
 3: .3       Probe Length (meters)
 4: 22.0     Cable Length (meters)
 5: 5551     MMMP Mux & Probe Selection
 6: 40       Loc [ N9_86     ]
 7: 0.1138   Mult
 8: -0.1758  Offset

44:  Do (P86)
 1: 54       Set Port 4 Low

45:  Do (P86)
 1: 10       Set Output Flag High (Flag 0)

46:  Real Time (P77)
 1: 110      Day,Hour/Minute (midnight = 0000)

47:  Sample (P70)
 1: 41       Reps
 2: 1        Loc [ S1_06____ ]

48:  End (P95
```

A.12 Mobile Weather station & light penetration of hedge-rows

```
;{CR10X}
;TITLE: SOLWETH.CSI
; Program for measurement weather for mobile weather station
;     when measuring light penetration of hedgerow plantings.
; Use HMP35C TEMPERATURE & RH PROBE (S/N 636980) wired as follows:
;     Red = + 12V, Yellow (power control) =  E2 ,
;     Green (RH) = SE 12,     Orange (Temp) = SE 11
;     Black (Temp Excitation) = Switched Excitation = E1,
;     Clear + White + Purple = Ground
; Albedo meter in Diff Channel 1 (Top) & 2 (Bottom)
; Diffuse Radiation Pyranometer in Diff channel 3 (Pyran No 1)


*Table 1 Program
          01:        10.0       Execution Interval (seconds)

1:  Temp (107) (P11)
 1: 1        Reps
 2: 11       SE Channel
 3: 1        Excite all reps w/E1
 4: 1        Loc [ AirTemp   ]
 5: 1.0      Mult
 6: 0.08     Offset

2:  Excite-Delay (SE) (P4)
 1: 1        Reps
 2: 5        2500 mV Slow Range
 3: 12       SE Channel
 4: 2        Excite all reps w/Exchan 2
 5: 15       Delay (units 0.01 sec)
 6: 2500     mV Excitation
 7: 2        Loc [ RH        ]
 8: 0.1026   Mult
 9: 2.0285   Offset
; Calibration for HMP35C (S/N 636980) is RH = 2.02852 + 1.02559X
;     where X is RH calculated by instruction P4.

3:  Z=X*F (P37)
 1: 2        X Loc [ RH        ]
 2: .01      F
 3: 7        Z Loc [ rh_frac   ]

4:  Saturation Vapor Pressure (P56)
 1: 1        Temperature Loc [ AirTemp   ]
 2: 8        Loc [ SVP       ]

5:  Z=X*Y (P36)
 1: 8        X Loc [ SVP       ]
 2: 7        Y Loc [ rh_frac   ]
 3: 9        Z Loc [ VP_kPa    ]

6:  Z=X-Y (P35)
 1: 8        X Loc [ SVP       ]
 2: 9        Y Loc [ VP_kPa    ]
 3: 10       Z Loc [ VPD_kPa   ]

7:  Volt (Diff) (P2)
 1: 1        Reps
```

```
 2: 33       25 mV 50 Hz Rejection Range
 3: 1        DIFF Channel
 4: 3        Loc [ AlbTop    ]
 5: 56.6352  Mult
 6: 0.0      Offset

 8:  Volt (Diff) (P2)
 1: 1        Reps
 2: 33       25 mV 50 Hz Rejection Range
 3: 2        DIFF Channel
 4: 4        Loc [ AlbBot    ]
 5: 51.1427  Mult
 6: 0.0      Offset

 9:  Volt (Diff) (P2)
 1: 1        Reps
 2: 33       25 mV 50 Hz Rejection Range
 3: 3        DIFF Channel
 4: 5        Loc [ Diffuse   ]
 5: 119.2    Mult
 6: 0.0      Offset

10:  Batt Voltage (P10)
 1: 6        Loc [ Batt_V    ]

11:  If time is (P92)
 1: 0        Minutes (Seconds --) into a
 2: 15       Interval (same units as above)
 3: 10       Set Output Flag High (Flag 0)

12:  Real Time (P77)
 1: 1220     Year,Day,Hour/Minute (midnight = 2400)

13:  Average (P71)
 1: 10       Reps
 2: 1        Loc [ AirTemp   ]

14:  If time is (P92)
 1: 0        Minutes (Seconds --) into a
 2: 1440     Interval (same units as above)
 3: 10       Set Output Flag High (Flag 0)

15:  Real Time (P77)
 1: 1200     Year,Day (midnight = 2400)

16:  Maximum (P73)
 1: 1        Reps
 2: 10       Value with Hr-Min
 3: 1        Loc [ AirTemp   ]

17:  Minimum (P74)
 1: 1        Reps
 2: 10       Value with Hr-Min
 3: 1        Loc [ AirTemp   ]

18:  Maximum (P73)
 1: 1        Reps
 2: 10       Value with Hr-Min
 3: 2        Loc [ RH        ]
```

```
19:  Minimum (P74)
 1: 1        Reps
 2: 10       Value with Hr-Min
 3: 2        Loc [ RH        ]

20:  Maximize (P73)
 1: 1        Reps
 2: 10       Value with Hr-Min
 3: 10       Loc [ VPD_kPa   ]

21:  Minimize (P74)
 1: 1        Reps
 2: 10       Value with Hr-Min
 3: 10       Loc [ VPD_kPa   ]

22:  Sample (P70)
 1: 1        Reps
 2: 6        Loc [ Batt_V    ]

* Table 2 Program
          02:         0.0000              Execution Interval (seconds)

* Table 3  Subroutines

End Program
```

A.13 Programme to calibrate seven tube solarimeters

```
;{CR10X}
;TITLE: SOLCAL00.CSI
; Program for calibrating 7 tube solarimeters
; & 7 Line Quantum Sensors (LQS)
; Use Eppley in Diff Channel 3 as Standard
; Use AM416 in Diff Channel 4 & 5, Pulsed thru'

* Table 1 Program
        01:     10.00           Execution Interval (seconds)

1:  Do (P86)
 1: 41      Set Port 1 High

2:  Beginning of Loop (P87)
 1: 0       Delay
 2: 6       Loop Count

3:  Do (P86)
 1: 72      Pulse Port 2

4:  Step Loop Index (P90)
 1: 2       Step

5:  Volt (Diff) (P2)
 1: 2       Reps
 2: 33      25 mV 50 Hz Rejection Range
 3: 4       DIFF Channel
 4: 6    -- Loc [ Sol1      ]
 5: 1       Mult
 6: 0       Offset

6:  End (P95)

7:  Do (P86)
 1: 51      Set Port 1 Low

8:  Volt (Diff) (P2)
 1: 2       Reps
 2: 33      25 mV 50 Hz Rejection Range
 3: 1       DIFF Channel
 4: 18      Loc [ LQS6     ]
 5: 1       Mult
 6: 0       Offset

9:  Volt (Diff) (P2)
 1: 1       Reps
 2: 33      25 mV 50 Hz Rejection Range
 3: 3       DIFF Channel
 4: 20      Loc [ Epply    ]
 5: 115     Mult
 6: .58     Offset

10:  If (X<=>F) (P89)
 1: 20      X Loc [ Epply    ]
 2: 3       >=
 3: 700     F
 4: 30      Then Do
```

```
11:  Z=X+F (P34)
 1: 20       X Loc [ Epply     ]
 2: -0.58    F
 3: 20       Z Loc [ Epply     ]

12:  Z=X*F (P37)
 1: 20       X Loc [ Epply     ]
 2: 1.07113  F
 3: 20       Z Loc [ Epply     ]

13:  Z=X+F (P34)
 1: 20       X Loc [ Epply     ]
 2: 0.58     F
 3: 20       Z Loc [ Epply     ]

14:  End (P95)

15:  Z=X*F (P37)
 1: 6        X Loc [ Sol1      ]
 2: 66.681   F
 3: 6        Z Loc [ Sol1      ]

16:  Z=X*F (P37)
 1: 7        X Loc [ Sol2      ]
 2: 66.98    F
 3: 7        Z Loc [ Sol2      ]

17:  Z=X*F (P37)
 1: 8        X Loc [ Sol3      ]
 2: 67.266   F
 3: 8        Z Loc [ Sol3      ]

18:  Z=X*F (P37)
 1: 9        X Loc [ Sol4      ]
 2: 71.336   F
 3: 9        Z Loc [ Sol4      ]

19:  Z=X*F (P37)
 1: 10       X Loc [ Sol5      ]
 2: 65.83    F
 3: 10       Z Loc [ Sol5      ]

20:  Z=X*F (P37)
 1: 11       X Loc [ Sol6      ]
 2: 65.076   F
 3: 11       Z Loc [ Sol6      ]

21:  Z=X*F (P37)
 1: 12       X Loc [ Sol7      ]
 2: 63.59    F
 3: 12       Z Loc [ Sol7      ]

22:  Z=X*F (P37)
 1: 13       X Loc [ LQS1      ]
 2: 439.06   F
 3: 13       Z Loc [ LQS1      ]

23:  Z=X*F (P37)
 1: 14       X Loc [ LQS2      ]
 2: 311.51   F
```

```
 3: 14       Z Loc [ LQS2      ]

24:  Z=X*F (P37)
 1: 15       X Loc [ LQS3      ]
 2: 364.08   F
 3: 15       Z Loc [ LQS3      ]

25:  Z=X*F (P37)
 1: 16       X Loc [ LQS4      ]
 2: 444.3    F
 3: 16       Z Loc [ LQS4      ]

26:  Z=X*F (P37)
 1: 17       X Loc [ LQS5      ]
 2: 405.38   F
 3: 17       Z Loc [ LQS5      ]

27:  Z=X*F (P37)
 1: 18       X Loc [ LQS6      ]
 2: 419.74   F
 3: 18       Z Loc [ LQS6      ]

28:  Z=X*F (P37)
 1: 19       X Loc [ LQS7      ]
 2: 423.34   F
 3: 19       Z Loc [ LQS7      ]

29:  Batt Voltage (P10)
 1: 1        Loc [ V_Batt    ]

30:  If time is (P92)
 1: 0        Minutes (Seconds --) into a
 2: 10       Interval (same units as above)
 3: 10       Set Output Flag High (Flag 0)

31:  Real Time (P77)
 1: 1220     Year,Day,Hour/Minute (midnight = 2400)

32:  Average (P71)
 1: 15       Reps
 2: 6        Loc [ Sol1      ]

33:  Sample (P70)
 1: 1        Reps
 2: 1        Loc [ V_Batt    ]


* Table 2 Program
            02:         0.0000              Execution Interval (seconds)

* Table 3  Subroutines

End Program
```